Control of Cellular Redox State and Biomass Synthesis

by

Sarah Mary Chang
B.S. Biochemistry and Molecular Biology
Pennsylvania State University (2016)

Submitted to the Department of Biology
in Partial Fulfillment of the Requirements for the Degree of

DOCTOR OF PHILOSOPHY

at the

MASSACHUSETTS INSTITUTE OF TECHNOLOGY

JUNE 2024

Authored by: Sarah M. Chang
Department of Biology
January 24, 2024

Certified by: Matthew G. Vander Heiden
Director, Koch Institute of Integrative Cancer Research
Lester Wolfe Professor of Molecular Biology
Thesis Supervisor

Accepted by: Mary Gehring
Professor of Biology
Member, Whitehead Institute
Director, Biology Graduate Committee

Control of Cellular Redox State and Biomass Synthesis

by

Sarah M. Chang

Submitted to the Department of Biology on January 24, 2024
in Partial Fulfillment of the Requirements for the Degree of
Doctor of Philosophy in Biology

Abstract

To proliferate, tumors must synthesize sufficient biomass, such as proteins, nucleotides, and lipids. Many nutrients that produce biomass undergo oxidation reactions that require the redox cofactor NAD+ as an electron acceptor. Thus, the cellular redox state, measured by the NAD+/NADH ratio, can constrain the synthesis of oxidized biomass. This dissertation aims to uncover the determinants of the cellular NAD+/NADH ratio and how the cellular redox state governs biosynthetic capabilities of cancer cells in response to elevated biomass demands. In serine depleted conditions, which increase the NAD+ demand to support serine synthesis, we find that modulating the NAD+/NADH ratio proportionally alters serine synthesis rates. We uncover that some cancer cells elevate mitochondrial respiration and increase the NAD+/NADH ratio following serine withdrawal while others do not. Increasing mitochondrial respiration is sufficient to elevate the NAD+/NADH ratio and improve serine synthesis and proliferation in serine depleted conditions. Exogenous lipid withdrawal can also elevate mitochondrial respiration and the NAD+/NADH ratio, leading to increased serine synthesis despite no change in serine demand. Together, we find that the cellular NAD+/NADH ratio is regulated by mitochondrial respiration in a cell and environment specific manner, impacting oxidative biosynthesis reactions to determine the proliferative capacity of cancer cells in different nutrient environments.

Thesis Supervisor: Matthew G. Vander Heiden
Title: Lester Wolfe Professor of Molecular Biology

Acknowledgements

I am extremely grateful to many people, whose deep support throughout my scientific training has made this thesis work possible. Firstly, I'd like to thank my advisor, Matt Vander Heiden, whose passion for science and steadfast enthusiasm taught me to be more fearless in pursuing my ideas. I have a true physician scientistic role model and friend in Matt, and I admire the way he cares for each of his trainees.

I'd like to thank the entire Vander Heiden lab, past and present, whose intelligence, generosity, patience, and comedy have hoisted me throughout my PhD. In particular, I'd like to thank Peggy Hsu, Allison Lau, Evan Lien, Zhaoqi Li, Kiera Sapp, and Alicia Darnell. Kiera and Alicia have given me an immeasurable amount of support and light in and out of the lab, and I profoundly cherish our friendship. Thank you to Muhammad Munim, Anya Shevzov-Zebrun, and Sonia Trojan for uplifting me time and time again. To have trained in the Vander Heiden lab alongside every talented, kind, and genuine individual, many of whom are now my close friends, is a true gift.

Thank you to my thesis committee Jackie Lees and Joey Davis. Before our first meeting, I yearned for new scientific perspectives and guidance after a period of confusion. I left the meeting beaming from our discussions with a new sense of clarity, and I was immediately excited for the opportunity to learn from them. I tremendously value their advice and am grateful for their support throughout my PhD. I would also like to thank Dr. Ed Chouchani for serving as my outside thesis examiner.

Thank you to my MD/PhD classmates, in particular Kaitavjeet Chowdhary, Elliot Akama-Garren, and Annabel Wang. I am lucky I get to run this marathon with them.

These acknowledgements would be incomplete without the deepest thank you to 143 Magazine Street. To Sofia Hu, Soley Olafsson, Daniel Michelson, Matt Shelley-Reade, Zhaoqi Li, Max Carter, Tony Gardella, Muhammad Munim, and Tony Scott, and to everyone who has made 143 Magazine Street the most beautiful community, you have my heart. I am blessed.

And thank you to my family – my father, mother, and brother Matthew – who remind me to never stop adding oil.

Table of Contents

Chapter 1: The Metabolic Requirements of Proliferation

Introduction

For cells to proliferate, sufficient biomass must be produced to enable cell division. Failure to meet biomass demands can restrict passage through the cell cycle, leading to cell cycle stalling, quiescence, or cell death. Producing biomass is particularly important for rapidly dividing cells, including cancer cells, which require robust and well-coordinated mechanisms to ensure adequate resources are obtained to meet the high metabolic demands of proliferation. These mechanisms must be dynamic in circumstances where synthesizing and acquiring the necessary metabolites for biomass production are challenged by nutrient limitations in the cellular environment. Inability to adapt to environmental changes reveals metabolic vulnerabilities that can be exploited to suppress cancer growth. Additionally, uncovering processes that allow cells to overcome obstacles to proliferation can be targeted, leading to novel therapeutic options.

Coordinated metabolic supply and demand is essential for many cellular processes. There are numerous variables that influence the acquisition of metabolic supply and the specific metabolic demands, including both cell-intrinsic and cell-extrinsic factors. Here, we will examine the pathways of biosynthesis, how they are altered in cancer, and the components that shape the availability of metabolic supplies required to meet the biosynthetic demands of proliferation.

The metabolic pathways in biosynthesis

Certain biomass precursors can be synthesized through various metabolic pathways while others must be acquired from the environment. Many nutrients acquired from the environment are used as substrates for the reactions that convert these environment nutrients to necessary components for proliferation. The key metabolic pathways in biosynthesis will be discussed in this section.

Central Carbon Metabolism

Central carbon metabolism is the conversion of carbon-containing molecules such as sugars to biomass and serves as a major branching off point for other biosynthetic pathways. Not only is it a major biosynthetic pathway, but it is also integral for ATP formation and the generation of redox cofactors necessary for both biosynthetic enzymes and antioxidant production. Central carbon metabolism encompasses glycolysis, the pentose phosphate pathway, and the tricarboxylic acid (TCA) cycle (**Figure 1**). A major substrate of central carbon metabolism is glucose, which is initially phosphorylated into glucose-6-phosphate (G6P) during the first step of glycolysis. G6P carbons can enter the pentose phosphate pathway, leading to the synthesis of ribose-5-phosphate, a precursor for nucleotides. The pentose phosphate pathway also yields the production of NADPH, a redox cofactor that is required for certain anabolic and biosynthetic reactions and integral for glutathione synthesis and antioxidant defense. The end product of glycolysis is the production of pyruvate, yielding 2 net ATP per glucose in the process. Pyruvate carbons carry two fates: conversion into lactate or entry into the mitochondria for further oxidation. Lactate does not contribute to biomass formation and is net secreted, serving as a waste product. However, pyruvate reduction to lactate leads to the generation of NAD+ via lactate dehydrogenase (LDH), causing glycolysis to be net redox neutral. Additionally, in

oxygen limiting or anaerobic environments, glucose fermentation into lactate allows cells to continue producing ATP when aerobic respiration by the mitochondria is unable to.

In the presence of oxygen, pyruvate, once transported into the mitochondria via the mitochondrial pyruvate carriers (MPC1/2) (Bricker, 2013), contributes carbons to the TCA cycle where it is further oxidized. The TCA cycle serves multiple metabolic roles including the synthesis of citrate, which contributes carbons for fatty acid synthesis. A major consequence of the TCA cycle is the generation of electron carriers such as NADH and $FADH_2$. These electron carriers donate electrons to the mitochondrial electron transport chain (ETC), situated on the inner mitochondrial membrane. The ETC encompasses four protein complexes, I-IV, as well as ATP synthase, known as complex V. Electrons are donated via NADH at complex I and $FADH_2$ at complex II and are carried through the ETC until they are captured by the terminal electron acceptor, O_2, via complex IV. Complexes I, III, and IV use the transfer of electrons to pump protons from the mitochondrial matrix against their chemical gradient into the mitochondrial intermembrane space, leading to a mitochondrial membrane potential. The energy stored in the proton gradient is harnessed by ATP synthase, allowing for the phosphorylation of ADP into ATP. The process of coupling the mitochondrial electron transport chain with ADP phosphorylation by the proton chemiosmotic gradient is termed oxidative phosphorylation and yields ~32 ATP per glucose. ATP can then be transported out of the mitochondrial in exchange for ADP via the ATP/ADP translocase, where it is needed for a variety of cellular processes, from facilitating transporter activity to cytoskeletal remodeling, protein synthesis, motor function, and signaling changes, among many others. In sum, central carbon metabolism encompasses major cellular pathways that provide cellular energy in

the form of ATP, generate redox cofactors, and produce integral biomass for growth and division, such as nucleotides, lipids, and amino acids.

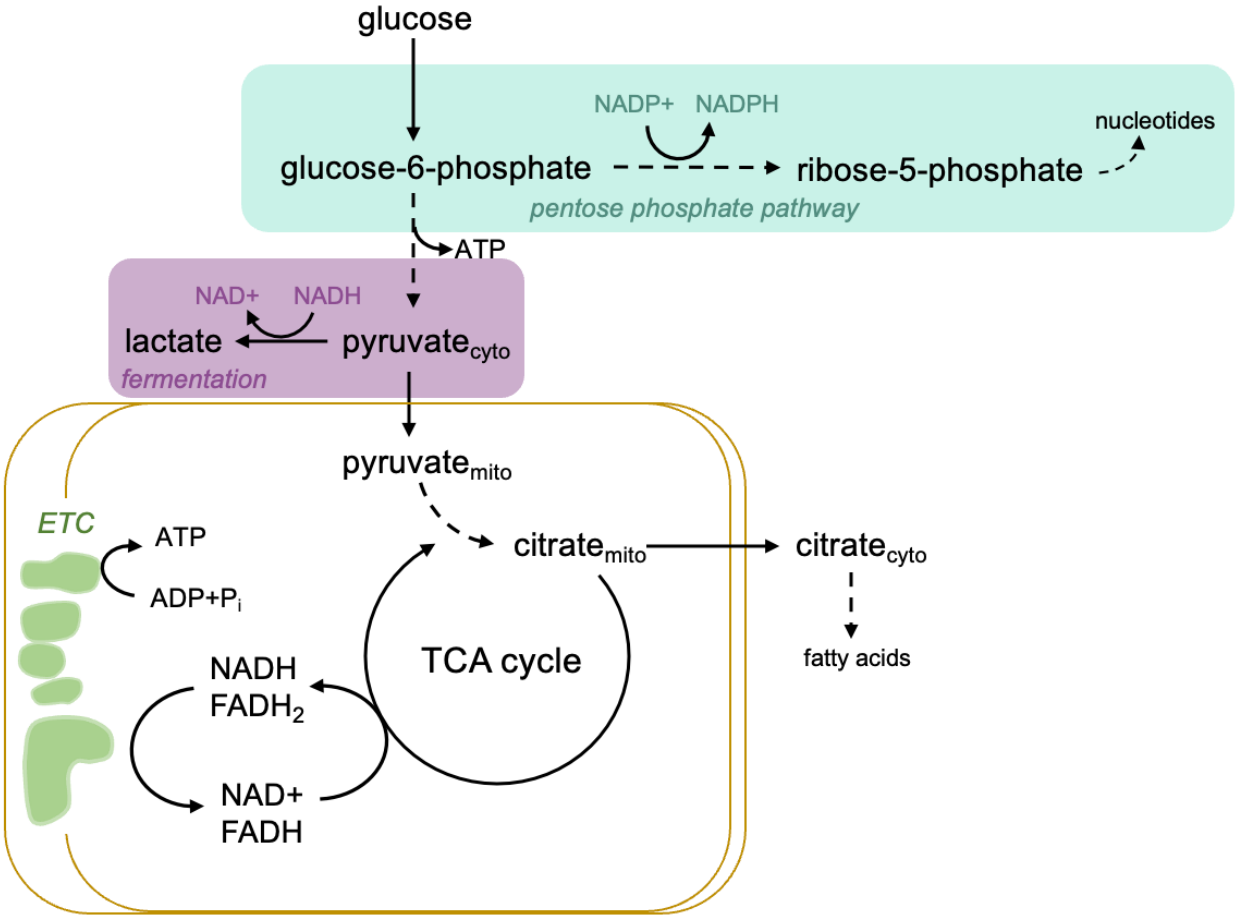

Figure 1. Overview of central carbon metabolism. Glucose is consumed by cells and is phosphorylated to glucose-6-phosphate, which can produce ribose-5-phosphate in the pentose phosphate pathway. At the end of glycolysis, glucose generates two net ATP and pyruvate, which can be converted to lactate via lactate dehydrogenase (LDH) or enter the mitochondria where it contributes carbons to the TCA cycle. The TCA cycle produces citrate, which is used for fatty acid synthesis, as well as the reducing equivalents NADH and $FADH_2$. Donation of electrons from NADH and $FADH_2$ to the mitochondrial electron transport chain (ETC) leads to the formation of a proton gradient in the inner mitochondrial membrane space that is used by ATP synthase to produce ATP in a process called oxidative phosphorylation.

Amino Acid Synthesis

Obtaining sufficient amino acids is a major requirement for dividing cells. In fact, amino acids make up the majority of cell mass in proliferating mammalian cells compared to glucose (Hosios, 2016). Not only are amino acids integral for protein synthesis, but

they also serve as precursors for other biomass components such as nucleotides and lipids. While some amino acids are essential and must be taken-up by cells from the environment, other amino acids can be produced through various biosynthetic reactions and are termed non-essential amino acids (NEAA).

Serine is a critical NEAA that is necessary for nucleotide synthesis, the production of sphingolipids, glutathione synthesis, as well as generating one-carbon units required for folate metabolism and methylation reactions. Additionally, other amino acids such as glycine and cysteine are produced from serine carbons. Serine is the second most highly consumed amino acids by cultured cancer cells after glutamine, emphasizing its significance for proliferation (Hosios, 2016). While serine can be consumed, cells are capable of synthesizing serine *de novo*. Serine is derived from glucose carbons, where the glycolytic intermediate 3-phosphoglycerate (3-PG) can branch off glycolysis into the three step serine synthesis pathway (**Figure 2**). 3-PG is converted to 3-phosphohydroxypyruvate (3-PHP) by the enzyme phosphoglycerate dehydrogenase (PHGDH), which requires the redox cofactor NAD+. 3-PHP is then converted to 3-phosphoserine (3-PS) by phosphoserine aminotransferase (PSAT1), which couples this conversion to the deamination of glutamate into α-ketoglutarate (α-KG). 3-PS is finally converted to serine via phosphoserine phosphatase (PSPH). Once serine is synthesized, it can directly be used to form the amino acid glycine via the enzyme serine hydroxymethyltransferase (SHMT). The SHMT-mediated reaction leads to the donation of a one carbon unit from serine to the folate cycle, which is integral for nucleotide synthesis. Cysteine, while available for uptake in its disulfide form cystine, can be

produced from serine and methionine, where the carbon backbone of cysteine is generated from serine and the sulfur group is derived from methionine.

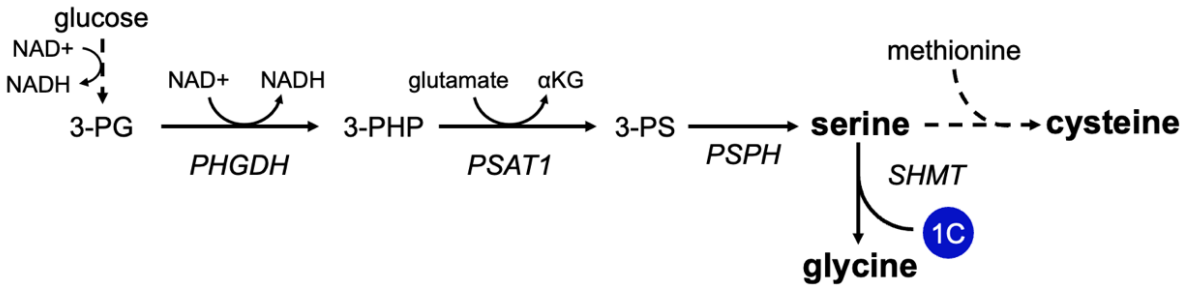

Figure 2. Overview of *de novo* serine, glycine, and cysteine synthesis. Serine is produced from glucose through three metabolic reactions. Serine can then be converted to the amino acids glycine and cysteine. Abbreviations: 3-PG, 3-phosphglycerate; PHGDH, phosphoglycerate dehydrogenase; 3-PHP, 3-phosphohydroxypyruvate; PSAT1, phosphoserine aminotransferase 1; αKG, α-ketoglutarate; 3-PS, 3-phosphoserine; PSPH, phosphoserine phosphatase; SHMT, serine hydroxymethyltransferase; 1C, 1-carbon

Glutamine is the highest consumed amino acid by cells in culture (Hosios, 2016). It serves multiple metabolic roles, acting as a proteinogenic amino acid, a nitrogen donor for nucleotide synthesis, as well as a precursor for other amino acids (**Figure 3**). The amino acid glutamate is formed from glutamine via the enzyme glutaminase. Glutamate can then be used to produce the amino acid proline in the mitochondria and synthesize ornithine, which leads to the arginine production via the urea cycle. Arginine synthesis requires the amino acid aspartate. *De novo* aspartate synthesis largely relies on glutamine carbons. Glutamine-derived glutamate is converted to α-KG either through glutamate dehydrogenase (GDH) or through a transamination reaction that couples the conversion of glutamate to α-KG with the conversion of another α-ketoacid such as pyruvate or oxaloacetate to an amino acid such as alanine or aspartate, respectively. Aspartate can then be produced from α-KG through two separate pathways. One pathway relies on the oxidative TCA cycle where α-KG is converted to oxaloacetate, which generates aspartate via aspartate aminotransferase or glutamate-oxaloacetate

transaminase (GOT). The other pathway relies on the reductive TCA cycle where α-KG is converted into isocitrate via isocitrate dehydrogenase, which requires a reducing equivalent such as NADPH or NADH. Isocitrate is then isomerized into citrate by aconitase, where citrate is converted to acetyl-CoA and oxaloacetate via cytosolic ATP citrate lyase. Oxaloacetate can then be converted to aspartate via cytosolic GOT1. Aspartate, like many other amino acids, is not only used for protein synthesis but also critical for the synthesis of asparagine via asparagine synthetase (ASNS) and purine nucleotides, where the conversion of inosine monophosphate (IMP) into adenine monophosphate (AMP) requires aspartate. Additionally, the production of the purine intermediate phosphoribosylaminoimidazolesuccinocarboxamide (SAICAR) by SAICAR synthetase requires aspartate.

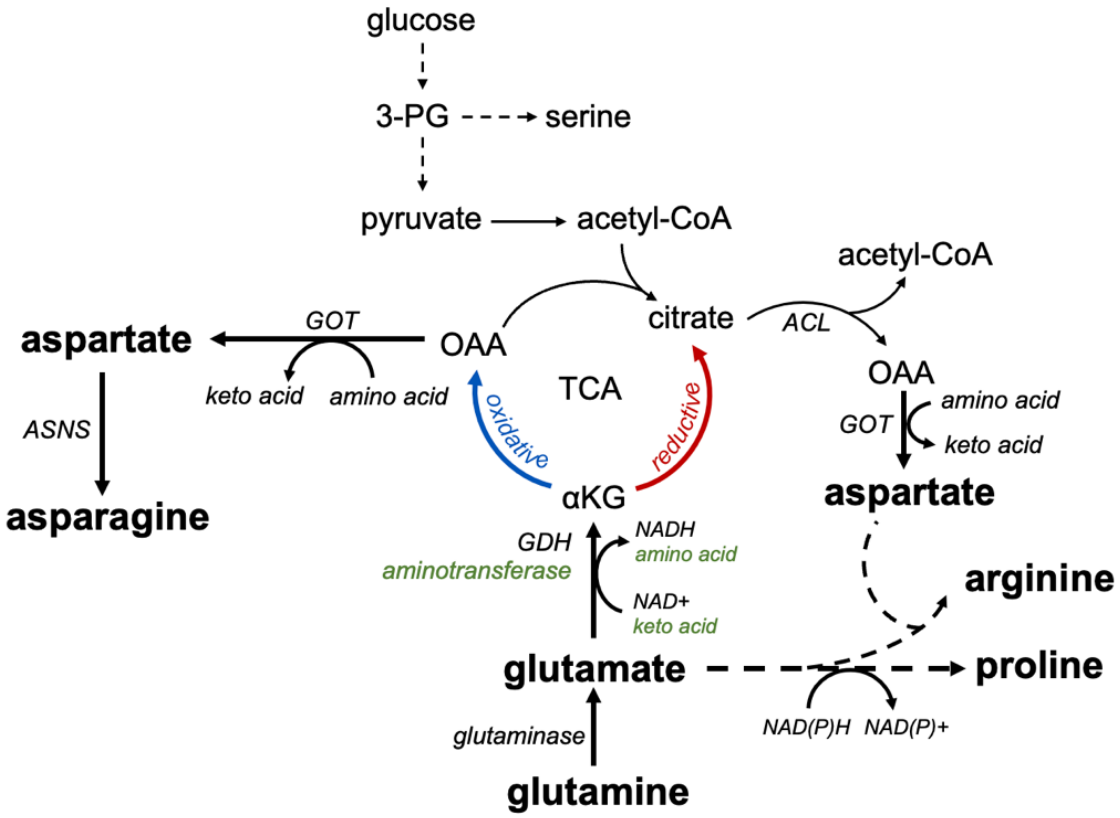

Figure 3. Amino acid synthesis is heavily interconnected. Glutamine is consumed by cells, where its carbons are used to produce glutamate, proline, arginine, aspartate, and asparagine. Abbreviations: 3-PG, 3-phosphoglycerate; ACL, ATP citrate lyase; OAA, oxaloacetate; GOT, glutamic-oxaloacetic transaminase; αKG, α-ketoglutarate; ASNS, asparagine synthetase; GDH, glutamate dehydrogenase

One Carbon Metabolism

The synthesis of RNA and DNA integrates numerous metabolic pathways, using specific amino acids, sugars, and one-carbon units to generate purine and pyrimidine nucleotides. Not only are one carbon (1C) units integral for nucleotide synthesis, but they also support multiple cellular processes such as amino acid homeostasis, methylation reactions, and redox homeostasis. The tremendous significance of the 1C metabolism, which encompasses the folate cycle, is reflected in the phenotypic consequences of folate deficiencies, including anemia and spina bifida.

The 1C or folate cycle spans across the cytosol and mitochondria where a majority of 1C units are derived from serine carbons. It has been shown that in most mammalian cells, both cancer and non-transformed, as well as in yeast, serine is cleaved into glycine primarily in the mitochondria by SHMT2 (**Figure 4**) (Lewis, 2014; Yang, 2016). SHMT2 transfers the β-carbon of serine to tetrahydrofolate (THF). THF is a folic acid derivative that is produced by the enzyme dihydrofolate reductase (DHFR) from the uptake of environmental folates. The transfer of the one carbon unit from serine onto THF leads to the production of 5,10-methylene-THF, which is converted to 10-formyl-THF by the mitochondrial enzyme methylenetetrahydrofolate dehydrogenase (MTHFD2) or MTHFD2-like (MTHFD2L), requiring NAD(P)+ as an electron acceptor. 10-formyl-THF is then converted to formate by MTHFD1-like (MTHFD1L), where formate can then traverse the mitochondria into the cytosol via an unknown mechanism (Kory, 2018). Formate in

the cytosol is converted by MTHFD1 back to 10-formyl-THF, which can be used for *de novo* purine synthesis or converted back to 5,10-methylene-THF by MTHFD1. Cytosolic 5,10-methylene-THF has three separate fates. One fate is its use for nucleotide synthesis in a reaction mediated by thymidylate synthase (TYMS), which couples the conversion of deoxyuridine monophosphate (dUMP) to deoxythymidine monophosphate (dTMP) with the conversion of 5,10-methylene-THF to dihydrofolate (DHF). DHF can then regenerate THF via DHFR. Another fate of 5,10-methylene-THF is for methionine synthesis. The enzyme methylenetetrahydrofolate reductase (MTHFR) catalyzes the conversion of 5,10-methylene-THF into 5-methyl-THF. 5-methyl-THF reacts with homocysteine via methionine synthase (MTR) to produce THF and methionine as part of the methionine cycle, which leads to the eventual production of S-adenosyl methionine (SAM), the methyl donor cofactor for methyltransferases. A third fate of 5,10-methylene-THF is its return to 1C cycle home base, where it is used to generate serine from glycine via SHMT1. Serine can then travel into the mitochondria through what is believed to be sideroflexin 1 (SFXN1) (Kory, 2018) and continue the 1C cycle.

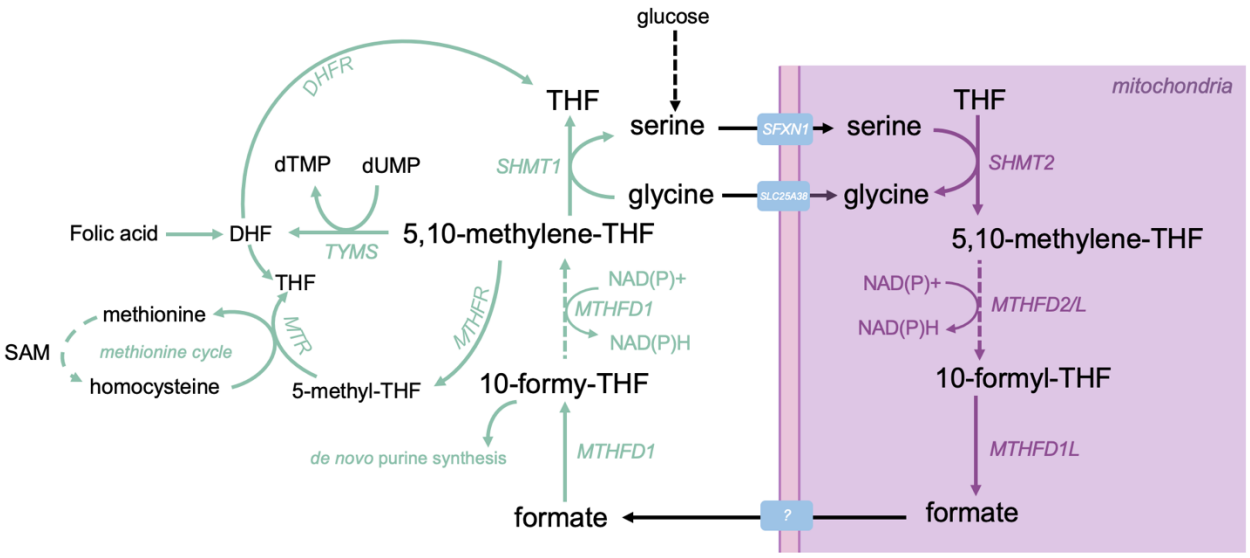

Figure 4. Overview of one carbon metabolism. Serine carbons generate one-carbon units used for nucleotide synthesis and contribute to the methionine cycle to produce methionine and carbon units for methylation reactions. Arrows in this figure are depicted as unidirectional and display the net direction found in most mammalian cells. However, flux through the 1C cycle and transport of serine, glycine, and formate across the mitochondria can be reversible. Abbreviations: THF, tetrahydrofolate; SHMT, serine hydroxymethyltransferase, MTHFD, methylenetetrahydrofolate dehydrogenase; MTHFDL, methylenetetrahydrofolate dehydrogenase-like; MTHFR, methylenetetrahydrofolate reductase; MTR, methionine synthase; SAM, S-adenosyl methionine; TYMS, thymidylate synthase; DHFR, dihydrofolate reductase; SFXN1, sideroflexin 1

Fatty Acid Synthesis

Lipids are an extremely diverse family of macromolecules, serving as mediators of signaling pathways, energy stores in the form of triglycerides, and components of the cell membrane. In fact, 50% of membrane mass is composed of lipids, including cholesterol, phospholipids, and sphingolipids (Hosios and Vander Heiden, 2018). While a large fraction of lipids and fatty acids are taken up from the environments, cells are able to perform *de novo* lipid synthesis. Lipid synthesis requires the production of cytosolic acetyl-CoA, the building block of fatty acids. In most mammalian cells, lipogenic acetyl-CoA is synthesized through two major metabolic pathways: glucose and glutamine oxidation. Glucose oxidation to make acetyl-CoA involves glycolysis and pyruvate oxidation by pyruvate dehydrogenase (PDH). Producing acetyl-CoA from glutamine requires the conversion of glutamine-derived glutamate to α-ketoglutarate (α-KG), which can be oxidatively metabolized through the TCA cycle or undergo reductive carboxylation to form citrate. Citrate can be transported out of the mitochondria via SLC25A1 and converted to oxaloacetate and acetyl-CoA by ATP-citrate lyase, producing lipogenic acetyl-CoA necessary for *de novo* lipid synthesis (**Figure 5**). In the first committed step of fatty acid synthesis, cytosolic acetyl-CoA is converted to malonyl-CoA via acetyl-CoA carboxylase (ACC). Then, fatty acid synthase (FASN) combines malonyl-CoA and acetyl-

CoA after each are transferred to acyl carrier proteins (ACP), generating fatty acids with the addition of more acetyl-CoA carbons in an iterative process that requires NADPH. This process leads to the production of the sixteen carbon-long saturated fatty acid, palmitate. Palmitate can undergo fatty acid elongation via elongases and/or desaturation via desaturases in the endoplasmic reticulum and serve as a precursor for other complex lipid species. The use of NADPH in fatty acid synthesis causes lipid synthesis to be viewed generally as a reductive anabolic process. However, the need to oxidize glucose and/or glutamine to generate lipogenic acetyl-CoA imparts a significant requirement for electron acceptor availability (Li, 2022) (see “Redox Requirement of Biomass Synthesis”).

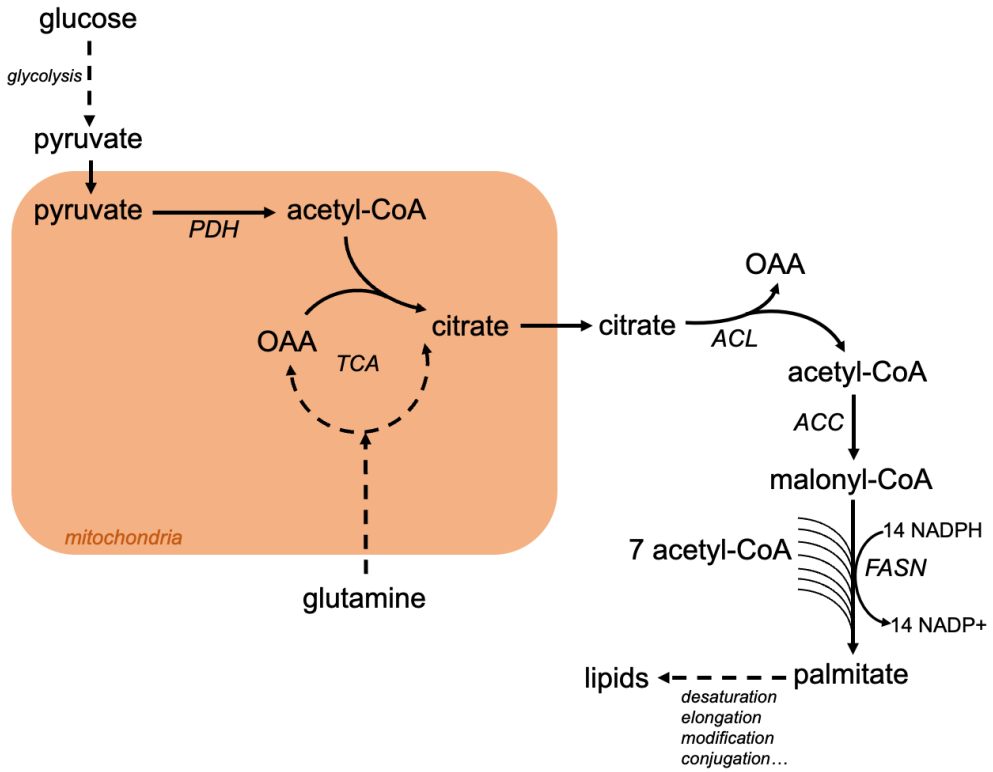

Figure 5. Overview of fatty acid synthesis. Glucose is oxidized to synthesize acetyl-CoA, which combines with OAA to synthesize citrate. Glutamine can undergo oxidative decarboxylation to produce OAA or reductive carboxylation to produce citrate. Once citrate is transported out of the mitochondria and cleaved into acetyl-CoA via ATP Citrate Lyase (ACL), fatty acid synthesis can take place. Abbreviations: PDH, pyruvate dehydrogenase, ACC, acetyl-CoA carboxylase, FASN, fatty acid synthase.

Biomass demands of cancer

Many biosynthetic pathways are altered in cancer. The high biosynthetic demands of rapid proliferation lead to changes in metabolism that are distinct to cancer compared to non-transformed cells. The aspects that modify and influence the biosynthetic pathways in cancer will be discussed in this section.

Aerobic Glycolysis or the Warburg Effect

In the 1920s, using different rat tumors and the Rous chicken sarcoma, Otto Warburg observed that cancer cells consume a tremendous amount of glucose compared to cells from normal tissues and ferment the glucose into lactate even in the presence of abundant oxygen (Warburg, 1923). Warburg's findings were also observed by Carl and Gerty Cori, who implanted tumors in one wing of a chicken and found increased lactate in the blood of the tumor-bearing wing (Cori, 1925). Upon considering the expected large energetic requirements for rapid proliferation, the tendency to ferment glucose into lactate, a waste product, appears paradoxical; glycolysis yields 2 ATP per glucose while aerobic respiration yields 30-32 ATP per glucose. This phenomenon is a major metabolic distinction between non-transformed cells and tumors and has been leveraged in patient settings. Fluorodeoxyglucose (FDG) – positron emission tomography (PET) is a procedure that enables imaging of tumors in the body by visualizing the uptake the radioactive glucose analog FDG by cancer cells in the body. This tendency to ferment glucose in the presence of oxygen, also called aerobic glycolysis, not only occurs in human cancer cells, but also has been observed in other rapidly proliferating eukaryotic cells. After Warburg's observations in 1929, English biochemist Herbert Crabtree

observed that the yeast *Saccharomyces cerevisiae* tended to ferment glucose into ethanol even in the presence of oxygen, a phenomenon now called the Crabtree effect (Crabtree, 1929). Additionally, lymphocytes and proliferating fibroblasts display aerobic glycolysis (Wang, 1976).

The Warburg effect has been actively investigated by the cancer metabolism field, and many hypotheses have been proposed. One long held hypothesis is that increasing glucose consumption and glycolysis leads to higher availability of glycolytic intermediates that are used for biosynthesis (Vander Heiden, 2009). Others argue that because glucose is a highly abundant nutrient, aerobic glycolysis allows rapidly dividing cells to better use glucose to produce ATP, which occurs at a higher rate compared to oxidative phosphorylation (Pfeiffer, 2001). Additionally, metabolic models have found that the proteome cost of respiration exceeds that of fermentation by almost two-fold, arguing that it is more net costly for proliferating cells to respire (Basan, 2015). However, the ATP requirement for proliferation has been interrogated. The ability for cancer cells to rapidly divide while being highly glycolytic suggests that ATP production through aerobic glycolysis is sufficient for proliferation. Consistently, cells exhibiting aerobic glycolysis have high ATP/ADP ratios (Deberardinis, 2008). A recent study identifies that one major consequence of glucose fermentation into lactate is the regeneration of NAD+. This study reveals that ATP synthase activity and excess ATP in rapidly proliferating cells hyperpolarize the mitochondrial membrane, limiting the ability for complex I to regenerate sufficient NAD+ required for biosynthetic reactions. Thus, it has been proposed that cancer cells increase glucose fermentation into lactate to maintain NAD+ regeneration via lactate dehydrogenase (LDH). Consistently, diverting pyruvate carbons into the TCA

cycle and suppressing LDH activity leads to a reduced cellular NAD+/NADH ratio and lower proliferation (Luengo, 2021). While elevated LDH activity can lead to increased NAD+ regeneration, glucose fermentation is redox neutral, as one unit of NAD+ is consumed by GAPDH per unit of NAD+ regenerated by LDH. It remains unclear what functional benefits cancer cells derive from excess glucose consumption. Further studies are being conducted to reveal the metabolic benefits of aerobic glycolysis as well as identify methods to target glucose uptake and lactate production in malignancy (Luengo et al., 2017).

The Biosynthetic Roles of Mitochondria in Cancer

Warburg originally hypothesized that cancer cells increase glucose fermentation due to defective mitochondria as a consequence of chronic hypoxia (Warburg, 1956). Warburg argued that because cancer cells did not follow the Pasteur Effect, when oxygen availability inhibits fermentation in yeast, their mitochondria must be unable to respire. However, tumors do not display diminished oxygen consumption and can consume oxygen as rapidly as normal tissues, shown by biochemists Dean Burk, who may be recognized for his development of the Lineweaver-Burk plot, and Sidney Weinhouse, who stated “it would be more accurate to state that anaerobic glycolysis is so high in tumors that a normal respiration and a normal Pasteur effect are incapable of eliminating it” (Burk, 1939; Weinhouse, 1956). Additionally, in cancer cell lines, the majority of cell mass is not derived from glucose carbons but from amino acids, where glutamine is the most consumed amino acid (Hosios, 2016).

Cancer cells are not only capable of performing mitochondrial respiration, but also require functional mitochondria for proliferation and tumorigenesis (Weinberg, 2010).

Suppressing mitochondrial respiration blocks cancer cell proliferation in culture and in tumor xenografts (Kroll, 1983; Wheaton, 2014). Additionally, it has long been observed that cancer cells without mtDNA, called ρ^0 cells, cannot proliferate unless supplemented with pyruvate and the nucleoside uridine (King, 1989). Because mtDNA encodes thirteen electron transport chain proteins, ρ^0 cells cannot respire. In fact, tumors without mtDNA display slow tumor growth only after the acquisition of mtDNA from surrounding host cells (Tan, 2015), arguing that cancer cells rely on mitochondrial respiration for proliferation.

The pyrimidine biosynthesis enzyme dihydroorotate dehydrogenase (DHODH) is a mitochondrial protein whose activity is coupled to the ETC by transferring electrons to coenzyme Q (CoQ), a lipid soluble component of the ETC that carries electrons from complexes I, II, and DHODH, among others, to complex III. Complex III then transfers its electrons to cytochrome c, and Complex IV oxidizes cytochrome c to reduce oxygen, the terminal electron acceptor (**Figure 6**). The supplementation of uridine compensates for the inability of respiration-deficient ρ^0 cells to synthesize pyrimidines due to suppressed DHODH activity. Reactivation of DHODH in ρ^0 cells by expressing alternative oxidase (AOX), a protein that replaces complex III and IV function by mediating electron transfer from CoQ to oxygen, can lead to tumor formation even in the context where ATP synthase was not functional, demonstrating that mitochondrial ATP production is not required for cancer growth (Bajzikova, 2019).

One major metabolic role of mitochondrial respiration besides ATP synthesis is to regenerate the electron acceptor NAD+ at complex I. Complex I receives electrons from NADH and then transfers electrons to CoQ, leading to the oxidation of NADH back to NAD+. In addition to uridine, ρ^0 cells require pyruvate supplementation in culture.

Pyruvate is an electron acceptor and can supply cells with oxidized NAD+ through lactate dehydrogenase activity. It was found that regeneration of NAD+ by complex I is vital to support aspartate biosynthesis, which is required for both protein and nucleotide synthesis (Birsoy, 2015; Sullivan, 2015). Consistently, supplementing respiration-deficient cells with the exogenous electron acceptor α-ketobutyrate, which regenerates NAD+ through dehydrogenase reactions akin to pyruvate, supports aspartate production in cancer cells to enable proliferation. Thus, the regeneration of NAD+ by complex I is a major biosynthetic function of mitochondria (further discussed in "Redox Requirements for Biomass Synthesis").

Succinate dehydrogenase (SDH) is a TCA cycle enzyme and also serves as complex II of the ETC. SDH oxidizes succinate to fumarate and requires flavin adenine dinucleotide (FAD) as a cofactor, producing $FADH_2$ which donates electrons to CoQ in the ETC. By converting succinate into fumarate, SDH maintains the biosynthetic functions of the TCA cycle such as amino acid and citrate synthesis. Interestingly, certain cancers possess loss-of-function mutations in SDH, leading to hereditary pheochromocytoma and paraganglioma as well as renal carcinoma (Astuti, 2001; Baysal, 2000). This suggests that certain tumors can rewire their metabolism to support proliferation to compensate for loss of SDH activity. It was recently shown that SDH, like complex I, can support cancer proliferation through aspartate synthesis. Mutant SDH cells adapt to SDH loss by concurrently suppressing complex I activity, decreasing the cellular NAD+/NADH ratio and enabling other metabolic pathways to synthesize aspartate (Hart, 2023). Thus, mitochondrial respiration can be dynamically tuned to the biosynthetic needs of

proliferating cells, demonstrating its essential metabolic roles that go beyond ATP synthesis.

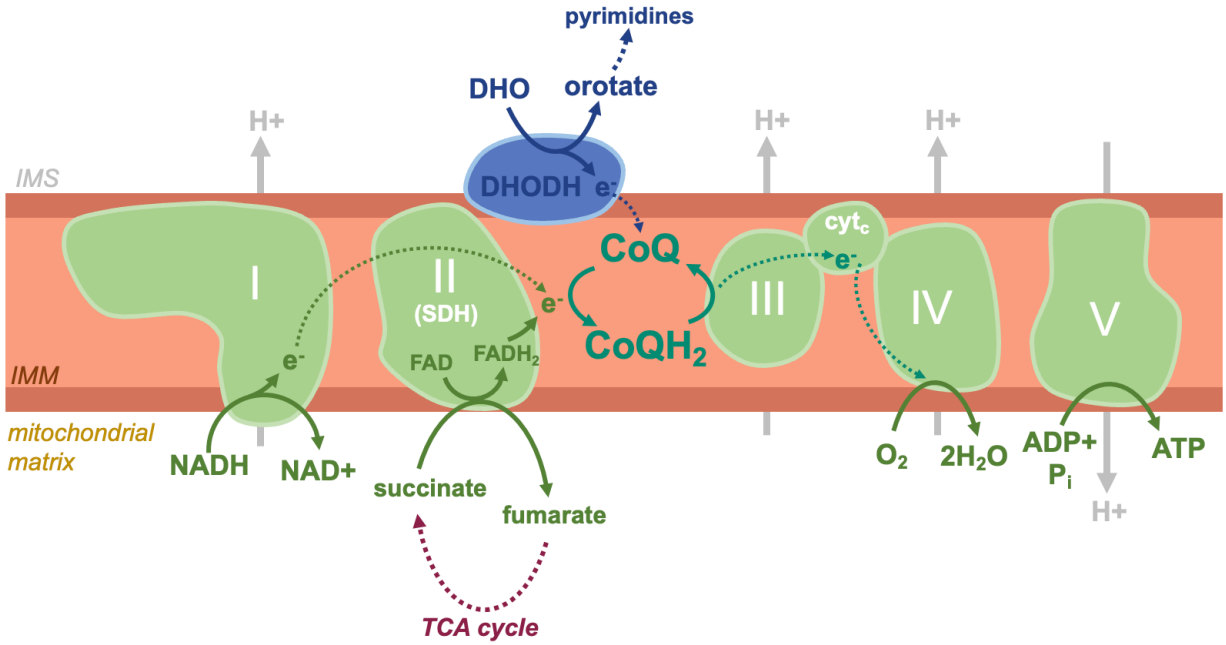

Figure 6. Mitochondrial respiration possesses numerous biosynthetic roles and is required for tumor formation. Electrons from reactions catalyzed by complex I, complex II, and DHODH reduce coenzyme Q. Complex III receives the electrons from coenzyme Q and transfers them to cytochrome c, which is oxidized by complex IV. Complex IV then reduces oxygen into water. As electrons flow down their energy gradient along the electron transport chain (ETC), protons are pumped by complexes I, III, and IV against their chemical gradient, generating a membrane potential across the inner mitochondrial membrane. This proton gradient is dissipated by ATP synthase, or complex V, to phosphorylate ADP into ATP. The ETC has many biosynthetic roles, including regenerating NAD+, which is required by many oxidative biosynthetic reactions, maintaining the TCA cycle, and supporting pyrimidine synthesis. Abbreviations: IMS, mitochondrial intermembrane space; IMM, inner mitochondrial membrane; DHO, dihydrooroate; DHODH, dihydroorotate dehydrogenase; SDH, succinate dehydrogenase; CoQ, coenzyme Q; $CoQH_2$, reduced coenzyme Q; cyt_c, cytochrome c

Cell-Intrinsic Metabolic Changes

Reprogrammed cellular metabolism is a hallmark of cancer (Hanahan, 2011). Many of the altered metabolic phenotypes are associated with activation of oncogenes and mutated tumor suppressor genes. Indeed, the signaling changes that lead to oncogenesis must be accompanied by metabolic changes that can successfully support

uncontrolled proliferation. Constitutive activation of KRAS leads to increased glucose uptake, glycolysis, and channeling of glucose carbons into the pentose phosphate pathway for ribose production (Ying, 2012). Oncogenic KRAS also alters glutamine metabolism by decreasing glutamate dehydrogenase-1 (GLUD1) activity and upregulating GOT1/2 expression (Son, 2013). Oncogenic c-myc increases lactate dehydrogenase A (LDH-A) expression and lactate production, which is required for c-myc mediated transformation (Shim, 1997). Hypoxia inducible factor (HIF) proteins are often overexpressed in numerous cancers and rewire metabolism (Wigerup, 2016). For example, HIF-1α can promote glycolysis by suppressing pyruvate oxidation in the mitochondria (Kim, 2006). In renal cell carcinoma, loss of von Hippel-Lindau (VHL), the E3 ubiquitin ligase that mediates the degradation of HIF-2α, causes HIF-mediated upregulation of tumor-promoting genes (Choueiri, 2020). The tumor suppressor LKB1 is deleted in several cancers and in Peutz-Jeghers syndrome, which encompasses the development of intestinal polyps and a higher cancer risk. LKB1 is a serine-threonine kinase that phosphorylates and activates AMP-activated protein kinase (AMPK), a master regulator of glucose and lipid metabolism in response to nutrient fluctuations and decreases in intracellular ATP. Together, LKB1 and AMPK ensure that cell growth is suppressed during energy stress, and loss of LKB1 causes dysregulated proliferation (Shackelford, 2009; Shaw, 2004).

Mutations in the TCA cycle enzymes SDH and fumarate hydratase (FH) lead to hereditary malignancies. Loss-of-function mutations in SDH subunits can cause familial paraganglioma, pheochromocytoma, and renal cell carcinoma (Astuti, 2001; Baysal, 2000; Vanharanta, 2004). Loss-of-function mutations in FH causes uterine fibroids, uterine

leiomyomata, and papillary renal cell cancer (Tomlinson, 2002). Additionally, mutations in isocitrate dehydrogenase-1 and 2 (IDH1/2) occur in several cancer types, including glioblastoma and acute myeloid leukemia (AML) (Losman, 2013). IDH mutations block the conversion of isocitrate to αKG. However, mutant IDH gains the ability to convert αKG to oncometabolite 2-hydroxyglutarate (2HG) (Dang, 2009). 2HG is a competitive inhibitor of αKG-dependent dioxygenases, including the prolyl hydroxylases that target HIF for degradation (Xu, 2011). Thus, the production of 2HG leads to HIF stabilization and HIF-mediated gene expression to promote oncogenesis.

Serine metabolism is often altered in cancer, where the enzymes in the *de novo* serine synthesis pathway are upregulated (Snell, 1984). In many cases, serine synthesis enzymes are upregulated downstream of oncogenic alterations. The transcription factor Nrf2, often dysregulated in lung cancers, induces the expression of PHGDH, PSAT1, and SHMT2 and elevates serine synthesis (DeNicola, 2015). Additionally, c-myc and HIF proteins can upregulate serine synthesis enzymes (Samanta, 2016; Sun, 2015). The presence of the tumor suppressor p53 supports cancer growth in serine and glycine depleted conditions. p53 wild-type cancer cells possess higher intracellular serine levels compared to p53-null cells, suggesting that p53 regulates serine synthesis (Maddocks, 2013). Certain tumor types, including melanoma and triple-negative breast cancer, possess gene copy number gains of PHGDH and elevated serine synthesis (Locasale, 2011; Possemato, 2011). Suppressing serine synthesis in tumors with high PHGDH levels decreases proliferation, demonstrating the importance of serine synthesis for select tumors to grow (DeNicola, 2015; Pacold, 2016; Possemato, 2011). The different

dependencies on PHGDH for tumor growth may be due to cell lineage, varying genetic alterations, and tissue location with different nutrient availabilities, in particular serine.

In sum, there are copious ways genetic mutations and gene expression changes can mediate metabolic rewiring that promote rapid proliferation and oncogenesis. Yet, genetic alterations and their corresponding expression changes are one of many variables that determine the metabolic dependencies of different cancers.

Metabolic Supply for Biomass Demands

The cancer metabolism field has highlighted the importance of cell-intrinsic factors such as enzyme expression in determining whether tumors can meet the biomass demands of proliferation. However, it has become more appreciated that cell-extrinsic factors play a major role in influencing the metabolic dependencies of tumors. Cancer cells can only meet their biomass demands if they are able to accumulate sufficient supplies required for biosynthesis. Metabolic supplies not only include the nutrients used to generate biomass, but are also influenced by the availability of redox cofactors and oxygen. The factors that affect the ability for cancer cells to obtain the metabolic supply for proliferation will be discussed in this section.

Nutrient Availability and Acquisition within the Tumor Microenvironment

Obtaining the nutrients needed for biomass production depends on the availability of these nutrients in the tumor microenvironment. This is an important experimental consideration when studying cancer metabolism. Indeed, changing the nutrient conditions in cell culture studies alters the metabolic pathways cancer cells depend on for growth and influences the success of therapeutics that target metabolism (Abbott, 2023a; Cantor,

2017; Gui, 2016; Muir, 2017; Sullivan, 2021). Culturing cells in media conditions that better reflect the nutrient availability in the tumor microenvironment will improve our understanding of different tumor metabolic dependencies and how to target metabolism in the appropriate settings.

While abundant nutrients are available in cell culture conditions, the levels of these nutrients are often hyper-physiological. For example, in many standard cell culture media such as Dulbecco's Modified Eagle Medium (DMEM), glucose levels are 25 mM while glucose is around 0.48 mM in healthy adult human plasma (Cantor, 2017). The concentration of the amino acid serine is 400 μM in DMEM while it is around 100 μM in human plasma (Cantor, 2017). Amino acids are largely in excess in standard culture conditions. In addition to sugars and amino acids, lipid composition and levels in culture differ from physiological settings, as cell culture media is often supplemented with 10% heat-inactivated fetal bovine serum (FBS) and loses the biological complexity of blood and tissue (Abbott, 2023a). Nucleosides such as cytidine and uridine, are absent in cell culture media while present in plasma, modifying the dependency on *de novo* nucleotide synthesis due to ability to salvage these nucleotide precursors from the environment (Diehl, 2022). As media formulations were produced to identify the minimal nutrients required to successfully grow cells in dishes, it is not surprising that the nutrient composition of culture media does not accurately mirror the nutrients available in the body (Eagle, 1955; Muir, 2018). In addition to nutrient levels, oxygen tension differs in culture settings compared to physiological settings. This contributes profound effects on the metabolic pathways performed by cells as oxygen is the most commonly used substrate in cellular biochemical reactions (Jain, 2020; Raymond, 2006). Cells grown in culture are

incubated at 21% oxygen, leading to an oxygen tension of ~140mmHg. However, oxygen tensions in the body are often lower, between 5 and 100mmHg (Ast, 2019). Additionally, diffusion of oxygen across media *in vitro* can limit the oxygen delivered to cells artificially (Krogh, 1919; Place, 2017).

Like tissues, tumors are supplied nutrients and oxygen from the vasculature. The importance of tumor vasculature for tumor growth is reflected in the success of anti-angiogenesis therapies, which stemmed from the finding that tumors relied on neovascularization for their growth (Folkman, 1963; 1971; Gimbrone, 1974). In order for tissues and tumors to access the nutrients available in the vasculature, the nutrients from the vasculature are transferred to interstitial spaces, generating an interstitial fluid that bathes cells (Wiig, 2012). Because the plasma nutrients must cross blood vessel walls, nutrients are inherently filtered, creating differences between the nutrients accessible to tumors in the interstitial fluid and the nutrients in plasma. Moreover, the interstitial fluid between healthy tissues and tumor-bearing tissues may differ due the differences in tumor vasculature, which are often tortuous and leaky with distinct blood vessel biology (Ruoslahti, 2002). Indeed, it was found that the tumor interstitial fluid (TIF) had lower glucose and higher lactate levels compared to normal interstitial fluid (NIF) (Burgess, 1962). The location in the body can also influence the composition of TIF. The tumor microenvironment is made up of many cells types, including stromal cells and immune cells. Thus, the tumor interstitial space is dynamic, with exchange not only between the tissue and vasculature but also between different cell types. This may be a reason why different tissue locations have distinct nutrient environments, as the cellular make-up of each tissue and the metabolic needs of these cell types vary. Indeed, TIF nutrient levels

differed between tumors with the same genotype placed in separate anatomical locations as well as between tumors with different tissue-of-origin but same genotype grafted in the same location (Sullivan, 2019a). Additionally, nutrient exchange and competition between tumor and stromal cells have been shown to impact tumor growth and resistance to chemotherapies (Dalin, 2019; Datta, 2022; Jeong, 2023). Whether tumor-specific or tissue-related factors have a larger impact on the nutrients availability in the tumor microenvironment is unclear. The finding that tumors with the same genotype but different tissue-of-origin in the same anatomical location have distinct TIF compositions argue that the tissue, not the oncogenic lesions, has a larger impact on nutrient availability. Consistently, it was recently found that the interstitial fluid of normal kidney tissues resembles that from matched kidneys with renal cell carcinoma (Abbott, 2023b).

Diet can also impact tumor nutrient availability, shape TIF contents, and influence tumor growth (Lien, 2019; 2021; Maddocks, 2017; Sullivan, 2019a). For example, caloric restriction can decrease circulating lipid levels to suppress tumor growth (Lien, 2021). Modifying dietary lipid composition can also impact tumor growth. In patients with pancreatic ductal adenocarcinoma (PDAC), consuming more plant based fats, which contain more unsaturated fatty acids, compared to animal based fats, is associated with increased survival (Lien, 2021). Lowering serine and glycine in the diet can reduce serum serine and glycine levels from 150 μM to 65 μM and reduce tumor growth (Maddocks, 2017; Sullivan, 2019b). Thus, modifying the diet can influence the nutrient composition of plasma, impacting metabolite accessibility in the tumor microenvironment.

Along with differences in tumor nutrient availability, successfully acquiring extracellular nutrients is vital for biomass synthesis. Cancer cells, unlike non-transformed

cells, demonstrate constitutive glucose, glutamine, and amino acid uptake downstream of oncogenic lesions (Pavlova, 2017). Certain cancers have developed strategies to efficiently scavenge nutrients to meet their biomass demands. For example, oncogenic Ras upregulates macropinocytosis, leading to the uptake of proteins that are liberated by lysosomes and supplying cells with free amino acids (Commisso, 2013). Many amino acid transporters function by exchange mechanisms. Thus, amino acid uptake largely depends on not only the availability of amino acids, both intracellularly and extracellularly, but also the amino acid composition of the nutrient environment. As an example, the amino acid asparagine can support and influence cancer cell proliferation by facilitating the uptake of other amino acids, including serine, arginine, and histidine (Krall, 2016). The solute carrier protein family (SLCs) facilitates the uptake of nutrients. Interestingly, the function of many SLC transporters are under characterized and have been studied in conditions that fail to reflect the tumor microenvironment. Examining the function of the SLC family across different physiological conditions will help identify the SLC transporters that contribute to tumor growth and the factors that influence their activity (Chidley, 2023).

Redox Requirements for Biomass Synthesis

Nutrient availability and acquisition heavily impact the biosynthetic capabilities of cells, as the ability to obtain sufficient nutrients, such as glucose and glutamine, enable the *de novo* synthesis of amino acids, lipids, and nucleotides to support proliferation. Yet, when nucleobases, lipids, and amino acids are present in the environment, they are readily acquired by cells, decreasing the need to synthesize these biomass precursors *de novo*. In certain cases, despite the ability to synthesize biomass precursors, cells still depend on their environmental uptake for proliferation (Diehl, 2019; Maddocks, 2013;

Sullivan, 2019b). However, in certain tumor nutrient environments, biomass precursors are depleted or unable to be acquired, requiring cancer cells to rely on *de novo* synthesis. For example, the mammary fat pad, cerebrospinal fluid, and brain interstitial fluid possess low serine levels that can limit tumor growth (Ngo, 2020; Sullivan, 2019b). Aspartate is poorly cell-permeable and cannot be acquired from tumors despite being present in the tumor nutrient environment (Sullivan, 2018). Specific low glycemic diets deplete environmental lipid availability (Lien, 2021). Many biomass precursors are more oxidized than the abundant nutrients that are available, such as glucose and glutamine. Consequently, for cells to produce oxidized biomass, sufficient electron acceptors must be available to enable the necessary oxidation reactions. Therefore, while the supply for nutrients that contribute carbon and nitrogen must be successfully obtained for biomass production, the supply of electron acceptors must also meet the biomass demands for successful proliferation.

Many oxidation-reduction reactions require the pyrimidine nucleotide cofactors nicotinamide adenine dinucleotide, NAD(H), and nicotinamide adenine dinucleotide phosphate NADP(H) or are transamination reactions (Hosios and Vander Heiden, 2018). NAD+ is a major redox cofactor that acts as an electron acceptor in oxidative biosynthetic reactions. Accumulating evidence has demonstrated that NAD+ availability can constrain the synthesis of biomass; when NAD+ availability is limited, cells are unable to generate sufficient biomass to divide (Bao, 2016; Birsoy, 2015; Diehl, 2019; Li, 2022; Sullivan, 2015). As mentioned previously, the synthesis of aspartate from glutamine heavily involves NAD+-requiring oxidation reactions in the oxidative direction of the TCA cycle. Likewise, while *de novo* lipid synthesis is generally viewed as a reductive process due to

its NADPH consumption, the synthesis of lipogenic acetyl-CoA involves many NAD+-requiring reactions, including both glucose oxidation and glutamine oxidation. Serine synthesis also increases NAD+ demand where the conversion of glucose to serine requires NAD+ at GADPH, one of the highest NAD+-utilizing reactions in proliferating cells (Shestov et al., 2014), and PHGDH (**Figure 7**).

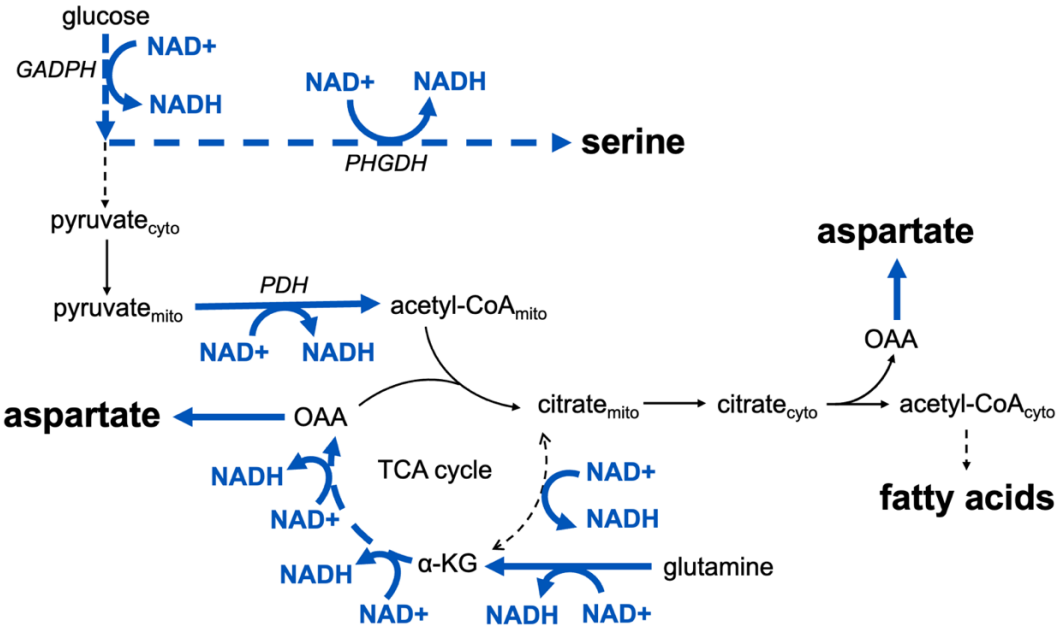

Figure 7. The NAD+ requirements for serine, aspartate, and fatty acid synthesis. Oxidation steps, including those that require NAD+ to act as an electron acceptor and transamination reactions are highlighted in blue. Abbreviations: GADPH, glyceraldehyde 3-phosphate dehydrogenase; PHGDH, phosphoglycerate dehydrogenase; PDH, pyruvate dehydrogenase; OAA, oxaloacetate; αKG, α-ketoglutarate; cyto, cytoplasmic; mito, mitochondrial

In environments where aspartate, lipids, and serine are unattainable, cells must maintain NAD+ availability to support the oxidation reactions that them. Indeed, suppressing NAD+ regeneration by complex I of the ETC ablates the ability for cells to produce aspartate, serine, and citrate for fatty acid synthesis. Cancer cells cultured without environmental serine and lipids are more sensitive to complex I inhibition because of the inability to perform *de novo* serine and fatty acid synthesis, and supplementation with exogenous electron acceptors restores the activity of these reactions and

proliferation in the nutrient depleted conditions (Diehl, 2019; Li, 2022; Sullivan, 2015). In addition to aspartate, serine, and lipids, synthesizing other non-essential amino acids and nucleotides also incur an NAD+-cost in cells. The NAD+ requirement for synthesizing these components *de novo* has been quantitatively modeled using flux balance analysis, revealing that *de novo* lipid synthesis, either through glucose oxidation or glutamine oxidation, has the largest calculated NAD+ requirement compared to other biosynthetic reactions (Li, 2022) (**Figure 8**).

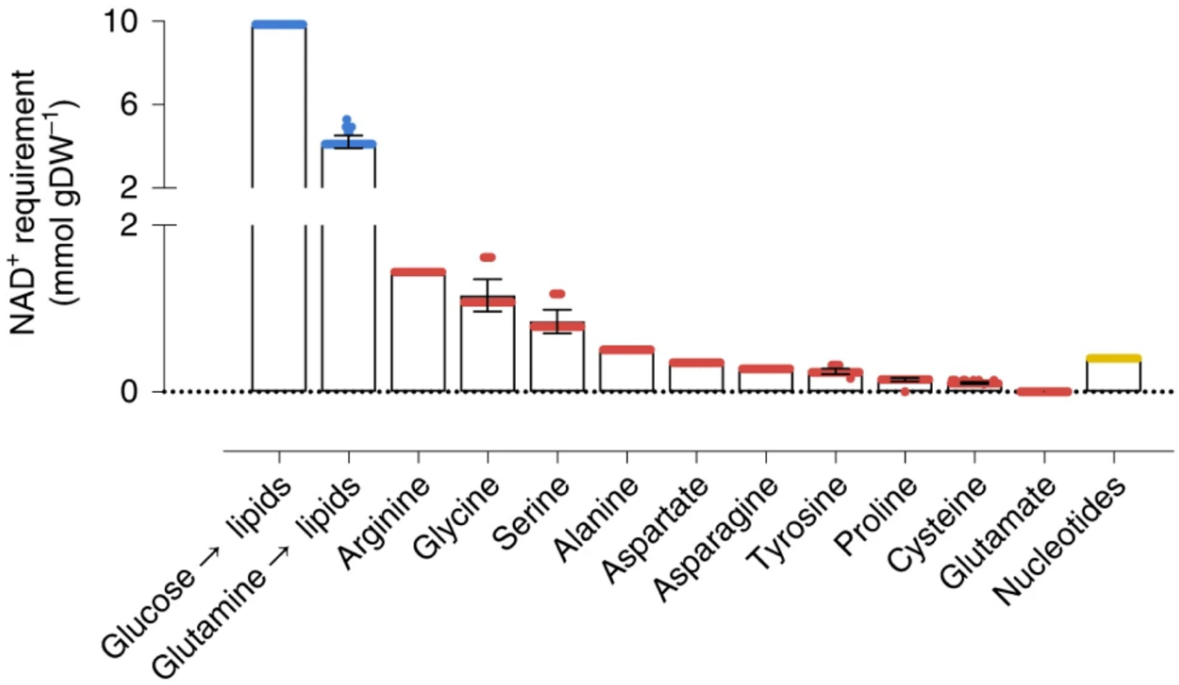

Figure 8. Quantitative model for the NAD+ consumption requirement of *de novo* biomass synthesis. From Li, 2022.

Together, these findings emphasize the importance of understanding the processes that allow cells to meet NAD+ demands and what controls NAD+ availability in environments where cells must rely on upregulating *de novo* biosynthesis to maintain proliferation. This may reveal new methods for targeting cancer cell proliferation in the nutrient environments and tissues that are most relevant.

Redox Homeostasis and Cellular Compartments

Biosynthetic reactions occur in different cellular compartments and require different redox cofactor pairs, namely NAD+/NADH and NADP+/NADPH. There are multiple factors that influence each redox cofactor pair, including the production and consumption of NAD(H) and NADP(H) that determine their absolute concentrations and the interconversion of the oxidized and reduced forms that establish the redox state (i.e., the NAD(P)+/NAD(P)H ratio) across different subcellular compartments. The maintenance of redox homeostasis across the cell is a heavily coordinated network that balances the processes that modulate the consumption, synthesis, and conversion within and between each redox pair.

The NAD+/NADH and NADP+/NADPH ratios generally play distinct biosynthetic functions. Because of the difference in redox potentials (-250mV for NAD+/NADH, -400mV for NADP+/NADPH) (Houtkooper, 2010), the NAD+/NADH redox pair generally drives oxidation reactions while the NADP+/NADPH redox pair drives reductive reactions. Intracellular levels of NAD(H) are significantly higher than NADP(H) (Pollak, 2007) and are highly compartmentalized. Mitochondrial NAD levels exceed cytoplasmic levels although this largely depends on the cell type (Stein, 2012). The absolute concentration of NAD(H) and NADP(H), like any metabolite, is determined by the rate of synthesis and rate of consumption or breakdown. NAD can be produced by *de novo* synthesis from tryptophan or salvaged from nicotinamide in humans (Bender, 1983; Collins, 1972). NADP is produced by the phosphorylation of NAD by NAD kinase (Pollak, 2007). Insufficient cellular levels of NAD(H) can impact the ability to perform certain oxidative biosynthetic reactions (Murphy, 2018), but in the context where oxidation of NADH into

NAD+ is blocked, supplementing cells with the NAD+ salvage precursor nicotinamide mononucleotide was unable to alter the cellular NAD+/NADH ratio or restore biomass synthesis (Diehl, 2019). This is because given a sufficient amount of total NAD, NAD+ and NADH rapidly exchange to maintain the NAD+/NADH ratio (Gui, 2016; Hart, 2023). Thus, while the absolute levels of NAD can have important impacts on the enzymes that consume NAD+, such as sirtuins and poly (ADP-ribose) polymerases (PARPs) (intracellular NAD(H) ranges from ~100-120 μM, roughly the K_m for NAD+-consuming enzymes), the redox state plays a larger role in influencing oxidative biosynthetic reactions (for example, the K_m of NAD+ is ~20μM for PHGDH, ~57μM for GADPH) (Phadke, 2015; Wang, 2023)

Generally, the amount of free NAD+ is much higher than NADH because more NADH is protein-bound, leading to cellular NAD+/NADH ratios that are greater than 1 in typical eukaryotic cells (Cambronne, 2020). In contrast, NADPH levels are significantly higher than NADP+ (Ying, 2008). It is generally believed that the mitochondrial membrane is impermeable to NAD, causing the NAD+/NADH ratio to be compartmentalized. In the cytoplasm, the NAD+/NADH ratio is roughly 700:1 while in the mitochondria, it is roughly 8:1 (Williamson, 1967). However, cytosolic NADH can be transferred to the mitochondria through the malate-aspartate shuttle (**Figure 9**) and the glycerol-3-phosphate shuttle (**Figure 10**). The predominant shuttle used to transport NADH into the mitochondria depends on the tissue. For example, the glycerol-3-phosphate shuttle is used in brown adipose tissue and skeletal muscle (Houštêk, 1975; Ohkawa, 1969) whereas the malate-aspartate shuttle is the dominant redox shuttle in the heart (Safer, 1971). In tumors, both shuttles are important for supporting proliferation, but the dependencies on each differ

between malignancies (Mráček, 2013; Sánchez-Jiménez, 1985). The malate-aspartate shuttle consists of cytosolic and mitochondrial malate dehydrogenase (MDH) and cytosolic and mitochondrial aspartate aminotransferase (GOT). NADH generated in the cytosol is used to reduce oxaloacetate into malate by MDH1, producing an NAD+ equivalent. Cytosolic malate is transported into the mitochondria through a dicarboxylate carrier, where it is converted back to oxaloacetate by MDH2, generating a mitochondrial NADH. The cycle is maintained by the conversion of oxaloacetate into aspartate by GOT2, which is transported to the cytosol by the aspartate-glutamate carrier, and cytosolic aspartate is converted to oxaloacetate by GOT1.

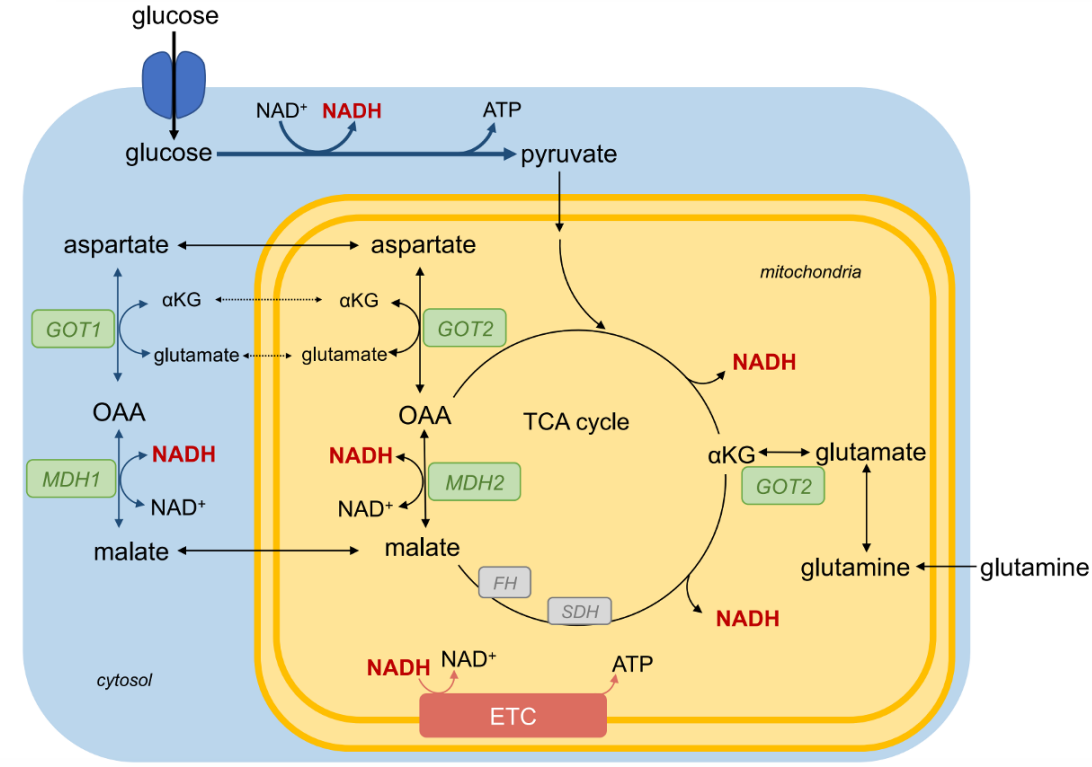

Figure 9. The malate-aspartate shuttle transfers NADH equivalents from the cytosol to the mitochondria. From (Chang, 2022). Abbreviations: αKG, α-ketoglutarate; GOT1/2, glutamic-oxaloacetic transaminase 1/2; SDH, succinate dehydrogenase; FH, fumarate hydratase; MDH1/2, malate dehydrogenase 1/2; OAA, oxaloacetate; ETC, electron transport chain

In the glycerol-3-phosphate shuttle, dihydroxyacetone phosphate (DHAP), which is produced during glycolysis, is reduced to glycerol-3-phosphate (G3P) by cytosolic glycerol-3-phosphate dehydrogenase (cG3PD), leading to the generation of NAD+. G3P is then oxidized back to DHAP by mitochondrial G3PD (mG3PD), which sits in the inner mitochondrial membrane. mG3PD uses FAD as an electron acceptor, generating $FADH_2$, which transfers its electrons to coenzyme Q in the mitochondrial electron transport chain, akin to succinate dehydrogenase.

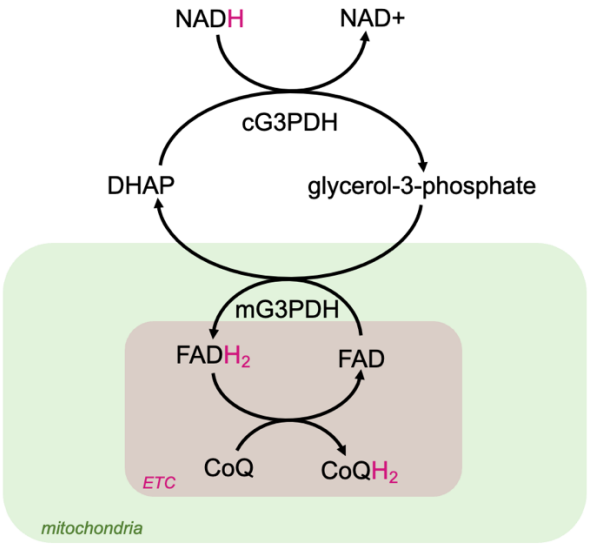

Figure 10. The glycerol-3-phosphate shuttle transfers NADH equivalents from the cytosol to the mitochondria. Abbreviations: DHAP, dihydroxyacetone phosphate; cG3PDH, cytosolic glycerol-3-phosphate dehydrogenase; mG3PDH, mitochondrial glycerol-3-phosphate dehydrogenase; CoQ(H_2), coenzyme Q; ETC, electron transport chain

It was recently shown that one driver of aerobic glycolysis is the saturation of the malate-aspartate shuttle and the glycerol-3-phosphate shuttle such that cytosolic NADH transfer to the mitochondria is maximized, leading to elevated lactate dehydrogenase activity, which allows for the re-oxidation of NADH back to NAD+ (Wang, 2022). This supports the finding that the demand for NAD+ is greater than the demand for ATP in rapidly

proliferating cells, and ATP synthase activity limits NAD+ regeneration due to hyperpolarization of the mitochondria (Luengo, 2021). The kinetics of mitochondrial respiration and the redox shuttles that drive mitochondrial respiration are limiting for the NAD+ requirement of proliferating cells, driving elevated NAD+ regeneration by lactate dehydrogenase. It was recently found that SLC25A1 functions as an NAD+ mitochondrial transporter and is important for regulating mitochondrial NAD(H) levels to influence TCA cycle activity and mitochondrial respiration (Kory, 2020; Luongo, 2020). Thus, there is much more to learn about the regulators of redox between compartments and the factors that regulate redox homeostasis.

How are cells able to maintain redox homeostasis across compartments in challenging environments? Given tumors rely on mitochondrial respiration for biomass production and proliferation, it remains unclear if and how tumors can support mitochondrial respiration and consequently oxidative biosynthetic reactions in hypoxic conditions. Indeed, culturing cells without lipids in hypoxic conditions is detrimental for cancer cell proliferation (Li, 2022). Interestingly, electron transport chain activity can be sustained in hypoxic conditions where in lieu of oxygen, fumarate can act as a terminal electron acceptor to maintain complex I and DHODH activity (Spinelli, 2021). Investigating the plasticity, regulators, and constraints of mitochondrial respiration will lead to significant progress in our understanding for how cancer cells maintain the redox requirements absolutely essential for biomass synthesis and proliferation. How these factors are altered in different tumor nutrient environments and in different cancer types will have important impacts on improving precision cancer therapies and suppressing metastasis.

Conclusion

Successful proliferation requires the coordinated balance between metabolic supply and demand, where the demand for biomass synthesis is significantly elevated in rapidly dividing cells like cancer. Whether cancer cells are able to supply the substrates required for biomass demands determines their proliferation. Many factors influence nutrient supply but can be broadly characterized into two categories: nutrient availability and nutrient acquisition. Nutrient availability is dependent on the anatomical location of the tumor, the tumor tissue-of-origin, exchange between tumor and stromal cells, degree of vascularization, and diet. Sufficient nutrient acquisition relies on the presence of required transporters and having the appropriate conditions to facilitate transport. In addition to nutrient availability, levels of oxygen and electron acceptors are crucial for meeting the biomass demands of cancer cells. The mitochondria plays a significant role in modulating the availability and dependencies on electron acceptor availability. However, the determinants of redox cofactor and electron acceptor availability is not well characterized, and further investigation will elucidate important processes that support cancer cell metabolism.

Cancer cells have evolved multiple mechanisms to adapt to metabolite supply challenges and have specific metabolic demands that distinguish cancer metabolism from the metabolism of non-transformed cells. One common adaptation to changes in nutrient availability is altering expression of biosynthetic enzymes and transporters. An additional adaptation is gaining diverse and opportunistic methods of mediating nutrient uptake. Moreover, metabolic pathway plasticity enables alternative routes of obtaining sufficient biomass when certain reactions are constrained. Some adaptations are cell-intrinsic and

downstream of oncogenic drivers or gene amplifications. Others are cell-extrinsic and occur in the immediate face of environmental obstacles. Understanding the adaptive metabolic constraints can be leveraged to generate imbalances between metabolic supply and demand and block tumor growth.

References

Abbott, K.L., Ali, A., Casalena, D., Do, B.T., Ferreira, R., Cheah, J.H., Soule, C.K., Deik, A., Kunchok, T., Schmidt, D.R., Renner, S., Honeder, S.E., Wu, W., Chan, S.H., Tseyang, T., Stoltzfus, A.T., Michel, S.L.J., Greaves, D., Hsu, P.P., Ng, C.W., Zhang, C.J., Farsidjani, A., Kent, J.R., Madariaga, M.L.L., Gramatikov, I.M.T., Matheson, N.J., Lewis, C.A., Clish, C.B., Rees, M.G., Roth, J.A., Griner, L.M., Muir, A., Auld, D.S., Vander Heiden, M.G. (2023a). Screening in serum-derived medium reveals differential response to compounds targeting metabolism. Cell Chemical Biology *30*, 1156-1168. https://doi.org/10.1016/j.chembiol.2023.08.007.

Abbott, K.L., Ali, A., Reinfeld, B.I., Deik, A., Subudhi, S., Landis, M.D., Hongo, R.A., Young, K.L., Kunchok, T., Nabel, C.S., Crowder, K.D., Kent, J.R., Madariaga, M.L.L., Jain, R.K., Beckermann, K.E., Lewis, C.A., Clish, C.B., Muir, A., Rathmell, K., Rathmell, J.C., Vander Heiden, M.G. (2023b). Metabolite profiling of human renal cell carcinoma reveals tissue-origin dominance in nutrient availability. bioRxiv *https://doi.org/10.1101/2023.12.24.573250*.

Ast, T., Mootha, V.K. (2019). Oxygen and mammalian cell culture: are we repeating the experiment of Dr. Ox? Nature Metabolism *1*, 858-860. https://doi.org/10.1038/s42255-019-0105-0.

Astuti, D., Latif, F., Dallol, A., Dahia, P.L.M., Douglas, F., George, E., Sköldberg, F.H., Husebye, E.S., Eng, C., Maher, E.R. (2001). Gene mutations in the succinate dehydrogenase subunit SDHB cause susceptibility to familial pheochromocytoma and to familial paraganglioma. American Journal of Human Genetics *69*, 49-54. 10.1086/321282

Bajzikova, M., Kovarova, J., Coelho, A.R., Boukalova, S., Oh, S., Rohlenova, K., Svec, D., Hubackova, S., Endaya, B., Judasova, K., Bezawork-Geleta, A., Kluckova, K., Chatre, L., Zobalova, R., Novakova, A., Vanova, K, Ezrova, Z., Maghzal, G.J., Novais, S.M., Olsinova, M., Krobova, L., Jin An, Y., Davidova, E., Nahacka, Z., Sobol, M., Cunha-Oliveira, T., Sandoval-Acuña, C., Strnad, H., Zhang, T., Huynh, T., Serafim, T.L., Hozak, P., Sardao, V.A., Koopman, W.J.H., Ricchetti, M., Oliveira, P.J., Kolar, F., Kubista, M., Truksa, J., Dvorakova-Hortova, K., Pacak, K., Gurlich, R., Stocker, R., Zhou, Y., Berridge, M.V., Park, S., Dong, L., Rohlena, J., Neuzil, J. (2019). Reactivation

of Dihydroorotate Dehydrogenase-Driven Pyrimidine Biosynthesis Restores Tumor Growth of Respiration-Deficient Cancer Cells. Cell Metabolism *29*, 399-416. 10.1016/j.cmet.2018.10.014.

Bao, X.R., Ong, S.-E., Goldberger, O., Peng, J., Sharma, R., Thompson, D. A., Vafai, S. B., Cox, A. G., Marutani, E., Ichinose, F., Goessling, W., Regev, A., Carr, S. A., Clish, C. B., & Mootha, V. K. (2016). Mitochondrial dysfunction remodels one-carbon metabolism in human cells. eLife *5*. https://doi.org/10.7554/elife.10575.

Basan, M., Hui, S., Okano, H., Zhang, Z., Shen, Y., Williamson, J.R., Hwa, T. (2015). Overflow metabolism in Escherichia coli results from efficient proteome allocation. nature *528*, 99-104.
Baysal, B.E., Ferrell, R.E., Willett-Brozick, J.E., Lawrence, E.C., Myssiorek, D., Bosch, A., van der Mey, A., Taschner, P.E., Rubinstein W.S., Myers, E.N., Richard, C.W., Cornelisse, C.J., Devilee, P., Devlin, B. (2000). Mutations in SDHD, a mitochondrial complex II gene, in hereditary paraganglioma. Science *287*, 848-851. 10.1126/science.287.5454.848.

Bender, D.A. (1983). Biochemistry of tryptophan in health and disease. Molecular Aspects of Medicine *6*. https://doi.org/10.1016/0098-2997(83)90005-5.

Birsoy, K., Wang, T., Chen, W.W., Freinkman, E., Abu-Remaileh, M., and Sabatini, D.M. (2015). An Essential Role of the Mitochondrial Electron Transport Chain in Cell Proliferation Is to Enable Aspartate Synthesis. Cell *162*, 540-551. https://doi.org/10.1016/j.cell.2015.07.016.

Bricker, D.K., Taylor, E.B., Schell, J.C., Orsak, T., Boutron, A., Chen, Y., Cox, J.E., Cardon, C.M., Van Vranken, J.G., Dephoure, N., Redin, C., Boudina, S., Gygi, S.P., Brivet, M., Thummel, C.S., Rutter, J. (2013). A Mitochondrial Pyruvate Carrier Required for Pyruvate Uptake in Yeast, Drosophila, and Humans. Science *337*, 96-100. 10.1126/science.1218099.

Burgess, E.A., Sylven, B. (1962). Glucose, lactate, and lactic dehydrogenase activity in normal interstitial fluid and that of solid mouse tumors. Cancer Research *22*, 581-588.
Burk, D. (1939). A colloquial consideration of the Pasteur and neo-Pasteur effects. Cold Spring Harbor Symposia on Quantitative Biology.

Cambronne, X.A., Kraus, W.L. (2020). Location, Location, Location: Compartmentalization of NAD+ Synthesis and Functions in Mammalian Cells. Trends in Biochemical Sciences *45*, 858-873.

Cantor, J.R., Abu-Remaileh, M., Kanarek, N., Freinkman, E., Gao, X., Louissaint, A., Lewis, C.A., Sabatini, D.M. (2017). Physiologic medium rewires cellular metabolism and reveals uric acid as an endogenous inhibitor of UMP synthase. Cell *169*, 258-272.e217. doi: 10.1016/j.cell.2017.03.023.

Chang, S.M., Vander Heiden, M.G. (2022). Inhibiting GLUTtony in cancer. Cell Chemical Biology *29*, 353-355. https://doi.org/10.1016/j.chembiol.2022.03.004.

Chidley, C., Darnell, A.M., Gaudio, B.L., Lien, E.C., Barbeau, A.M., Vander Heiden, M.G., Sorger, P.K. (2023). A CRISPRi/a screening platform to study cellular nutrient transport in diverse microenvironments. bioRxiv. https://doi.org/10.1101/2023.01.26.525375.

Choueiri, T.K., Kaelin, W.G. (2020). Targeting the HIF2–VEGF axis in renal cell carcinoma. Nature Medicine *26*, 1519-1530. https://doi.org/10.1038/s41591-020-1093-z.
Collins, P.B., Chaykin, S. (1972). The Management of Nicotinamide and Nicotinic Acid in the Mouse. Journal of Biological Chemistry *247*, 778-783. https://doi.org/10.1016/S0021-9258(19)45675-5.

Commisso, C., Davidson, S.M., Soydaner-Azeloglu, R.G., Parker, S.J., Kamphorst, J.J., Hackett, S., Grabocka, E., Nofal, M., Drebin, J.A., Thompson, C.B., Rabinowitz, J.D., Metallo, C.M., Vander Heiden, M.G., Bar-Sagi, D. (2013). Macropinocytosis of protein is an amino acid supply route in Ras-transformed cells. Nature *497*, 633-637. 10.1038/nature12138.

Cori, C.F., Cori, G.T. (1925). The carbohydrate metabolism of tumors: II. changes in the sugar, lactic acid, and CO2-combining power of blood passing through a tumor. Journal of Biological Chemistry *65*, 397-405.

Crabtree, H.G. (1929). Observations on the Carbohydrate Metabolism of Tumours. Biochemical Journal *23*, 536-545. 10.1042/bj0230536.

Dalin, S., Sullivan, M.R., Lau, A.N., Grauman-Boss, B., Mueller, H.S., Keridl, E., Fenoglio, S., Luengo, A., Lees, J.A., Vander Heiden, M.G., Lauffenburger, D.A., Hemann, M.T. (2019). Deoxycytidine Release from Pancreatic Stellate Cells Promotes Gemcitabine Resistance. Cancer Research *79*, 5723-5733. 10.1158/0008-5472.CAN-19-0960.

Dang, L., White, D.W., Gross, S., Bennett, B.D., Bittinger, M.A., Driggers, E.M., Fantin, V.R., Jang, H.G., Jin, S., Keenan, M.C., Marks, K.M., Prins, R.M., Ward, P.S., Yen, K.E., Liau, L.M., Rabinowitz, J.D., Cantley, L.C., Thompson, C.B., Vander Heiden, M.G., Su, S.M. (2009). Cancer-associated IDH1 mutations produce 2-hydroxyglutarate. Nature *462*, 739-744. 10.1038/nature08617.

Datta, R., Sivanand, S., Lau, A.N., Florek, L.V., Barbeau, A.M., Wyckoff, J., Skala, M.C., Vander Heiden, M.G. (2022). Interactions with stromal cells promote a more oxidized cancer cell redox state in pancreatic tumors. Science Advances *8*. 10.1126/sciadv.abg6383.

Deberardinis, R.J., Lum, J.J., Hatzivassiliou, G., Thompson, C.B. (2008). The Biology of Cancer: Metabolic Reprogramming Fuels Cell Growth and Proliferation. Cell Metabolism *7*, 11-20.

DeNicola, G.M., Chen P., Mullarky E., Sudderth, J.A., Hu, Z., Wu, D., Tang, H., Xie, Y., Asara J.M., Huffman, K.E., Wistuba, I.I., Minna, J.D., DeBerardinis, R.J., Cantley, L.C. (2015). NFR2 regulates serine biosynthesis in non-small cell lung cancer. Nature Genetics *47*, 1475-1481. 10.1038/ng.3421.

Diehl, F.F., Lewis, C.A., Fiske, B.P., Vander Heiden, M.G. (2019). Cellular redox state constrains serine synthesis and nucleotide production to impact cell proliferation. Nature Metabolism *1*, 861-867. doi:10.1038/s42255-019-0108-x.
Diehl, F.F., Miettinen, T.P., Elbashir, R., Nabel, C.S., Darnell, A.M., Do, B.T., Manalis, S.R., Lewis, C.A., Vander Heiden, M.G. (2022). Nucleotide imbalance decouples cell growth from cell proliferation. Nature Cell Biology *24*, 1252-1264. https://doi.org/10.1038/s41556-022-00965-1.

Eagle, H. (1955). Nutrient Needs of Mammalian Cells in Tissue Culture. Science *122*, 501-504. 10.1126/science.122.3168.50.

Folkman, J. (1971). Tumor Angiogenesis: Therapeutic Implications. New England Journal of Medicine *285*, 1182-1186. 10.1056/NEJM197111182852108.

Folkman, J., Long, D.M., Becker, F. (1963). Growth and metastasis of tumor in organ culture. Cancer *16*, 453-467. https://doi.org/10.1002/1097-0142(196304)16:4<453::AID-CNCR2820160407>3.0.CO;2-Y.

Gimbrone, M.A., Cotran, R.S., Leapman, S.B., Folkman, J. (1974). Tumor growth and neovascularization: an experimental model using the rabbit cornea. Journal of the National Cancer Institute *52*, 413-427. 10.1093/jnci/52.2.413.

Gui, D.Y., Sullivan, L.B., Luengo, A., Hosios, A.M., Bush, L.N., Gitego, N., Davidson, S.M., Freinkman, E., Thomas, C.J., Vander Heiden, M.G. (2016). Environment dictates dependence on mitochondrial complex I for NAD+ and aspartate production and determines cancer cell sensitivity to metformin. Cell Metabolism *24*, 716-727. 10.1016/j.cmet.2016.09.006.

Hanahan, D., Weinberg, R.A. (2011). Hallmarks of Cancer: The Next Generation. Cell *144*, 646–674. https://doi.org/10.1016/j.cell.2011.02.013.

Hart, M.L., Quon, E., Vigil, A.B.G., Engstrom, I.A., Newson, O.J., Davidsen, K., Hoellerbauer, P., Carlisle, S.M., Sullivan, L.B. (2023). Mitochondrial redox adaptations enable alternative aspartate synthesis in SDH-deficient cells eLIfe *12*. 10.7554/eLife.78654.

Hosios, A.M., Hecht, V.C., Danai, L.V., Johnson, M.O., Rathmell, J.C., Steinhauser, M.L., Manalis, S.R., Vander Heiden, M.G. (2016). Amino acids rather than glucose account for the majority of cell mass in proliferating mammalian cells. Developmental Cell *36*, 540-549. doi: 10.1016/j.devcel.2016.02.012.

Hosios, A.M., and Vander Heiden, M.G. (2018). The redox requirement of proliferation mammalian cells. Journal of Biological Chemistry *293*, 7490-7498. https://doi.org/10.1074/jbc.TM117.000239.

Houštêk, J., Cannon, B., Lindberg, O. (1975). Glycerol-3-Phosphate Shuttle and Its Function in Intermediary Metabolism of Hamster Brown-Adipose Tissue. European Journal of Biochemistry *54*, 11-18. https://doi.org/10.1111/j.1432-1033.1975.tb04107.x.
Houtkooper, R.H., Cantó C., Wanders, R.J., Auwerx, J. (2010). The Secret Life of NAD+: An Old Metabolite Controlling New Metabolic Signaling Pathways. Endocrine Reviews *31*, 194-223.

Jain, I.H., Calvo, S.E., Markhard, A.L., Skinner, O.S., To, T., Ast, T., Mootha, V.K. (2020). Genetic Screen for Cell Fitness in High or Low Oxygen Highlights Mitochondrial and Lipid Metabolism. Cell *181*, 716-727. 10.1016/j.cell.2020.03.029.

Jeong, Y., Rogers, T.J., Anderson, C.E., Lien, E. (2023). Tumor lipid metabolism: a mechanistic link between diet and cancer progression. Current Opinion in Biotechnology *84*. https://doi.org/10.1016/j.copbio.2023.102993.

Kim, J., Tchernyshyov, I., Semenza, G., Dang, C.V. (2006). HIF-1-mediated expression of pyruvate dehydrogenase kinase: A metabolic switch required for cellular adaptation to hypoxia. Cell Metabolism *3*, 177-185. 10.1016/j.cmet.2006.02.002.

King, M.P., Attardi, G. (1989). Human cells lacking mtDNA: repopulation with exogenous mitochondria by complementation Science *246*, 500-503. 10.1126/science.2814477.

Kory, N., Uit De Bos, J., Van Der Rijt, S., Jankovic, N., Güra, M., Arp, N., Pena, I.A., Prakash, G., Chan, S.H., Kunchok, T., Lewis, C.A., Sabatini, D.M. (2020). MCART1/SLC25A51 is required for mitochondrial NAD transport. Science Advances *6*. doi:10.1126/sciadv.abe5310.

Kory, N., Wyant, G.A., Prakash, G., uit de Bos, J., Bottanelli, F., Pacold, M.E., Ham Chan, S., Lewis, C.A., Wang, T., Keys, H.R., Guo, Y., Sabatini, D.M. (2018). SFXN1 is a mitochondrial serine transporter required for one-carbon metabolism. Science *362*. 10.1126/science.aat9528.

Krall, A.S., Xu, S., Graeber, T.G., Braas, D., Christofk, H.R. (2016). Asparagine promotes cancer cell proliferation through use as an amino acid exchange factor. Nature Communications *11457*. https://doi.org/10.1038/ncomms11457.

Krogh, A. (1919). The rate of diffusion of gases through animal tissues, with some remarks on the coefficient of invasion. The Journal of Physiology *52*, 391-408. 10.1113/jphysiol.1919.sp001838.

Kroll, W., Loffler, M., Schneider, F. (1983). Energy parameters, macromolecular synthesis and cell cycle progression of in vitro grown Ehrlich ascites tumor cells after inhibition of oxidative ATP synthesis by oligomycin Zeitschrift für Naturforschung C *38*, 604-612.

Lewis, C.A., Parker, S.J., Fiske, B.P., McCloskey, D., Gui, D.Y., Green, C.R., Vokes N.I., Feist, A.M., Vander Heiden, M.G., Metallo, C.M. (2014). Tracing Compartmentalized NADPH Metabolism in the Cytosol and Mitochondria of Mammalian Cells. Molecular Cell *55*, 253-263. https://doi.org/10.1016/j.molcel.2014.05.008.

Li, Z., Ji, B.W., Dixit, P.D., Lien, E.C., Tchourine, K., Hosios, A.M., Abbott, K.L., Westermark, A.M., Gorodetsky, E.F., Sullivan, L.B., Vander Heiden, M.G., Vitkup, D. (2022). Cancer cells depend on environmental lipids for proliferation when electron acceptors are limited. Nature Metabolism *4*, 711-723. https://doi.org/10.1038/s42255-022-00588-8.

Lien, E.C., Vander Heiden, M.G. (2019). A framework for examining how diet impacts tumour metabolism. Nature Reviews Cancer *19*, 651-661. https://doi.org/10.1038/s41568-019-0198-5.

Lien, E.C., Westermark, A.M., Zhang, Y., Yuan, C., Li, Z., Lau, A., Sapp, K.M., Wolpin, B.M., Vander Heiden, M.G. (2021). Low glycaemic diets alter lipid metabolism to influence tumour growth. Nature *599*, 302-307. 10.1038/s41586-021-04049-2.

Locasale, J.W., Grassian, A.R., Melman, T., Lyssiotis, C.A., Mattaini, K.R., Bass, A.J., Heffron, G., Metallo, C.M., Muranen, T., Sharfi, H., Sasaki, A.T., Anastasiou, D., Mullarky, E., Vokes, N.I., Sasaki, M., Beroukhim, R., Stephanopoulos, G., Ligon, A.H., Meyerson, M., Richardson, A.L., Chin, L., Wagner, G., Asara, J.M., Brugge, J.S., Cantley, L.C., Vander Heiden, M.G. (2011). Phosphoglycerate dehydrogenase diverts glycolytic flux and contributes to oncogenesis. Nature Genetics *43*, 869-874. 10.1038/ng.890.

Losman, J., Kaelin, W.G. (2013). What a difference a hydroxyl makes: mutant IDH, (R)-2-hydroxyglutarate, and cancer. Genes and Development *27*, 836-852. 10.1101/gad.217406.113.

Luengo, A., Gui, D.Y., and Vander Heiden, M.G. (2017). Targeting Metabolism for Cancer Therapy. Cell Chemical Biology *24* (*9*), 1161-1180. 10.1016/j.chembiol.2017.08.028.

Luengo, A., Li, Z., Gui, D.Y., Sullivan, L.B., Zagorulya, M., Do, B.T., Ferreira, R., and Naamati, A., Ali, A., Lewis, C. A., Thomas, C. J., Spranger, S., Matheson, N. J., &

Vander Heiden, M. G. (2021). Increased demand for NAD+ relative to ATP drives aerobic glycolysis. Molecular Cell *81*, 691–707. https://doi.org/10.1016/j.molcel.2020.12.012.

Luongo, T.S., Eller, J.M., Lu, M., Niere, M., Raith, F., Perry, C., Bornstein, M.R., Oliphint, P., Wang, L, McReynolds, M.R., Migaud, M.E., Rabinowitz, J.D., Johnson, F.B., Johnsson, K., Ziegler, M., Cambronne, X.A., Baur, J.A. (2020). SLC25A51 is a mammalian mitochondrial NAD+ transporter. Nature *588*, 174-179. https://doi.org/10.1038/s41586-020-2741-7.

Maddocks, O.D.K., Athineos, D., Cheung, E. C., Lee, P., Zhang, T., Van Den Broek, N. J. F., Mackay, G. M., Labuschagne, C. F., Gay, D., Kruiswijk, F., Blagih, J., Vincent, D. F., Campbell, K. J., Ceteci, F., Sansom, O. J., Blyth, K., & Vousden, K. H. (2017). Modulating the therapeutic response of tumours to dietary serine and glycine starvation. Nature *544*, 372–376. https://doi.org/10.1038/nature22056.

Maddocks, O.D.K., Berkers, C. R., Mason, S. M., Zheng, L., Blyth, K., Gottlieb, E., & Vousden, K. H. (2013). Serine starvation induces stress and p53-dependent metabolic remodelling in cancer cells. Nature *493* (*7433*), 542–546. https://doi.org/10.1038/nature11743.

Mráček, T., Brahota, Z., Houštek, J. (2013). The function and the role of the mitochondrial glycerol-3-phosphate dehydrogenase in mammalian tissues. Biochimica et Biophysica Acta *1827*, 401-410. https://doi.org/10.1016/j.bbabio.2012.11.014.

Muir, A., Danai, L.V., Gui, D.Y., Waingarten, C.Y., Lewis, C.A., Vander Heiden, M.G. (2017). Environmental cystine drives glutamine anaplerosis and sensitizes cancer cells to glutaminase inhibition. eLife *6*. https://doi.org/10.7554/eLife.27713.001.

Muir, A., Vander Heiden, M.G. (2018). The nutrient environment affects therapy. Science *360*, 962-963. 10.1126/science.aar5986.

Murphy, J.P., Giacomantonio, M. A., Paulo, J. A., Everley, R. A., Kennedy, B. E., Pathak, G. P., Clements, D. R., Kim, Y., Dai, C., Sharif, T., Gygi, S. P., & Gujar, S. (2018). The NAD+ Salvage Pathway Supports PHGDH-Driven Serine Biosynthesis. Cell Reports *24*, 2381–2391.e2385. https://doi.org/10.1016/j.celrep.2018.07.086.

Ngo, B., Kim, E., Osorio-Vasquez, V., Doll, S., Bustraan, S., Liang, R. J., Luengo, A., Davidson, S. M., Ali, A., Ferraro, G. B., Fischer, G. M., Eskandari, R., Kang, D. S., Ni, J., Plasger, A., Rajasekhar, V. K., Kastenhuber, E. R., Bacha, S., Sriram, R. K., … Pacold, M. E. (2020). Limited Environmental Serine and Glycine Confer Brain Metastasis Sensitivity to PHGDH Inhibition. Cancer Discovery *10*, 1352–1373. https://doi.org/10.1158/2159-8290.cd-19-1228.

Ohkawa, K., Vogt, M.T., Farber, E. (1969). Unusually high mitochondrial alpha glycerolphosphate dehydrogenase activity in rat brown adipose tissue. Journal of Cell Biology *41*, 441-449. https://doi.org/10.1083/jcb.41.2.441.

Pacold, M.E., Brimacombe, K.R., Chan, S.H., Rohde, J.M., Lewis, C.A., Swier, L., Possemato, R., Chen, W.W., Sullivan, L.B., Fiske, B.P., Cho, S., Freinkman, E., Birsoy, K., Abu-Remaileh, M., Shaul, Y.D., Liu, C.M., Zhou, M., Koh, M.J., Chung, H., Davidson, S.M., Luengo, A., Wang, A.Q., Xu, X., Yasgar, A., Liu, L., Rai, G., Westover, K.D., Vander Heiden, M.G., Shen, M., Gray, N.S., Boxer, M.B., Sabatini, D.M. (2016). A PHGDH inhibitor reveals coordination of serine synthesis and one-carbon unit fate. Nature Chemical Biology *12*, 452-458. 10.1038/nchembio.2070.
Pavlova, N.N., Thompson, C.B. (2017). The Emerging Hallmarks of Cancer Metabolism. Cell Metabolism *23*, 27-47. 10.1016/j.cmet.2015.12.006.

Pfeiffer, T., Schuster, S., and Bonhoeffer, S. (2001). Cooperation and Competition in the Evolution of ATP-Producing Pathways. Science *292*, 504-507. DOI: 10.1126/science.1058079.

Phadke, M., Krynetskaia, N., Mishra, A., Barrero, C., Merali, S., Gothe, S.A., Krynetskiy, E. (2015). Disruption of NAD+ binding site in glyceraldehyde 3-phosphate dehydrogenase affects its intranuclear interactions. World Journal of Biological Chemistry *6*, 366-378. 10.4331/wjbc.v6.i4.366.

Place, T.L., Domann, F.E., Case, A.J. (2017). Limitations of Oxygen Delivery to Cells in Culture: An
Underappreciated Problem in Basic and Translational Research. Free Radical Biology and Medicine *113*, 311-322. 10.1016/j.freeradbiomed.2017.10.003.

Pollak, N., Dölle, C., Ziegler, M. (2007). The power to reduce: pyridine nucleotides – small molecules with a multitude of functions. Biochemical Journal *402*, 205-218.

Possemato, R., Marks, K.M., Shaul, Y.D., Pacold, M.E., Kim, D., Birsoy, K., Sethumadhavan, S., Woo, H., Jang, H.G., Jha, A.K., Chen, W.W., Barrett, F.G., Stransky, N., Tsun, Z., Cowley, G.S., Barretina, J., Kalaany, N.Y., Hsu, P.P., Ottina, K., Chan, A.M., Yuan, B., Garrayway, L.A., Root, D.E., Mino-Kenudson, M., Brachtel, E.F., Driggers, E.M., Sabatini, D.M. (2011). Functional genomics reveals serine synthesis is essential in PHGDH-amplified breast cancer. Nature *476*, 346-350. 10.1038/nature10350.

Raymond, J., Segrè, D. (2006). The effect of oxygen on biochemical networks and the evolution of complex life. Science *311*, 1764-1767. 10.1126/science.1118439

Ruoslahti, E. (2002). Specialization of tumour vasculature. Nature Reviews Cancer *2*, 83-90. https://doi.org/10.1038/nrc724.

Safer, B., Smith, C.M., Williamson, J.R. (1971). Control of the transport of reducing equivalents across the mitochondrial membrane in perfused rat heart. Journal of Molecular and Cellular Cardiology *2*, 111-124. https://doi.org/10.1016/0022-2828(71)90065-4.

Samanta, D., Park, Y., Andrabi, S.A., Shelton, L.M., Gilkes, D.M., Semenza, G. (2016). PHGDH Expression Is Required for Mitochondrial Redox Homeostasis, Breast Cancer Stem Cell Maintenance, and Lung Metastasis. Cancer Research *76*, 4430-4442. 10.1158/0008-5472.CAN-16-0530.

Sánchez-Jiménez, F., Martínez, P., Núñez de Castro, I., Olavarría, J.S. (1985). The function of redox shuttles during aerobic glycolysis in two strains of Ehrlich ascites tumor cells. Biochimie *67*. 10.1016/s0300-9084(85)80055-9.

Shackelford, D.B., Shaw, R.J. (2009). The LKB1–AMPK pathway: metabolism and growth control in tumour suppression. Nature Reviews Cancer *9*, 563-575. https://doi.org/10.1038/nrc2676.

Shaw, R.J., Kosmatka, M., Bardeesy, N., Hurley, R.L., Witters, L.A., DePinho, R.A., Cantley, L.C. (2004). The tumor suppressor LKB1 kinase directly activatesAMP-activated kinase and regulates apoptosisin response to energy stress. PNAS *101*, 3329-3335. 10.1073pnas.0308061100.

Shestov, A.A., Liu, X., Ser, Z., Cluntun, A.A., Hung, Y.P., Huang, L., Kim, D., Le, A., Yellen, G., Albeck, J.G., and Locasale, J.W. (2014). Quantitative determinants of aerobic glycolysis identify flux through the enzyme GAPDH as a limiting step. eLife. 10.7554/eLife.03342.

Shim, H., Dolde, C., Lewis, B.C., Wu, C., Dang, G., Jungmann, R.A., Dalla-Favera, R., Dang, C.V. (1997). c-Myc transactivation of LDH-A: Implications for tumor metabolism and growth. PNAS *94*, 6658-6663. 10.1073/pnas.94.13.6658.

Snell, K. (1984). Enzymes of serine metabolism in normal, developing and neoplastic rat tissues. Advances in Enzyme Regulation *22*, 325-400. https://doi.org/10.1016/0065-2571(84)90021-9.

Son, J., Lyssiotis, C.A., Ying, H., Wang, X., Hua, S., Ligorio, M., Perera, R.M., Ferrone, C.R., Mullarky, E., Shyh-Chang, N., Kang, Y., Fleming, J.B., Bardeesy, N., Asara, J.M., Haigis, M.C., DePinho, R.A., Cantley, L.C., Kimmelman, A.C. (2013). Glutamine supports pancreatic cancer growth through a KRAS-regulated metabolic pathway. Nature *496*, 101-105. 10.1038/nature12040.

Spinelli, J.B., Rosen, P.C., Sprenger, H., Puszynska, A.M., Mann, J.L., Roessler, J.M., Cangelosi, A.L., Henne, A., Condon, K.J., Zhang, T., Kunchok, T., Lewis, C.A., Chandel, N.S., Sabatini, D.M. (2021). Fumarate is a terminal electron acceptor in

themammalian electron transport chain. Science *374*, 1227-1237. 10.1126/science.abi749.

Stein, L.R., Imai, S. (2012). The dynamic regulation of NAD metabolism in mitochondria. Trends in Endocrinology & Metabolism *23*, 420-428. 10.1016/j.tem.2012.06.005.

Sullivan, L.B., Gui, D.Y., Hosios, A.M., Bush, L.N., Freinkman, E., Vander Heiden M.G. (2015). Supporting Aspartate Biosynthesis Is an Essential Function of Respiration in Proliferation Cells. Cell *162*, 552-563. doi:10.1016/j.cell.2015.07.017.

Sullivan, L.B., Luengo, A., Danai, L.V., Bush, L.N., Diehl, F.F., Hosios, A.M., Lau, A.N., Elmiligy, S., Malstrom, S., Lewis, C.A., Vander Heiden, M.G., (2018). Aspartate is an endogenous metabolic limitation for tumour growth. . Nature Cell Biology *20*, 782-788. doi:10.1038/s41556-018-0125-0.

Sullivan, M.R., Danai, L. V., Lewis, C. A., Chan, S. H., Gui, D. Y., Kunchok, T., Dennstedt, E. A., Vander Heiden, M. G., Muir, A. (2019a). Quantification of microenvironmental metabolites in murine cancers reveals determinants of tumor nutrient availability. eLife *8*. https://doi.org/10.7554/elife.44235.

Sullivan, M.R., Darnell, A.M., Reilly, M.R., Kunchok, T., Joesch-Cohen, L., Rosenberg, D., Ali, A., Rees, M.G., Roth, J.A., Lewis, C.A., Vander Heiden, M.G. (2021). Methionine synthase is essential for cancer cell proliferation in physiological folate environments. Nature Metabolism *3*, 1500-1511. https://doi.org/10.1038/s42255-021-00486-5.

Sullivan, M.R., Mattaini, K.R., Dennstedt, E.A., Nguyen, A.A., Reilly, M.F., Meeth, K., Muir, A., Darnell, A.M., Bosenberg, M.W., Lewis, C.A., Vander Heiden, M.G. (2019b). Increased serine synthesis provides an advantage for tumors arising in tissues where serine levels are limiting. Cell Metabolism *29*, 1410-1421,e1414. doi: 10.1016/j.cmet.2019.02.015.

Sun, L., Song, L., Wan, Q., Wu, G., Li, X., Wang, Y., Wang, J., Liu, Z., Zhong, X., He, X., Shen, S., Pan, X., Li, A., Wang, Y., Gao, P., Tang, H., Zhang, H. (2015). cMyc-mediated activation of serine biosynthesis pathway is critical for cancer progression under nutrient deprivation conditions. Cell Research *25*, 429-444. https://doi.org/10.1038/cr.2015.33.

Tan, A.S., Baty, J.W., Dong, L, Bezawork-Geleta, A., Endaya, B. Goodwin, J., Bajzikova, M., Kovarova, J., Peterka, M., Yan, B., Pesdar, E.A., Sobol, M., Filimonenko, A., Stuart, S., Vondrusova, M., Kluckova, K., Sachaphibulkij, K., Rohlena, J., Hozak, P., Truksa, J., Eccles, D., Haupt, L.M., Griffiths, L.R., Neuzil, J., Berridge, M.V. (2015). Mitochondrial genome acquisition restores respiratory function and tumorienic potential of cancer cells without mitochondrial DNA. Cell Metabolism *21*, 81-94.

Tomlinson, I.P.M., Alam, N.A., Rowan, A.J., Barclay, E., Jaeger, E.E.M., Kelsell, D., Leigh, I., Gorman, P., Lamlum, H., Rahman, S., Roylance, R.R., Olpin, S., Bevan, S.,

Barker, K., Hearle, N., Houlston, R.S., Kiuru, M., Lehtonen, R., Karhu, A., Vilkki, S., Laiho, P., Eklund, C., Vierimaa, O., Aittomäki, K., Hietala, M., Sistonen, P., Paetau, A., Salovaara, R., Herva, R., Launonen, V., Aaltonen, L.A., Multiple Leiomyoma Consortium (2002). Germline mutations in FH predispose to dominantly inherited uterine fibroids, skin leiomyomata and papillary renal cell cancer. Nature Genetics *30*, 406-410. 10.1038/ng849.

Vander Heiden M.G., C., L.C., Thompson, C.B. (2009). Understanding the Warburg Effect: The Metabolic Requirements of Cell Proliferation. Science *324*, 1029-1033. 10.1126/science.1160809.

Vanharanta, S., Buchta, M., McWhinney, S.R., Virta, S.K., Peçzkowska, M., Morrison, C.D., Lehtonen, R., Januszewicz, A., Järvinen, H., Juhola, M., Mecklin, J., Pukkala, E., Herva, R., Kiuru, M., Nupponen, N.N., Aaltonen, L.A., Neumann, H.P.H, Eng, C. (2004). Early-Onset Renal Cell Carcinoma as a Novel Extraparaganglial Component of SDHB-Associated Heritable Paraganglioma. American Journal of Human Genetics *74*, 153-159. 10.1086/381054.

Wang, K., Luo, L., Fu, S., Wang, M., Wang, Z., Dong, L., Wu, X., Dai, L., Peng, Y., Shen, G., Chen, H., Nice, E.C., Wei, X., Huang, C. (2023). PHGDH arginine methylation by PRMT1 promotes serine synthesis and represents a therapeutic vulnerability in hepatocellular carcinoma. Nature Communications *14*. https://doi.org/10.1038/s41467-023-36708-5.

Wang, T., Marquardt, C., Foker, J. (1976). Aerobic glycolysis during lymphocyte proliferation. Nature *261*, 702-705.

Wang, Y., Stancliffe, E., Fowle-Grider, R., Wang, R., Wang, C., Schwaiger-Haber, M., Shriver, L.P., Patti, G.J. (2022). Saturation of the mitochondrial NADH shuttles drives aerobic glycolysis in proliferating cells. Molecular Cell *82*, 3270-3283. https://doi.org/10.1016/j.molcel.2022.07.007.

Warburg, O. (1923). Versuche an überlebendem Carcinomgewebe (Methoden). Biochem Zeitschr. *142*, 317-333.

Warburg, O. (1956). On respiratory impairment in cancer cells. Science *124*, 269-270.

Weinberg, F., Hamanaka, R., Wheaton, W.W., Weinberg, S., Joseph, J., Lopez, M., Kalyanaraman, B., Mutlu, G.M., Budinger, G.R., Chandel, N.S. (2010). Mitochondrial metabolism and ROS generation are essential for Kras-mediated tumorigenicity. PNAS *107*, 8788-8793.

Weinhouse, S. (1956). On Respiratory Impairment in Cancer Cells. Science *124*, 267-269.

Wheaton, W.W., Weinberg, S.E., Hamanaka R.B., Soberanes, S., Sullivan L.B., Anso E., Glasauer A., Dufour E., Mutlu G.M., Budigner, G.S., Chandel N.S. (2014). Metformin inhibits mitochondrial complex I of cancer cells to reduce tumorigenesis. eLife *3*.

Wigerup, C., Påhlman, S., Bexell, D. (2016). Therapeutic targeting of hypoxia and hypoxia-inducible factors in cancer. Pharmacology & Therapeutics *164*, 152-169. 10.1016/j.pharmthera.2016.04.009.

Wiig, H., Swartz, M.A. (2012). Interstitial Fluid and Lymph Formation and Transport: Physiological Regulation and Roles in Inflammation and Cancer. Physiological Reviews *92*, 1005-1060. https://doi.org/10.1152/physrev.00037.2011.
Williamson, D.H., Lund, P., Krebs, H.A. (1967). The Redox State of Free Nicotinamide-Adenine Dinucleotide in the Cytoplasm and Mitochondria of Rat Liver. Biochemical Journal *103*, 514-527.

Xu, W., Yang, H., Liu, Y., Yang, Y., Wang, P., Kim S., Ito, S., Yang, C., Wang, P., Xiao, M., Liu, L., Jiang, W., Liu, J., Zhang, J., Wang, B., Frye, S., Zhang, Y., Xu, Y., Lei, Q., Guan, K., Zhao, S., Xiong, Y. (2011). Oncometabolite 2-Hydroxyglutarate Is a Competitive Inhibitor of α-Ketoglutarate-Dependent Dioxygenases. Cancer Cell *19*, 17-30. 10.1016/j.ccr.2010.12.014.

Yang, M., Vousden, K.H. (2016). Serine and one-carbon metabolism in cancer. Nature Reviews Cancer *16*, 651-662. 10.1038/nrc.2016.81.

Ying, H., Kimmelan, A.C., Lyssiotis, C.A., Hua, S., Chu G.C., Fletcher-Sanaikone, E., Locasale, J.W., Son, J., Zhang, H., Coloff, J.L., Yan, H., Wang, W., Chen, S., Viale, A., Zheng, H., Paik, J., Lim, C., Guimaraes, A.R., Martin, E.S., Chang, J., Hezel, A.F., Perry, S.R., Hu, J., Gan, B., Xiao, Y., Asara, J.M., Weissleder, R., Wang, Y.A., Chin, L., Cantley, L.C., DePinho, R.A. (2012). Oncogenic Kras Maintains Pancreatic Tumors through Regulation of Anabolic Glucose Metabolism. Cell *149*, 656-679. 10.1016/j.cell.2012.01.058.

Ying, W. (2008). NAD+/NADH and NADP+/NADPH in Cellular Functions andCell Death: Regulation and Biological Consequences. Antioxidants & Redox Signaling *10*, 179-206.

Chapter 2: Endogenous cellular redox state is regulated by mitochondrial respiration to facilitate serine synthesis in serine depleted environments

This chapter is under preparation for submission for publication.

Authors: Sarah M. Chang[1], Muhammad B. Munim[1], Sonia E. Trojan[1,2], Anya Shevzov-Zebrun[1], Keene L. Abbott[1], and Matthew G. Vander Heiden[1,3]

Affiliations:
[1]Koch Institute for Integrative Cancer Research and Department of Biology, Massachusetts Institute of Technology, Cambridge, MA, USA.
[2]Jagiellonian University Medical College, Faculty of Medicine, Chair of Medical Biochemistry, Krakow, Poland
[3]Dana-Farber Cancer Institute, Boston, MA, USA.

Author Contributions

Conceptualization: **SMC,** MGVH; Intellectual Discussion: **SMC**, MBM, MGVH; Proliferation rates: **SMC**, SET, ASZ; Kinetic Isotope Tracing: **SMC**, SET; Immunoblotting: **SMC**, SET; NAD+/NADH measurements: **SMC**, SET; Oxygen consumption: **SMC**; Overexpression constructs: KLA; Cell line generation: **SMC**; Writing: **SMC**; Editing: **SMC**, MBM, SET, ASZ, MGVH; Funding Acquisition: MGVH

Abstract

The cellular NAD+/NADH ratio can constrain biomass production and influence proliferation. However, what determines the NAD+/NADH ratio in different nutrient environments and whether differences in endogenous NAD+/NADH ratio across cancers influence biosynthesis capacities is unknown. In this study, we find that a subset of cancer cells increase the NAD+/NADH ratio following serine deprivation due to elevated mitochondrial respiration. Increasing mitochondrial respiration, through uncoupling the mitochondrial electron transport chain from ATP synthesis or increasing the cellular NAD+ demand by removing environmental lipids, is sufficient to raise the NAD+/NADH ratio. This leads to greater serine synthesis to enable proliferation in serine depleted conditions. Taken together, these data show that mitochondrial respiration increases following serine or lipid deprivation, with different responses among cancer cells. This impacts the endogenous NAD+/NADH ratio to influence oxidative biomass synthesis, suggesting that control of the NAD+/NADH ratio can have a major impact on what nutrient environments are compatible for cancer cell proliferation.

Introduction

Many cancer cells have altered metabolism compared to normal cells in part due to the elevated biosynthetic demands of rapid proliferation (Deberardinis, 2008; Faubert, 2020; Hanahan, 2011; Pavlova, 2017; Vander Heiden, 2017). One important biomass component is the non-essential amino acid serine, which plays multiple metabolic roles and acts as a precursor for a variety of molecules, including proteins, nucleic acids, and lipids. Serine generates the amino acids glycine and cysteine to produce glutathione and donates one carbon units to contribute to nucleotide synthesis, folate metabolism, and S-

adenosylmethionine (SAM) production for methylation reactions. Additionally, serine is used to generate phospholipid head groups and sphingolipid species. Thus, acquiring sufficient serine from the environment or *de novo* synthesis is crucial to support cancer proliferation. Serine metabolism is often altered in cancers, including the upregulation of serine synthesis pathway enzymes (Ducker, 2018; Newman, 2017; Yang, 2016). Phosphoglycerate dehydrogenase (PHGDH) catalyzes the first step of the serine synthesis pathway and is upregulated downstream of tumor-promoting elements including Nrf2 (DeNicola, 2015), c-Myc (Sun, 2015), and Kras (Maddocks, 2017). Many cancers, notably melanoma and triple negative breast cancer, exhibit gene copy number gains of PHGDH (Locasale, 2011; Possemato, 2011). Increased PHGDH protein is associated with higher serine synthesis and improved proliferation in environments where serine is depleted, such as the breast (Sullivan, 2019b) and brain microenvironments (Ngo, 2020). However, despite elevating serine synthesis, tumor growth can still be limited by low environmental serine, and greater serine availability is required for maximal cancer proliferation (Labuschagne, 2014; Maddocks, 2013; 2017; Sullivan, 2019b). What constrains serine synthesis from fully supporting proliferation in low serine environments remains unclear. A better understanding of the determinants that regulate serine synthesis may improve targeting this pathway in the appropriate nutrient contexts and highlight how cancer cells adapt metabolism to thrive in new environments, including metastasis.

In addition to serine synthesis enzyme expression, serine synthesis can be constrained by the cellular redox state, which is reflected by the NAD+/NADH ratio (Baksh, 2020; Bao, 2016; Diehl, 2019). The synthesis of oxidized biomass precursors requires

regeneration of the redox cofactor NAD+ to act as an electron acceptor. There is accumulating evidence that NAD+ availability limits biomass production, including the synthesis of aspartate (Birsoy, 2015; Sullivan, 2015), asparagine (Krall, 2021), lipids (Li, 2022), serine (Baksh, 2020; Bao, 2016; Diehl, 2019), and nucleotides (Bao, 2016; Diehl, 2019). Serine synthesis from glucose involves two oxidation reactions that require NAD+: the glycolytic enzyme glyceraldehyde 3-phosphate dehydrogenase (GADPH) and PHGDH. Experimentally blunting NAD+ regeneration from NADH by blocking the mitochondrial electron transport chain ablates serine synthesis and increases cancer cell sensitivity to serine withdrawal (Bao, 2016; Diehl, 2019; Gravel, 2014). Serine synthesis and proliferation can be restored by supplementing cells with exogenous electron acceptors, demonstrating that serine synthesis can be impacted by external changes to electron acceptor availability (Diehl, 2019). However, whether the endogenous cellular redox state influences the magnitude of serine synthesis and proliferation rate in serine depleted conditions is not well understood. Additionally, whether cancer cells actively regulate the NAD+/NADH ratio to support elevated serine synthesis following serine withdrawal is unknown.

In this study, we investigated the contribution of the endogenous cellular redox state to serine synthesis, and more broadly, to oxidized biomass production. We uncover heterogeneity among how the cellular NAD+/NADH ratio responds to serine withdrawal across different cancers. Despite an increased demand for NAD+ to synthesize serine, certain cancers paradoxically increase the NAD+/NADH ratio through elevated mitochondrial respiration. This increase in mitochondrial respiration and NAD+/NADH ratio increases serine synthesis to confer a proliferative advantage over cancers that lack

this response and exhibit an unaltered NAD+/NADH ratio following serine withdrawal. Interestingly, the observed elevation of the NAD+/NADH ratio in some cells is specific to serine withdrawal and does not occur upon lipid depletion, a nutrient environment that raises oxidative citrate demand (Li, 2022). However, in cells with no redox response to serine withdrawal, lipid depletion can increase mitochondrial respiration to raise the cellular NAD+/NADH ratio. Surprisingly, this results in improved serine synthesis and proliferation in serine depleted conditions. Together, these findings illustrate that the endogenous cellular redox ratio is differentially responsive to environmental conditions across different cancers, impacting oxidative biomass production. This demonstrates that the NAD+/NADH ratio can determine what metabolic pathways are available to cells and influence the nutrient environments that are compatible with specific cancers.

Results

Modulating the cellular NAD+/NADH ratio proportionally alters serine synthesis

While previous studies have demonstrated that NAD+ availability can affect the ability to produce oxidized biomass, it remains unclear whether the NAD+/NADH ratio is related to the magnitude of serine synthesis flux. To test this, we varied the cellular NAD+/NADH ratio upon serine withdrawal and measured the serine synthesis rate in non-small cell lung cancer A549 cells, which exhibit transcriptional upregulation of PHGDH (DeNicola, 2015). We increased the NAD+/NADH ratio by treating cells with the exogenous electron acceptor alpha-ketobutyrate (AKB), which can be reduced to alpha-hydroxybutyrate to regenerate NAD+ via lactate dehydrogenase (Sullivan, 2015). We decreased the NAD+/NADH ratio by treating cells with rotenone, an inhibitor of complex I of the mitochondrial electron transport chain (ETC), which regenerates NAD+ (**Figure**

1A). AKB and rotenone dose-dependently increased and decreased the cellular NAD+/NADH ratio, respectively (**Figure 1B**). To measure serine synthesis rate in cells, we performed kinetic isotope tracing using uniformly ^{13}C-labeled glucose (U-^{13}C-glucose) to measure serine production over time via gas chromatography-mass spectrometry (GC-MS). Intracellular serine, including newly synthesized serine, rapidly exchanges with the extracellular environment (Labuschagne, 2014). Thus, measuring intracellular serine may under-represent the production of isotopically labeled serine. To mitigate this technical issue, we collected both media and cells to detect all newly synthesized serine produced from glucose (M+3 serine) at each time point (**Figure 1C**). We find that increasing the cellular NAD+/NADH ratio with AKB led to proportionally higher serine synthesis rates whereas lowering the cellular NAD+/NADH ratio with rotenone led to a dose-dependent decrease in serine synthesis rates (**Figure 1D**). These changes in serine synthesis occurred without altering PHGDH protein levels (**Supplementary Figure 1A,B**). When comparing the NAD+/NADH ratio with the corresponding serine synthesis rates following AKB or rotenone treatment, we find that serine synthesis is positively correlated with the cellular NAD+/NADH ratio (**Figure 1E**). Accordingly, increasing the NAD+/NADH ratio led to increased proliferation upon serine withdrawal, while decreasing the NAD+/NADH ratio led to decreased proliferation following serine withdrawal (**Figure 1F,G**), as previously observed (Diehl, 2019). Similarly, proliferation rate in response to serine depletion was also positively correlated with the NAD+/NADH ratio (**Supplementary Figure 1C**). Together, these data demonstrate that the cellular NAD+/NADH ratio correlates with serine synthesis flux following serine deprivation, and changing the NAD+/NADH ratio is

sufficient to proportionally modulate serine synthesis and the ability to proliferate in serine deprived conditions.

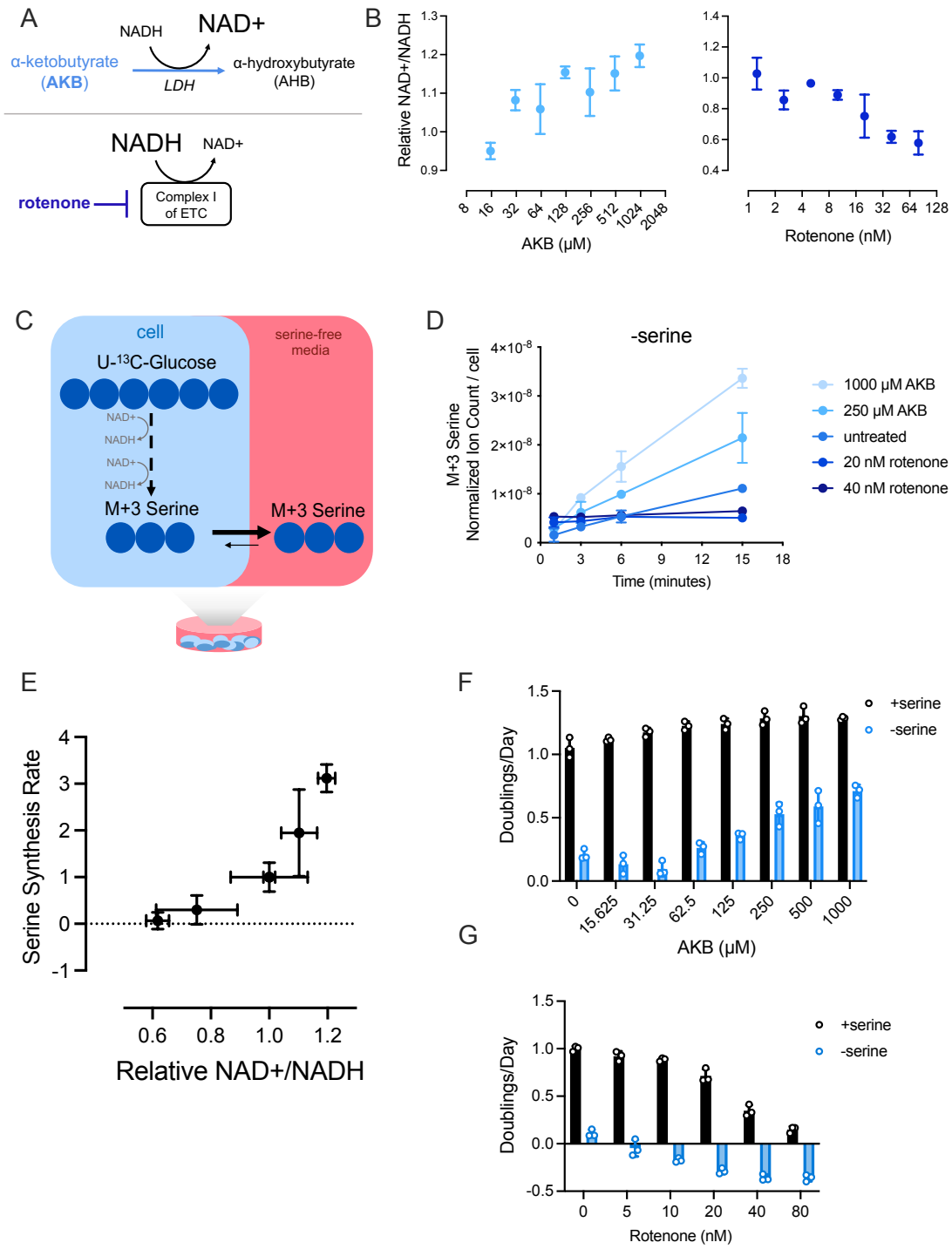

Figure 1. The NAD+/NADH ratio is directly proportional to serine synthesis rate. (A) α-ketobutyrate (AKB) is an exogenous electron acceptor that promotes the oxidation of NADH into

NAD+ through its conversion to α-hydroxybutyrate (AHB). Rotenone suppresses complex I of the mitochondrial electron transport chain (ETC) to block NADH oxidation into NAD+. **(B)** NAD+/NADH ratios relative to untreated conditions upon addition of increasing doses of AKB (left) and rotenone (right) under serine starvation, n=3. **(C)** U-^{13}C-glucose isotope tracing into serine (M+3), displaying the NAD+ requirement to convert glucose into serine. Under serine starvation, serine rapidly effluxes from cells into culture media. Thus, cells and media were analyzed at each time point of kinetic tracing to capture M+3 serine production. **(D)** Kinetic U-^{13}C-glucose tracing conducted in cells deprived of serine with indicated treatments for 24 hours prior to commencing tracing. Serine ion counts were normalized to internal standard norvaline and cell number, n=3. **(E)** Serine synthesis rate from kinetic U-^{13}C-glucose tracing in (D) was quantified and correlated with corresponding NAD+/NADH ratios in each condition. NAD+/NADH ratios were normalized to untreated values. **(F,G)** Proliferation rate of cells grown with and without serine with indicated concentrations of AKB (**F**) or rotenone (**G)** for 3 days, n=3. All experiments were conducted in A549 cells. All values are means ± SD.

Elevated NAD+/NADH ratio is associated with greater serine synthesis and ability to proliferate following serine withdrawal

Given that the NAD+/NADH ratio can correlate with serine synthesis rate, we next investigated whether differences in serine synthesis across cancer cells were related to the endogenous cellular NAD+/NADH ratio following serine withdrawal. We measured the proliferation rate of a panel of different cancer cells and found a wide range of sensitivity to serine deprivation (**Figure 2A**, **Supplementary Figure 2A, Supplementary Table 1**). Because PHGDH expression is closely associated with proliferation in serine low conditions, we first measured PHGDH protein expression to examine whether this could fully explain differences in environmental serine dependence. As expected, cells known to have low PHGDH protein expression (MCF7, MDA-MB-231) (Possemato, 2011) were most sensitive to serine withdrawal. In contrast, cells with very high PHGDH protein levels were more resistant to serine withdrawal (A375), and overexpressing PHGDH in MDA-MB-231 cells rescues proliferation when grown without serine, as previously observed (Possemato, 2011; Sullivan, 2019b) (**Supplementary Figure 2A-D**). However, despite the known relationship between PHGDH protein expression and proliferation in low serine conditions, some cells with higher PHGDH protein proliferated slower in serine depleted

conditions compared to cells with lower PHGDH protein (**Supplementary Figure 2A-D**). This was most notable when comparing A549 and H1299 cells. H1299 cells express less PHGDH protein compared to A549 cells despite exhibiting faster proliferation in serine depleted conditions (**Figure 2A, Supplementary Figure 2B-D**). To better characterize this differential response to serine withdrawal, we performed kinetic U-^{13}C-glucose isotope tracing in A549 and H1299 cells cultured with and without serine and confirmed that differences in serine synthesis corresponded with differences in proliferation (**Figure 2B**). We next hypothesized that endogenous cellular redox differences might contribute to the variability in sensitivity to serine withdrawal across cells with similar PHGDH protein levels (Calu6, A549, PaTu8988T, MIA PaCa-2, H1299, and HCT116) (**Supplementary Figure 2D**). To test this, we measured their cellular NAD+/NADH ratio in the presence and absence of exogenous serine and find that serine starvation led to an elevated NAD+/NADH ratio in some cells, while the NAD+/NADH ratio was minimally affected in others (**Figure 2C, Supplementary Figure 2E**). To test if the increase in the NAD+/NADH ratio was related to proliferation in serine depleted conditions, we compared the NAD+/NADH ratio with proliferation rate following serine withdrawal in these cells. Strikingly, cells with elevated cellular NAD+/NADH ratios following serine withdrawal collectively proliferated faster compared to cells with unchanged NAD+/NADH ratios when cultured in conditions without exogenous serine (**Figure 2D**). This relationship between NAD+/NADH ratio and proliferation following serine withdrawal was also observed in cancers where PHGDH protein expression could explain differences in sensitivity to serine withdrawal. A375 cells elevated the NAD+/NADH ratio while MCF7 and MDA-MB-231 cells did not significantly alter the NAD+/NADH ratio following serine

withdrawal (**Supplementary Figure 2F**). Taken together, these data argue that the endogenous cellular NAD+/NADH ratio responds to serine availability in a cell-dependent manner and correlates with proliferation in serine depleted environments.

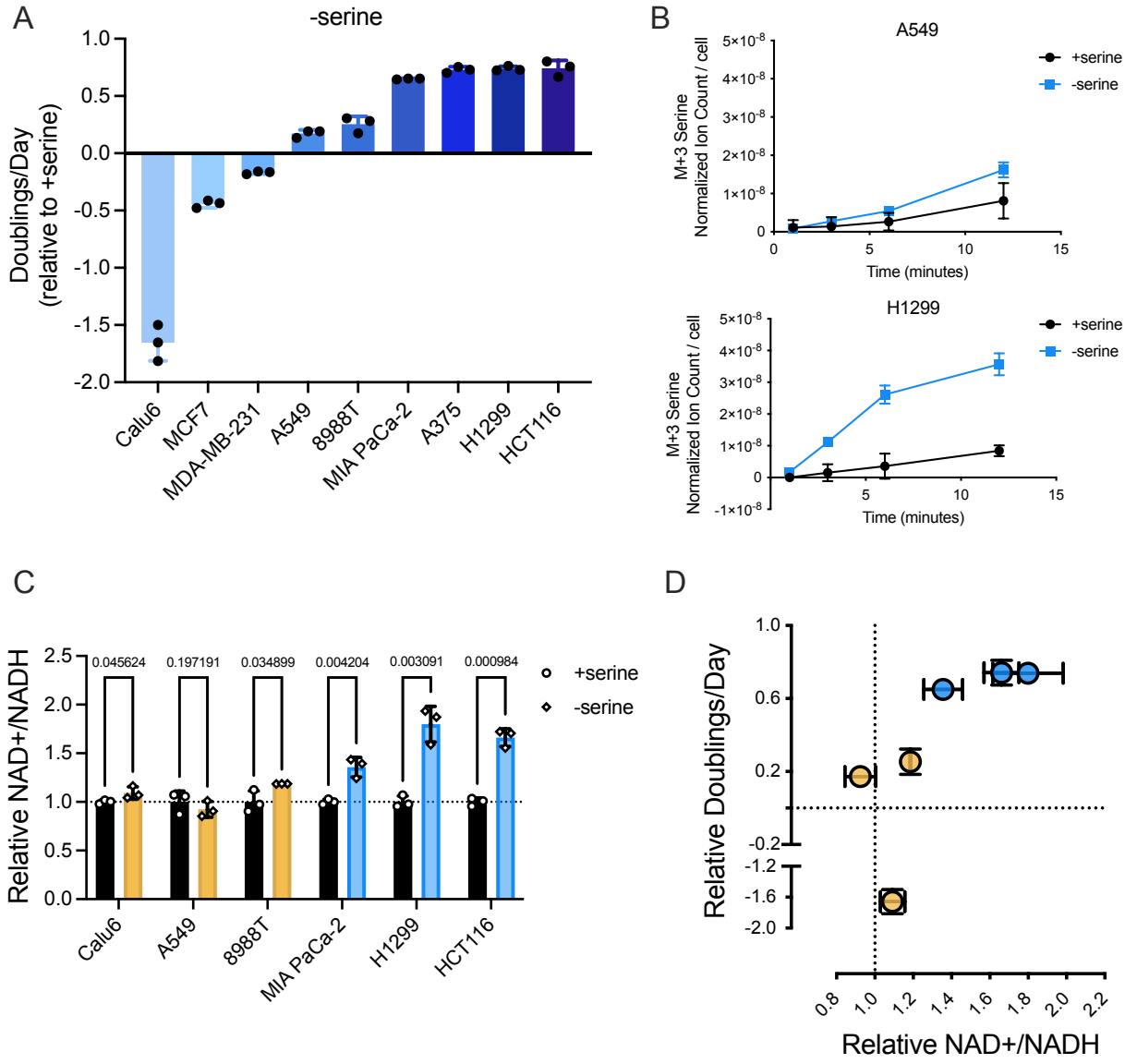

Figure 2. Changes in the endogenous NAD+/NADH ratio differ between cancer cells in response to serine withdrawal and correlate with proliferation in serine depleted conditions. (A) Proliferation rate (doublings per day) of indicated cancer cells grown with and without exogenous serine for three days, normalized to proliferation rate in serine-replete conditions per cell line, n=3. **(B)** Kinetic U-^{13}C-glucose isotope tracing into serine in cells starved of serine for 24 hours. Serine ion counts were normalized to internal standard norvaline and cell number, n=3. **(C)** NAD+/NADH ratios of indicated cells cultured with and without serine for 24 hours. Yellow indicates cells with unaltered NAD+/NADH ratios and blue indicates cells with elevated NAD+/NADH ratios following serine withdrawal. Values were normalized to NAD+/NADH

ratios measured in serine-replete conditions per cell line, n=3. **(D)** Correlation of NAD+/NADH ratios and proliferation rates for cells examined in (C) following serine withdrawal. Data points denote different cell lines. All values are means ± SD. P-values were calculated by unpaired Student's t-test.

Increased mitochondrial respiration is associated with an elevated NAD+/NADH ratio and greater serine synthesis

An elevated NAD+/NADH ratio upon serine starvation is unexpected because increased serine synthesis increases the demand for NAD+ to support GAPDH and PHGDH activity (Diehl, 2019; Maddocks, 2017). Thus, the NAD+/NADH ratio would be predicted to decrease due to higher consumption of NAD+ and elevated NADH production (**Supplementary Figure 3A**). The paradoxical elevation of the NAD+/NADH ratio suggested that cells must regulate NAD+ regeneration following serine withdrawal to facilitate serine synthesis. One cellular process that regenerates NAD+ from NADH is glucose fermentation into lactate via lactate dehydrogenase (LDH) (**Supplementary Figure 3B**). However, lactate secretion relative to glucose consumption was not elevated following serine deprivation across cells, consistent serine acting as an allosteric activator of pyruvate kinase M2 (PMK2) (Chaneton, 2012; Gao, 2018; Labuschagne, 2014; Maddocks, 2013) (**Supplementary Figure 3C**). Mitochondrial respiration is another major process that regenerates NAD+ from NADH via complex I. Thus, we hypothesized that higher cellular NAD+/NADH ratios might be linked to increased mitochondrial respiration. Indeed, cells with elevated NAD+/NADH ratios following serine deprivation exhibited higher mitochondrial respiration (**Figure 3A**). In contrast, cells with unaltered NAD+/NADH ratios following serine withdrawal did not elevate mitochondrial respiration (**Figure 3A**). To further explore the mitochondrial respiration response to serine deprivation, we cultured H1299 (redox responsive) and A549 (redox unresponsive) cells

in varying amounts of extracellular serine and measured mitochondrial respiration. H1299 cells displayed a dose-dependent decrease in mitochondrial respiration with increasing levels of extracellular serine levels up to 100 μM of serine, an extracellular serine concentration where proliferation is not further improved with increased serine availability (**Supplementary Figure 3D**), while A549 mitochondrial respiration was largely unresponsive to changes in extracellular serine levels (**Figure 3B**). Similarly, increasing environmental serine led to a dose-dependent decrease in the NAD+/NADH ratio in H1299 cells (**Figure 3C**). These changes corresponded with decreasing serine synthesis rates (**Supplementary Figure 3E**). In contrast, A549 cells maintained an unchanged NAD+/NADH ratio in response to increasing serine levels (**Figure 3E),** although they exhibited a decrease in serine synthesis rate with greater extracellular serine availability (**Figure 3F, Supplementary Figure 3F**). PHGDH protein levels did not change as extracellular serine levels were increased (**Supplementary Figure 3G**). The increase in mitochondrial respiration observed in H1299 cells as serine availability decreased from 100 to 0 μM serine positively correlated with changes in the NAD+/NADH ratio while no such relationship was observed in A549 cells (**Figure 3G,H**). Consistent with the findings that the NAD+/NADH ratio proportionally modulates serine synthesis, the NAD+/NADH ratio also positively correlated with serine synthesis rates in H1299 cells (**Figure 3G**). Together, these findings suggest that the rise in the NAD+/NADH ratio in response to decreasing serine availability in select cancers is linked to elevated mitochondrial respiration and serine synthesis rates.

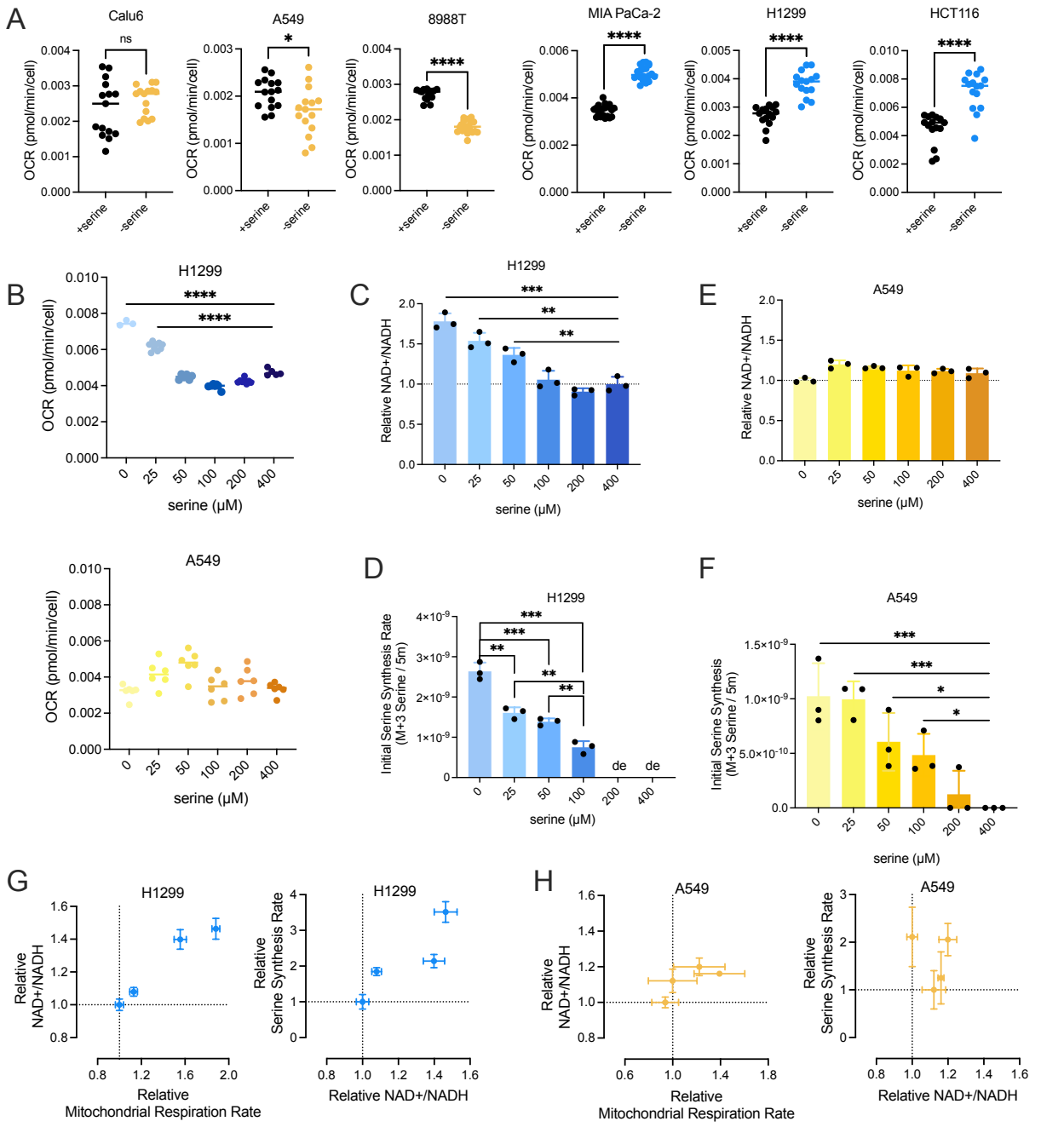

Figure 3. Elevated mitochondrial respiration is associated with increased NAD+/NADH ratios and serine synthesis rates. (A) Mitochondrial oxygen consumption rate (OCR) in cells cultured with and without serine for 24 hours, n=14-20. Values are averages across three repeat measurements, *p<0.05, ****p<0.0001, "ns" denotes not significant. **(B)** Mitochondrial OCR in cells (H1299 top, A549 bottom) cultured with indicated concentrations of serine for 24 hours, n=3-9, ****p<0.0001. **(C)** NAD+/NADH ratios of H1299 cells cultured with indicated concentrations of serine for 24 hours. Values are normalized to 400μM serine (serine concentration in DMEM), n=3. **(D)** Quantification of kinetic U-^{13}C-glucose tracing into serine in H1299 cells cultured with indicated concentrations of serine for 24 hours. Values are normalized ion counts of serine per cell produced between 1 and 6 minutes of tracing, "de" notes detection error, n=3, **p<0.01, ***p<0.005. **(E)** NAD+/NADH ratios of A549 cells cultured with indicated concentrations of serine

for 24 hours. Values are normalized to 400μM serine (serine concentration in DMEM), n=3. **(F)** Quantification of kinetic U-^{13}C-glucose tracing into serine in A549 cells cultured with indicated concentrations of serine for 24 hours. Values are normalized ion counts of serine per cell produced between 1 and 6 minutes of tracing, n=3, "ns" denotes not significant, *p<0.05, ***p<0.005. **(G,H)** Mitochondrial OCR plotted against NAD+/NADH ratios (left) and NAD+/NADH ratios plotted against serine synthesis rates (right) of H1299 (G) and A549 (H) cells cultured in 0, 25, 50, and 100 μM serine for 24 hours. Values are normalized to measurements from the 100 μM serine condition. All values are means ± SD. P-values were calculated by unpaired Student's t-test.

Mitochondrial respiration governs the endogenous cellular NAD+/NADH ratio and influences serine synthesis rate

We next wanted to determine whether changes in mitochondrial respiration following serine withdrawal directly affects the NAD+/NADH ratio and serine synthesis rate. To test this, we treated redox unresponsive cells (cells that do not elevate the NAD+/NADH ratio following serine withdrawal) with the proton ionophore FCCP (trifluoromethoxy carbonylcyanide phenylhydrazone). FCCP leads to the equilibration of the proton gradient generated by the mitochondrial electron transport chain (ETC) across the inner mitochondrial membrane and uncouples ETC activity from ATP synthase. Consequently, increased ETC activity can increase NAD+ regeneration and the cellular NAD+/NADH ratio (Luengo, 2021) (**Figure 4A**). We find that treating redox unresponsive cells with FCCP improved proliferation in serine depleted conditions in a dose-dependent manner as well as a small increase in proliferation in serine-replete conditions (**Figure 4B, Supplementary Figure 4A**). In contrast, FCCP did not alter the proliferation of redox responsive cells cultured without serine (**Figure 4B, Supplementary Figure 4B**). Improved proliferation following serine depletion in response to FCCP treatment was accompanied by higher serine synthesis rates (**Figure 4C, Supplementary Figure 5A-D**). As expected, uncoupling mitochondrial respiration from ATP synthase with FCCP led to elevated mitochondrial respiration in both redox responsive and unresponsive cells

(**Figure 4D, Supplementary Figure 4C**). However, FCCP only improved serine synthesis when it also elevated the cellular NAD+/NADH ratio (**Figure 4E, Supplementary Figure 4D**). The unchanged NAD+/NADH ratio yet increased mitochondrial respiration in select cancer cells after FCCP treatment could be due to saturation of complex I activity, and another constraint on serine synthesis limits proliferation in serine depleted environments. One possible constraint is PHGDH protein expression. Indeed, overexpressing PHGDH in redox responsive cells fully rescues proliferation, while simultaneous PHGDH overexpression and FCCP treatment had a greater improvement on proliferation of redox unresponsive cells following serine withdrawal (**Supplementary Figure 4E,F**). To confirm that FCCP increased serine synthesis and proliferation due to the elevated NAD+/NADH ratio that accompanies increased respiration, we treated cells with the complex I inhibitor rotenone in conjunction with FCCP. Rotenone treatment ablated the ability of FCCP to improve proliferation and serine synthesis and blocked the increase in the NAD+/NADH ratio (**Figure 4F-H, Supplementary Figure 5E,F**). In contrast, treating cells with oligomycin, an ATP synthase inhibitor, did not suppress the ability of FCCP to improve proliferation, supporting that the effect of FCCP is driven by the increased NAD+/NADH ratio induced by complex I (**Supplemental Figure 4G**). Moreover, FCCP treatment did not increase PHGDH protein expression or glucose consumption, indicating that improved proliferation and serine synthesis is not caused by changes in serine synthesis enzyme expression or carbon availability for serine synthesis (**Supplemental Figure 4H,I**). Together, these data argue that mitochondrial respiration can govern the endogenous cellular NAD+/NADH ratio and directly influence the serine synthesis rate in response to serine withdrawal.

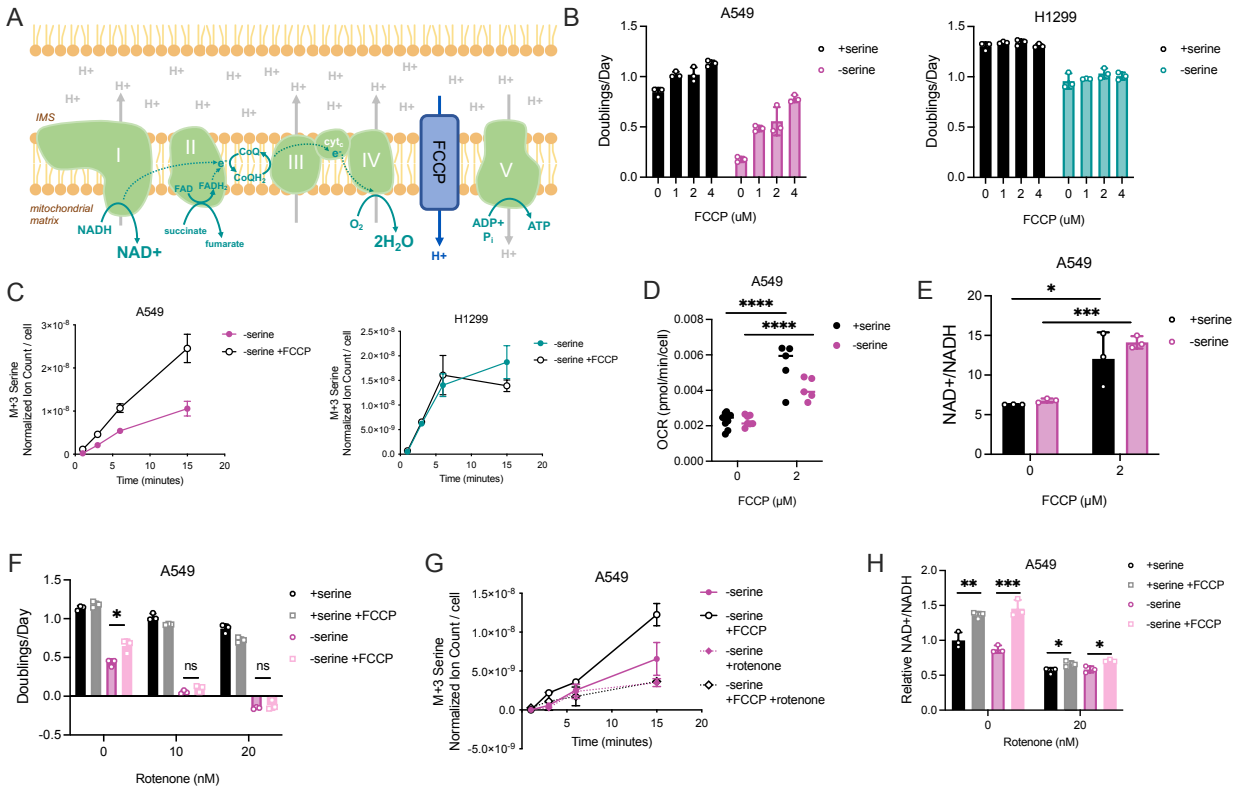

Figure 4. Mitochondrial respiration governs the endogenous cellular NAD+/NADH ratio and influences serine synthesis rate. (A) Schematic depicting the mitochondrial electron transport chain (ETC) and the protonophore activity of FCCP that uncouples the ETC from ATP synthase activity. CoQ(H_2) indicates the oxidized and reduced (H_2) forms of coenzyme Q, cyt_c denotes cytochrome c. **(B)** Proliferation rate (doublings per day) of cells cultured with and without serine with indicated concentrations of FCCP for three days, n=3. **(C)** Kinetic U-^{13}C-glucose tracing into serine (M+3) of cells cultured without serine, with and without 2 μM FCCP treatment for 24 hours, n=3. Total ion counts of serine were normalized to norvaline added as an internal standard and cell number. **(D)** Mitochondrial oxygen consumption rate (OCR) of cells cultured with and without serine with indicated FCCP treatment for 24 hours, n=5-9. Values are averages from three repeat measurements ****p<0.001. **(E)** NAD+/NADH ratio of cells treated with and without serine with indicated FCCP treatment for 24 hours, n=3, *p<0.05 ***p<0.005. **(F)** Proliferation rate (doublings per day) of cells treated with and without serine, FCCP (2 μM), and indicated concentrations of rotenone for three days, *p<0.05. **(G)** Kinetic U-^{13}C-glucose tracing into serine (M+3) of cells treated with and without serine, FCCP (2 μM), and rotenone (20 nM), n=3. Total ion counts of serine were normalized to norvaline added as an internal standard and cell number. **(H)** NAD+/NADH ratio of cells treated with and without serine, FCCP (2 μM), and rotenone (20 nM). NAD+/NADH values were normalized to the +serine condition, n=3, *p<0.05, **p<0.01, ***p<0.005. All values are means ± SD. P-values were calculated by unpaired Student's t-test.

Lipid depletion can increase mitochondrial respiration and improve proliferation in serine depleted conditions

Oxidative biosynthetic reactions other than serine synthesis can also be constrained by the NAD+/NADH ratio (Sullivan, 2015), including synthesis of citrate for lipid production (Li, 2022). We considered whether the ability to increase mitochondrial respiration in response to low extracellular serine was specific to serine withdrawal or a general response to increased NAD+ demand. Lipogenic citrate can be produced through glucose oxidation, which requires NAD+ for glycolysis and pyruvate dehydrogenase (PDH) activity. It can also be synthesized via glutamine oxidation, which requires NAD+ for tricarboxylic acid (TCA) cycle reactions (**Figure 5A**). Lipid deprivation can elevate mitochondrial respiration in some cells, and decreasing the NAD+/NADH ratio by inhibiting the mitochondrial electron transport chain suppresses lipogenic citrate synthesis via glucose and glutamine oxidation. Citrate synthesis can be restored by raising the NAD+/NADH ratio with exogenous electron acceptor supplementation (Li, 2022). To test whether increasing mitochondrial respiration is specific to serine withdrawal, we withdrew lipids from the extracellular environment by stripping the culture medium of all lipids (Hosios, 2018) and measured mitochondrial oxygen consumption rate (OCR). Interestingly, mitochondrial respiration increased following lipid withdrawal in A549 cells, which do not elevate mitochondrial respiration following serine depletion. In contrast, mitochondrial respiration did not significantly change following lipid depletion in H1299 cells, which do elevate mitochondrial respiration following serine withdrawal (**Figure 5B**). This suggests that the unchanged mitochondrial respiration upon serine starvation in A549 cells is not due to inherent electron transport chain dysfunction. Consistent with mitochondrial respiration governing the NAD+/NADH ratio, cells displaying elevated mitochondrial respiration upon lipid withdrawal exhibit increased NAD+/NADH ratios

compared to that observed in lipid-replete conditions (**Figure 5C**). We next asked if the elevated mitochondrial respiration following lipid withdrawal would be maintained upon serine depletion in cells that do not alter mitochondrial respiration after serine withdrawal alone. To test this, we withdrew both serine and lipids from the environment and measured mitochondrial respiration. Cells with unaltered mitochondrial respiration following serine withdrawal increased mitochondrial respiration following dual serine and lipid starvation (**Figure 5D**). In contrast, cells that elevated mitochondrial respiration after serine depletion but not lipid depletion maintained a similar mitochondrial respiration rate following concurrent serine and lipid withdrawal as serine withdrawal alone (**Figure 5D**). Changes in mitochondrial respiration corresponded to similar shifts in the NAD+/NADH ratio following simultaneous serine and lipid depletion (**Figure 5E**). Given that lipid deprivation raised mitochondrial respiration and the NAD+/NADH ratio in cells that did not exhibit these changes following serine deprivation, we asked if withdrawing exogenous lipids would increase the serine synthesis rate of serine deprived cells due to a higher NAD+/NADH ratio. To test this, we performed kinetic U-^{13}C-glucose tracing to measure serine synthesis in cells depleted of exogenous serine and lipids. Indeed, only cells that exhibited an increased NAD+/NADH ratio in lipid-depleted conditions had elevated serine synthesis following concurrent serine and lipid depletion compared to serine depletion alone (**Figure 5F, Supplementary Figure 6A-D**). This increase in serine synthesis corresponded with improved proliferation in serine and lipid depleted conditions (**Figure 5G**). Lastly, we examined whether FCCP treatment would additively improve proliferation of serine and lipid deprived cells or if the action of FCCP was functionally redundant to lipid or serine deprivation when they cause an increase in the NAD+/NADH ratio. We

predicted that if lipid withdrawal and FCCP treatment were redundant, the mechanism by which they increase NAD+/NADH ratio would be similar. While FCCP treatment improved the proliferation of serine depleted A549 cells, FCCP did not significantly improve the proliferation upon concurrent serine and lipid depletion (**Figure 5H**). As expected, FCCP did not alter the proliferation of serine depleted H1299 cells cultured with or without lipids (**Figure 5H**). Together, these findings show that mitochondrial respiration is differentially responsive to serine and lipid deprivation in a cell specific manner, and either uncoupling mitochondrial respiration from ATP synthase with FCCP or depriving nutrients that lead to increased mitochondrial respiration raises the NAD+/NADH ratio to support increased oxidative reactions, improving serine synthesis and proliferation in serine depleted environments.

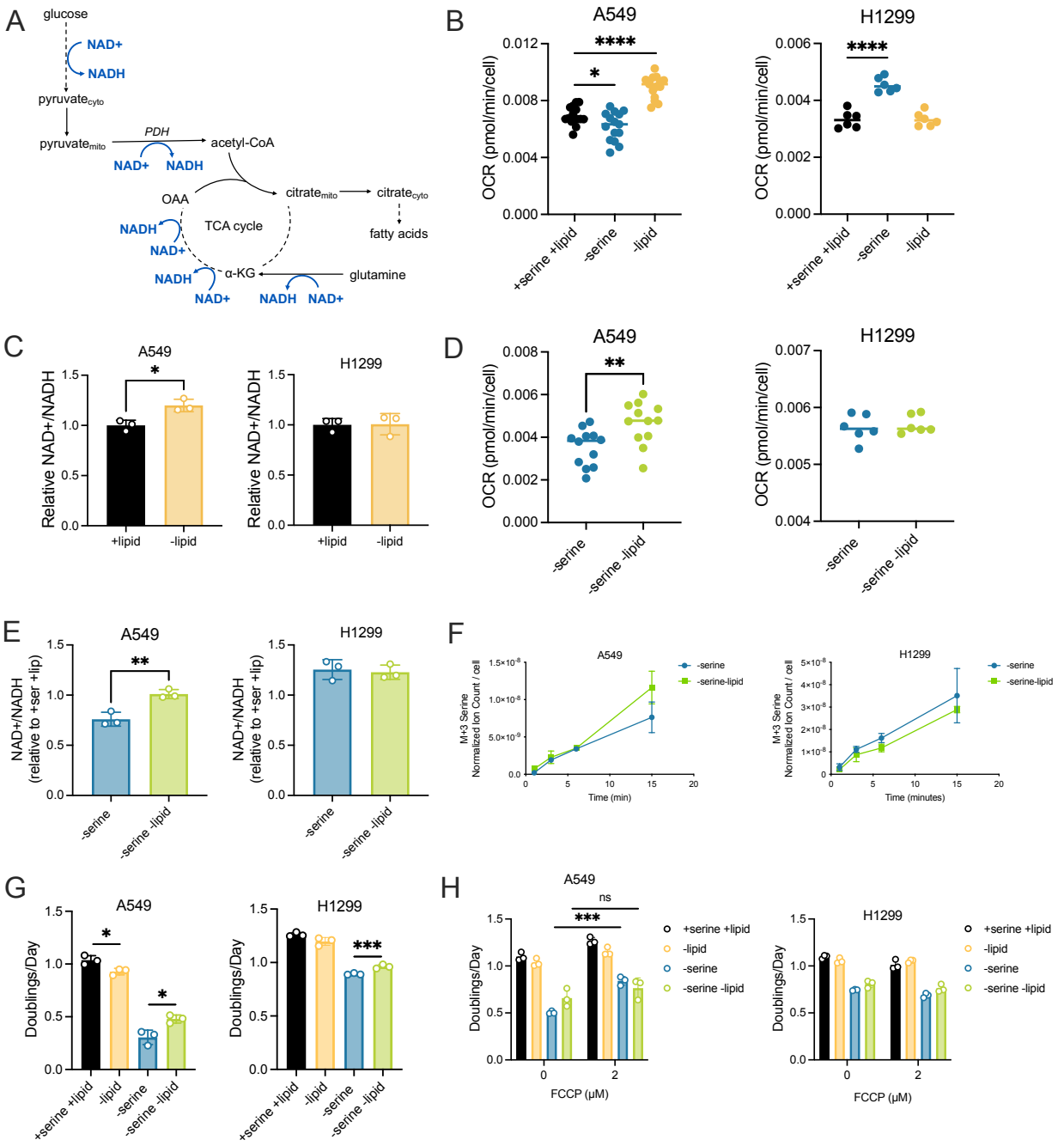

Figure 5. Lipid depletion raises mitochondrial respiration and the NAD+/NADH ratio in a cell specific manner to influence serine synthesis and proliferation in serine depleted conditions. (A) Schematic showing the NAD+ requirements for producing lipogenic citrate via glucose and glutamine oxidation. Abbreviations: PDH, pyruvate dehydrogenase; αKG, α-ketoglutarate; OAA, oxaloacetate. **(B)** Mitochondrial oxygen consumption rate (OCR) of A549 (left) or H1299 (right) cells grown in complete culture conditions or starved of either serine or lipids for 24 hours. Values are the average of three repeat measurements, n=6-15, *p<0.05, ****p<0.001. **(C)** NAD+/NADH ratios of A549 (left) or H1299 (right) cells grown with or without lipids for 24 hours. Values are normalized to the +lipid condition, n=3, *p<0.05. **(D)** Mitochondrial OCR of A549 (left) or H1299 (right) cells starved of serine and grown with or without lipids for 24 hours. Values

are the average of three repeat measurements, n=6-12, **p<0.01. **(E)** NAD+/NADH ratio of A549 (left) or H1299 (right) cells starved of serine and grown with or without lipids for 24 hours. Values are normalized to the +serine +lipid condition, n=3, **p<0.01. **(F)** Kinetic U-^{13}C-glucose tracing into serine (M+3) in A549 (left) or H1299 (right) cells starved of serine and grown with or without lipids for 24 hours. Serine ion counts are normalized to internal standard norvaline and cell number, n=3. **(G)** Proliferation rate (doublings per day) of A549 (left) or H1299 (right) cells grown with or without serine or lipids, as indicated, for three days, n=3, *p<0.05, ***p<0.005. **(H)** Proliferation rate (doublings per day) of A549 (left) or H1299 (right) cells grown with or without serine or lipids with 2 μM FCCP. All values are means ± SD. P-values were calculated by unpaired Student's t-test.

Discussion

Cancer cells require sufficient serine to build biomass for proliferation. Despite the ability to synthesize serine, serine synthesis capacity is limited, and uptake of extracellular serine may still be needed for maximal proliferation (Maddocks, 2017; Sullivan, 2019b). However, the tumor nutrient environment poses challenges, as extracellular serine availability can vary in different tissue locations, limiting tumor growth (Ngo, 2020; Sullivan, 2019b). In this study, we uncover that cellular redox state is a significant determinant of serine synthesis capacity and modulates cancer sensitivity to serine depleted environments independent of PHGDH expression. We reveal that mitochondrial respiration in a subset of cancers increases following serine deprivation and is sufficient to raise the NAD+/NADH ratio and govern serine synthesis rate. Interestingly, the control of the NAD+/NADH ratio by mitochondrial respiration is specific to not only the cancer, but also the nutrient demand, as lipid deprivation can also lead to elevated mitochondrial respiration, with different cancers responsive to lipid depletion and serine depletion.

Regardless of whether mitochondrial respiration was higher because of serine withdrawal, uncoupled mitochondrial respiration due to FCCP treatment, or lipid withdrawal, the increase in mitochondrial respiration was accompanied by an increase in the NAD+/NADH ratio, elevating serine synthesis in serine-depleted conditions. The

paradoxical improvement of proliferation upon simultaneous serine and lipid deprivation opposes the assumption that cancer cell proliferation is carbon limited in nutrient restricted environments. Rather, redox state is an important determinant of pathway activity if the required enzymes are expressed and can change in particular nutrient environments to shape dependencies on the uptake of multiple metabolites. This highlights the importance of considering different tumor nutrient environments, as a variety of metabolite levels have been measured in the extracellular environment of different tumors and normal tissues (Abbott, 2023a; Cantor, 2017; Ferraro, 2021; Muir, 2018; Ngo, 2020; Sullivan, 2019a). For example, cancer cells are less sensitive to serine and glycine deprivation in Plasmax, a physiological culture media that reflects metabolite levels found in human blood (Vande Voorde, 2019), due to the presence of hypoxanthine (Hennequart, 2021). Interestingly, Plasmax contains four-fold less fetal bovine serum (2.5%) than many standard culture medias (10% for DMEM) (Hennequart, 2021), which may modulate lipid availability and also contribute to this phenotype. One physiological environment that is deprived of both serine and lipids is the brain microenvironment, which can be a site of metastasis for many cancers (Ferraro, 2021; Jin, 2020; Ngo, 2020). While studies have focused on the role of enzyme expression in determining whether certain tumor cells can successfully synthesize serine and lipids to colonize the brain (e.g., PHGDH (Ngo, 2020), FASN (Ferraro, 2021), and SREBP (Jin, 2020)), our findings highlight the control of the NAD+/NADH ratio as an additional factor that governs the activity of serine synthesis, and potentially other pathways that produce oxidized biomass, influencing whether cancer cells can grow in different tissue environments.

We and many others find that mitochondrial respiration is a main regulator of the NAD+/NADH ratio (Birsoy, 2015; Luengo, 2021; Sullivan, 2015). What dictates whether certain cancers increase mitochondrial respiration in response to elevated oxidized biomass demands is unknown. Of the cancer types examined in this study, neither genetic driver lesions or tissue-of-origin can distinguish those that elevate mitochondrial respiration following serine withdrawal (See Supplementary Table 1). However, the ability of FCCP to improve proliferation of cells with unchanged mitochondrial respiration following serine withdrawal in serine replete conditions is intriguing. We have previously found that treating cells with gramicidin D, which permeabilizes cells to sodium and potassium and consequently increases ATP consumption by stimulating Na+/K+-ATPases, can elevate mitochondrial respiration and the NAD+/NADH ratio (Bertholet, 2019; Buttgereit, 1995; Luengo, 2021; Nobes, 1989; Vander Heiden, 1999). This suggests that ATP synthase insufficiency may restrain complex I activity to different extents across cancers, modulating the endogenous NAD+/NADH ratio and sensitivity to serine depletion. Interestingly, it was recently shown that FCCP induces proton leak through the ADP/ATP translocase, which transports ATP out of the mitochondria in exchange for ADP to promote ATP synthase activity (Bertholet, 2022). Additionally, lipid synthesis consumes a significant amount of ATP through the action of ATP citrate lyase, which uses ATP to produce each acetyl-CoA molecule to build fatty acids (Chypre, 2012). One unifying mechanism by which both lipid deprivation and FCCP could elevate complex I activity, and by consequence the NAD+/NADH ratio, is through modulating ATP consumption and would only impact cancers where ATP synthase limits complex I.

How serine deprivation leads some cancer cells to increase mitochondrial respiration is unknown. Because serine availability tunes mitochondrial respiration and the NAD+/NADH ratio in a dose-dependent manner, it is likely that serine availability modulates the levels of electron transport chain substrates or activators. The regulation of complex I activity is highly complex, influenced by substrate availability, function of other electron transport chain complexes (Hart, 2023), ATP synthase activity (Luengo, 2021), and structural and assembly alterations (Maranzana, 2013), among many others (Wirth, 2016), all of which can be independently regulated. What process downstream of serine deprivation leads to increased complex I activity and NAD+/NADH ratios requires further study. Nevertheless, these findings highlight the importance of complex I activity in determining the cellular NAD+/NADH ratio and consequently the activity of oxidative biosynthetic pathways to influence what nutrient environments permit cancer proliferation. Further examination of how different cancers modulate the NAD+/NADH ratio in response to nutrient environments and different tissue locations will reveal whether this allows select cancers to adapt to specific conditions. Better understanding of what processes to target and what cancers and conditions should be targeted will help generate more precise therapeutic treatments.

Acknowledgements

We thank Emma Dawson, Grace Wolczanski, and Alejandra Rosario-Crespo for technical assistance. We thank all members of the Vander Heiden lab for helpful discussions. This research was supported by the National Cancer Institute of the NIH under award number F30CA268633 (SMC) and award numbers R35CA242379, R01CA201276, and P30CA14051 (MGVH). MGVH also acknowledges support from a Faculty Scholar grant

from the Howard Hughes Medical Institute, SU2C, a division of the Entertainment Industry Foundation, the Lustgarten Foundation, the MIT Center for Precision Cancer Medicine, and the Ludwig Center at MIT.

Material and Methods

Cell Culture Experiments

Cell lines were maintained in Dulbecco's Modified Eagle's Medium (DMEM) without sodium pyruvate (Corning 50-013-PC) supplemented with sodium bicarbonate (Sigma S6014) and 10% heat-inactivated Fetal Bovine Serum (FBS). All cells were cultured at 37°C with 5% CO_2, tested for mycoplasma contamination regularly, and confirmed negative before experimentation. Cell line information is listed in Supplementary Table 1.

Proliferation Assays

Cells were plated in six-well plates in 2 ml of DMEM with 10% heat-inactivated FBS at an initial seeding density of 40,000 cells. Cells were permitted to settle overnight, and cells on a six-well dish were counted to calculate the starting cell number at the start of the experiment. For all remaining plates, cells were washed three times with 1ml of 1X PBS and 2 ml of treatment media was added to each well. All treatment media was made with 10% dialyzed FBS. Serine-free medium was made by adding a mix of amino acids (Sigma Aldrich) at DMEM concentrations lacking serine and glycine to DMEM with low glucose, without pyruvate, and amino acids (US Biological D9800-13-50L). Glucose and glycine were supplemented for a final concentration for 25 mM and 0.4 mM, respectively. Three days after the initial treatment, cells were quantified using a Cellometer (Nexcelom Bioscience) or cells were quantified using a sulforhdamine B (SRB) (Sigma Aldrich

230162) colorimetric assay. All SRB measurements are normalized to a blank. Proliferation rates were calculated with the following formula:

Doublings per day = log_2(final cell count / initial cell count) / (total # of treatment days)

NAD+/NADH Measurements

NAD+/NADH measurements were performed using the NAD/NADH-Glo Assay (Promega G9072) with a modified version of manufacturer instructions as previously reported (Sullivan, 2015). Cells were plated at an initial seeding density of 20,000 cells (A549, H1299, HCT116) or 40,000 cells (Calu6, MDA-MB-231). Cells were permitted to settle overnight. The next day, cells were washed once with 1X PBS and then incubated with 2 ml of treatment media for the indicated times prior to preparation of cell extracts. For extraction, cells were washed once in ice cold 1X PBS and extracted in 100 µl ice-cold 1% dodecyltrimethylammonium bromide (DTAB) in 0.2N NaOH diluted 1:1 with 1X PBS. Each sample was flash-frozen in liquid nitrogen and immediately stored at -80°C. To measure NADH, 10 µl of sample was moved to PCR tubes, diluted with 10 µl of DTAB, and incubated at 75 °C for 30 min, where basic conditions selectively degrade NAD+. To measure NAD+, 10 µl of the samples was moved to PCR tubes containing 30 µl DTAB and 20 µl 0.4 N HCl and incubated at 60°C for 15 min, where acidic conditions selectively degrade NADH. Samples were then allowed to equilibrate to room temperature and quenched by neutralizing with 20 µl 0.25 M Tris in 0.2 N HCl (for NADH) or 20 µl 0.5 M Tris base (for NAD+). Manufacturer instructions were followed thereafter to measure NAD+/NADH using a luminometer (Tecan Infinite M200Pro). A standard curve with representative samples was done with each assay to confirm that NAD+ and NADH measurements were in the linear range of detection.

Glucose Consumption and Lactate Secretion Measurements

Cells were plated at a density of 40,000 cells per well in a six well plate. The next day, cells were washed three times with 1X PBS before 2 ml of treatment media were added to each well. In parallel, 2 ml of treatment media were added to plates without cells. An initial cell number before beginning treatment was quantified (Cellometer). 72 hours later, media was collected from exponentially proliferating cells with a parallel collection of media from empty wells, which we used to measure initial media concentrations. Cell number was quantified (Cellometer) along with the volume of media on cells to consider evaporative changes to metabolite concentrations that may have occurred over 72 hours in culture. Glucose concentrations from media samples were measured on a YSI-2900 Biochemistry Analyzer (Yellow Spring Instruments). Every assay included a glucose (Sigma Aldrich G8270) standard curve (0, 2.5, 5, 10, 20, and 40 mM glucose in DMEM media) and lactate (Sigma Aldrich 71716) standard curve (0, 1.25, 2.5, 5, 10, and 20 mM sodium lactate in DMEM media). To calculate consumption rate per cell for a given nutrient, fmol of glucose or lactate over time were plotted relative to the area under the curve (fmol / cells · time) of an exponential function fit to the number of cells at the start of the assay and after 72 hours of treatment, as previously described (Hosios, 2016).

Oxygen Consumption Measurements

An Agilent Seahorse Bioscience Extracellular Flux Analyzer (XFe96) was used to measure oxygen consumption rates (OCR). Cells were plated at 20,000 – 40,000 cells per well in a Seahorse Bioscience 96-well plate in 80 µl of DMEM without pyruvate supplemented with 10% heat-inactivated FBS. Cells were not plated on the perimeter of the plate to avoid edge effect. The following day, cells were washed twice with 180 µl of

treatment media supplemented with 10% of dialyzed FBS before incubating cells with 180 µl of treatment media for the indicated time prior to OCR data acquisition. The day before OCR data acquisition, the XFe96 cartridge was hydrated by submerging the sensor cartridge in 200 µl of sterile water per well of the utility plate. Parafilm was wrapped around the perimeter of the cartridge to avoid evaporation. The XFe96 cartridge was then incubated in a 37°C non-CO_2 incubator overnight. The next day, at least two hours before data acquisition, the water in the utility plate was replaced with 200 µl of the Agilent XF Calibrant per well and the sensory cartridge was submerged and returned to the 37°C non-CO_2 incubator until OCR was ready to be measured. After OCR data acquisition, six to eight wells per treatment condition were collected for cell number quantification (Cellometer) to normalize OCR values. Basal OCR was calculated by subtracting residual OCR, the OCR remaining following the addition of rotenone and antimycin A (final concentration of 2 µM).

Kinetic U-^{13}C-Glucose Isotope Tracing Experiments

Cells were seeded at 150,000 cells per well in a six-well plate in 2ml of DMEM without pyruvate supplemented with 10% heat-inactivated FBS. The following day, cells were washed once with 1ml of 1X PBS and then incubated in 2ml of treatment media supplemented with 10% dialyzed FBS for the indicated treatment time and when metabolic steady state is reached. Two hours before the start of the kinetic isotope tracing, media on cells was exchanged with fresh treatment media with 10mM unlabeled glucose. To measure serine labeling over time, cells and media were extracted together. Before the initiation of the kinetic U-^{13}C-glucose isotope tracing, cells were washed three times with 1X PBS and then cultured with 400 µl of tracing medium containing 10 mM of U-^{13}C-

glucose (Cambridge Isotope Laboratories, CLM-481-0) for the rapid time points. Tracing media was equivalent to treatment media except with 10 mM of U-^{13}C- glucose. Following incubation, 1.6ml of extraction buffer containing ice cold 100% HPLC-grade methanol (Sigma Aldrich, 646377) with norvaline (Sigma, N7627) was added onto cells with tracing media for a final sample volume of 2 ml (1.6 ml of extraction buffer with 400 µl of tracing media) and a final concentration of 1 µg per 400 µl norvaline. 1.6 ml of the lysate was placed into a fresh Eppendorf tube and then vortexed at 4°C at maximum speed for ten minutes and then spun down at 4°C at maximum speed for thirty minutes. The supernatant was collected and then dried under nitrogen gas to prepare for metabolic analysis.

Gas Chromatography-Mass Spectrometry (GC-MS) Polar Metabolite Measurements

Dried samples were derivatized by adding 16 µl of methoxamine reagent (Thermo Fisher, TS-45950) and incubated for an hour at 37°C followed by addition of 20 µl of *N*-*tert*-butyldimethylsilyl-*N*-methyltrifluoroacetamide with 1% *tert*-butyldimethylchlorosilane (Sigma 375934) and incubation of two hours at 60°C. Samples were then centrifuged at maximum speed for ten minutes, and 20 µl of supernatant was used for analysis. Following derivatization, samples were analyzed using a DB-35MS column (30 m × 0.25 mm i.d. × 0.25 µm, Agilent J&W Scientific) in an Agilent 7890 gas chromatograph coupled to an Agilent 5975C mass spectrometer (GC–MS).

Immunoblotting

Cells were washed with ice cold 1X PBS and lysed in cold RIPA buffer containing Halt Protease and Phosphatase Inhibitor Cocktail (Thermo Scientific 78442). Lysates were

clarified by rocking samples for thirty minutes at 4°C and then spun at maximum speed for ten minutes for collection of supernatant. Protein concentration was calculating using the BCA Protein Assay (Pierce, 23225) with BSA as a standard. Lysates were resolved by SDS-PAGE using NuPAGE 4-12% Bis-Tris Protein Gels and run at 100V. Proteins were transferred onto nitrocellulose membranes via wet transfer at 100V. Membranes were blocked in 5% BSA in TBST before incubating membranes with primary antibodies at 4°C overnight. The next day, membranes were washed three times with TBST at room temperature and then incubated in secondary antibodies for one hour at room temperature. The primary antibodies used were PHGDH (Sigma Aldrich, HPA021241 [1:1000]) and HSP90 (Cell Signaling Technology, 4874 [1:1000]). The secondary antibodies used were anti-rabbit IgG horseradish peroxidase-linked antibody (1:4000 dilution; Cell Signaling Technologies, 7074S) or anti-mouse IgG horseradish peroxidase-linked antibody (1:4000, 7076S).

Cell Line Generation

Cell lines overexpressing either EGFP or human PHGDH were generated via lentiviral infection. pLJM1-EGFP was obtained from Addgene (Addgene plasmid # 19319). pLJM1-PHGDH was constructed using pLJM1-Empty (Addgene plasmid # 91980) as a backbone. pLJM1-Empty was digested using NheI and EcoRI and gel purified. PHGDH insertion was amplified with the following oligonucleotide primers, where the capitalized sequence denotes PHGDH homology:

PHGDH F: agtgaaccgtcagatccggctagcgccaccATGGCTTTTGCAAATCTGCG

PHGDH R: tactgccatttgtctcgaggtcgagaattcTTAGAAGTGGAACTGGAAGGCT

PHGDH insert was gradient PCR amplified using Phusion High-Fidelity DNA

polymerase (NEB M0530) from 60 to 70°C and gel purified. Digested pLJM1-Empty and amplified PHGDH insert were assembled via Gibson Assembly, and the resulting plasmid was transformed, and validated by Sanger sequencing. Lentiviral production was done by transfecting constructs into LentiX293T cells with Mirus Transit293T (Mirus Bio MIR2700) following manufacturer's protocol. Briefly, 800,000 cells were plated per well in a 6 well plate in DMEM-pyruvate media with 10% heat-inactivated FBS. The next day, cells were transfected with 1.6 µg vector (either pLJM1-EGFP or pLJM1-PHGDH), 800 ng of pMDLg (Addgene plasmid # 12251) packaging plasmid, 400 ng of pMD2.G (Addgene plasmid # 12259) envelope plasmid, and 400 ng of pRSV-REV (Addgene plasmid # 12253) in OptiMEM (Thermo Fisher Scientific 31985070). DNA transfection mix was incubated with cells for 24 hours before harvesting virus. Sub-confluent cells were infected with 1 ml of virus-containing media in each well of a 6 well plate with polybrene (8 µg/ml, EMD Millipore TR-1003-G). 24 hours after infection, selection with puromycin (Sigma Aldrich P7255) began. All experiments with generated cell lines were conducted on a polyclonal cell population.

Statistics and Reproducibility

All statistical tests using experimental data were performed with Prism 10 software. No statistical method was used to predetermine sample sizes. Samples sizes were chosen based on pilot experiments using three or more technical replicates. Certain data points were excluded from Seahorse analyzer assays due to premature injection of rotenone and antimycin. The experiments were not randomized and the investigators were not blinded during experiments nor data analysis.

References

Abbott, K.L., Ali, A., Casalena, D., Do, B.T., Ferreira, R., Cheah, J.H., Soule, C.K., Deik, A., Kunchok, T., Schmidt, D.R., Renner, S., Honeder, S.E., Wu, W., Chan, S.H., Tseyang, T., Stoltzfus, A.T., Michel, S.L.J., Greaves, D., Hsu, P.P., Ng, C.W., Zhang, C.J., Farsidjani, A., Kent, J.R., Madariaga, M.L.L., Gramatikov, I.M.T., Matheson, N.J., Lewis, C.A., Clish, C.B., Rees, M.G., Roth, J.A., Griner, L.M., Muir, A., Auld, D.S., Vander Heiden, M.G. (2023). Screening in serum-derived medium reveals differential response to compounds targeting metabolism. Cell Chemical Biology *30*, 1156-1168. https://doi.org/10.1016/j.chembiol.2023.08.007.

Baksh, S.C., Todorova, P.K., Gur-Cohen, S., Hurwitz, B., Ge, Y., Novak, J.S.S., Tierney, M.T., dela Cruz-Racelis, J., Fuchs, E., Finley, L.W.S. (2020). Extracellular serine controls epidermal stem cell fate and tumour initiation. Nature Cell Biology *22*, 779-790. https://doi.org/10.1038/s41556-020-0525-9.

Bao, X.R., Ong, S.-E., Goldberger, O., Peng, J., Sharma, R., Thompson, D. A., Vafai, S. B., Cox, A. G., Marutani, E., Ichinose, F., Goessling, W., Regev, A., Carr, S. A., Clish, C. B., & Mootha, V. K. (2016). Mitochondrial dysfunction remodels one-carbon metabolism in human cells. eLife *5*. https://doi.org/10.7554/elife.10575.

Bertholet, A.M., Chouchani, E. T., Kazak, L., Angelin, A., Fedorenko, A., Long, J. Z., Vidoni, S., Garrity, R., Cho, J., Terada, N., Wallace, D. C., Spiegelman, B. M., & Kirichok, Y. (2019). H+ transport is an integral function of the mitochondrial ADP/ATP carrier. Nature *571*, 515–520. https://doi.org/10.1038/s41586-019-1400-3.

Bertholet, A.M., Natale, A.M., Bisignano, P., Suzuki, J., Fedorenko, A., Hamilton, J., Brustovestky, T., Kazak, L., Garrity, R., Chouchani, E.T., Brustovetsky, N., Grabe, M., Kirichok, Y. (2022). Mitochondrial uncouplers induce proton leak by activating AAC and UCP1. Nature *606*, 180-187. 10.1038/s41586-022-04747-5.

Birsoy, K., Wang, T., Chen, W.W., Freinkman, E., Abu-Remaileh, M., Sabatini, D.M. (2015). An Essential Role of the Mitochondrial Electron Transport Chain in Cell Proliferation Is to Enable Aspartate Synthesis. Cell *162*, 540-551. https://doi.org/10.1016/j.cell.2015.07.016.

Buttgereit, F., Brand, M.D. (1995). A hierarchy of ATP-consuming processes in mammalian cells. Biochemical Journal *312*, 163-167. A hierarchy of ATP-consuming processes in mammalian cells.

Cantor, J.R., Abu-Remaileh, M., Kanarek, N., Freinkman, E., Gao, X., Louissaint, A., Lewis, C.A., Sabatini, D.M. (2017). Physiologic medium rewires cellular metabolism and reveals uric acid as an endogenous inhibitor of UMP synthase. Cell *169*, 258-272.e217. doi: 10.1016/j.cell.2017.03.023.

Chaneton, B., Hillman, P., Zheng, L., Martin, A.C.L., Maddocks, O.D.K., Chokkathukalam, A., Coyle, J.E., Jankevics, A., Holding, F.P., Vousden, K.H., Frezza, C., O'Reilly, M., Gottlieb, E. (2012). Serine is a natural ligand and allosteric activator of pyruvate kinase M2. Nature *491*, 458-462. 10.1038/nature11540.

Chypre, M., Zaidi, N., Smans, K. (2012). ATP-citrate lyase: a mini-review. Biochemical and Biophysical Research Communications *422*, 1-4. https://doi.org/10.1016/j.bbrc.2012.04.144.

Deberardinis, R.J., Lum, J.J., Hatzivassiliou, G., Thompson, C.B. (2008). The Biology of Cancer: Metabolic Reprogramming Fuels Cell Growth and Proliferation. Cell Metabolism *7*, 11-20.

DeNicola, G.M., Chen P., Mullarky E., Sudderth, J.A., Hu, Z., Wu, D., Tang, H., Xie, Y., Asara J.M., Huffman, K.E., Wistuba, I.I., Minna, J.D., DeBerardinis, R.J., Cantley, L.C. (2015). NFR2 regulates serine biosynthesis in non-small cell lung cancer. Nature Genetics *47*, 1475-1481. 10.1038/ng.3421.

Diehl, F.F., Lewis, C.A., Fiske, B.P., Vander Heiden, M.G. (2019). Cellular redox state constrains serine synthesis and nucleotide production to impact cell proliferation. Nature Metabolism *1*, 861-867. doi:10.1038/s42255-019-0108-x.

Ducker, G.S., Rabinowitz, J.D. (2018). One-Carbon Metabolism in Health and Disease. Cell Metabolism *25*, 27-42. 10.1016/j.cmet.2016.08.009.

Faubert, B., Solmonson, A., Deberardinis, R.J. (2020). Metabolic reprogramming and cancer progression. Science *368*. DOI: 10.1126/science.aaw5473.

Ferraro, G.B., Ali, A., Luengo, A., Kodack, D.P., Deik, A., Abbott, K.L., Bezwada, D., Blanc, L., Prideaux, B., Jin, X., Possada, J.M., Chen, J., Chin, C.R., Amoozgar, Z., Ferreira, R., Chen, I., Naxerova, K., Ng, C., Westermark, A.M., Duquette, M., Roberge, S., Lindeman, N.I., Lyssiotis, C.A., Nielsen, J., Housman, D.E., Duda, D.G., Brachtel, E., Golub, T.R., Cantley, L.C., Asara, J.M., Davidson, S.M., Fukumua, D., Dartois, V.A., Clish, C.B., Jain, R.K., Vander Heiden, M.G. (2021). Fatty acid synthesis is required for breast cancer brain metastasis. Nature Cancer *in press*. 10.1038/s43018-021-00183-y.

Gao, X., Lee, K., Reid, M.A., Sanderson, S.M., Qiu, C., Li, S., Liu, J., Locasale, J.W. (2018). Serine Availability Influences Mitochondrial Dynamics and Function through Lipid Metabolism. Cell Reports *22*, 3507-3520. https://doi.org/10.1016/j.celrep.2018.03.017.

Gravel, S., Hulea, L., Toban, N., Birman, E., Blouin, M., Zakikhani, M., Zhao, Y., Topisirovic, I., St-Pierre, J., Pollak, M. (2014). Serine Deprivation Enhances Antineoplastic Activity of Biguanides. Cancer Research *74*, 7521-7533. https://doi.org/10.1158/0008-5472.CAN-14-2643-T.

Hanahan, D., Weinberg, R.A. (2011). Hallmarks of Cancer: The Next Generation. Cell *144*, 646–674. https://doi.org/10.1016/j.cell.2011.02.013.

Hart, M.L., Quon, E., Vigil, A.B.G., Engstrom, I.A., Newson, O.J., Davidsen, K., Hoellerbauer, P., Carlisle, S.M., Sullivan, L.B. (2023). Mitochondrial redox adaptations enable alternative aspartate synthesis in SDH-deficient cells eLIfe *12*. 10.7554/eLife.78654.

Hennequart, M., Labuschagne, C.F., Tajan, M., Pilley, S.E., Cheung, E.C., Legrave, N.M., Driscoll, P.C., Vousden, K.H. (2021). The impact of physiological metabolite levels on serine uptake, synthesis and utilization in cancer cells. Nature Communications *12*. https://doi.org/10.1038/s41467-021-26395-5.

Hosios, A.M., Hecht, V.C., Danai, L.V., Johnson, M.O., Rathmell, J.C., Steinhauser, M.L., Manalis, S.R., Vander Heiden, M.G. (2016). Amino acids rather than glucose account for the majority of cell mass in proliferating mammalian cells. Developmental Cell *36*, 540-549. doi: 10.1016/j.devcel.2016.02.012.

Hosios, A.M., Li, Z., Lien, E.C., Vander Heiden, M.G. (2018). Preparation of Lipid-Stripped Serum for the Study of Lipid Metabolism in Cell Culture. Bio-protocol *8*. 10.21769/BioProtoc.2876

Jin, X., Demere, Z., Nair, K., Ali, A., Ferraro, G. B., Natoli, T., Deik, A., Petronio, L., Tang, A. A., Zhu, C., Wang, L., Rosenberg, D., Mangena, V., Roth, J., Chung, K., Jain, R. K., Clish, C. B., Vander Heiden, M. G., & Golub, T. R. (2020). A metastasis map of human cancer cell lines. Nature *588*, 331-336. https://doi.org/10.1038/s41586-020-2969-2.

Krall, A.S., Mullen, P.J., Surjano, F., Momcilovic, M., Schmid, E.W., Halbrook, C.J., Thambundit, A., Mittelman, S.D., Lyssiotis, C.A., Shackelford, D.B., Knott, S.R.V., Christofk, H.R. (2021). Asparagine couples mitochondrial respiration to ATF4 activity and tumor growth. Cell Metabolism *33*, 1013-1026. https://doi.org/10.1016/j.cmet.2021.02.001.

Labuschagne, C.F., van den Broek, N.J.F., Mackay, G.M., Vousden, K.H., Maddocks, O.D.K. (2014). Serine, but not glycine, supports one-carbon metabolism and proliferation of cancer cells. Cell Reports *7*. doi: 10.1016/j.celrep.2014.04.045.

Li, Z., Ji, B.W., Dixit, P.D., Lien, E.C., Tchourine, K., Hosios, A.M., Abbott, K.L., Westermark, A.M., Gorodetsky, E.F., Sullivan, L.B., Vander Heiden, M.G., Vitkup, D. (2022). Cancer cells depend on environmental lipids for proliferation when electron acceptors are limited. Nature Metabolism *4*, 711-723. https://doi.org/10.1038/s42255-022-00588-8.

Locasale, J.W., Grassian, A.R., Melman, T., Lyssiotis, C.A., Mattaini, K.R., Bass, A.J., Heffron, G., Metallo, C.M., Muranen, T., Sharfi, H., Sasaki, A.T., Anastasiou, D.,

Mullarky, E., Vokes, N.I., Sasaki, M., Beroukhim, R., Stephanopoulos, G., Ligon, A.H., Meyerson, M., Richardson, A.L., Chin, L., Wagner, G., Asara, J.M., Brugge, J.S., Cantley, L.C., Vander Heiden, M.G. (2011). Phosphoglycerate dehydrogenase diverts glycolytic flux and contributes to oncogenesis. Nature Genetics *43*, 869-874. 10.1038/ng.890.

Luengo, A., Li, Z., Gui, D. Y., Sullivan, L. B., Zagorulya, M., Do, B. T., Ferreira, R., Naamati, A., Ali, A., Lewis, C. A., Thomas, C. J., Spranger, S., Matheson, N. J., & Vander Heiden, M. G. (2021). Increased demand for NAD+ relative to ATP drives aerobic glycolysis. Molecular Cell *81*, 691–707. https://doi.org/10.1016/j.molcel.2020.12.012.

Maddocks, O.D.K., Athineos, D., Cheung, E. C., Lee, P., Zhang, T., Van Den Broek, N. J. F., Mackay, G. M., Labuschagne, C. F., Gay, D., Kruiswijk, F., Blagih, J., Vincent, D. F., Campbell, K. J., Ceteci, F., Sansom, O. J., Blyth, K., & Vousden, K. H. (2017). Modulating the therapeutic response of tumours to dietary serine and glycine starvation. Nature *544*, 372–376. https://doi.org/10.1038/nature22056.

Maddocks, O.D.K., Berkers, C. R., Mason, S. M., Zheng, L., Blyth, K., Gottlieb, E., & Vousden, K. H. (2013). Serine starvation induces stress and p53-dependent metabolic remodelling in cancer cells. Nature *493* (*7433*), 542–546. https://doi.org/10.1038/nature11743.

Maranzana, E., Barbero, G., Ida Falasca, A., Lenaz, G., Luisa Genova, M. (2013). Mitochondrial Respiratory Supercomplex Association Limits Production of Reactive Oxygen Species from Complex I. Antioxidants & Redox Signaling *19*, 1469-1480. 10.1089/ars.2012.4845.

Muir, A., Vander Heiden, M.G. (2018). The nutrient environment affects therapy. Science *360*, 962-963. 10.1126/science.aar5986.

Newman, A.C., Maddocks, O.D.K. (2017). One-carbon metabolism in cancer. British Journal of Cancer *116*, 1499-1504. https://doi.org/10.1038/bjc.2017.118.

Ngo, B., Kim, E., Osorio-Vasquez, V., Doll, S., Bustraan, S., Liang, R. J., Luengo, A., Davidson, S. M., Ali, A., Ferraro, G. B., Fischer, G. M., Eskandari, R., Kang, D. S., Ni, J., Plasger, A., Rajasekhar, V. K., Kastenhuber, E. R., Bacha, S., Sriram, R. K., … Pacold, M. E. (2020). Limited Environmental Serine and Glycine Confer Brain Metastasis Sensitivity to PHGDH Inhibition. Cancer Discovery *10*, 1352–1373. https://doi.org/10.1158/2159-8290.cd-19-1228.

Nobes, C.D., Lakin-Thomas, P.L., Brand, M.D. (1989). The contribution of ATP turnover by the Na+/K+-ATPase to the rate of respiration of hepatocytes: Effects of thyroid status and fatty acids. Biochimica Et Biophysica Acta (BBA) - Bioenergetics *976*, 241-245. https://doi.org/10.1016/S0005-2728(89)80236-1.

Pavlova, N.N., Thompson, C.B. (2017). The Emerging Hallmarks of Cancer Metabolism. Cell Metabolism *23*, 27-47. 10.1016/j.cmet.2015.12.006.

Possemato, R., Marks, K.M., Shaul, Y.D., Pacold, M.E., Kim, D., Birsoy, K., Sethumadhavan, S., Woo, H., Jang, H.G., Jha, A.K., Chen, W.W., Barrett, F.G., Stransky, N., Tsun, Z., Cowley, G.S., Barretina, J., Kalaany, N.Y., Hsu, P.P., Ottina, K., Chan, A.M., Yuan, B., Garrayway, L.A., Root, D.E., Mino-Kenudson, M., Brachtel, E.F., Driggers, E.M., Sabatini, D.M. (2011). Functional genomics reveals serine synthesis is essential in PHGDH-amplified breast cancer. Nature *476*, 346-350. 10.1038/nature10350.

Sullivan, L.B., Gui, D.Y., Hosios, A.M., Bush, L.N., Freinkman, E., Vander Heiden M.G. (2015). Supporting Aspartate Biosynthesis Is an Essential Function of Respiration in Proliferation Cells. Cell *162*, 552-563. doi:10.1016/j.cell.2015.07.017.

Sullivan, M.R., Danai, L. V., Lewis, C. A., Chan, S. H., Gui, D. Y., Kunchok, T., Dennstedt, E. A., Vander Heiden, M. G., Muir, A. (2019a). Quantification of microenvironmental metabolites in murine cancers reveals determinants of tumor nutrient availability. eLife *8*. https://doi.org/10.7554/elife.44235.

Sullivan, M.R., Mattaini, K.R., Dennstedt, E.A., Nguyen, A.A., Reilly, M.F., Meeth, K., Muir, A., Darnell, A.M., Bosenberg, M.W., Lewis, C.A., Vander Heiden, M.G. (2019b). Increased serine synthesis provides an advantage for tumors arising in tissues where serine levels are limiting. Cell Metabolism *29*, 1410-1421,e1414. doi: 10.1016/j.cmet.2019.02.015.

Sun, L., Song, L., Wan, Q., Wu, G., Li, X., Wang, Y., Wang, J., Liu, Z., Zhong, X., He, X., Shen, S., Pan, X., Li, A., Wang, Y., Gao, P., Tang, H., Zhang, H. (2015). cMyc-mediated activation of serine biosynthesis pathway is critical for cancer progression under nutrient deprivation conditions. Cell Research *25*, 429-444. https://doi.org/10.1038/cr.2015.33.

Vande Voorde, J., Ackermann, T., Pfetzer, N., Sumpton, D., Mackay, G., Kalna, G., Nixon, C., Blyth, K., Gottlieb, E., Tardito, S. (2019). Improving the metabolic fidelity of cancer models witha physiological cell culture medium. Science Advances *5*. 10.1126/sciadv.aau7314.

Vander Heiden, M.G., Chandel, N.S., Schumacker, P.T., Thompson, C.B. (1999). Bcl-xL Prevents Cell Death following Growth Factor Withdrawal by Facilitating Mitochondrial ATP/ADP Exchange. Molecular Cell *3*, 159-167. https://doi.org/10.1016/S1097-2765(00)80307-X.

Vander Heiden, M.G., Deberardinis R.J. (2017). Understanding the Intersections between Metabolism and Cancer Biology. Cell *168*, 657-669. doi:10.1016/j.cell.2016.12.039.

Wirth, C., Brandt, U., Hunte, C., Zickermann, V. (2016). Structure and function of mitochondrial complex I. Biochimica Et Biophysica Acta (BBA) - Bioenergetics *1857*, 902-914. https://doi.org/10.1016/j.bbabio.2016.02.013.

Yang, M., Vousden, K.H. (2016). Serine and one-carbon metabolism in cancer. Nature Reviews Cancer *16*, 651-662. 10.1038/nrc.2016.81.

Supplementary Figures

Supplementary Figure 1

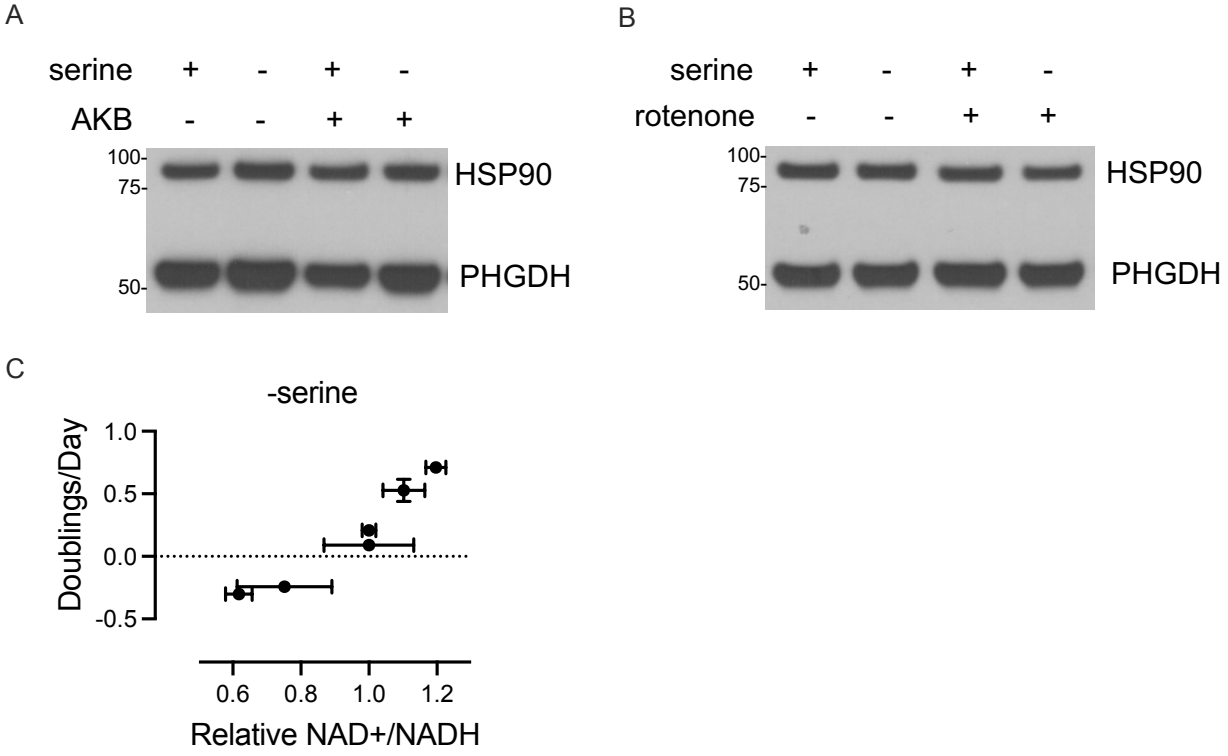

Supplementary Figure 1. α-ketobutyrate (AKB) and rotenone do not change PHGDH protein levels despite altering the NAD+/NADH ratio and proliferation upon serine withdrawal. (A,B) Immunoblot measuring PHGDH protein levels in A549 cells grown with and without serine, AKB, or rotenone, as indicated for 24 hours. HSP90 was used as a loading control. **(C)** NAD+/NADH ratios following AKB treatment (250μM, 1mM) or rotenone treatment (20nM, 40nM) were correlated with raw proliferation rate in A549 starved of serine. NAD+/NADH ratio values were measured after 24 hour treatment. Proliferation rates were measured after 3 days of treatment. Values represent mean ± SD.

Supplementary Figure 2

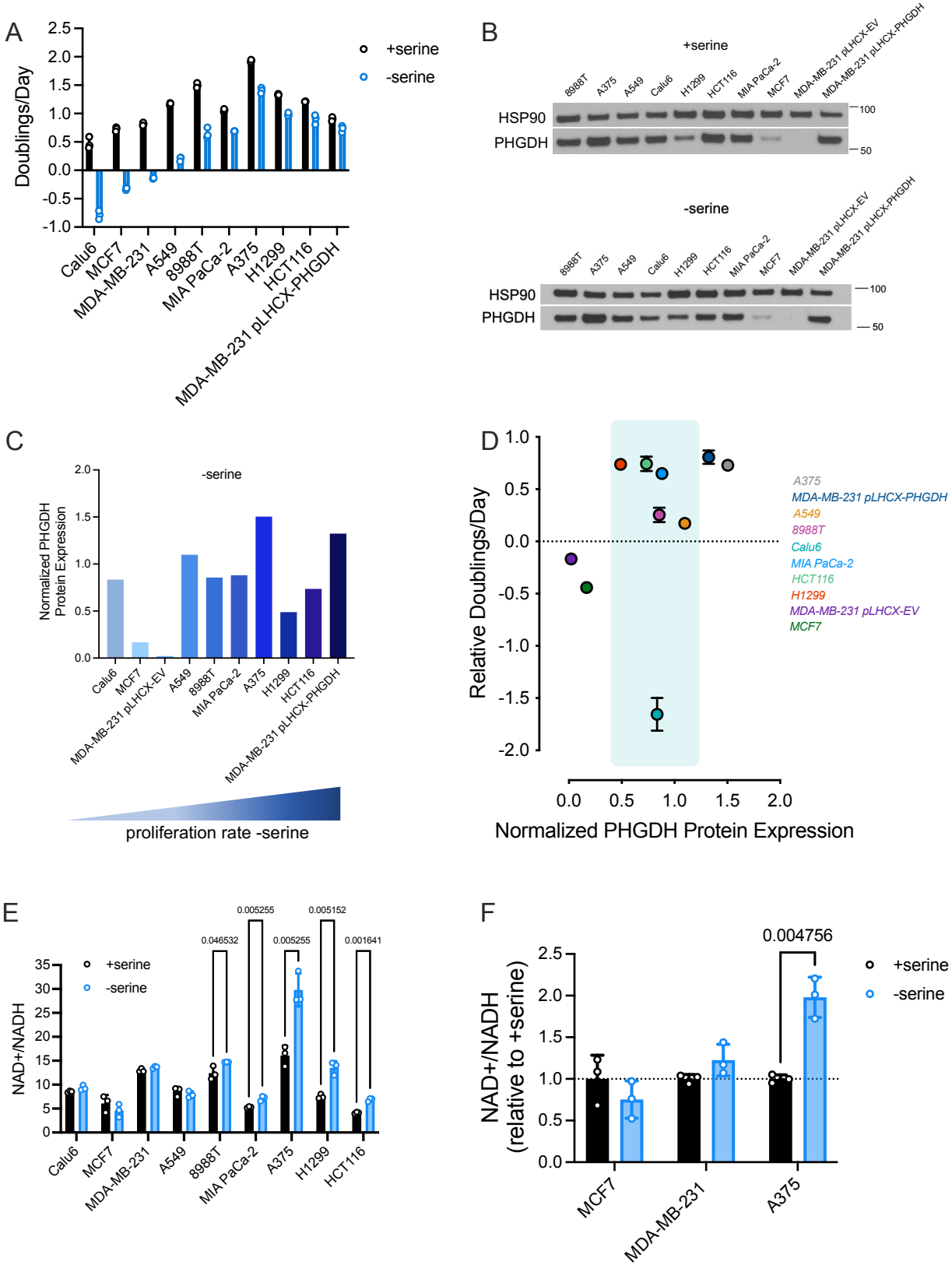

Supplementary Figure 2. Examining PHGDH protein expression and NAD+/NADH ratio contributions to proliferation following serine deprivation. (A) Unnormalized proliferation rates (doublings per day) of cells cultured with and without serine for three days, n=3. **(B)** Immunoblots measuring PHGDH protein levels in cells cultured with serine (top) and without serine (bottom) for 24 hours. HSP90 was used as a loading control. **(C)** PHGDH protein quantification from -serine conditions normalized to HSP90 loading control, plotted in order of cells most to least sensitive to serine withdrawal. **(D)** Normalized PHGDH protein levels from (C) plotted against proliferation rate normalized to +serine conditions per individual cancer cell. Legend depicts each cell line in the color of its corresponding data point. Light blue box encapsulates cells we examined for alterations in NAD+/NADH ratio due to similar PHGDH protein expression despite variation in proliferation without serine. **(E)** Unnormalized NAD+/NADH ratios from each cell type cultured with and without serine for 24 hours, n=3. **(F)** NAD+/NADH ratios of MCF7 and MDA-MB-231, which have low PHGDH protein expression and A375, which has high PHGDH protein expression. Cells were cultured with and without serine for 24 hours. Values are normalized to +serine conditions per cell type, n=3. All p-values calculated by unpaired Student's t-test. All values represent means ± SD.

Supplementary Figure 3

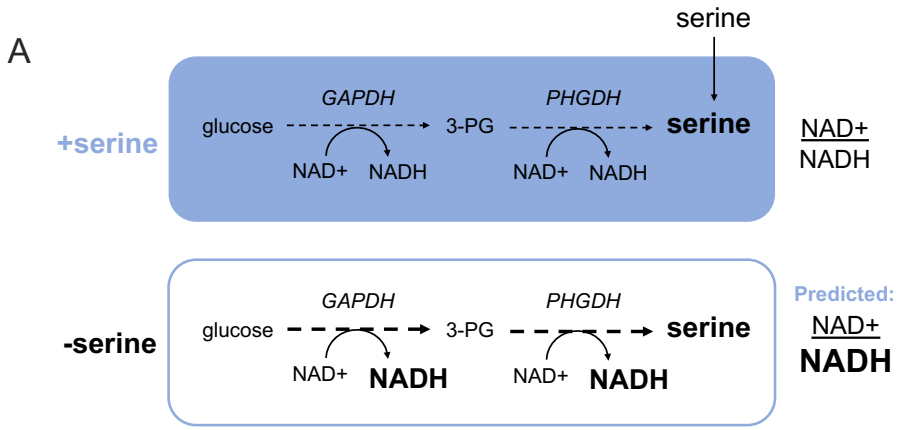

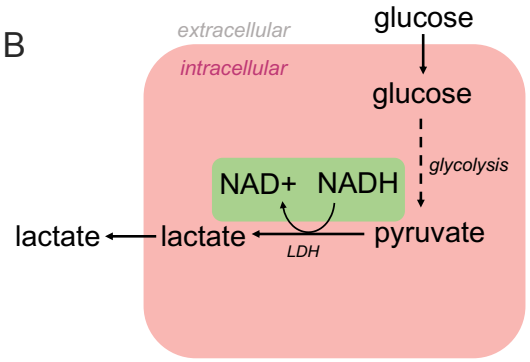

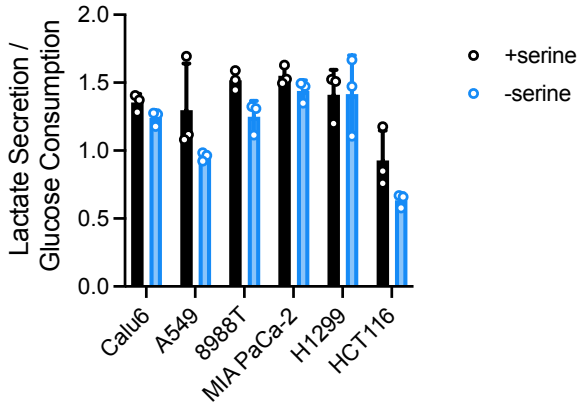

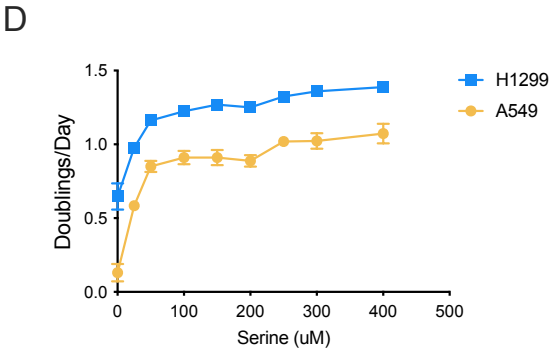

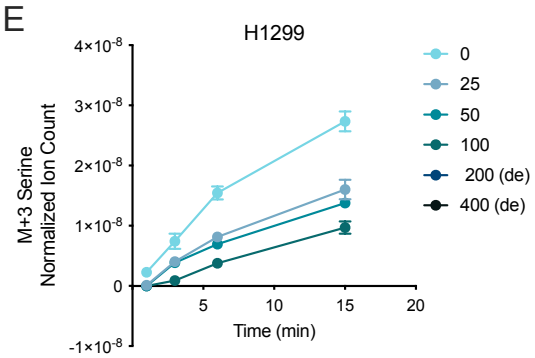

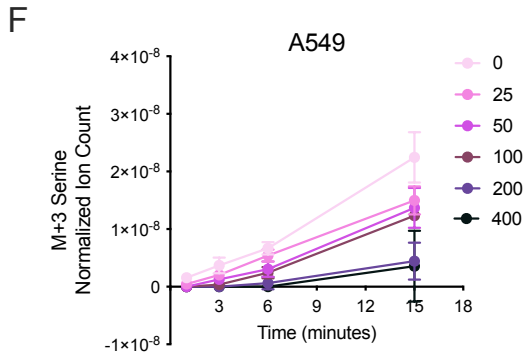

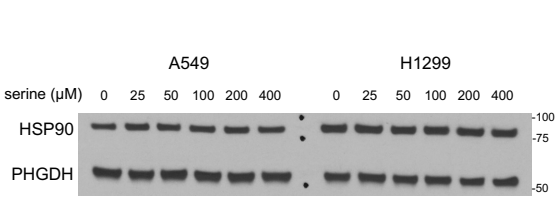

Supplementary Figure 3. Examining PHGDH protein expression and NAD+/NADH ratio contributions to proliferation following serine deprivation. (A) Schematic depicting predictions to cellular NAD+/NADH ratio in response to serine withdrawal. Serine deprivation leads to elevated serine synthesis in cells capable of producing serine. Because serine synthesis consumes NAD+ and generates NADH, we predicted that serine deprivation due to higher serine synthesis would lead to lower NAD+/NADH ratios. **(B)** Schematic depicting lactate production from glucose via glycolysis and lactate dehydrogenase (LDH) as a major NAD+ regenerating process. Lactate is rapidly exchanged between intracellular and extracellular compartments. Thus, measuring lactate secretion relative to glucose consumption is used as a readout for LDH activity. **(C)** Lactate secretion rate normalized to glucose consumption rate in indicated cells grown with and without serine for 72 hours, n=3. **(D)** Proliferation rate (doublings per day) of A549 and H1299 cells grown with indicated concentrations of serine for three days with media replenished every day to avoid serine depletion, n=3. **(E,F)** Kinetic U-^{13}C-glucose tracing into serine in H1299 (E) and A549 (F) cells grown in indicated concentrations of serine for 24 hours. Values are total ion counts of M+3 serine normalized to internal standard norvaline and cell number, “de” denotes detection error, n=3. **(G)** Immunoblot measuring PHGDH protein levels in A549 or H1299 cells cultured with indicated concentrations of serine for 24 hours. HSP90 was used as a loading control. All values are means ± SD.

Supplementary Figure 4

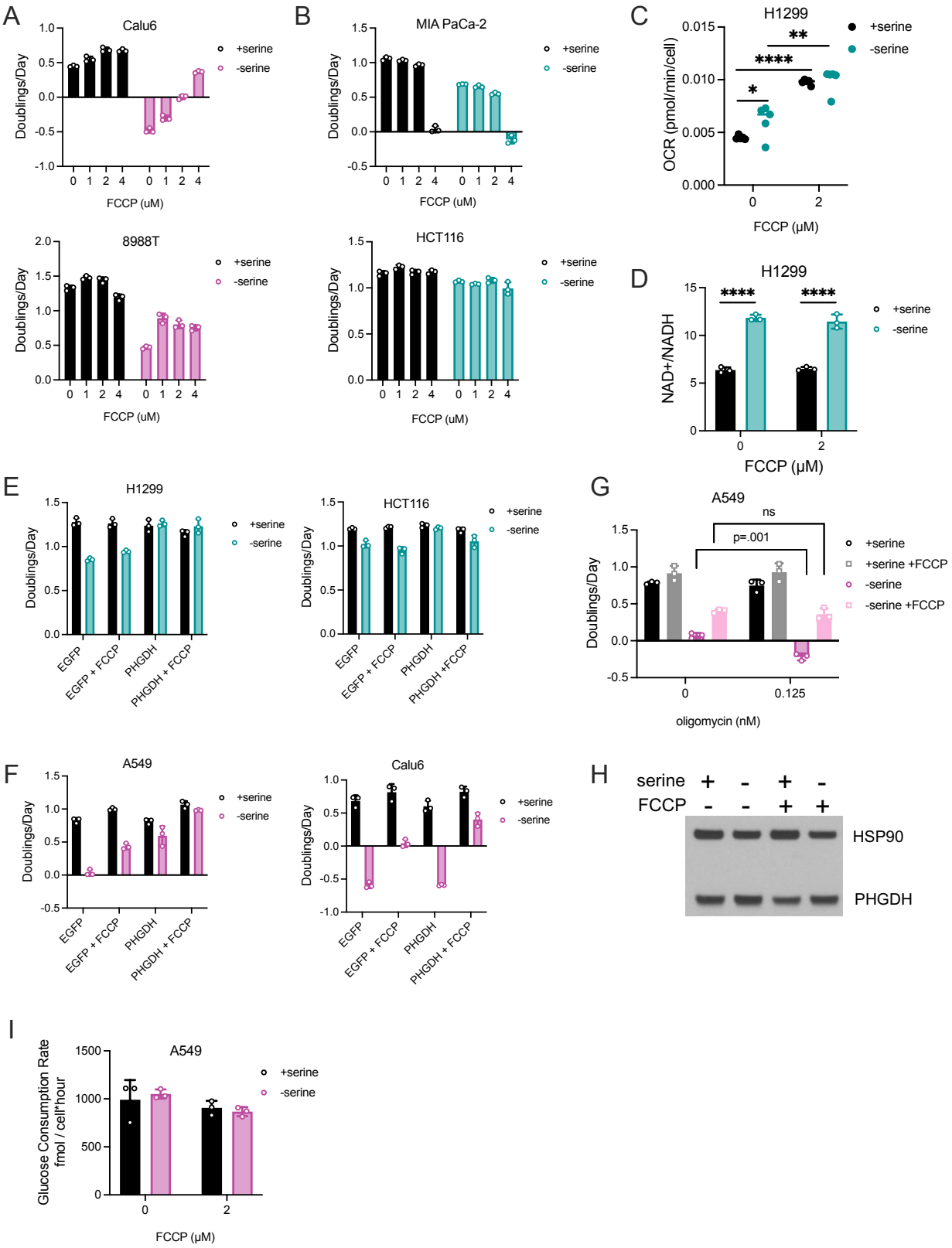

Supplementary Figure 4. FCCP improves serine synthesis and proliferation in serine depleted conditions in redox unresponsive cells. (A) Proliferation rate (doublings per day) of redox unresponsive cells grown with and without serine and indicated concentrations of FCCP for three days, n=3. **(B)** Proliferation rate (doublings per day) of redox responsive cells grown with and without serine and indicated concentrations of FCCP for three days, n=3. **(C)** Mitochondrial oxygen consumption rate (OCR) in H1299 cells grown with and without serine and indicated concentrations of FCCP for 24 hours, n=5. Values are averages of three repeat measurements, *p<0.05, **p<0.01, ****p<0.001. **(D)** NAD+/NADH ratio of H1299 cells cultured with and without and indicated concentrations of FCCP for 24 hours, n=3, ****p<0.001. **(E)** Proliferation rate (doublings per day) of redox responsive cells expressing pLJM1-EGFP (EGFP) and pLJM1-PHGDH (PHGDH) cultured with and without serine and FCCP (2μM) for three days, n=3. **(F)** Proliferation rate (doublings per day) of redox unresponsive cells expressing pLJM1-EGFP (EGFP) and pLJM1-PHGDH (PHGDH) cultured with and without serine and FCCP (2μM) for three days, n=3. **(G)** Proliferation rate (doublings per day) of A549 cells treated with and without serine, 2μM FCCP, and 0.125nM oligomycin for three days, n=3. **(H)** Immunoblot measuring PHGDH protein levels in A549 cells grown with and without serine and FCCP (2μM) for 24 hours. HSP90 was used as a loading control. **(I)** Glucose consumption rates of A549 cells cultured with and without serine and FCCP (2μM) for 72 hours, n=3. All values are means ± SD. P-values were calculated by unpaired Student's t-test.

Supplementary Figure 5

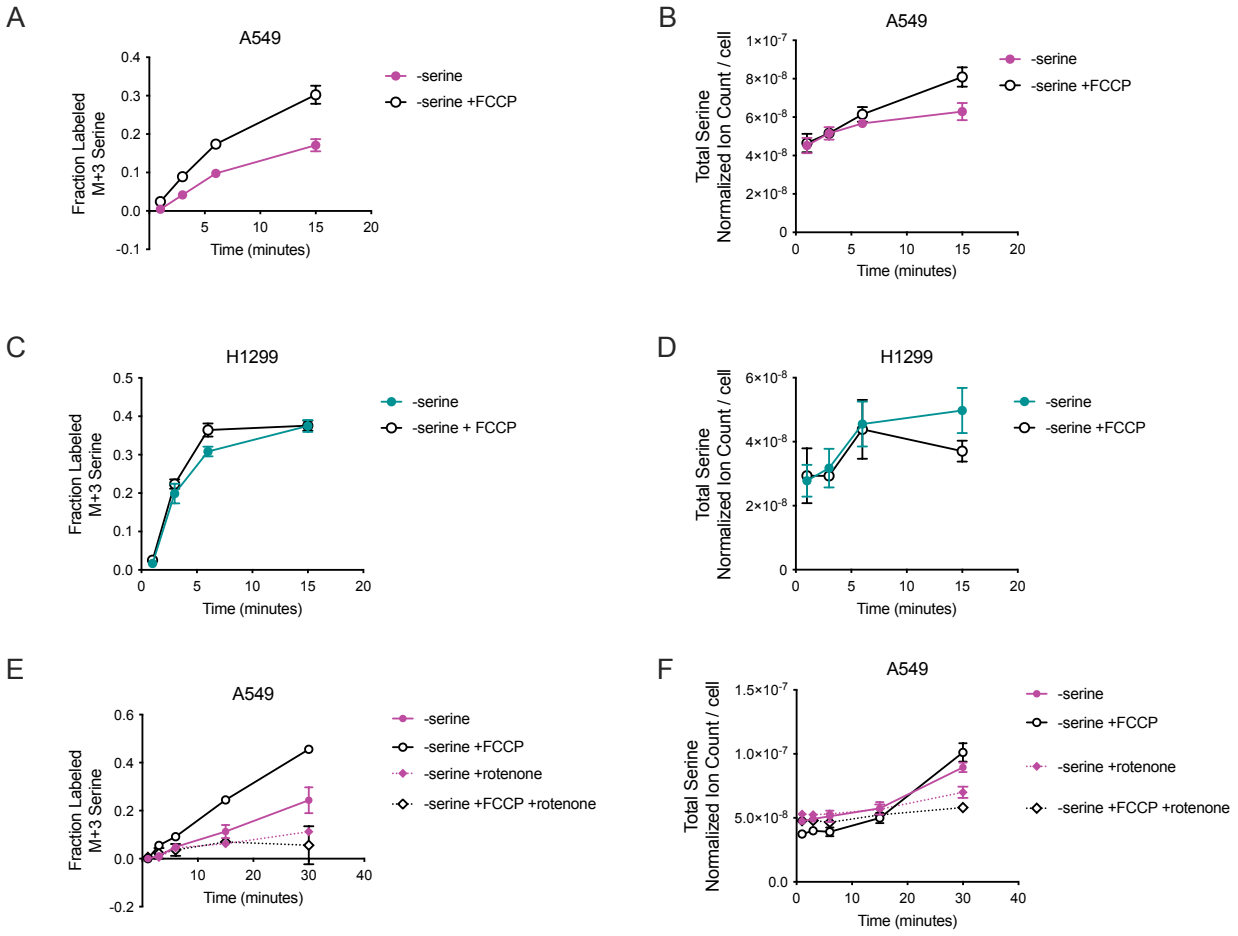

Supplementary Figure 5. Kinetic U-^{13}C-glucose tracing into serine following serine withdrawal and FCCP treatment. (A) Fraction of serine pool labeled fully by glucose (M+3 serine) over time in A549 cells deprived of serine treated with and without 2 μM FCCP for 24 hours prior to tracing. **(B)** Total serine in A549 cells deprived of serine treated with and without 2 μM FCCP for 24 hours prior to tracing. **(C)** Fraction of serine pool labeled fully by glucose (M+3 serine) over time in H1299 cells deprived of serine treated with and without 2 μM FCCP for 24 hours prior to tracing. **(D)** Total serine in H1299 cells deprived of serine treated with and without 2 μM FCCP for 24 hours prior to tracing. **(E)** Fraction of serine pool labeled fully by glucose (M+3 serine) over time in A549 cells deprived of serine treated with and without 2 μM FCCP and 20nM rotenone for 24 hours prior to tracing. **(F)** Total serine pool labeled fully by glucose (M+3 serine) over time in A549 cells deprived of serine treated with and without 2 μM FCCP and 20nM rotenone for 24 hours prior to tracing. All serine ion counts were normalized to internal standard norvaline and cell number. N=3 for all conditions and values represent means ± SD.

Supplementary Figure 6

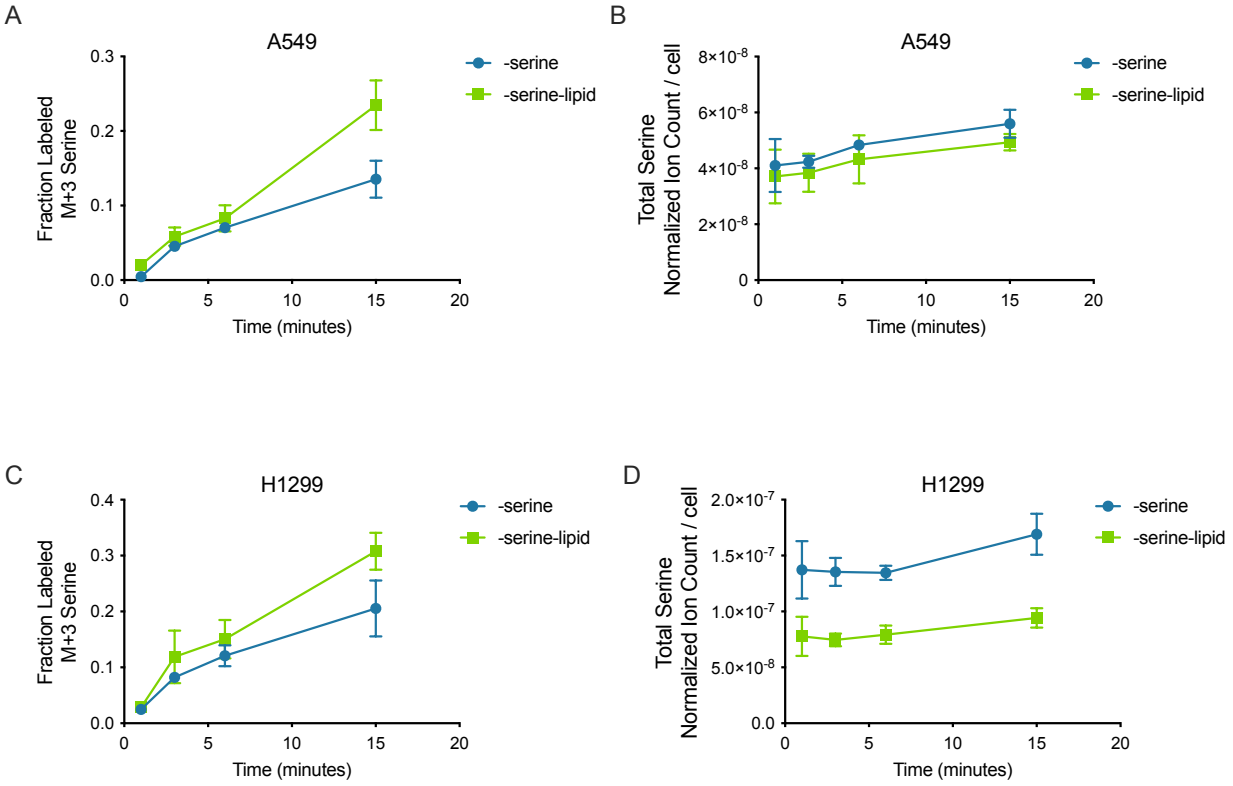

Supplementary Figure 6. Kinetic U-^{13}C-glucose tracing into serine upon serine and lipid withdrawal. (A) Fraction of total serine pool that is labeled by glucose (M+3 serine) over the course of tracing in A549 cells starved of serine grown with and without lipids, n=3. **(B)** Total serine levels in A549 cells starved of serine grown with and without lipids. Values are normalized to internal standard norvaline and cell number, n=3. **(C)** Fraction of total serine pool that is labeled by glucose (M+3 serine) over the course of tracing in H1299 cells starved of serine grown with and without lipids, n=3. **(D)** Total serine levels in H1299 cells starved of serine grown with and without lipids. Values are normalized to internal standard norvaline and cell number, n=3. All values are means ± SD.

Supplementary Table 1

Cell Line	Genetic Mutations	Cancer Type	Source
Calu6	Kras Q61K TP53 R196*	Lung Adenocarcinoma	pleural effusion
A549	Kras G12S Stk11 Q37*	Lung Adenocarcinoma	lung
PaTu 8988T	Kras G12V TP53 R282W Smad4 del EP300 del	PDAC	liver metastasis
MIA PaCa-2	Kras G12C TP53 R248W CDKN2A del	PDAC	pancreas
H1299	Nras Q61K TP53 del	Lung Adenocarcinoma	lymph node metastasis
HCT116	Kras G13D BRCA2 I2675Dfs CDKN2A mut EP300 mut PIK3CA H1047R PPMID L450* TGFBR2 K128Sfs	Colon Carcinoma	colon
A375	BRAF V600E CDKNA E61* TERTc.1-146C>T	Melanoma	skin
MDA-MB-231	BRAF G464V Kras G13D TP53 R280K CDKN2A/B del TERTc.1-146C>T	Triple Negative Breast Adenocarcinoma	pleural effusion
MCF7	PIK3CA E545K GATA3 D336Gfs CDKN2A del	ER+ HER2- Breast Carcinoma	pleural effusion

Chapter 3: Regulation of mitochondrial respiration by serine availability

Authors: Sarah M. Chang[1], Sonia E. Trojan[1,2], Keene L. Abbott[1], and Matthew G. Vander Heiden[1,3]

Affiliations:
[1]Koch Institute for Integrative Cancer Research and Department of Biology, Massachusetts Institute of Technology, Cambridge, MA, USA.
[2]Jagiellonian University Medical College, Faculty of Medicine, Chair of Medical Biochemistry, Krakow, Poland
[3]Dana-Farber Cancer Institute, Boston, MA, USA.

Author Contributions

Conceptualization: **SMC**; Overexpression constructs: KLA; Proliferation rates: **SMC**, SET; Kinetic Isotope Tracing: **SMC**; Immunoblotting: **SMC**; NAD+/NADH measurements: **SMC**, SET; Oxygen consumption: **SMC**; Writing: **SMC**; Editing: **SMC**; Funding Acquisition: MGVH

Abstract

Nutrient availability differs across different tumor microenvironments, constraining the ability of tumors to meet the biomass demands for proliferation. The non-essential amino acid serine can be depleted in tumor nutrient environments and limit tumor growth. While many cancer cells are capable of synthesizing serine, the cellular redox state (NAD+/NADH) influences the rate of serine synthesis. We have found that select cancer cells increase mitochondrial respiration following serine withdrawal, raising the NAD+/NADH ratio and increasing serine synthesis to provide a proliferative advantage over cancer cells that do not elevate mitochondrial respiration in response to serine depletion. How serine availability alters mitochondrial respiration in some cell lines and not others is unknown. Here, we characterize NADH-generating reactions, complex I-linked respiration, and mitochondrial membrane potential under serine withdrawal to uncover that the rise in mitochondrial respiration is not solely driven by mass action. Instead, elevated complex I-linked respiration is coupled to ATP synthase activity. These data suggest ATP synthase function is influenced by serine availability differently across cancers, impacting mitochondrial electron transport chain activity and the cellular NAD+/NADH ratio to govern serine synthesis rates.

Introduction

To proliferate, cells must accumulate sufficient lipids, amino acids, and nucleotides to produce the biomass needed for division. While some biomass components are available from the environment, nutrient availability varies across both tumor and tissue environments. For example, pancreatic cancers are poorly vascularized, leading to depletion of select nutrients environments (Banh, 2020; Commisso, 2013; Datta, 2022;

Kamphorst, 2015). Relative to levels in plasma, pancreatic cancer interstitial fluid is depleted of the amino acid arginine (Sullivan, 2019a), and the brain microenvironment is depleted of the amino acid serine and lipids (Ferraro, 2021; Jin, 2020; Ngo, 2020). In order for cancer cells to proliferate in different tissue nutrient environments, they must adapt metabolism to produce missing environmental metabolites to generate sufficient biomass for proliferation (Abbott, 2023b; Ferraro, 2021; Jin, 2020; Li, 2022; Muir, 2018). One strategy that cancers employ is by upregulating nutrient scavenging mechanisms, such as macropinocytosis (Commisso, 2013; Perera, 2015). Another is increasing the expression of nutrient transporters (Pavlova, 2017) or increasing the expression of biosynthetic enzymes needed to meet the biomass demands of proliferation. However, the ways in which cancer adapts to different conditions is not completely understood.

Serine is a significant biomass precursor that is required not only for synthesizing proteins, but also nucleotides and specific lipid species. Thus acquiring sufficient serine is essential for tumor growth. Serine availability can be limiting for tumor growth in some tissues, including the breast and brain microenvironments (Ngo, 2020; Sullivan, 2019b). Cancer cells adapt to serine depletion by increasing the activity of *de novo* serine synthesis. This can be accomplished by upregulating the expression of serine synthesis pathway enzymes (DeNicola, 2015; Ngo, 2020; Possemato, 2011; Sullivan, 2019b). However, even with high expression of the serine synthesis pathway, serine synthesis can be constrained by the cellular redox state, or the NAD+/NADH ratio (Chapter 2) (Diehl, 2019), leading to the persistent requirement for environmental serine to support for maximal proliferation.

The serine synthesis pathway converts glucose into serine where NAD+ is required by glyceraldehyde-3-phosphate dehydrogenase (GAPDH) and phosphoglycerate dehydrogenase (PHGDH). We found that the endogenous cellular NAD+/NADH ratio is altered in response to serine withdrawal and that this response varies across cancer cells (Chapter 2). Some cancers increase the NAD+/NADH ratio in response to serine withdrawal, while in others, the NAD+/NADH ratio is unchanged, leading to differential serine synthesis activity despite similar protein expression of the serine synthesis pathway. The ability to elevate the cellular NAD+/NADH ratio is due to increased mitochondrial respiration (Chapter 2), but what enables the differential response in mitochondrial respiration to serine depletion is not known.

Here, we aim to uncover the processes that lead some cancers to elevate mitochondrial respiration and raise the cellular NAD+/NADH ratio in response to serine withdrawal. We characterize NADH-generating metabolic reactions in cells grown with and without serine to reveal that the increase in mitochondrial respiration is not likely driven by changes in substrate availability for mitochondrial complex I. Instead, our data suggest that the ability to increase mitochondrial respiration is linked to differential ATP synthase activity that either enables or suppresses complex I-driven respiration in a cell-dependent manner.

Results

Mitochondrial respiration increases acutely following serine withdrawal

Changes in mitochondrial respiration can be broadly categorized into three processes: mass action-driven changes (i.e., higher electron input into the mitochondrial ETC), changes in enzyme levels (i.e., increased ETC protein), and alterations to enzyme

activity (i.e., higher ETC activity per unit of electron input). We considered that if the changes to mitochondrial respiration were driven by increased substrate availability for complex I or elevated enzyme activity, serine withdrawal would lead to acute increases in mitochondrial respiration while changes to protein expression would occur at a slower time scale. To test this, we first aimed to characterize the kinetics of the response. We deprived cells of serine for 2, 4, 6, and 24 hours and measured mitochondrial oxygen consumption rate (OCR). We find that serine withdrawal after just 2 hours leads to an increase in mitochondrial respiration that is sustained for 24 hours (**Figure 1A-D**). To obtain greater kinetic clarity of the response, we acutely supplemented extracellular serine to cells while measuring OCR, as serine rapidly exchanges between extracellular and intracellular compartments (Labuschagne, 2014). Acute serine supplementation led to no difference in mitochondrial respiration rate in cells deprived of serine for either 6 or 24 hours (**Figure 1E,F)**. We next questioned whether mitochondrial respiration would be restored over longer time periods following serine addition. Thus, we deprived serine for 6 hours and then exposed cells to serine for one hour before measuring mitochondrial OCR. Indeed, after one hour, mitochondrial respiration returned to levels observed in cells continuously cultured with serine (**Figure 1G**). These data suggest that changes to mitochondrial respiration are responsive to serine deprivation over a time scale of approximately one hour.

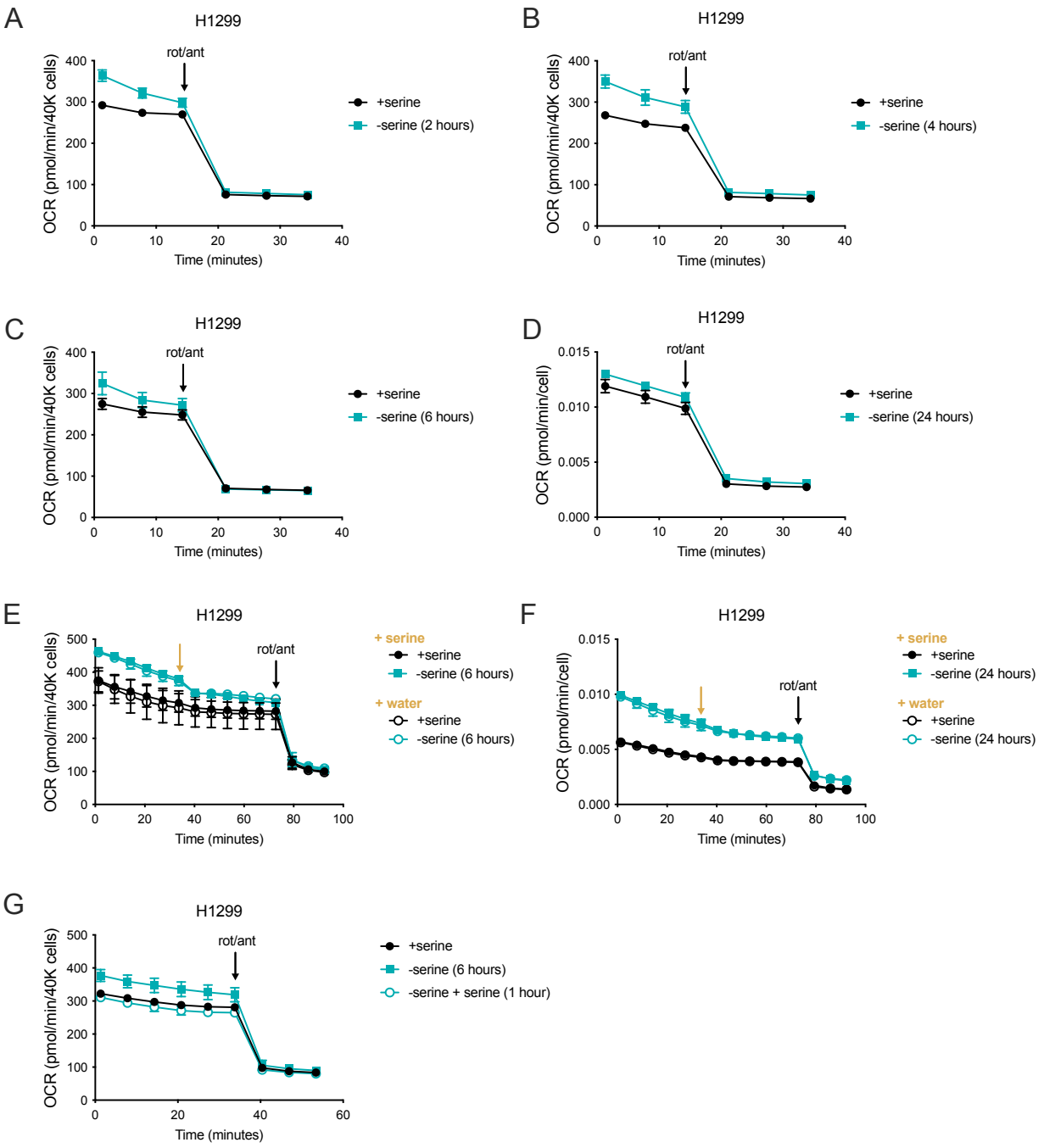

Figure 1. Mitochondrial respiration acutely increases following serine withdrawal. Mitochondrial oxygen consumption rate (OCR) was measured in H1299 cells deprived of serine for **(A)** 2 hours **(B)** 4 hours, **(C)** 6 hours, and **(D)** 24 hours before treatment with rotenone and antimycin A (rot/ant) to block all mitochondrial OCR. **(E)** H1299 cells were deprived of serine for 6 hours and basal OCR, OCR following a rapid supplementation of serine (final concentration 0.4mM) or water vehicle, and residual OCR following rot/ant injection. **(F)** OCR measurements of H1299 cells deprived of serine for 24 hours after serine (final 0.4mM) or water and rot/ant treatment. **(G)** OCR measurements after 6 hour serine depletion or 6 hour serine depletion with

re-supplementation of 0.4mM serine for 1 hour. **(A-D)** n=30, **(E-G)** n=15. Values denote mean ± SD.

Pyruvate dehydrogenase activity but not oxidative decarboxylation is higher in cells that increase mitochondrial respiration following serine withdrawal

The lack of a more rapid response upon serine re-supplementation is notable on a signaling and metabolic time scale, suggesting that the elevation in mitochondrial respiration is not necessarily driven by increased substrate availability or signaling responses that alter enzyme activity, as both would be expected to occur with much faster kinetics. However, given the lack of clarity on how metabolic reactions linked to the ETC change and what modifications to ETC activity could occur following serine withdrawal, the kinetic response cannot completely rule out these possibilities. To better explore the potential causes for increased mitochondrial respiration, we characterized major metabolic pathways that could alter electron input into the ETC upon serine deprivation: serine synthesis, lactate production, pyruvate dehydrogenase, and the TCA cycle. We have previously shown that serine synthesis from glucose is increased and lactate dehydrogenase activity is unchanged or lower in response to serine deprivation (Chapter 2). Pyruvate dehydrogenase (PDH) catalyzes the conversion of mitochondrial pyruvate into acetyl-CoA. Acetyl-CoA and oxaloacetate (OAA) produce citrate by citrate synthase (CS) (**Figure 2A**). To characterize PDH activity, we performed kinetic isotope tracing using uniformly ^{13}C-labeled glucose (U-^{13}C-glucose) to monitor the citrate formation, which will contain two ^{13}C carbons if generated by CS (M+2 citrate). We find that PDH activity is higher 24 hours after serine withdrawal in cells that elevate mitochondrial respiration following serine deprivation, but not in cells with unaltered mitochondrial respiration (**Figure 2B, Supplementary Figure 1A-D**). While elevated PDH activity can

raise mitochondrial respiration in complete media conditions (Luengo, 2021), increasing PDH activity with the pyruvate dehydrogenase kinase (PDK) inhibitor AZD7545 does not improve proliferation of serine deprived cells (**Supplementary Figure 1E,F**). This sugests that increased PDH activity alone does not mediate the proliferative advantage observed in cells with higher mitochondrial respiration. To measure TCA cycle activity, we performed kinetic isotope tracing using uniformly ^{13}C-labeled glutamine (U-^{13}C-glutamine) and monitored the labeling of TCA cycle metabolites over time (**Figure 2A**). Interestingly, we find no meaningful difference in the production of α-ketoglutarate, succinate, fumarate, malate, or aspartate (as a proxy for oxaloacetate) from glutamine in cells with and without elevated mitochondrial respiration upon serine deprivation (**Figure 2C-G, Supplementary Figure 2A-G, Supplementary Figure 3A-E, Supplementary Figure 4A-G**). Notably, we observe no difference in succinate and fumarate labeling over time, suggesting that complex II activity is unaltered.

In contrast, the production of citrate significantly differed following serine withdrawal in cells with elevated mitochondrial respiration. We find that total intracellular citrate levels are only increased in cells that increase mitochondrial respiration upon serine deprivation (**Supplementary Figure 2H, Supplementary Figure 4H**). Additionally, citrate produced through both oxidative decarboxylation (M+4 citrate) and reductive carboxylation (M+5 citrate) from glutamine is elevated only in cells that increase mitochondrial respiration upon serine withdrawal (**Figure 2H-I, Supplementary Figure 3F-G**). Given no difference in M+4 succinate, fumarate, malate, and aspartate labeling between serine deplete and replete cells, the increase in M+4 citrate is likely not from increased oxidative decarboxylation but instead from increased citrate synthase activity

or PDH activity, where acetyl-CoA availability is elevated and OAA levels are not limiting. Reductive carboxylation converts αKG to isocitrate via isocitrate dehydrogenase (IDH1/2/3). This reaction generates NAD+ or NADP+, depending on the active IDH isozyme. Thus, increasing reductive carboxylation not only avoids the reduction of NAD+ to NADH required for oxidative decarboxylation, but also allows the regeneration of an oxidized redox cofactor.

Curiously, we also find a significant population of M+6 citrate in cells with elevated mitochondrial respiration following serine starvation, where 15% of the citrate pool is M+6 compared to 2% in cells with no change in mitochondrial respiration despite the total citrate pool being larger in cells with elevated mitochondrial respiration following serine withdrawal (**Supplementary Figure 5A-C**). The production of M+6 citrate requires the presence of fully labeled OAA (M+4) and acetyl-CoA (M+2) from U-^{13}C-glutamine. The only known process that leads to the production of glutamine-derived mitochondrial acetyl-CoA is if pyruvate is derived from glutamine carbons. Indeed, we also see the presence of fully labeled pyruvate (M+3 pyruvate) (**Supplementary Figure 5A,D-I**). Pyruvate can be produced from glutamine by cytosolic malic enzyme 1 (ME1) or a mitochondrial malic enzyme (ME2/3), all of which require NADP+ as an electron acceptor and generate NADPH. Whether malic enzyme activity benefits serine synthesis or is a consequence of other metabolic changes downstream of serine withdrawal has yet to be determined. Together, these data demonstrate that while oxidative decarboxylation, a major NADH-producing pathway that donates electrons to the ETC, is largely unaltered, serine synthesis and PDH activity are elevated, potentially contributing NADH reducing equivalents to raise mitochondrial respiration in response to serine withdrawal.

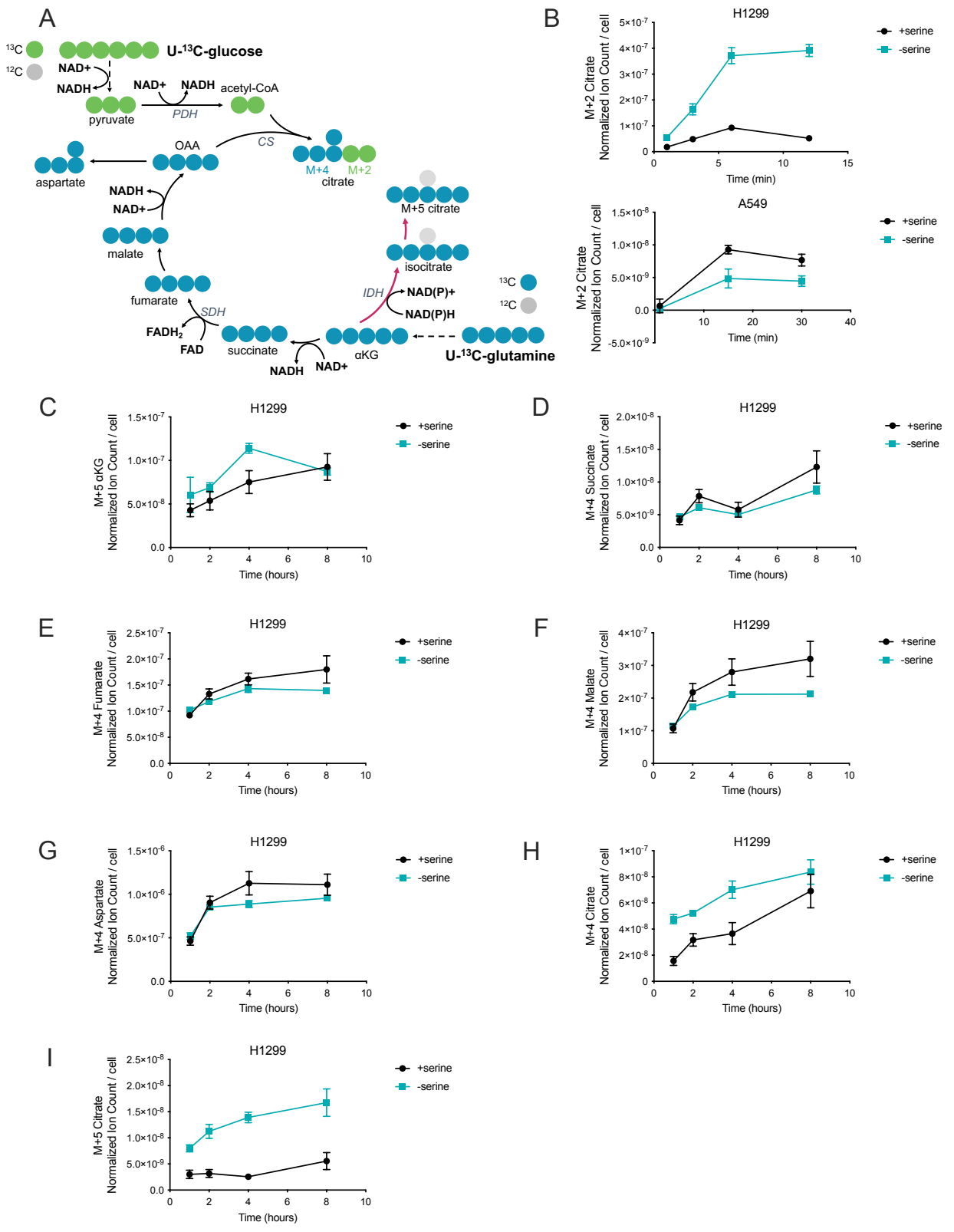

Figure 2. Pyruvate dehydrogenase and TCA cycle activity following serine deprivation. (A) Schematic displaying kinetic U-^{13}C-glucose and U-^{13}C-glutamine tracing patterns. **(B)** Kinetic U-

^{13}C-glucose tracing into citrate in cells deprived of serine for 24 hours. **(C-I)** Kinetic U-^{13}C-glutamine tracing into TCA metabolites α-ketoglutarate, succinate, fumarate, malate, aspartate, and citrate in cells deprived of serine for 24 hours. All values are mean of n=3 ± SD. Abbreviations: PDH, pyruvate dehydrogenase; CS, citrate synthase; IDH, isocitrate dehydrogenase, SDH; succinate dehydrogenase; αKG, α-ketoglutarate.

PHGDH overexpression blocks the increase in mitochondrial respiration following serine withdrawal

To further test whether NADH generated from elevated serine synthesis and PDH activity drive the increase in mitochondrial respiration, we overexpressed PHGDH and measured mitochondrial oxygen consumption rate. We hypothesized that increasing PHGDH protein levels could lead to higher serine synthesis and raise NADH, driving increased mitochondrial respiration in responsive cells. PHGDH overexpression led to increased serine synthesis, full restoration of proliferation in cells with elevated mitochondrial respiration, and partial restoration of proliferation in cells with unaltered mitochondrial respiration due to NAD+ limitation following serine withdrawal, as previously observed (**Figure 3A-D, Supplementary Figure 6A-C**) (Chapter 2). However, despite elevating serine synthesis, PHGDH overexpression suppressed the increase in mitochondrial respiration in cells that are capable of elevating mitochondrial respiration in response to serine deprivation (**Figure 3E,F**). Consistent with our previous findings that mitochondrial respiration determines the cellular NAD+/NADH ratio, PHGDH overexpression also blocked the rise in the NAD+/NADH ratio exhibited by mitochondrial-responsive serine starved cells (**Figure 3G,H**). These data suggest that elevated serine synthesis and consequently increased NADH production does not directly lead to the increase in mitochondrial respiration. Instead, our findings argue that another metabolic consequence of PHGDH overexpression, potentially elevated levels of serine (**Supplementary Figure 6C**) or a serine-derived metabolite is sufficient to impact

mitochondrial respiration and the cellular redox ratio in cells that endogenously increase mitochondrial respiration following serine withdrawal. This is consistent with extracellular serine availability dose-dependently tuning mitochondrial respiration as previously observed (Chapter 2).

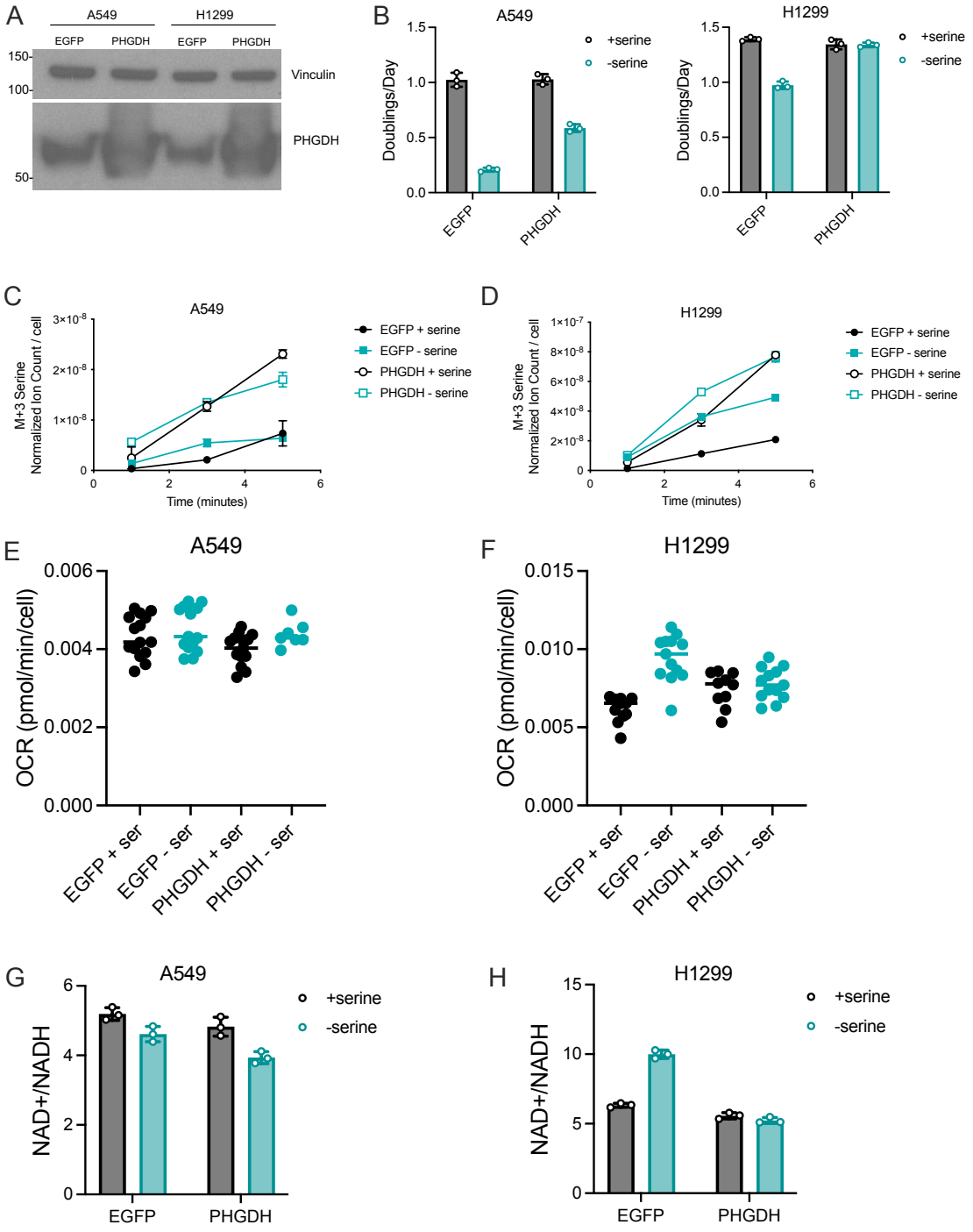

Figure 3. PHGDH overexpression blocks the rise in mitochondrial respiration and NAD+/NADH ratio following serine withdrawal. (A) Immunoblot displaying PHGDH protein levels in cells expressing pLJM1-EGFP (EGFP) or pLJM1-PHGDH (PHGDH). Vinculin is used as a loading control. **(B)** Proliferation rate of cells expressing EGFP or PHGDH and deprived of serine over three days, n=3. **(C-D)** Kinetic U-^{13}C-glucose tracing into serine (M+3) after starving cells of serine for 24 hours, n=3. Total ion counts were normalized to external standard norvaline and cell number. **(E-F)** Mitochondrial oxygen consumption rate (OCR) of cells expressing EGFP or PHGDH after 24 hour serine starvation, n=7-15. **(G-H)** Whole cell NAD+/NADH ratio of cells expressing EGFP or PHGDH after 24 hour serine starvation, n=3. All values are means ± SD.

Higher complex I-linked respiration is associated with increases in mitochondrial respiration following serine starvation

We wondered if elevated pyruvate dehydrogenase (PDH) activity led to increased mitochondrial respiration as has previously been shown (Luengo, 2021). To begin exploring this question, we deprived cells of serine and measured complex I-linked respiration of mitochondria *in situ* by permeabilizing the plasma membrane. By supplementing permeabilized cells with the same amount of pyruvate and malate, which produce NADH via PDH and malate dehydrogenase, respectively, we can measure and compare complex I activity between cells exposed to serine replete and depleted conditions (Chance, 1955a; Divakaruni, 2022; Gui, 2016). We hypothesized that elevated PDH activity might increase NADH production and drive higher mitochondrial respiration. We performed this experiment in cells that do and do not elevate mitochondrial respiration following serine withdrawal to compare the contribution of altered PDH activity, which is only elevated in cells with higher mitochondrial respiration (**Figure 2B, Supplementary Figure 1A-D**). Indeed, we find that serine depleted cells with elevated PDH activity have higher complex I-linked respiration compared to serine replete cells, while serine depleted cells with unaltered PDH activity have unchanged complex I-linked respiration (**Figure 4A,B**). Notably, while mitochondrial mass, as stained by MitoTracker Green, was elevated in H1299 cells deprived of serine, it was not elevated in HCT116 cells, which also increase

mitochondrial respiration following serine withdrawal (**Figure 4C, Supplemental Figure 1A**). Moreover, electron transport chain protein expression was unchanged following serine withdrawal in all cells deprived of serine (**Figure 4D**). Together these data demonstrate that cells that increase mitochondrial respiration following serine withdrawal possess higher complex I-linked respiration independent of ETC protein expression.

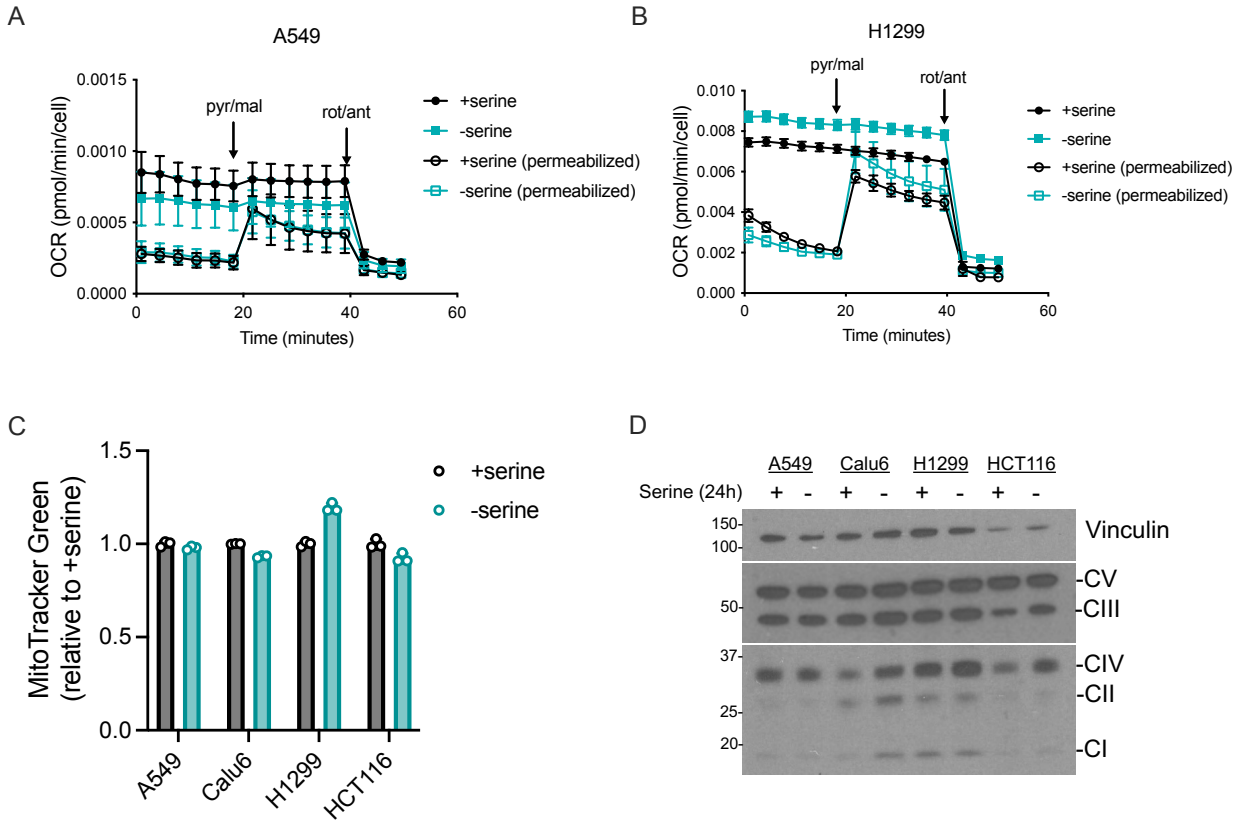

Figure 4. Higher complex I-linked respiration is associated with elevated mitochondrial respiration following serine withdrawal independent of mitochondrial ETC protein expression. (A-B) Mitochondrial oxygen consumption rate (OCR) was measured in intact or permeabilized cells after 24 hours of serine starvation basally and after the addition of pyruvate and malate (pyr/mal). Rotenone and antimycin A (rot/ant) were added to suppress all mitochondrial OCR, n=15. **(C)** MitoTracker Green staining of cells starved of serine for 24 hours. Values are normalized to the Alexa Fluor-488 median values obtained in the +serine condition per each cell type, n=3. **(D)** Immunoblot displaying complex I-V protein levels in cells grown with and without serine for 24 hours. Vinculin was used as a loading control. Values in **(A-C)** are means ± SD.

While these data are consistent with altered PDH activity contributing to increased mitochondrial respiration, there are many caveats to this interpretation. First, treating cells

with a PDH activator alone should elevate complex I-linked respiration. We have yet to conduct this control experiment needed to interpret our results. Additionally, these data do not rule out the possibility that changes to intrinsic ETC activity, as opposed to changes to electron input, yield the increase in complex I-linked respiration (Divakaruni, 2022). In fact, the inability of PDH activation to improve proliferation of cells that do not elevate mitochondrial respiration in response to serine deprivation argues that the increase in complex I-linked respiration is not due to PDH activation alone. If it were, PDH activation would drive higher complex I-linked respiration and subsequently raise the NAD+/NADH ratio to support higher serine synthesis and proliferation in serine-depleted conditions, similar to what is observed in cells that respond to serine withdrawal with higher mitochondrial respiration and NAD+/NADH ratios.

We considered the possibility of another major NADH source that could affect mitochondrial respiration related to serine metabolism: the one carbon cycle. The one carbon cycle uses serine carbons to generate one carbon units required for nucleotide synthesis. The one carbon cycle is heavily compartmentalized, spanning the cytosol and the mitochondria where each compartment contains parallel sets of enzymes that transfer one carbon units via folate cofactors, moving electrons between compartments in the process. Transporters for serine, glycine, and formate, key components of the one carbon cycle facilitate exchange of these metabolites between the mitochondria and cytosol (Kory, 2018; Lunetti, 2016). Accumulating evidence suggests that in most proliferating mammalian cells, the net direction of the one carbon cycle transfers cytosolic serine into the mitochondria (Ducker, 2018; García-Martínez, 1993; Herbig, 2002; Lewis, 2014; Tibbetts, 2010; Yang, 2016), which leads to the conversion of serine into glycine via the

mitochondrial enzyme serine hydroxymethyltransferase 2 (SHMT2). SHMT2 uses tetrahydrofolate (THF) and generates 5,10-methylene-THF. 5,10-methylene-THF is eventually converted into formate via the mitochondrial enzyme methylenetetrahydrofolate dehydrogenase (MTHFD2), which reduces NAD+ into NADH. Thus, alterations in MTHFD2 flux can lead to changes in mitochondrial NADH production, impacting mitochondrial respiration. We have yet to examine the flux through the mitochondrial one carbon cycle, which can be done using isotope tracing (Lewis, 2014). However, changes in the one carbon cycle upon serine deprivation appear unlikely to elevate mitochondrial respiration. Serine deprivation leads to the depletion of one carbon units for nucleotide synthesis, as formate supplementation in serine starved cells restores one carbon units and nucleotide levels (Bao, 2016; Diehl, 2019; Labuschagne, 2014). This demonstrates that activity through one carbon metabolism is decreased upon serine deprivation. Additionally, while the presence of glycine in our serine depleted media could contribute to one carbon metabolism, extracellular glycine in the absence of serine withdraws one carbon units away from the one carbon cycle due to SHMT-mediated synthesis of serine from glycine (Labuschagne, 2014). Moreover, previous studies have linked the importance of one carbon metabolism to mitochondrial respiration, as the production of 10-formy THF is important for mitochondrial translation of mitochondrial proteins needed for respiration (Minton, 2018). Additionally, serine catabolism by the one carbon cycle is a major producer of NADH when mitochondrial respiration is suppressed (Yang, 2020). Together, our observation that serine starvation, which decreases one carbon metabolism, stimulates mitochondrial respiration is at odds with the relationship between one carbon metabolism and mitochondrial function, suggesting that the elevation

in mitochondrial respiration may not be due to changes in one carbon metabolism. In fact, the proliferation advantage conferred by elevating mitochondrial respiration by uncoupling agents would argue that raising mitochondrial respiration can improve one carbon metabolism, perhaps through stimulating MTHFD2 activity, as opposed to the other way around. However, experiments to directly test this would need to be conducted to lend further clarity to these possibilities.

Differential ATP synthase activity influences complex I in serine-depleted conditions

Our data are less consistent the possibility that increased electron input into the ETC leads to the rise in mitochondrial respiration following serine withdrawal. Thus, we considered that the increase in complex I-linked respiration may be due to changes in ETC activity. In our previous studies, we found that increasing mitochondrial respiration with the uncoupler FCCP raises the NAD+/NADH ratio, serine synthesis rate, and proliferation of cells that do not endogenously elevate mitochondrial respiration following serine deprivation. On the other hand, treating cells that do increase mitochondrial respiration following serine withdrawal with FCCP led to no difference in serine synthesis rates and proliferation (Chapter 2). In conducting these experiments, we were struck by the ability for FCCP to specifically raise proliferation of cells that do not increase mitochondrial respiration after serine depletion even when they are cultured with serine. This suggested that in contrast to FCCP-unresponsive cells, mitochondrial ATP excess or ATP synthase activity may inherently limit NAD+ regeneration by complex I, constraining proliferation in complete media conditions (Luengo, 2021) and hyperpolarizing the mitochondrial membrane upon serine depletion. Thus, we first asked

whether serine deprivation altered the mitochondrial membrane potential differently between cells that increase mitochondrial respiration following serine withdrawal and those that do not. We measured mitochondrial membrane potential using TMRE, a positively charged dye that accumulates in the mitochondria due to the negative membrane potential; the more hyperpolarized the mitochondrial membrane potential, the higher the TMRE staining (Crowley, 2016; Perry, 2018). We hypothesized that serine deprivation would lead to mitochondrial membrane hyperpolarization in cells that cannot elevate mitochondrial respiration, but not in those that do elevate mitochondrial respiration. However, after normalizing to mitochondrial content, serine starvation hyperpolarized the mitochondrial membrane potential equally across the cancer cells we examined (**Figure 5A, Supplementary Figure 7A,B**). As a control, we used FCCP, which indeed depolarized the mitochondrial membrane potential across cells (**Supplementary Figure 7C,D**). We note that the mitochondrial membrane potential may still be different across cells, but we cannot compare the absolute mitochondrial membrane potentials across cell types due to differences in cell volume that could impact the intensity of TMRE and MitoTracker Green.

Hyperpolarization of the mitochondrial membrane potential occurs if the relative proton transport into the mitochondrial intermembrane space exceeds the release of protons back into the mitochondrial matrix. This can be due to multiple possibilities: 1. Increased proton input with unchanged proton output; 2. Unchanged proton input with decreased proton output; 3. Increased proton input that exceeds an increase in proton output; 4. Decreased proton output that exceeds a decrease in proton input; and 5. Increased proton input with decreased proton output (**Figure 5B**). An increase in proton

input can be due to both increased ETC substrate or an increase in intrinsic ETC activity per unit of substrate. Given that cells with elevated mitochondrial respiration exhibit increased NAD+/NADH ratios and higher complex-I linked respiration following serine withdrawal, we postulated that these cells either have increased proton input with unchanged proton output (**Figure 5B, model 1**), increased proton input that exceeds an increase in proton output (**Figure 5B, model 3**), or increased proton input with decreased proton output (**Figure 5B, model 5**), consistent with the raised NAD+/NADH ratio upon serine deprivation. In contrast, because cells that do not increase mitochondrial respiration following serine depletion do not elevate the NAD+/NADH ratio and have unaltered complex I-linked respiration, we postulated that they would exhibit no change in proton input or lower proton input with decreased proton output (**Figure 5B, models 2 or 4, respectively**). Specifically, we hypothesized that suppressed ATP synthase activity could lead to decreased proton output as ATP synthase releases protons down their chemical gradient into the mitochondrial matrix. ATP synthase insufficiency suppresses ETC activity, specifically complex I activity, akin to treatment with oligomycin, an ATP synthase inhibitor that hyperpolarizes the mitochondrial membrane and lowers the cellular NAD+/NADH ratio (Sullivan, 2015).

Thus, we wondered whether ATP synthase activity differed between cells that can and cannot increase mitochondrial respiration in response to serine deprivation. ATP synthase activity is regulated by ADP availability from ATP turnover in cells. Promoting ATP consumption elevates ATP synthase activity and increases mitochondrial respiration (Bertholet, 2019; Brown, 1992; Chance, 1955b). If ATP synthase insufficiency limits mitochondrial respiration and subsequently the NAD+/NADH ratio in cells that do not

increase mitochondrial respiration following serine withdrawal, we would predict that increasing ATP consumption would relieve mitochondrial membrane hyperpolarization and raise complex I activity to increase the NAD+/NADH ratio, serine synthesis, and proliferation under serine starvation. While we have yet to test all aspects of this hypothesis, we did treat cells that either do or do not increase mitochondrial respiration in response to serine withdrawal with gramicidin D. Gramicidin D increases ATP hydrolysis by Na+/K+-ATPases to promote ATP synthase activity and depolarize the mitochondrial membrane potential (Luengo, 2021; Nobes, 1989; Vander Heiden, 1999). Interestingly, gramicidin D mildly improves proliferation of cells that do not elevate mitochondrial respiration following serine withdrawal while having no impact on the proliferation of cells that do elevate mitochondrial respiration (**Figure 5C**). These data argue that ATP synthase insufficiency hyperpolarizes the mitochondrial membrane potential, blocking complex I activity during serine starvation in cells that do not raise mitochondrial respiration following serine withdrawal. This is consistent with FCCP, which depolarizes the mitochondrial membrane potential, raising the NAD+/NADH ratio and providing a proliferative advantage in serine-deprived conditions (**Supplementary Figure 7E,F**) (Chapter 2). Interestingly, it has recently been shown that FCCP can induce uncoupled respiration through the activity of the ADP/ATP translocase (AAC), which transports ATP out of the mitochondria in exchange for ADP transport into the mitochondria (Bertholet, 2022). Thus, FCCP may stimulate mitochondrial respiration via its protonophore activity and by supporting ATP synthase activity (at 1 μM FCCP, 20% of FCCP-induced respiration is reported to be dependent on AAC activity (Bertholet, 2022)).

Based on these data, we hypothesized that a difference that could explain why some cells elevate mitochondrial respiration and others do not following serine withdrawal is ATP synthase activity. We postulated that cells that do elevate mitochondrial respiration in response to serine deprivation also increase ATP synthase activity, allowing complex I activity to increase. An alternative possibility is that another mechanism independent of ATP synthase, such as an uncoupling protein, enables sufficient proton output that does not constrain complex I activity. We distinguished between these two possibilities by measuring oligomycin-insensitive mitochondrial respiration. Because oligomycin is an ATP synthase inhibitor, we can uncover whether the rise in mitochondrial respiration following serine withdrawal is coupled or uncoupled to ATP synthase activity. We first measured mitochondrial respiration in intact cells grown with and without serine. We find that the rise in mitochondrial respiration following serine withdrawal is ablated upon exposure to oligomycin, suggesting an increase in mitochondrial respiration that involves ATP synthase (**Figure 5D).** Cells that do not increase mitochondrial respiration following serine withdrawal have lower oligomycin-insensitive respiration compared to serine-replete cells, consistent with a greater dependence on ATP synthase activity (**Supplementary Figure 7G**). We next asked whether the increase in coupled mitochondrial respiration is related to complex I activity. Thus, we permeabilized cells and measured complex I-linked respiration following oligomycin addition. Indeed, the increase in complex I-linked respiration is oligomycin-sensitive, arguing that complex I activity is coupled ATP synthase activity (**Figure 5E**). Together, these data suggest that the increase in mitochondrial respiration following serine withdrawal is coupled to ATP

synthase activity, consistent with our hypothesis that ATP synthase activity can support the increase in complex I that occurs following serine withdrawal.

Interestingly, while FCCP does not alter serine synthesis and confers no proliferative advantage to cells that endogenously raise mitochondrial respiration following serine withdrawal, FCCP still elevates mitochondrial respiration, demonstrating their mitochondria are not at maximal respiratory capacity (Chapter 2). However, FCCP minimally alters the cellular NAD+/NADH ratio (**Supplementary Figure 7E**), consistent with FCCP not affecting serine synthesis and proliferation. Additionally, FCCP equally depolarizes the mitochondrial membrane potential in all cells following serine withdrawal (**Supplementary Figure 7F**). Why FCCP raises mitochondrial respiration and depolarizes the mitochondrial membrane potential without affecting the NAD+/NADH ratio is unclear. We speculate that complex I activity may be at maximal activity following serine withdrawal, consistent with sufficient ATP synthase activity enabling an increase in complex I activity. If complex I activity was limited by the mitochondrial membrane potential, FCCP and gramicidin D treatment would increase in the NAD+/NADH ratio. Additionally, because there are multiple other electron inputs to the ETC, FCCP may still increase oxygen consumption rates independent of complex I. Together, this suggests that serine deprivation stimulates maximum complex I activity in cells with sufficient ATP synthase activity (mitochondrial responders) or suppresses ATP synthase to constrain complex I activity in other cells (mitochondrial non-responders) (**Figure 6A-E**).

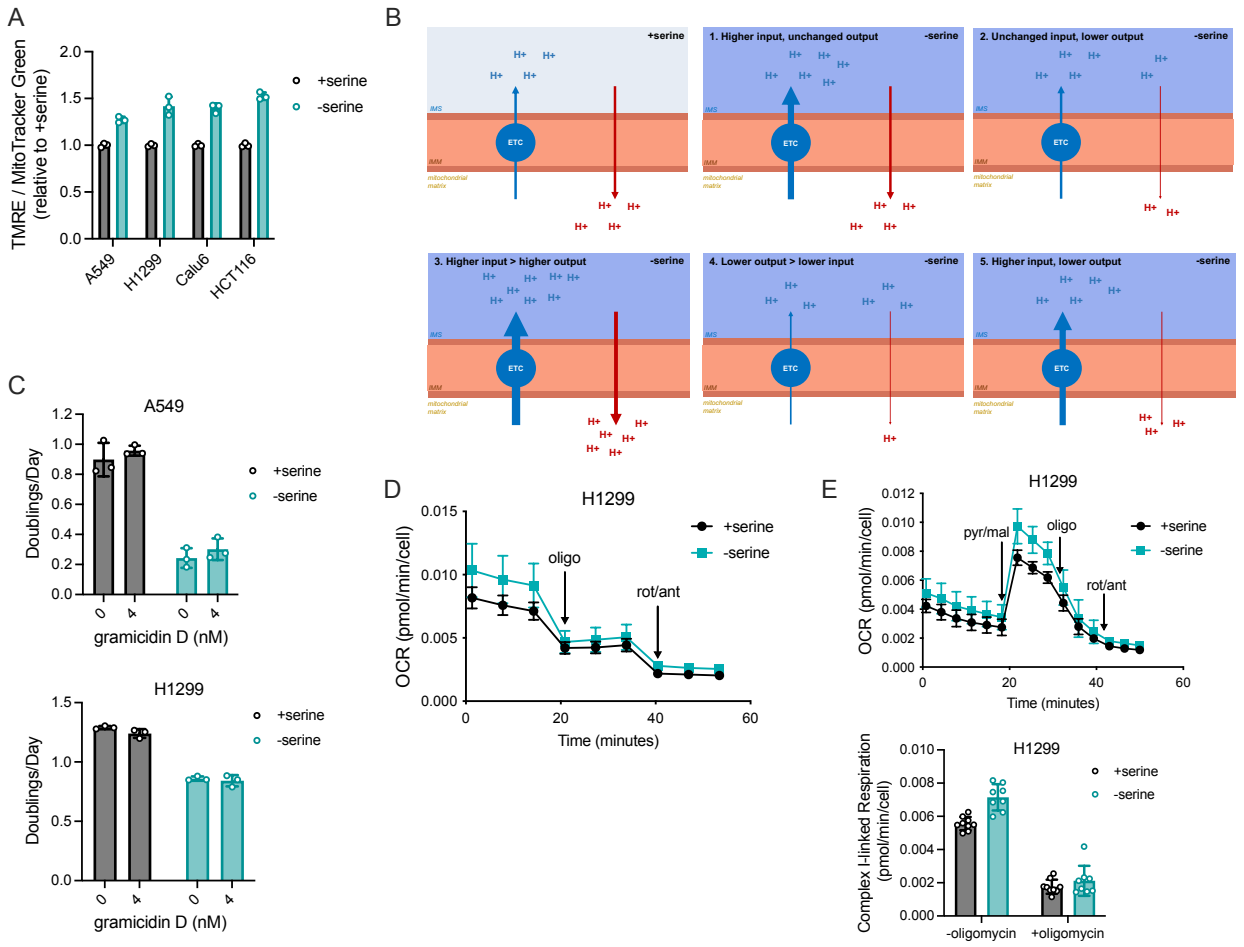

Figure 5. Serine withdrawal differentially impacts ATP synthase to influence complex I activity and mitochondrial membrane potential. (A) TMRE staining normalized to MitoTracker Green staining in cells grown with and without serine for 24 hours. Median TMRE values were normalized to median MitoTracker Green values and then normalized by values obtained in +serine conditions per each cell type, n=3. **(B)** Models depicting possible processes that lead to mitochondrial membrane hyperpolarization upon serine deprivation. **(C)** Proliferation rate of cells treated with gramicidin D with and without serine over three days. **(D)** Oxygen consumption rates (OCR) in intact cells starved of serine for 24 hours and then treated with oligomycin (oligo). Rotenone and antimycin A (rot/ant) were added to ablate all mitochondrial OCR (n=15). **(E)** OCR of permeabilized cells starved of serine for 24 hours. Injections: pyruvate and malate (pyr/mal), oligomycin (oligo), and rotenone with antimycin A (rot/ant), n=8-10. Top: kinetic OCR measurements, Bottom: quantification of complex I-linked respiration before and after oligomycin injection adjusting for residual OCR (OCR remaining after rot/ant injection). All values are means ± SD.

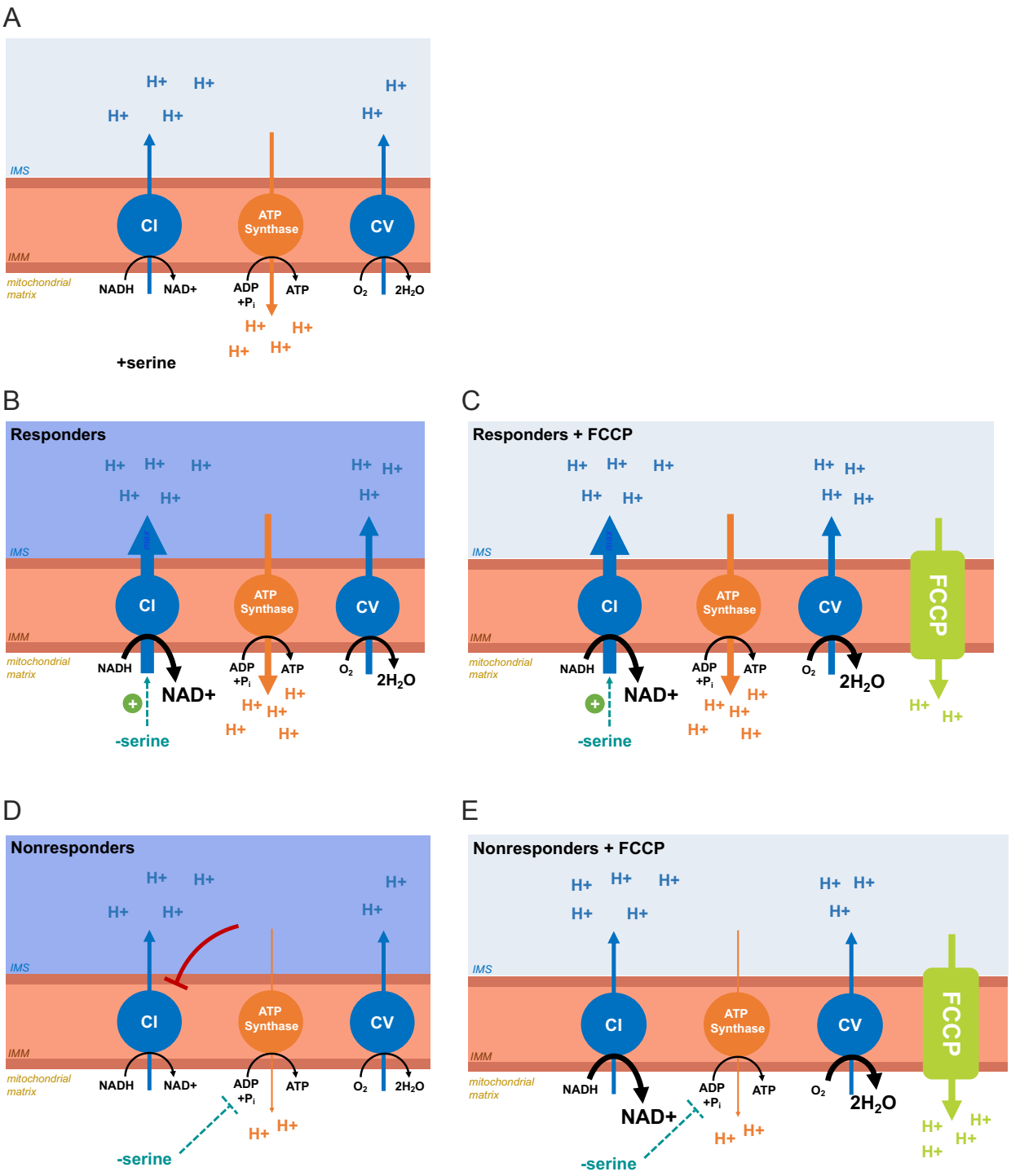

Figure 6. Model detailing the mitochondrial differences between cells that do and do not increase mitochondrial respiration following serine withdrawal. (A) In complete culture conditions, Complex I (CI) oxidizes NADH to NAD+, delivering electrons to the electron transport chain (ETC), and pumping protons into the mitochondrial intermembrane space (IMS). Electrons from the ETC are transferred to oxygen by complex IV (CIV), pumping protons into the IMS. The proton gradient in the IMS is harnessed by ATP synthase to convert ADP into ATP, allowing protons to travel down their gradient. **(B)** Upon serine deprivation in responder cells, complex I

activity is increased, allowing for greater NAD+ regeneration and proton transfer into the IMS. Increased ETC activity leads to greater oxygen consumption by CIV, which also transfers protons into the IMS. The elevation in oxygen consumption is coupled to ATP synthase activity, allowing maximal complex I activity by releasing protons down their gradient to produce ATP. **(C)** When responder cells are starved of serine, complex I activity is at maximal capacity. Thus upon FCCP treatment, complex I activity does not change, but facilitates increased uncoupled mitochondrial respiration, depolarizing the mitochondrial membrane and raising oxygen consumption. **(D)** In non-responder cells, we propose that serine deprivation blunts ATP synthase activity, leading to mitochondrial membrane hyperpolarization that constrains complex I activity. This causes no change in the NAD+/NADH ratio and oxygen consumption. **(E)** However, FCCP can induce uncoupled mitochondrial respiration, depolarizing the mitochondrial membrane and lifting the constraint on complex I activity to increase the NAD+/NADH ratio that can support greater serine synthesis.

Discussion

Cancer cells rely on *de novo* serine synthesis in serine-depleted environments to continue proliferating. The cellular NAD+/NADH ratio in part determines flux through *de novo* serine synthesis, influencing the ability for cancer cells to proliferate when serine levels are low. Cancer cells differ in their endogenous cellular NAD+/NADH ratio in response to varying nutrient environments. In this study, we aimed to uncover how serine depletion leads some cancers to raise mitochondrial respiration (responder cells) while having no impact on the mitochondrial respiration of other cancers (non-responder cells). By examining the activity of different electron carrier producing pathways upon serine withdrawal, we find that only responder cells have elevated pyruvate dehydrogenase activity, while both responder and non-responders cells have unaltered oxidative TCA cycle activity. Interestingly, we find that responder cells demonstrate higher reductive TCA cycle activity and potentially greater malic enzyme activity. It is striking that proportional elevation of reductive carboxylation and malic enzyme activity is redox neutral, where reductive carboxylation regenerates an NADP+ equivalent while malic enzyme consumes an NADP+ equivalent. Given that serine synthesis is constrained by

NAD+ availability, it is possible that serine deprived cells may bypass NAD+ consumption by malate dehydrogenase in the oxidative TCA cycle if malate is instead converted to pyruvate, which can re-enter the TCA cycle as acetyl-CoA to continue TCA cycle activity. This would avoid consuming an NAD+ equivalent which could be utilized for serine synthesis. Alternatively, as serine is required for glutathione synthesis and NADPH generation through the one carbon cycle, serine deprivation can lead to decreased glutathione and NADPH production (DeNicola, 2015; Lewis, 2014; Maddocks, 2013; Zhang, 2021; Zhou, 2017). Potentially, one adaptation to loss of NADPH production through the one carbon cycle is to increase malic enzyme-derived NADPH at a greater rate than IDH-mediated NADPH consumption. Why an elevation in reductive carboxylation and malic enzyme activity would occur in cells that elevate mitochondrial respiration upon serine deprivation and not others is not clear. The malic enzyme-mediated bypass of malate dehydrogenase may be due to saturation of the malate-aspartate shuttle in cells with elevated mitochondrial respiration. If complex I activity is maximal upon serine deprivation, it is also possible that malate-aspartate shuttle activity would correspondingly increase given the higher complex I capacity for NADH equivalents. In this way, perhaps the glutamine-derived pyruvate, which is likely generated by malic enzyme activity, is “overflow” metabolism as a consequence of maximal complex I and subsequently malate-aspartate shuttle activity.

It is not known what drives the increase in complex I activity in response to serine deprivation. The data argue that the elevation in complex I activity is not due to greater substrate availability. Instead, our data suggests that complex I activity is modulated directly by serine or a serine-derived metabolite. If complex I activity were modulated by

NADH production from elevated serine synthesis, PHGDH overexpression would increase, not decrease mitochondrial respiration as we observed. The ability to titrate down mitochondrial respiration activity simply by dose-dependently increasing serine availability (Chapter 2) would argue that complex I is directly or indirectly responsive to serine availability, not a signaling pathway downstream of serine availability, which we would predict might lead to a step function-like relationship. From our knowledge, it has not been shown that complex I activity can be directly regulated by a non-substrate metabolite. Curiously, structures of complex I suggest that the rotenone-inhibited subunit of complex I has homology with the electron input module of formate dehydrogenases, which convert formate to carbon dioxide (Efremov, 2012). As serine is needed for the production of formate, it would be interesting to uncover whether complex I itself is sensitive to formate levels or other one carbon cycle metabolites. Additionally, serine availability can impact mitochondrial morphology, which influences ETC activity (Gao, 2018; Yao, 2019), and could impact electron transport chain assembly, which has previously been shown to modulate complex I activity (Lucas, 2018).

Our data allude to a significant role of ATP synthase in modulating complex I activity. ATP synthase activity is modulated by ATP turnover. Because serine is important for purine nucleotide synthesis, it is possible that cells have different capacities to generate ADP to influence ATP synthase capacity, as serine deprivation decreases adenine nucleotides (AMP, ADP, and ATP) (DeNicola, 2015; Diehl, 2019; Labuschagne, 2014; Maddocks, 2013; Maddocks, 2016; Ngo, 2020). Additionally, a major regulator of ATP synthase activity is the ability to transport ATP out of the mitochondria and ADP into the mitochondria through ADP/ATP translocases, which release protons from the

mitochondrial intermembrane space into the matrix to influence the mitochondrial membrane potential (Bertholet, 2019). Moreover, because serine activates pyruvate kinase M2 (PKM2), which converts phosphoenolpyruvate to pyruvate and produces an ATP, serine deprivation suppresses pyruvate kinase M2 and decreases ATP production (Chaneton, 2012). Different PKM2 expression and/or activity could differentially influence mitochondrial ATP synthesis. Together, varying abilities to mediate ADP/ATP exchange, as well as differences in adenine nucleotide production and consumption, could lead to differences in ATP synthase function, affecting complex I activity, the NAD+/NADH ratio, and serine synthesis.

Acknowledgements

We thank members of the Vander Heiden lab for helpful discussions, particularly Muhammad Munim. This research was supported by the National Cancer Institute of the NIH under award number F30CA268633 (SMC) and award numbers R35CA242379, R01CA201276, and P30CA14051 (MGVH). MGVH also acknowledges support from a Faculty Scholar grant from the Howard Hughes Medical Institute, SU2C, a division of the Entertainment Industry Foundation, the Lustgarten Foundation, the MIT Center for Precision Cancer Medicine, and the Ludwig Center at MIT.

Material and Methods

Cell Culture Experiments

Cell lines were maintained in Dulbecco's Modified Eagle's Medium (DMEM) without sodium pyruvate (Corning 50-013-PC) supplemented with sodium bicarbonate

(Sigma S6014) and 10% heat-inactivated Fetal Bovine Serum (FBS). All cells were cultured at 37°C with 5% CO_2, tested for mycoplasma contamination regularly, and confirmed negative before experimentation.

Proliferation Assays

Cells were plated in six-well plates in 2ml of DMEM with 10% heat-inactivated FBS at an initial seeding density of 40,000 cells. Cells were permitted to settle overnight, and cells on a six-well dish were counted to calculate the starting cell number at the start of the experiment. For all remaining plates, cells were washed three times with 1ml of 1X PBS and 2ml of treatment media was added to each well. All treatment media was made with 10% dialyzed FBS. Serine-free medium was made by adding a mix of amino acids (Sigma Aldrich) at DMEM concentrations lacking serine and glycine to DMEM with low glucose, without pyruvate, and amino acids (US Biological D9800-13-50L). Glucose and glycine were supplemented for a final concentration for 25mM and 0.4mM, respectively. Three days after the initial treatment, cells were quantified using a Cellometer (Nexcelom Bioscience) or cells were quantified using a sulforhdamine B (SRB) (Sigma Aldrich 230162) colorimetric assay. All SRB measurements are normalized to a blank. Proliferation rates were calculated with the following formula:

Doublings per day = log_2(final cell count / initial cell count) / (total # of treatment days)

NAD+/NADH Measurements

NAD+/NADH measurements were performed using the NAD/NADH-Glo Assay (Promega G9072) with a modified version of manufacturer instructions as previously reported (Sullivan, 2015). Cells were plated at an initial seeding density of 20,000 cells

(A549, H1299, HCT116) or 40,000 cells (Calu6, MDA-MB-231). Cells were permitted to settle overnight. The next day, cells were washed once with 1X PBS and then incubated with 2ml of treatment media for the indicated times prior to preparation of cell extracts. For extraction, cells were washed once in ice cold 1X PBS and extracted in 100 µl ice-cold 1% dodecyltrimethylammonium bromide (DTAB) in 0.2N NaOH diluted 1:1 with 1X PBS. Each sample was flash-frozen in liquid nitrogen and immediately stored at -80°C. To measure NADH, 10 µl of sample was moved to PCR tubes, diluted with 10 µl of DTAB, and incubated at 75 °C for 30 min, where basic conditions selectively degrade NAD+. To measure NAD+, 10 µl of the samples was moved to PCR tubes containing 30 µl DTAB and 20 µl 0.4 N HCl and incubated at 60°C for 15 min, where acidic conditions selectively degrade NADH. Samples were then allowed to equilibrate to room temperature and quenched by neutralizing with 20 µl 0.25 M Tris in 0.2 N HCl (for NADH) or 20 µl 0.5 M Tris base (for NAD+). Manufacturer instructions were followed thereafter to measure NAD+/NADH using a luminometer (Tecan Infinite M200Pro). A standard curve with representative samples was done with each assay to confirm that NAD+ and NADH measurements were in the linear range of detection.

Oxygen Consumption Measurements

An Agilent Seahorse Bioscience Extracellular Flux Analyzer (XFe96) was used to measure oxygen consumption rates (OCR). Cells were plated at 20,000 – 40,000 cells per well in a Seahorse Bioscience 96-well plate in 80 µl of DMEM without pyruvate supplemented with 10% heat-inactivated FBS. Cells were not plated on the perimeter of the plate to avoid edge effects. The following day, cells were washed twice with 180 µl of treatment media supplemented with 10% of dialyzed FBS before incubating cells with 180

µl of treatment media for the indicated time prior to OCR data acquisition. The day before OCR data acquisition, the XFe96 cartridge was hydrated by submerging the sensor cartridge in 200 µl of sterile water per well of the utility plate. Parafilm was wrapped around the perimeter of the cartridge to avoid evaporation. The XFe96 cartridge was then incubated in a 37°C non-CO_2 incubator overnight. The next day, at least two hours before data acquisition, the water in the utility plate was replaced with 200 µl of the Agilent XF Calibrant per well and the sensory cartridge was submerged and returned to the 37°C non-CO_2 incubator until OCR was ready to be measured. To measure oxygen consumption from permeabilized cells, we followed manufacturer's protocols (Agilent Seahorse XF Plasma Membrane Permeabilizer). In brief, after indicated treatment, cells were washed three times with warm 1X mitochondrial assay buffer (220mM mannitol, 70mM sucrose, 10mM KH_2PO_4, 5mM $MgCl_2$, 2mM HEPES, 1mM EGTA, 0.2% w/v fatty acid free BSA) before addition of XF PMP (1nM final, Agilent p/n 102504-100) and adenosine 5'-diphosphate (ADP) monopotassium salt dihydrate (4mM final, Sigma Aldrich 72696-48-1) to begin permeabilization. Cell were incubated with XF PMP and ADP for thirty minutes before the start of the assay. To measure complex-I linked respiration, pyruvic acid (10mM final, Sigma Aldrich 107360) and malic acid (1mM final, Sigma Aldrich M1000) were injected. To measure oligomycin-insensitive respiration, oligomycin A (1.5uM final, Sigma Aldrich 75351) was injected onto cells. After OCR data acquisition, six to eight wells per treatment condition were collected for cell number quantification (Cellometer) to normalize OCR values. Basal OCR was calculated by subtracting residual OCR, the OCR remaining following the addition of rotenone and

antimycin A (final concentration of 2 μM). Complex I-linked respiration was calculated by subtracting residual OCR from OCR after pyruvic acid and malic acid addition.

Kinetic U-^{13}C-Glucose and U-^{13}C-Glutamine Isotope Tracing Experiments

Cells were seeded at 150,000 cells per well in a six-well plate in 2ml of DMEM without pyruvate supplemented with 10% heat-inactivated FBS. The following day, cells were washed once with 1ml of 1X PBS and then incubated in 2ml of treatment media supplemented with 10% dialyzed FBS for the indicated treatment time and when metabolic steady state is reached. Two hours before the start of the kinetic isotope tracing, media on cells was exchanged with fresh treatment media mirroring the same conditions of the tracing medium with unlabeled glucose and glutamine. Before the initiation of the kinetic isotope tracing, cells were washed three times with 1X PBS and then cultured with 1 ml of tracing medium containing 10 mM of U-^{13}C-glucose (Cambridge Isotope Laboratories, CLM-481-0) or 2 mM of U-^{13}C-glutamine (Cambridge Isotope Laboratories, CLM-1822) for the appropriate time points. Following incubation, cells were washed twice with ice cold blood bank saline as quickly as possible and lysed with 500 μl of ice cold 80% HPLC-grade methanol (Sigma Aldrich, 646377) in HPLC-grade water (Sigma Aldrich, 270733) with 1 μg per 400 μl norvaline (Sigma, N7627) to use as an internal extraction standard. Lysates were then vortexed at 4°C at maximum speed for ten minutes and then spun down at 4°C at maximum speed for thirty minutes. The supernatant was collected and then dried under nitrogen gas to prepare for metabolic analysis.

Gas Chromatography-Mass Spectrometry (GC-MS) Polar Metabolite Measurements

Dried samples were derivatized by adding 16 µl of methoxamine reagent (Thermo Fisher, TS-45950) and incubated for an hour at 37°C followed by addition of 20 µl of *N*-*tert*-butyldimethylsilyl-*N*-methyltrifluoroacetamide with 1% *tert*-butyldimethylchlorosilane (Sigma 375934) and incubation of two hours at 60°C. Samples were then centrifuged at maximum speed for ten minutes, and 20 µl of supernatant was used for analysis. Following derivatization, samples were analyzed using a DB-35MS column (30 m × 0.25 mm i.d. × 0.25 µm, Agilent J&W Scientific) in an Agilent 7890 gas chromatograph coupled to an Agilent 5975C mass spectrometer (GC–MS).

Cell Line Generation

Cell lines overexpressing either EGFP or human PHGDH were generated via lentiviral infection. pLJM1-EGFP was obtained from Addgene (Addgene plasmid # 19319). pLJM1-PHGDH was constructed using pLJM1-Empty (Addgene plasmid # 91980) as a backbone. pLJM1-Empty was digested using NheI and EcoRI and gel purified. PHGDH insertion was amplified with the following oligonucleotide primers, where the capitalized sequence denotes PHGDH homology:

PHGDH F: agtgaaccgtcagatccggctagcgccaccATGGCTTTTGCAAATCTGCG

PHGDH R: tactgccatttgtctcgaggtcgagaattcTTAGAAGTGGAACTGGAAGGCT

PHGDH insert was gradient PCR amplified using Phusion High-Fidelity DNA polymerase (NEB M0530) from 60 to 70°C and gel purified. Digested pLJM1-Empty and amplified PHGDH insert were assembled via Gibson Assembly, and the resulting plasmid was transformed, and validated by Sanger sequencing. Lentiviral production was done by transfecting constructs into LentiX293T cells with Mirus Transit293T (Mirus Bio MIR2700) following manufacturer's protocol. Briefly, 800,000 cells were plated per

well in a 6 well plate in DMEM-pyruvate media with 10% heat-inactivated FBS. The next day, cells were transfected with 1.6 µg vector (either pLJM1-EGFP or pLJM1-PHGDH), 800 ng of pMDLg (Addgene plasmid # 12251) packaging plasmid, 400 ng of pMD2.G (Addgene plasmid # 12259) envelope plasmid, and 400 ng of pRSV-REV (Addgene plasmid # 12253) in OptiMEM (Thermo Fisher Scientific 31985070). DNA transfection mix was incubated with cells for 24 hours before harvesting virus. Sub-confluent cells were infected with 1 ml of virus-containing media in each well of a 6 well plate with polybrene (8 µg/ml, EMD Millipore TR-1003-G). 24 hours after infection, selection with puromycin (Sigma Aldrich P7255) began. All experiments with generated cell lines were conducted on a polyclonal cell population.

Immunoblotting

Cells were washed with ice cold 1X PBS and lysed in cold RIPA buffer containing Halt Protease and Phosphatase Inhibitor Cocktail (Thermo Scientific 78442). Lysates were clarified by rocking samples for thirty minutes at 4°C and then spun at maximum speed for ten minutes for collection of supernatant. Protein concentration was calculating using the BCA Protein Assay (Pierce, 23225) with BSA as a standard. Lysates were resolved by SDS-PAGE using NuPAGE 4-12% Bis-Tris Protein Gels and run at 100V. Proteins were transferred onto nitrocellulose membranes via wet transfer at 100V. Membranes were blocked in 5% BSA in TBST before incubating membranes with primary antibodies at 4°C overnight (HSP90 [1:1000] Cell Signaling Technology 4874; Vinculin [1:1000] Cell Signaling Technology 13901S; PHGDH [1:1000] Sigma Aldrich HPA021241; OxPhos Rodent Cocktail [1:1000] Thermo Fisher 45-8099). The next day, membranes were washed three times with TBST at room temperature and then incubated in

secondary antibodies for one hour at room temperature. The secondary antibody used was anti-rabbit IgG horseradish peroxidase-linked antibody (1:4000 dilution; Cell Signaling Technologies, 7074S) or anti-mouse IgG horseradish peroxidase-linked antibody (1:4000, 7076S).

TMRE and MitoTracker Green Staining

Cells were plated at a density of 150,000 cells per well in a six-well plate in 2ml of DMEM-pyruvate media supplemented with 10% heat-inactivated FBS. Cells were allowed to settle overnight. The next day, cells were treated as indicated. Following treatment, cells were co-stained with 50nM of TMRE (tetramethylrhodamine, ethyl ester) (Thermo Fischer T669) and 20nM of MitoTracker Green FM (Invitrogen M7514) for 20 minutes. Following staining, media was aspirated, cells were washed with 1ml of 1XPBS, and trypsinized and collected in complete media with TMRE and MitoTracker Green. Cells were spun down for 3 minutes at 1,000rpm and resuspended in 1ml of 1XPBS with indicated concentrations of TMRE and MitoTracker Green before flow cytometry analysis on a FACSCanto II (BD Biosciences). Data processing was conducted using FlowJo V10.6.1.

References

Abbott, K.L., Ali, A., Reinfeld, B.I., Deik, A., Subudhi, S., Landis, M.D., Hongo, R.A., Young, K.L., Kunchok, T., Nabel, C.S., Crowder, K.D., Kent, J.R., Madariaga, M.L.L., Jain, R.K., Beckermann, K.E., Lewis, C.A., Clish, C.B., Muir, A., Rathmell, K., Rathmell, J.C., Vander Heiden, M.G. (2023). Metabolite profiling of human renal cell carcinoma reveals tissue-origin dominance in nutrient availability. bioRxiv *https://doi.org/10.1101/2023.12.24.573250*.

Banh, R.S., Biancur, D.E., Yamamoto, K., Sohn, A.S.W., Walters, B., Kuljanin, M., Gikandi, A., Wang, H., Mancias, J.D., Schneider, R.J., Pacold, M.E., Kimmelman, A.C.

(2020). Neurons Release Serine to Support mRNA Translation in Pancreatic Cancer. Cell *183*, 1202-1218. 10.1016/j.cell.2020.10.016.

Bao, X.R., Ong, S.-E., Goldberger, O., Peng, J., Sharma, R., Thompson, D. A., Vafai, S. B., Cox, A. G., Marutani, E., Ichinose, F., Goessling, W., Regev, A., Carr, S. A., Clish, C. B., & Mootha, V. K. (2016). Mitochondrial dysfunction remodels one-carbon metabolism in human cells. eLife *5*. https://doi.org/10.7554/elife.10575.

Bertholet, A.M., Chouchani, E. T., Kazak, L., Angelin, A., Fedorenko, A., Long, J. Z., Vidoni, S., Garrity, R., Cho, J., Terada, N., Wallace, D. C., Spiegelman, B. M., & Kirichok, Y. (2019). H+ transport is an integral function of the mitochondrial ADP/ATP carrier. Nature *571*, 515–520. https://doi.org/10.1038/s41586-019-1400-3.

Bertholet, A.M., Natale, A.M., Bisignano, P., Suzuki, J., Fedorenko, A., Hamilton, J., Brustovestky, T., Kazak, L., Garrity, R., Chouchani, E.T., Brustovetsky, N., Grabe, M., Kirichok, Y. (2022). Mitochondrial uncouplers induce proton leak by activating AAC and UCP1. Nature *606*, 180-187. 10.1038/s41586-022-04747-5.

Brown, G.C. (1992). Control of respiration and ATP synthesis in mammalian mitochondria and cells. Biochemical Journal *284*, 1-13. 10.1042/bj2840001.

Chance, B., Williams, G.R. (1955a). Respiratory Enzymes in Oxidative Phosphorylation. Journal of Biological Chemistry *217*, 409-427.

Chance, B., Williams, G.R. (1955b). Respiratory Enzymes in Oxidative Phosphorylation VI. The Effects of Adenosine Diphosphate on Azide-Treated Mitochondria. Journal of Biological Chemistry *221*, 477-489.

Chaneton, B., Hillman, P., Zheng, L., Martin, A.C.L., Maddocks, O.D.K., Chokkathukalam, A., Coyle, J.E., Jankevics, A., Holding, F.P., Vousden, K.H., Frezza, C., O'Reilly, M., Gottlieb, E. (2012). Serine is a natural ligand and allosteric activator of pyruvate kinase M2. Nature *491*, 458-462. 10.1038/nature11540.

Commisso, C., Davidson, S.M., Soydaner-Azeloglu, R.G., Parker, S.J., Kamphorst, J.J., Hackett, S., Grabocka, E., Nofal, M., Drebin, J.A., Thompson, C.B., Rabinowitz, J.D., Metallo, C.M., Vander Heiden, M.G., Bar-Sagi, D. (2013). Macropinocytosis of protein is an amino acid supply route in Ras-transformed cells. Nature *497*, 633-637. 10.1038/nature12138.

Crowley, L.C., Christensen, M.E., Waterhouse, N.J. (2016). Measuring Mitochondrial Transmembrane Potential by TMRE Staining. Cold Spring Harbor Protocols *2016*. 10.1101/pdb.prot087361.

Datta, R., Sivanand, S., Lau, A.N., Florek, L.V., Barbeau, A.M., Wyckoff, J., Skala, M.C., Vander Heiden, M.G. (2022). Interactions with stromal cells promote a more oxidized

cancer cell redox state in pancreatic tumors. Science Advances *8*. 10.1126/sciadv.abg6383.

DeNicola, G.M., Chen P., Mullarky E., Sudderth, J.A., Hu, Z., Wu, D., Tang, H., Xie, Y., Asara J.M., Huffman, K.E., Wistuba, I.I., Minna, J.D., DeBerardinis, R.J., Cantley, L.C. (2015). NFR2 regulates serine biosynthesis in non-small cell lung cancer. Nature Genetics *47*, 1475-1481. 10.1038/ng.3421.

Diehl, F.F., Lewis, C.A., Fiske, B.P., Vander Heiden, M.G. (2019). Cellular redox state constrains serine synthesis and nucleotide production to impact cell proliferation. Nature Metabolism *1*, 861-867. doi:10.1038/s42255-019-0108-x.

Divakaruni, A.S., Jastroch, M. (2022). A practical guide for the analysis, standardization, and interpretation of oxygen consumption measurements. Nature Metabolism *4*, 978-994. 10.1038/s42255-022-00619-4.

Ducker, G.S., Rabinowitz, J.D. (2018). One-Carbon Metabolism in Health and Disease. Cell Metabolism *25*, 27-42. 10.1016/j.cmet.2016.08.009.

Efremov, R.G., Sazanov, L.A. (2012). The coupling mechanism of respiratory complex I — A structural and evolutionary perspective. Biochimica Et Biophysica Acta (BBA) - Bioenergetics *1817*, 1785-1795. https://doi.org/10.1016/j.bbabio.2012.02.015.

Ferraro, G.B., Ali, A., Luengo, A., Kodack, D.P., Deik, A., Abbott, K.L., Bezwada, D., Blanc, L., Prideaux, B., Jin, X., Possada, J.M., Chen, J., Chin, C.R., Amoozgar, Z., Ferreira, R., Chen, I., Naxerova, K., Ng, C., Westermark, A.M., Duquette, M., Roberge, S., Lindeman, N.I., Lyssiotis, C.A., Nielsen, J., Housman, D.E., Duda, D.G., Brachtel, E., Golub, T.R., Cantley, L.C., Asara, J.M., Davidson, S.M., Fukumua, D., Dartois, V.A., Clish, C.B., Jain, R.K., Vander Heiden, M.G. (2021). Fatty acid synthesis is required for breast cancer brain metastasis. Nature Cancer *in press*. 10.1038/s43018-021-00183-y.

Gao, X., Lee, K., Reid, M.A., Sanderson, S.M., Qiu, C., Li, S., Liu, J., Locasale, J.W. (2018). Serine Availability Influences Mitochondrial Dynamics and Function through Lipid Metabolism. Cell Reports *22*, 3507-3520. https://doi.org/10.1016/j.celrep.2018.03.017.

García-Martínez, L.F., Appling, D.R. (1993). Characterization of the Folate-Dependent Mitochondrial Oxidation of Carbon 3 of Serine. Biochemistry *32*, 4671-4676. https://doi.org/10.1021/bi00068a027.

Gui, D.Y., Sullivan, L.B., Luengo, A., Hosios, A.M., Bush, L.N., Gitego, N., Davidson, S.M., Freinkman, E., Thomas, C.J., Vander Heiden, M.G. (2016). Environment dictates dependence on mitochondrial complex I for NAD+ and aspartate production and determines cancer cell sensitivity to metformin. Cell Metabolism *24*, 716-727. 10.1016/j.cmet.2016.09.006.

Herbig, K., Chiang, E., Lee, L., Hills, J., Shane, B., Stover, P.J. (2002). Cytoplasmic serine hydroxymethyltransferase mediates competition between folate-dependent deoxyribonucleotide and S-adenosylmethionine biosynthesis. Journal of Biological Chemistry *277*, 38381-38389. 10.1074/jbc.M205000200.

Jin, X., Demere, Z., Nair, K., Ali, A., Ferraro, G. B., Natoli, T., Deik, A., Petronio, L., Tang, A. A., Zhu, C., Wang, L., Rosenberg, D., Mangena, V., Roth, J., Chung, K., Jain, R. K., Clish, C. B., Vander Heiden, M. G., & Golub, T. R. (2020). A metastasis map of human cancer cell lines. Nature *588*, 331-336. https://doi.org/10.1038/s41586-020-2969-2.

Kamphorst, J.J., Nofal, M., Commisso, C., Hackett, S.R., Lu, W., Grabocka, E., Vander Heiden, M.G., Miller, G., Drebin, J.A., Bar-Sagi, D., Thompson, C.B., Rabinowitz, J.D. (2015). Human pancreatic cancer tumors are nutrient poor and tumor cells actively scavenge extracellular protein. Cancer Research *75*, 544-553. 10.1158/0008-5472.CAN-14-2211.

Kory, N., Wyant, G.A., Prakash, G., uit de Bos, J., Bottanelli, F., Pacold, M.E., Ham Chan, S., Lewis, C.A., Wang, T., Keys, H.R., Guo, Y., Sabatini, D.M. (2018). SFXN1 is a mitochondrial serine transporter required for one-carbon metabolism. Science *362*. 10.1126/science.aat9528.

Labuschagne, C.F., van den Broek, N.J.F., Mackay, G.M., Vousden, K.H., Maddocks, O.D.K. (2014). Serine, but not glycine, supports one-carbon metabolism and proliferation of cancer cells. Cell Reports *7*. doi: 10.1016/j.celrep.2014.04.045.

Lewis, C.A., Parker, S.J., Fiske, B.P., McCloskey, D., Gui, D.Y., Green, C.R., Vokes N.I., Feist, A.M., Vander Heiden, M.G., Metallo, C.M. (2014). Tracing Compartmentalized NADPH Metabolism in the Cytosol and Mitochondria of Mammalian Cells. Molecular Cell *55*, 253-263. https://doi.org/10.1016/j.molcel.2014.05.008.

Li, Z., Ji, B.W., Dixit, P.D., Lien, E.C., Tchourine, K., Hosios, A.M., Abbott, K.L., Westermark, A.M., Gorodetsky, E.F., Sullivan, L.B., Vander Heiden, M.G., Vitkup, D. (2022). Cancer cells depend on environmental lipids for proliferation when electron acceptors are limited. Nature Metabolism *4*, 711-723. https://doi.org/10.1038/s42255-022-00588-8.

Lucas, S., Chen, G., Aras, S., Wang, J. (2018). Serine catabolism is essential to maintain mitochondrial respiration in mammalian cells. Life Science Alliance *1*. e201800036.

Luengo, A., Li, Z., Gui, D. Y., Sullivan, L. B., Zagorulya, M., Do, B. T., Ferreira, R., Naamati, A., Ali, A., Lewis, C. A., Thomas, C. J., Spranger, S., Matheson, N. J., & Vander Heiden, M. G. (2021). Increased demand for NAD+ relative to ATP drives aerobic glycolysis. Molecular Cell *81*, 691–707. https://doi.org/10.1016/j.molcel.2020.12.012.

Lunetti, P., Damiano, F., De Benedetto, G., Siculella, L., Penetta, A., Muto, L., Paradies, E., Marobbio, C.M.T., Dolce, V., Capobianco, L. (2016). Characterizations of Human and Yeast Mitochondrial Glycine Carriers with Implications for Heme Biosynthesis and Anemia. Journal of Biological Chemistry *291*, 19746-19759. 10.1074/jbc.M116.736876.

Maddocks, O.D.K., Berkers, C. R., Mason, S. M., Zheng, L., Blyth, K., Gottlieb, E., & Vousden, K. H. (2013). Serine starvation induces stress and p53-dependent metabolic remodelling in cancer cells. Nature *493* (*7433*), 542–546. https://doi.org/10.1038/nature11743.

Maddocks, O.D.K., Labuschagne, C.F., Adams, P.D., Vousden, K.H. (2016). Serine Metabolism Supports the Methionine Cycle and DNA/RNA Methylation through De Novo ATP Synthesis in Cancer Cells. Molecular Cell *61*, 210-221. 10.1016/j.molcel.2015.12.014.

Minton, D.R., Nam, M., McLaughlin, D.J., Shin, J., Bayraktar, E.C., Alvarez, S.W., Sviderskiy, V.O., Papagiannakopoulos, T., Sabatini, D.M., Birsoy, K., Possemato, R. (2018). Serine Catabolism by SHMT2 is Required for Proper Mitochondrial Translation Initiation and Maintenance of Formylmethionyl-tRNAs. Molecular Cell *69*, 610-621. https://doi.org/10.1016/j.molcel.2018.01.024.

Muir, A., Vander Heiden, M.G. (2018). The nutrient environment affects therapy. Science *360*, 962-963. 10.1126/science.aar5986.

Ngo, B., Kim, E., Osorio-Vasquez, V., Doll, S., Bustraan, S., Liang, R. J., Luengo, A., Davidson, S. M., Ali, A., Ferraro, G. B., Fischer, G. M., Eskandari, R., Kang, D. S., Ni, J., Plasger, A., Rajasekhar, V. K., Kastenhuber, E. R., Bacha, S., Sriram, R. K., … Pacold, M. E. (2020). Limited Environmental Serine and Glycine Confer Brain Metastasis Sensitivity to PHGDH Inhibition. Cancer Discovery *10*, 1352–1373. https://doi.org/10.1158/2159-8290.cd-19-1228.

Nobes, C.D., Lakin-Thomas, P.L., Brand, M.D. (1989). The contribution of ATP turnover by the Na+/K+-ATPase to the rate of respiration of hepatocytes: Effects of thyroid status and fatty acids. Biochimica Et Biophysica Acta (BBA) - Bioenergetics *976*, 241-245. https://doi.org/10.1016/S0005-2728(89)80236-1.

Pavlova, N.N., Thompson, C.B. (2017). The Emerging Hallmarks of Cancer Metabolism. Cell Metabolism *23*, 27-47. 10.1016/j.cmet.2015.12.006.

Perera, R.M., Stoykova, S., Nicolay, B.N., Ross, K.N., Fitamant, J., Boukhali, M., Lengrand, J., Deshpande, V., Selig, M.K., Ferrone, C.R., Settleman, J., Stephanopoulos, G., Dyson, N.J., Zoncu, R., Ramaswamy, S., Haas, W., Bardeesy, N. (2015). Transcriptional control of autophagy-lysosome function drives pancreatic cancer metabolism. Nature *524*, 361-365. 10.1038/nature14587.

Perry, S.W., Norman, J.P., Barbieri, J., Brown, E.B., Gelbard, H.A. (2018). Mitochondrial membrane potential probes and the proton gradient: a practical usage guide. BioTechniques *50*. https://doi.org/10.2144/000113610.

Possemato, R., Marks, K.M., Shaul, Y.D., Pacold, M.E., Kim, D., Birsoy, K., Sethumadhavan, S., Woo, H., Jang, H.G., Jha, A.K., Chen, W.W., Barrett, F.G., Stransky, N., Tsun, Z., Cowley, G.S., Barretina, J., Kalaany, N.Y., Hsu, P.P., Ottina, K., Chan, A.M., Yuan, B., Garrayway, L.A., Root, D.E., Mino-Kenudson, M., Brachtel, E.F., Driggers, E.M., Sabatini, D.M. (2011). Functional genomics reveals serine synthesis is essential in PHGDH-amplified breast cancer. Nature *476*, 346-350. 10.1038/nature10350.

Sullivan, L.B., Gui, D.Y., Hosios, A.M., Bush, L.N., Freinkman, E., Vander Heiden M.G. (2015). Supporting Aspartate Biosynthesis Is an Essential Function of Respiration in Proliferation Cells. Cell *162*, 552-563. doi:10.1016/j.cell.2015.07.017.

Sullivan, M.R., Danai, L. V., Lewis, C. A., Chan, S. H., Gui, D. Y., Kunchok, T., Dennstedt, E. A., Vander Heiden, M. G., Muir, A. (2019a). Quantification of microenvironmental metabolites in murine cancers reveals determinants of tumor nutrient availability. eLife *8*. https://doi.org/10.7554/elife.44235.

Sullivan, M.R., Mattaini, K.R., Dennstedt, E.A., Nguyen, A.A., Reilly, M.F., Meeth, K., Muir, A., Darnell, A.M., Bosenberg, M.W., Lewis, C.A., Vander Heiden, M.G. (2019b). Increased serine synthesis provides an advantage for tumors arising in tissues where serine levels are limiting. Cell Metabolism *29*, 1410-1421,e1414. doi: 10.1016/j.cmet.2019.02.015.

Tibbetts, A.S., Appling, D.R. (2010). Compartmentalization of Mammalian Folate-Mediated One-Carbon Metabolism. Annual Review of Nutrition *30*, 57-81. 10.1146/annurev.nutr.012809.104810.

Vander Heiden, M.G., Chandel, N.S., Schumacker, P.T., Thompson, C.B. (1999). Bcl-xL Prevents Cell Death following Growth Factor Withdrawal by Facilitating Mitochondrial ATP/ADP Exchange. Molecular Cell *3*, 159-167. https://doi.org/10.1016/S1097-2765(00)80307-X.

Yang, L., Carlos Garcia Canaveras, J., Chen, Z., Wang, L., Liang, L., Jang, C., Mayr, J.A., Zhang, Z., Mhergurovich, J.M., Zhan, L., Joshi, S., Hu, Z., McReynolds, M.R., Su, X., White, E., Morscher, R.J., Rabinowitz, J.D. (2020). Serine Catabolism Feeds NADH when Respiration Is Impaired. Cell Metabolism *31*, 809-821. https://doi.org/10.1016/j.cmet.2020.02.017.

Yang, M., Vousden, K.H. (2016). Serine and one-carbon metabolism in cancer. Nature Reviews Cancer *16*, 651-662. 10.1038/nrc.2016.81.

Yao, C., Wang, R., Wang, Y., Kung, C., Weber, J.D., Patti, G.J. (2019). Mitochondrial fusion supports increased oxidative phosphorylation during cell proliferation. eLife *8*. 10.7554/eLife.41351.

Zhang, Z., TeSlaa, T., Xu, X., Zeng, X., Yang, L., Xing, G., Tesz, G.J., Clasquin, M.F., Rabinowitz, J.D. (2021). Serine catabolism generates liver NADPH and supports hepatic lipogenesis. Nature Metabolism *3*, 1608-1620. https://doi.org/10.1038/s42255-021-00487-4.

Zhou, X., He, L., Wu, C., Zhang, Y., Wu, X., Yin, Y. (2017). Serine alleviates oxidative stress via supporting glutathione synthesis and methionine cycle in mice. Molecular Nutrition and Food Research *61*. https://doi.org/10.1002/mnfr.201700262.

Supplementary Figures

Supplementary Figure 1

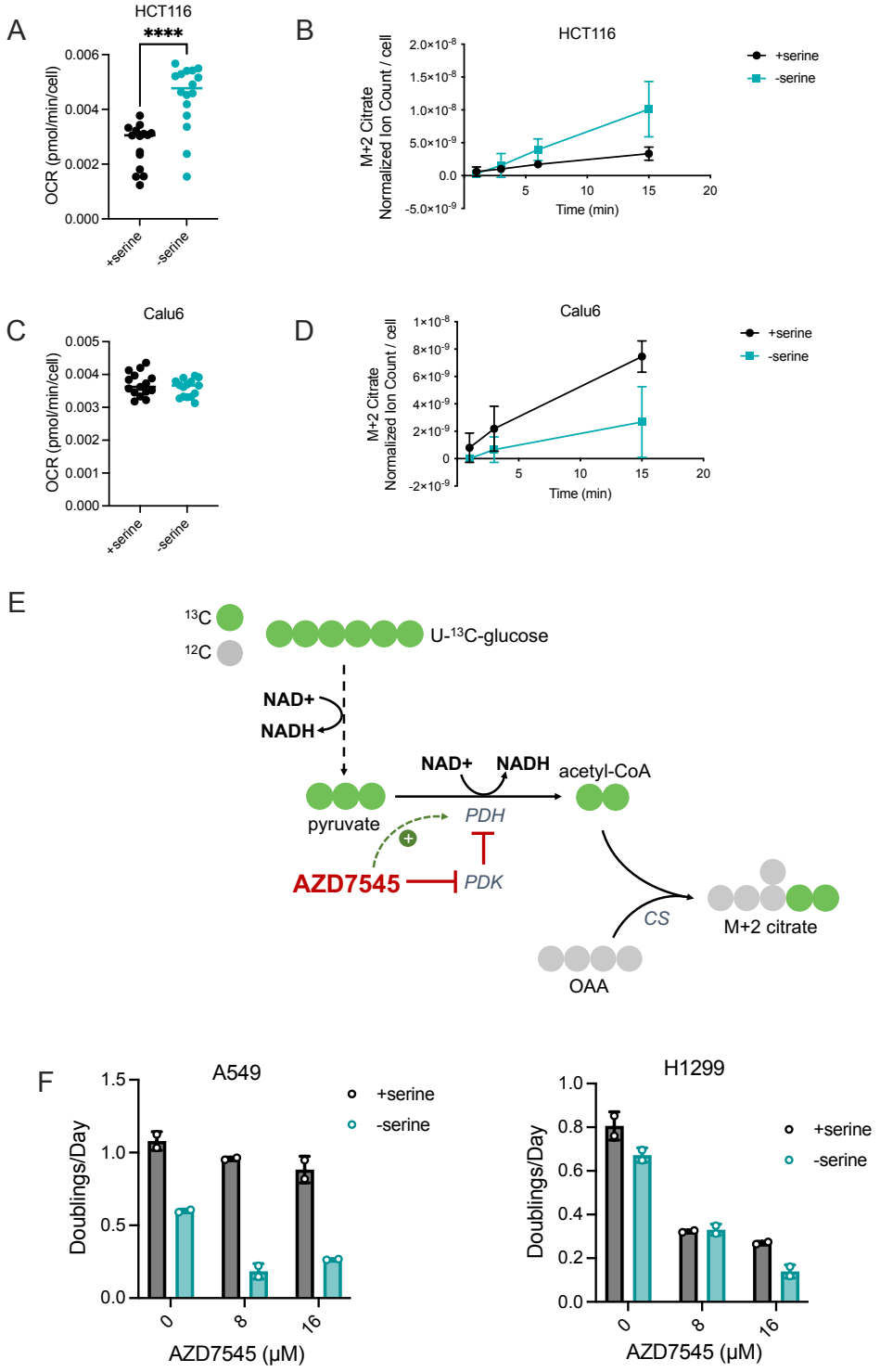

Supplementary Figure 1. Elevated pyruvate dehydrogenase activity does not confer a proliferative advantage in serine-depleted conditions. (**A**) Mitochondrial OCR in HCT116 cells deprived of serine for 24 hours, n=15 ****p<0.001, unpaired t-test. (**B**) Kinetic U-^{13}C-glucose

tracing into citrate in HCT116 cells starved of serine for 24 hours, n=3 (**C**) Mitochondrial OCR in Calu6 cells starved of serine for 24 hours, n=15. (**D**) Kinetic U-^{13}C-glucose tracing into citrate in Calu6 cells starved of serine for 24 hours, n=3. (**E**) Schematic demonstrating U-^{13}C-glucose tracing pattern into citrate and AZD7545 inhibition of pyruvate dehydrogenase kinase (PDK), which suppress pyruvate dehydrogenase (PDH) activity. (**F**) Proliferation rate of cells treated with and without serine with indicated concentrations of AZD7545 over three days, n=2. Values are mean ± SD.

Supplementary Figure 2

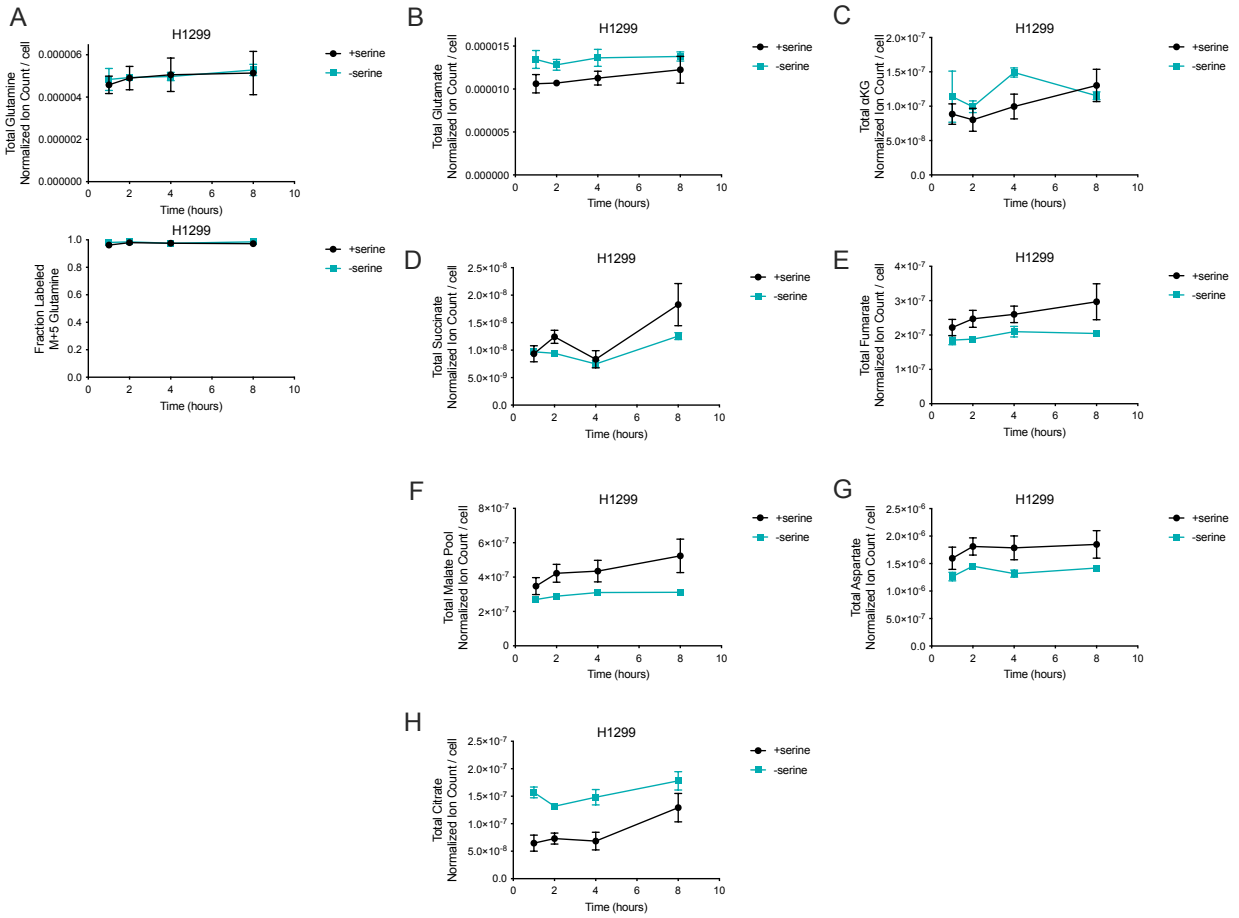

Supplementary Figure 2. Total metabolite pool sizes from U-^{13}C-glutamine tracing in H1299. H1299 cells were deprived of serine for 24 hours before commencing U-^{13}C-glutamine tracing. **(A)** Total glutamine levels (top), fraction of glutamine pool labeled with U-^{13}C-glutamine (bottom) over the course of tracing **(B-H)** Total levels of TCA metabolites over the course of tracing. All values are normalized to external standard norvaline and cell number and denote means ± SD, n=3.

Supplementary Figure 3

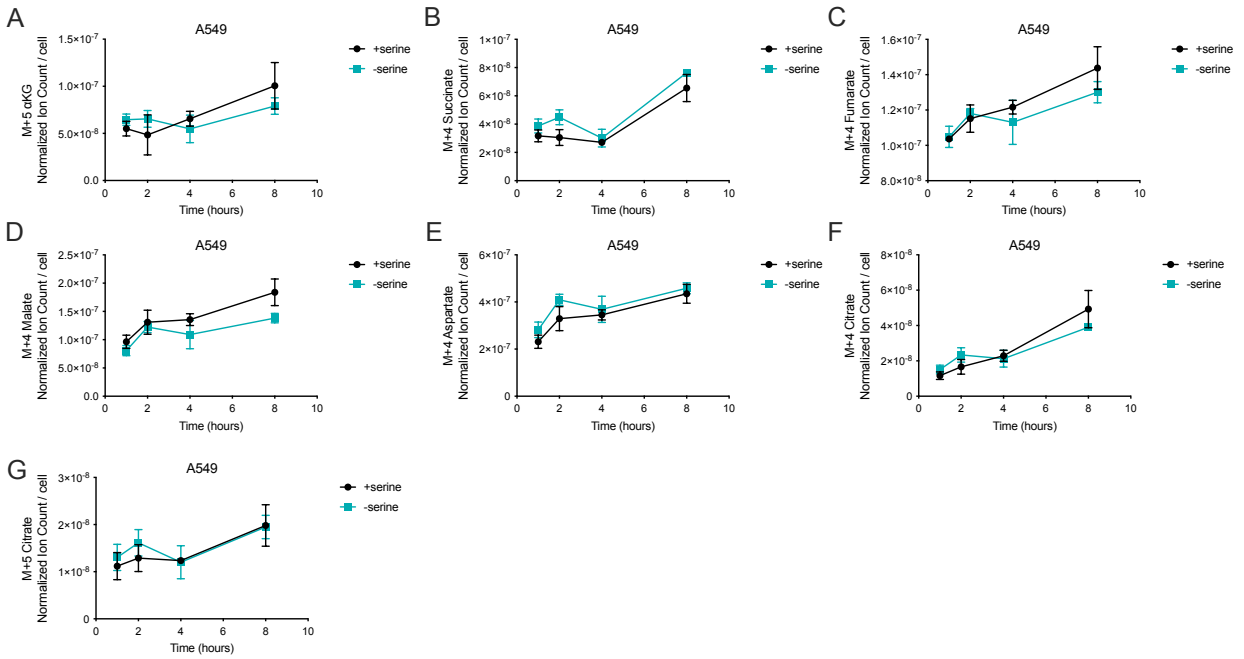

Supplementary Figure 3. TCA cycle activity is unchanged following serine deprivation in A549 cells (A-G) Kinetic U-^{13}C-glutamine tracing into TCA metabolites α-ketoglutarate, succinate, fumarate, malate, aspartate, and citrate in cells deprived of serine for 24 hours. All values are mean of n=3 ± SD.

Supplementary Figure 4

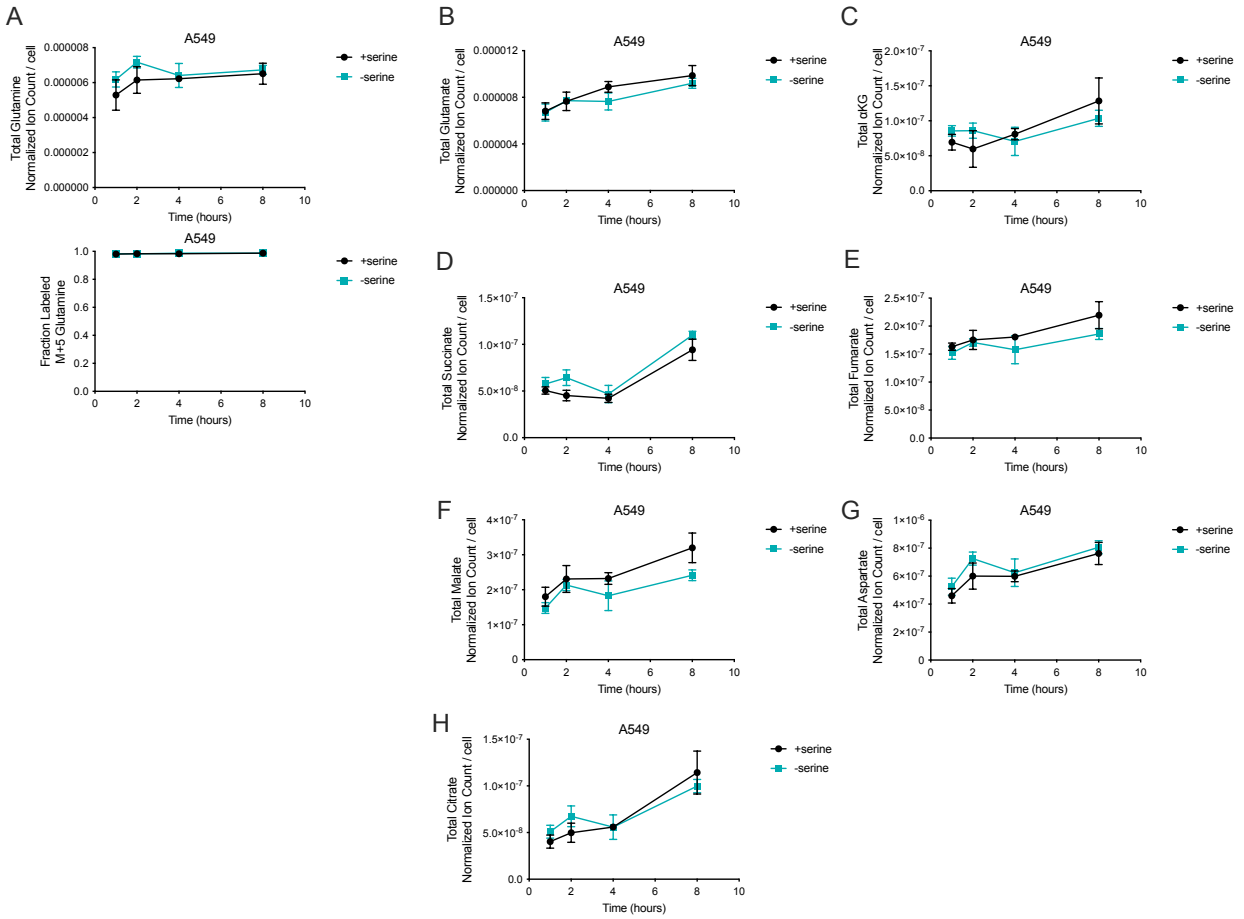

Supplementary Figure 4. Total metabolite pool sizes from U-^{13}C-glutamine tracing in A549. A549 cells were deprived of serine for 24 hours before commencing U-^{13}C-glutamine tracing. **(A)** Total glutamine levels (top), fraction of glutamine pool labeled with U-^{13}C-glutamine (bottom) over the course of tracing **(B-H)** Total levels of TCA metabolites over the course of tracing. All values are normalized to external standard norvaline and cell number and denote means ± SD, n=3.

Supplementary Figure 5

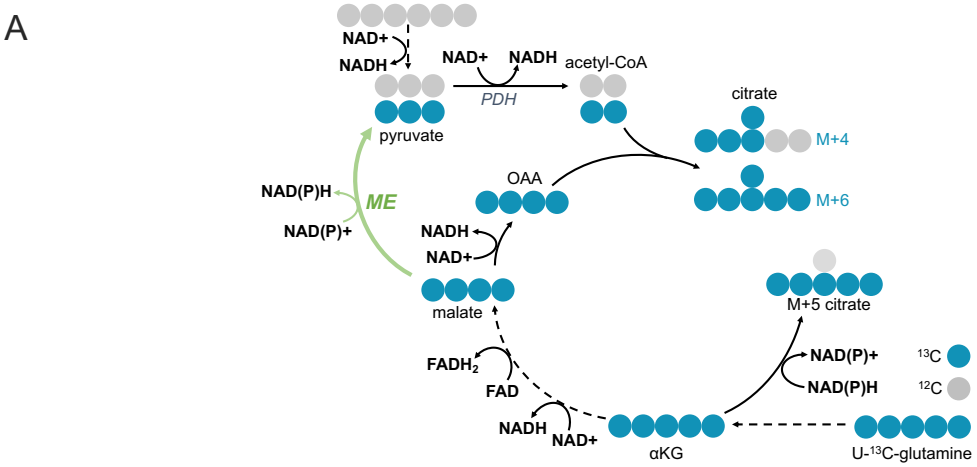

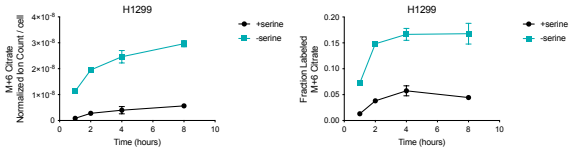

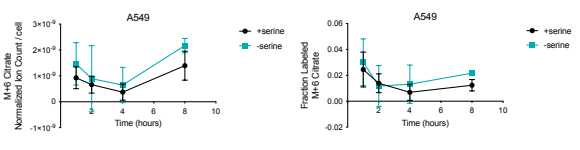

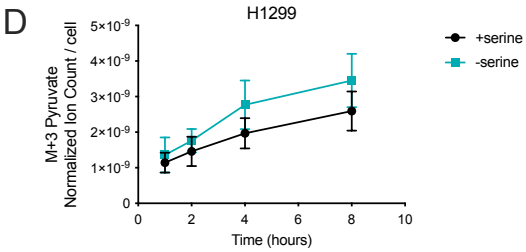

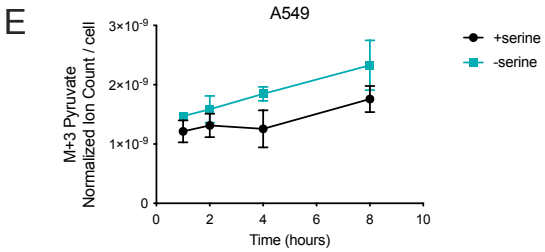

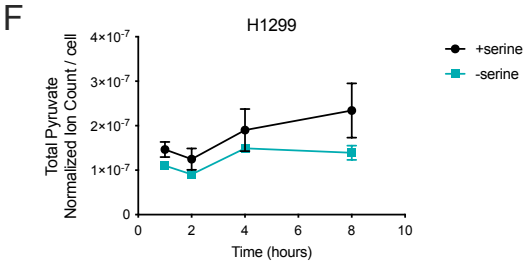

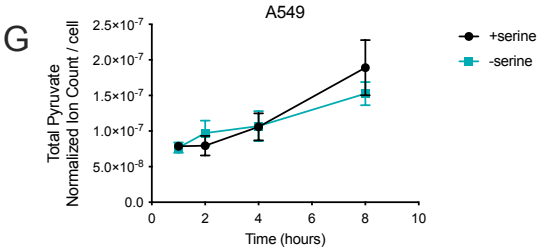

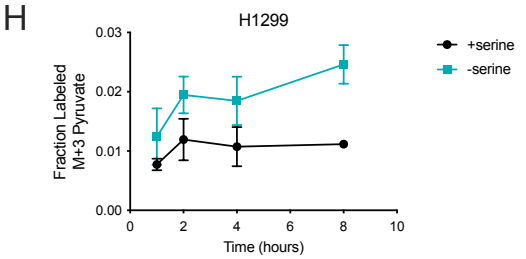

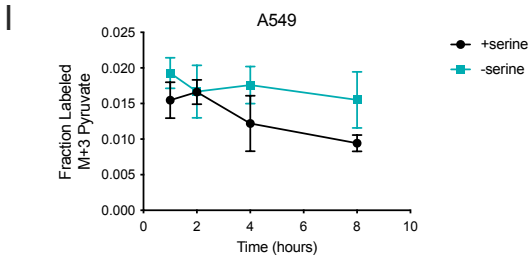

Supplementary Figure 5. H1299 cells deprived of serine produce glutamine-derived pyruvate used for citrate synthesis. (A) Schematic depicting the production of M+6 citrate from U-^{13}C-glutamine, predicted to be due to the conversion of fully labeled malate (M+4) into pyruvate (M+3) by malic enzyme, which requires NADP+. **(B)** H1299 kinetic U-^{13}C-glutamine tracing into M+6 citrate (left), fraction of citrate pool that is M+6 (right). **(C)** A549 kinetic U-^{13}C-glutamine tracing into M+6 citrate (left), fraction of citrate pool that is M+6 (right). **(D-E)** Kinetic U-^{13}C-glutamine tracing into M+3 pyruvate. **(F-G)** Total pyruvate pool over the course of tracing. (**H-I)** Fraction of pyruvate pool fully labeled from glutamine (M+3). Cells were deprived of serine for 24 hours before commencing U-^{13}C-glutamine tracing. All values are normalized to external standard norvaline and cell number and denote means ± SD, n=3.

Supplementary Figure 6

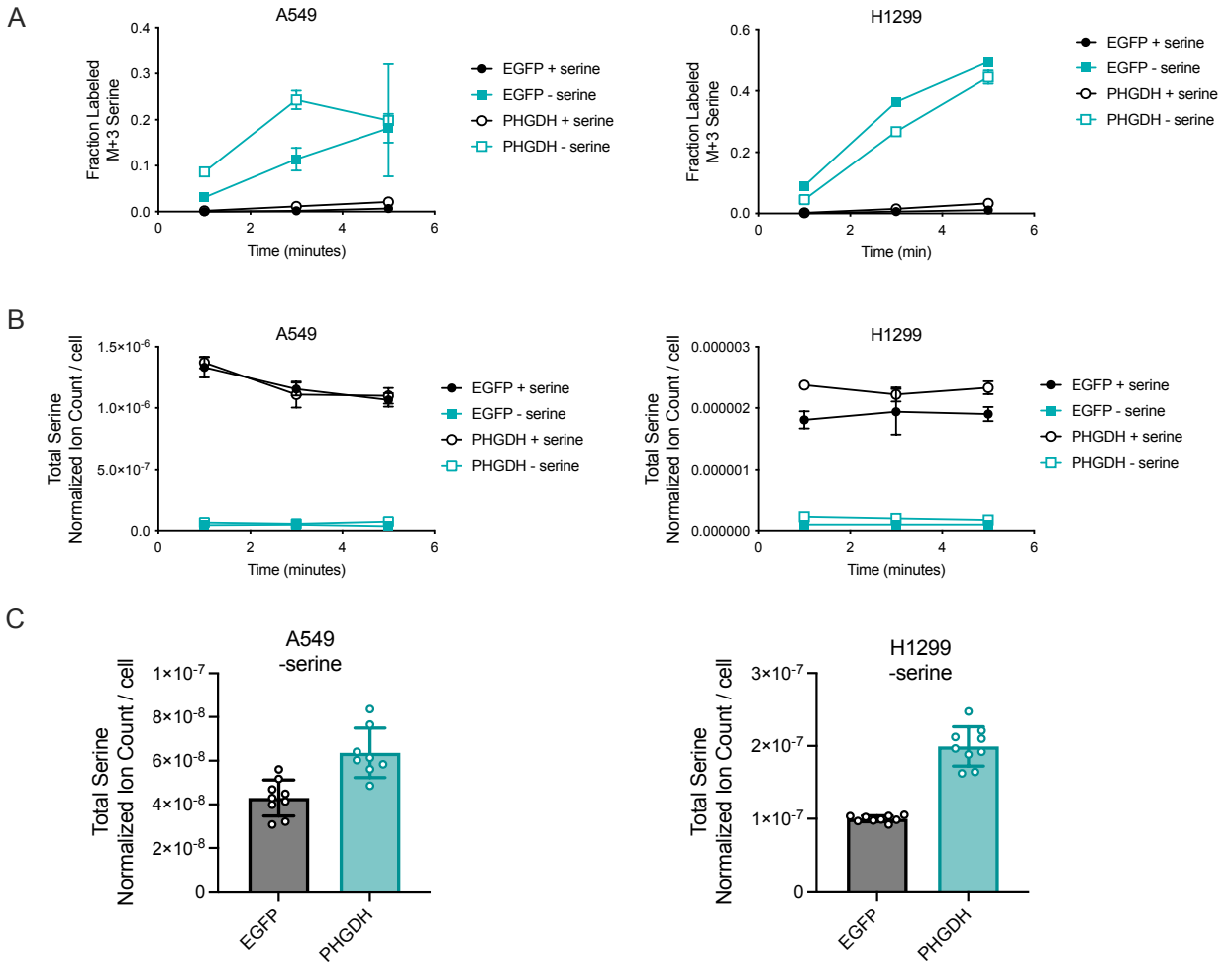

Supplementary Figure 6. PHGDH overexpression elevates serine production and total serine levels following serine withdrawal. (A) U-^{13}C-glucose kinetic tracing into serine displaying the fraction of intracellular serine pool that is synthesized by glucose (M+3) in cells expressing pLJM1-EGFP (EGFP) or pLJM1-PHGDH (PHGDH) after 24 hour serine starvation, n=3. **(B)** Total intracellular serine levels in cells expressing EGFP or PHGDH with and without 24 hours of serine starvation over the course of U-^{13}C-glucose tracing, normalized to external standard norvaline and cell number, n=3. **(C)** Total intracellular serine levels in cells expressing

EGFP or PHGDH after 24 hours of serine starvation only, where each data point is the mean of n=3, and is from each time point over the course of tracing. Values denote means ± SD.

Supplementary Figure 7

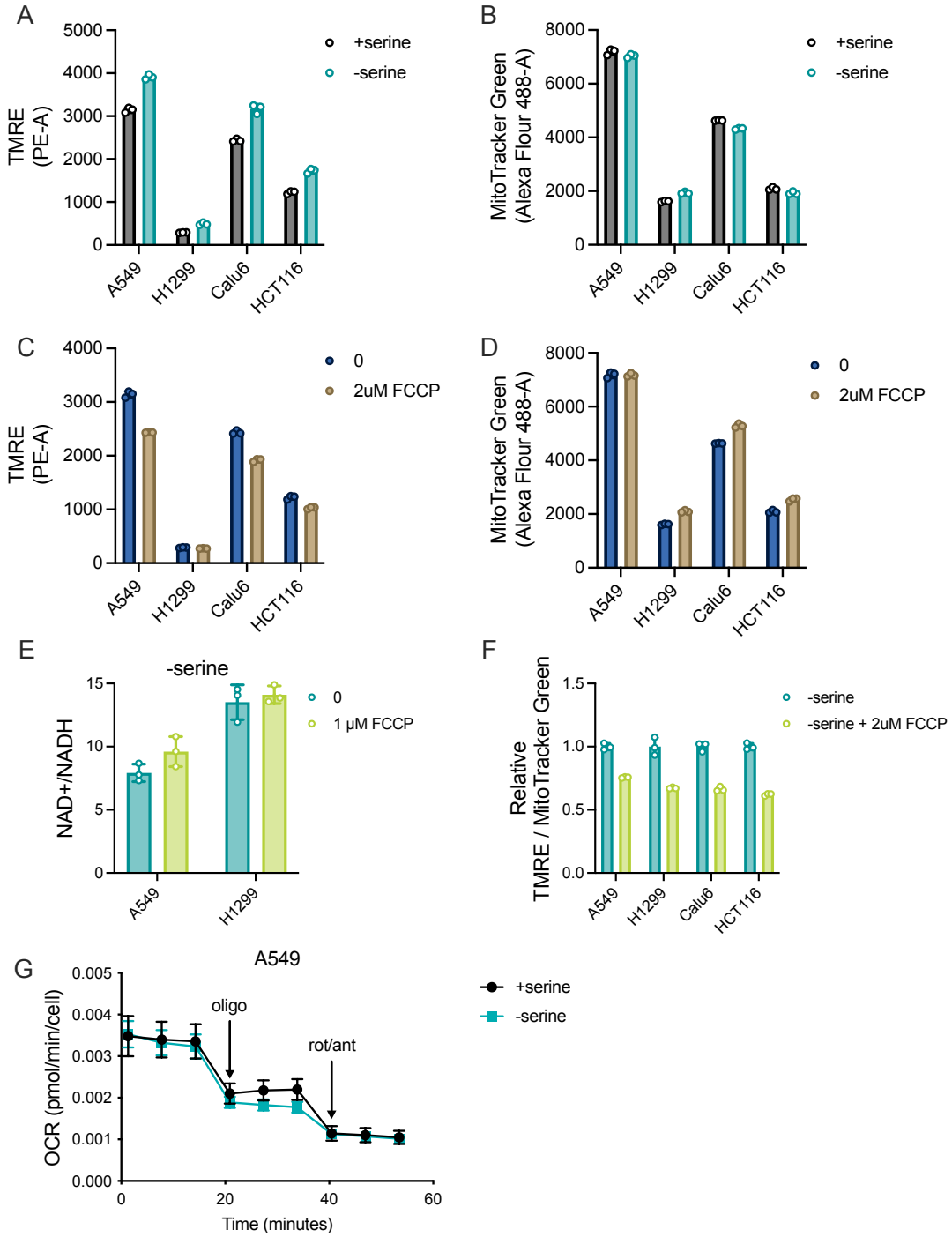

Supplementary Figure 7. Characterizing mitochondrial activity following serine deprivation and FCCP treatment. (A) Raw TMRE median values of cells grown with and without serine for 24 hours, n=3. **(B)** Raw MitoTracker Green median values of cells grown with and without serine for 24 hours, n=3. **(C)** Raw TMRE median values of cells treated with and without 2 μM FCCP for

two hours, n=3. **(D)** Raw MitoTracker Green median values of cells treated with and without 2 μM FCCP for two hours, n=3. **(E)** NAD+/NADH ratios of cells treated with 1 μM FCCP for two hours, n=3. **(F)** TMRE median values normalized to MitoTracker Green media values of cells starved of serine for 24 hours with and without treatment of 2 μM FCCP for two hours. Values are relative to the +serine condition per each cell type, n=3. **(G)** Oxygen consumption rates (OCR) in cells grown with and without serine for 24 hours. Injections: oligomycin (oligo), and rotenone with antimycin A (rot/ant). All values are means ± SD.

Chapter 4: Discussion and Future Studies

Summary

Many dynamic systems require the balance between supply and demand to function. For example, a new restaurant in Cambridge with amazing shrimp cocktail may have a generous supply of fresh shrimp, but if the demand is low, revenue will be strained. A baby guinea pig has a high demand for nutritious Timothy Hay and fresh vegetables to grow into a strong alpha rodent, but if the supply of its food is low, it can only dream of being the strongest in its herd. A tired medical or graduate student has a high academic demand, but their productivity wanes when the supply of sleep or caffeine is limited. Cellular proliferation is not much different, requiring the coordination between metabolic supply and biomass demands for successful cell division.

One important requirement for sufficient biomass synthesis is NAD+ availability. Limited NAD+ availability or a low cellular NAD+/NADH ratio can constrain the synthesis of amino acids (Diehl, 2019; Krall, 2016; Sullivan, 2015), lipids (Li, 2022), and nucleotides (Bao, 2016; Diehl, 2019), influencing metabolic dependencies and proliferation in different nutrient environments. In this dissertation, we aimed to uncover how the cellular NAD+/NADH ratio is determined in varying nutrient environments and whether differences in this process determine biosynthesis capacities across cancers. Specifically, we studied how cancer cells regulate the NAD+/NADH ratio in response to greater serine synthesis demand. We found that the NAD+/NADH ratio is directly proportional to serine synthesis, where tuning the NAD+/NADH ratio higher leads to greater serine synthesis and tuning the NAD+/NADH lower decreases serine synthesis without impacting expression of phosphoglycerate dehydrogenase (PHGDH), the enzyme that catalyzes

the first step in serine synthesis. We reveal that mitochondrial respiration is a major determinant of the cellular NAD+/NADH ratio. Certain cancers raise the NAD+/NADH ratio following serine withdrawal by elevating mitochondrial respiration and other cancers do not alter mitochondrial respiration under the same serine depleted conditions. Accordingly, cells that raise mitochondrial respiration have higher NAD+/NADH ratios, greater serine synthesis, and improved proliferation in serine depleted conditions. We also find that increasing mitochondrial respiration is sufficient to raise the NAD+/NADH ratio and improve serine synthesis. For certain cancers, the change in NAD+/NADH ratio following serine withdrawal was a better predictor for resistance to serine depletion than PHGDH protein expression.

Interestingly we find that mitochondrial respiration is regulated by nutrient conditions differently across cancers. While serine and lipid synthesis are both constrained by the NAD+/NADH ratio, certain cancers only increase mitochondrial respiration in response to serine withdrawal while others only increase mitochondrial respiration in response to lipid withdrawal. To understand what drives the different mitochondrial responses, we investigated the mechanisms that allow certain cells to increase mitochondrial respiration and the NAD+/NADH ratio following serine deprivation. Our data suggest that serine levels regulate complex I-linked respiration independent of electron carrier formation, and the capacity to raise complex I-linked respiration and the NAD+/NADH ratio may be determined by ATP synthase activity. These findings highlight the significance of complex I activity and the NAD+/NADH ratio for influencing biomass production. Better understanding how the NAD+/NADH ratio in different nutrient environments is regulated may reveal novel processes that impact how cancers meet

biomass demands to successfully proliferate in diverse tumor nutrient environments across the body.

Discussion

Different tumor types experience varying microenvironments influenced by their anatomical location (Abbott, 2023b; Sullivan, 2019a), stromal cell population (Apiz Saab, 2023; Datta, 2022; Lyssiotis, 2017), and vascularization (Vaupel, 1989; Wiig, 2012). Yet regardless of the nutrient environment, the biomass demands for proliferation are shared. Given the same nutrient challenges, cancers may have varying abilities to meet the biomass demands due to different expression of transporters (Bhutia, 2016; Chidley, 2023; Chike Nwosu, 2023; Papalazarou, 2023), biosynthetic enzymes levels (DeNicola, 2015; Jin, 2020; Lomelino, 2017; Ngo, 2020; Sullivan, 2019b; 2021), antioxidant defenses (DeNicola, 2011; Maddocks, 2013; Sporn, 2012), among other cell-intrinsic factors. Our work underscores another important determinant of biomass synthesis: control of the NAD+/NADH ratio. Future work further examining the coordination between the NAD+/NADH ratio and oxidized biomass synthesis, NAD+/NADH ratio compartmentalization, regulation of complex I activity and mitochondrial respiration, and the role of the NAD+/NADH ratio in metabolic adaptation and metastasis will shed further light on what nutrient environments can support proliferation for specific cancers.

What oxidative reactions are influenced by changes to the NAD+/NADH ratio?

NAD+ is a required redox cofactor for essential metabolic processes, including glycolysis and the TCA cycle, which are integral pillars for other biosynthetic reactions including lipid and amino acid production. Our data demonstrate that serine withdrawal

can increase the NAD+/NADH ratio, elevating serine synthesis and pyruvate dehydrogenase activity but not affecting NAD+ requiring reactions in the TCA cycle. What determines which reactions are impacted by a given change in NAD+/NADH is nontrivial. In theory, altering the NAD+/NADH ratio should influence the favorability of any reaction that uses these redox cofactors. In a controlled system, measuring how changes in the NAD+/NADH ratio would impact a redox reaction could be accomplished following thermodynamic principles. However, a plethora of variables in the cell could generate specificity for select reactions that are functionally changed by fluctuations in the NAD+/NADH, including the steady state concentration of substrate and products, the K_m for substrates of different enzymes, enzyme expression, and the presence of activators or inhibitors.

The intracellular concentration of NAD(H) lies between 200-500 μM in the cytosol and in the millimolar range in the mitochondria (Canto, 2016) while the K_m for NAD+ of many redox enzymes are much lower. For example, the K_m for NAD+ of PHGDH has been reported to be between 23 – 148 μM (Murtas, 2021; Wang, 2023), 110 μM of pyruvate dehydrogenase (Siess, 1976), and 67 μM of α-ketoglutarate dehydrogenase (Siess, 1976). In fact, analysis of multiple metabolite concentrations and K_m values find that NAD+, as well as ATP, are almost always saturating (Park, 2016). Thus, small fluctuations in the absolute concentration of NAD(H) alone will not have a large effect on reaction rates. However, changes in the relative ratio of NAD+ to NADH levels may have pronounced effects. In a simple system, altering the steady state NAD+/NADH ratio, like changing the concentration of the substrates and products, changes the free energy of the reaction to influence how favorable the reaction is. This alters the steady state

concentrations of products, impacting the favorability of the next reaction that uses these products. Because of the integrated coupling of metabolic reactions, a small perturbation in one set of metabolites could have substantial effects on multiple reactions (Nielsen, 2003). One study reported that increasing the NAD+/NADH ratio can nearly double the free energy drop in glycolysis (Park, 2016). While shifting the NAD+/NADH ratio does not impact the kinetics of the redox reaction (unless altering the ratio influences enzyme function, which has been documented (Pettit, 1975; Shimizu, 2018; Vemuri, 2007)) shifting the equilibrium concentrations of downstream metabolites may impact the rate of other reactions, depending on K_m values.

The tangled metabolic network makes it difficult to determine what phenotype is the chicken versus the egg. The way metabolism has been historically taught has largely given NAD+ the role as a chicken, where the NAD+/NADH ratio would be passively determined by the sum of all NAD+/NADH coupled reactions. While we cannot rule out that increasing serine synthesis demand elevates the NAD+/NADH ratio by shifting fluxes of all other NAD+/NADH coupled reactions, our data suggest that the NAD+/NADH ratio is regulated by mitochondrial respiration to facilitate metabolic pathway activity. In this scenario, the NAD+/NADH ratio is the relative egg and greater serine synthesis (and other oxidation reactions) is the downstream chicken. There is evidence that supports the importance of cellular redox state for determining metabolic fluxes. Engineering redox shifts by expressing bacterial NADH oxidases is sufficient to influence the activity of multiple dehydrogenases in yeast and reduce fermentation (Vemuri, 2007). It is intriguing to consider that physiological changes in nutrient availability is sufficient to alter the NAD+/NADH ratio and influence a specific set of redox reactions, regardless of the

nutrient demand. For example, when serine withdrawal increases the NAD+/NADH ratio, citrate production also increases, despite no change in cellular citrate demand. When lipid withdrawal increases the NAD+/NADH ratio, does serine production also rise when there is abundant extracellular serine? Would more dramatic increases in the NAD+/NADH ratio begin to influence the oxidation reactions in the TCA cycle or another set of redox reactions? Future work could uncover what metabolic redox reactions are affected by specific fluctuations in the cellular NAD+/NADH ratio across diverse nutrient demands.

NAD+/NADH compartmentalization

One aspect that could generate selectivity for which reactions are affected by a given change in the NAD+/NADH ratio is compartmentalization of redox state. In the cytoplasm, the NAD+/NADH ratio is roughly 700:1 while in the mitochondria, it is 8:1 (Williamson, 1967). In our study, we examine the impact of how whole cell changes in the NAD+/NADH ratio impact serine synthesis, which occurs in the cytosol. We link the change in the NAD+/NADH ratio following serine withdrawal to differences in complex I activity. How would changes in the mitochondria and the mitochondrial redox environment influence a redox-sensitive cytosolic reaction? The redox states of the mitochondria and cytosol are linked by the malate-aspartate shuttle and glycerol-3-phosphate shuttle. It has been shown that inhibiting the malate-aspartate shuttle suppresses *de novo* serine synthesis due to decreases in the NAD+/NADH ratio (Broeks, 2023; van Karnebeek, 2019). Additionally, data from genetically encoded NAD+/NADH biosensors find that the mitochondrial and cytosolic redox states are communicated through the malate-aspartate shuttle (Hu, 2021). Given that aspartate efflux out of the mitochondria requires the mitochondrial proton motive force (Lanoue, 1974), the malate-aspartate shuttle is

seemingly unidirectional where cytosolic NADH (i.e., NADH generated by PHGDH) is oxidized by malate dehydrogenase 1 (MDH1) and reducing equivalents in the form of malate are transported into the mitochondria (Borst, 2020). The flux through the malate-aspartate shuttle is dependent on the activity of transamination reactions, dicarboxylate transporters, TCA cycle function, and electron transport chain activity. Thus, increasing mitochondrial respiration in response to serine withdrawal would presumably promote malate-aspartate shuttle activity and cytosolic NADH oxidation by MDH1 and increase the whole cell NAD+/NADH ratio. Currently, there is no direct data showing the malate-aspartate shuttle activity is elevated following serine depletion. However, α-ketobutyrate supplementation, which increases the cellular NAD+/NADH through cytosolic lactate dehydrogenase (Sullivan, 2015), can improve the proliferation of H1299 cells, which endogenously increase mitochondrial respiration following serine withdrawal (**Figure 1**). In contrast, FCCP treatment, which raises the NAD+/NADH ratio through elevating mitochondrial respiration, has no effect on H1299 proliferation in serine depleted environments (Chapter 2). This suggests that the malate-aspartate shuttle may be saturated, which has been observed in tumor cells (Wang, 2022), and limit the cytosolic NADH oxidation needed to support maximal serine synthesis

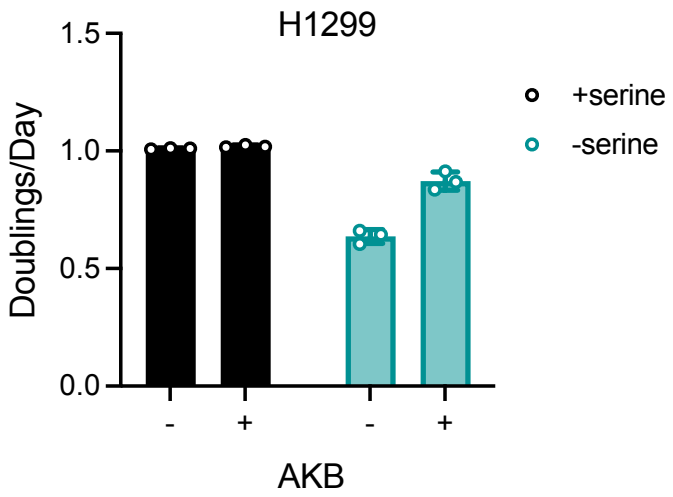

Figure 1. Effect of 1mM AKB treatment on H1299 proliferation in serine depleted conditions.

We found that uncoupling mitochondrial respiration with FCCP led to greater mitochondrial respiration rates, an elevated cellular NAD+/NADH ratio, and improved serine synthesis in cells that do not endogenously increase mitochondrial respiration in response to serine depletion. Because FCCP increases electron transport chain activity, we would predict that the elevated NAD+/NADH ratio is a reflection of mitochondrial redox state. However, the malate-aspartate shuttle requires a sufficient mitochondrial proton force, which is suppressed by uncouplers (Borst, 2020). Thus, it is not clear how greater NAD+ availability in the mitochondria caused by FCCP treatment would meet the increased cytosolic NAD+ demand required to support serine synthesis. Perhaps elevated complex II activity due to FCCP treatment would stimulate the glycerol-3-phosphate shuttle, which relies on the activity of complex II to oxidize $FADH_2$ to FADH, to support cytosolic NADH oxidation.

Uncovering the compartmentalized changes to redox status under different nutrient demands will provide better resolution for how fluctuations in mitochondrial respiration influences the cellular NAD+/NADH ratio and what pathways would be

impacted. At this point, we do not know how increases in mitochondrial respiration impact the mitochondrial NAD+/NADH ratio relative to the cytosolic NAD+/NADH ratio. Additionally, it is unclear whether endogenous increases in the mitochondrial respiration upon serine depletion lead to similar compartmentalized changes to the NAD+/NADH ratio as FCCP treatment despite both raising the whole cell NAD+/NADH ratio. It is not likely that the compartmentalized changes are equal given they impact mitochondria differently; serine deprivation hyperpolarizes the mitochondrial membrane while FCCP depolarizes it (Chapter 3). Investigating how the malate-aspartate shuttle activity is regulated in response to changes in mitochondrial respiration and nutrient demands, and how components of the shuttle differ between cancers can enhance our understanding of how shifts in NAD+ and NADH balance are communicated between cellular compartments to shape cancer metabolic dependencies.

How does nutrient environment modulate complex I activity?

We found that serine deprivation leads to higher complex I-linked mitochondrial respiration in certain cancers. What processes downstream of serine deprivation modify complex I activity? Complex I, also known as the NADH-ubiquinone oxidoreductase, is an L shaped complex containing 44 protein subunits with one segment of the complex extending into the mitochondrial matrix. This segment contains the binding site for NADH, flavin mononucleotide (FMN), and a chain of iron-sulfur clusters. Together, FMN and the iron-sulfur clusters carry electrons from NADH to coenzyme Q, or ubiquinone, and eventually onto a terminal electron acceptor of the mitochondrial ETC. Another portion of complex I is embedded into the inner mitochondrial membrane, which contains one iron-sulfur cluster and the catalytic site for ubiquinone reduction. The membrane arm also

facilitates proton translocation from the mitochondrial matrix into the intermembrane space (Fiedorczuk, 2018; Sharma, 2016; Tuschen, 1990).

Complex I activity can be regulated by changes in its subunit expression and assembly (Bhardwaj, 2021; Dieckmann, 1994). Seven subunits are encoded by the mitochondrial genome and thirty-eight are encoded by the nuclear genome. Of the 44 subunits, 14 are considered the functional core of the enzyme, which include all seven mitochondrially encoded subunits, and are highly conserved across species (Leif, 1993; Sharma, 2016). For successful formation of complex I and other ETC complexes, the nuclear and mitochondrially encoded subunits must properly assemble together. The membrane arm of complex I, which includes all seven mitochondrially encoded complex I subunits, and the matrix arm are independently assembled. How do cells coordinate the expression of nuclear and mitochondrially encoded in response to changes in nutrient environment? Studies examining ETC assembly in yeast shifted from fermentative to respiratory metabolism found that nuclear-encoded ETC mRNA was rapidly induced in response to changes in nutrient availability while mitochondrial ETC messages were induced relatively slower, suggesting that environmental responses impact ETC activity through changes in nuclear subunit expression (Couvillion, 2016). Consistently, changes in cytosolic translation of ETC components due to nutrient shifts impacted mitochondrial translation, but perturbations to mitochondrial translation did not influence nutrient-dependent cytosolic ETC translation, demonstrating that changes in nuclear gene expression can coordinate both mitochondrial and cytosolic translation to facilitate complex I assembly in response to nutrient demands (Couvillion, 2016). Another mechanism that has been implicated in coordinating nuclear and mitochondrial

transcription is ATP levels, where mitochondrial promoters are sensitive to ATP levels, and transcript abundance is correlated with respiration but only when it is coupled to ATP synthase activity (Amiott, 2006). This would be one process by which ATP synthase activity could impact complex I in addition to modulating the mitochondrial membrane potential (Luengo, 2021). In our studies, we measured the expression of NDUF8, a nuclear-encoded complex I subunit, in serine depleted conditions and found no change. However, because complex I is a large molecular machine that requires coordination between two compartments, it is possible that shifts in serine availability could influence complex I expression and assembly to alter its activity.

In addition to assembly of complex I alone, assembly with other ETC complexes and the formation of supercomplexes could modulate respiratory activity (Lapuente-Brun, 2013). Structures for the supercomplex containing complexes I, III, and IV as well as I and III have been elucidated by cryo-electron microscopy (Gu, 2016; Letts, 2016), but their physiological functions have not been fully characterized, and whether they possess physiological functions has been debated. One study finds that supercomplexes are rearranged in response to changes in electron source and nutrient conditions (Greggio, 2017). Another study showed that NADH-dependent respiration can be modified by supercomplex formation and different supercomplexes have separate coenzyme Q pools that alter complex I activity (Calvo, 2020). While the physiological functions of supercomplexes are unclear, examining how electron transport chain assembly and structure in different environments could highlight how mitochondrial respiration is regulated under varying nutrient demands to modify redox state.

Despite the integral metabolic function of complex I, our understanding of how its activity is regulated is nascent and convoluted. Not only is complex I itself a large molecular machine that is influenced by a plethora of variables, but it is also dynamically influenced by other ETC complexes, ATP synthase activity, the mitochondrial membrane potential, and fluctuations of ETC inputs. There remain many unanswered questions relating how changes in nutrient environment regulate mitochondrial respiration.

Cellular NAD+/NADH and metastasis

Nutrient availability differs across tissues. Our data poses the possibility that the NAD+/NADH ratio can influence biomass production and impact metastatic colonization. For example, brain metastases from different tumors were found to upregulate serine synthesis, and promoting serine synthesis enabled metastatic spread to the brain, a serine low environment (Ngo, 2020). Likewise, greater expression of fatty acid synthase was observed in brain metastases from breast tumors to adapt to decreased lipid availability in the brain microenvironment (Ferraro, 2021). Changing the cellular NAD+/NADH ratio could facilitate metabolic adaptation to different tissue sites. However, there are conflicting studies. Despite the importance of mitochondrial respiration for tumor growth (Bajzikova, 2019; Birsoy, 2015; Dong, 2017; King, 1989; Sullivan, 2015; Tan, 2015), one study found that enhancing complex I activity or increasing the NAD+/NADH ratio by providing animals NAD precursors inhibited growth and metastasis of triple negative breast tumors by increasing autophagy (Santidrian, 2013). Another study found that complex I dysfunction promotes tumorigenesis by inducing oxidative stress (Sharma, 2011), though this is at odds with many findings that show oxidative stress suppresses metastasis (Le Gal, 2015; Piskounova, 2016; Tasdogan, 2021). Regardless, these

findings do highlight an important balance that cancer cells must walk when regulating mitochondrial respiration – supporting biomass production in nutrient depleted microenvironments and limiting the production of reactive oxygen species (ROS), which are significantly generated by mitochondria respiration (Gravel, 2014). One process that could facilitate this balance is uncoupling mitochondrial respiration. Uncoupling proteins (UCP) enable higher mitochondrial respiration and complex I activity, yet limit ROS generation (Derdak, 2008; Zhao, 2019), and are highly expressed in certain cancers (Caggiano, 2024). Much is unknown about the exact roles mitochondrial respiration and the cellular NAD+/NADH ratio may play in the formation of metastasis. They likely play heterogenous roles depending on tissue and metastasis site and should be further investigated to increase the resolution of what processes are important for specific tumor types and nutrient environments.

Conclusion

In this dissertation, we investigated how nutrient environment and cellular redox status are coordinated to balance metabolic supply and demand. We have highlighted mitochondrial respiration as a major integrator that could facilitate biomass synthesis upon nutrient changes. Additionally, we have shown that varying capacities to regulate mitochondrial respiration and different endogenous redox states can selectively alter certain oxidation reactions to generate distinct biosynthesis phenotypes across cancers that can explain what nutrient environments are compatible with proliferation. Future work investigating the way cellular redox state shapes metabolic vulnerabilities between cancers will give insight into what constrains or allows metabolic plasticity to improve our understanding of how cancer metabolism promotes malignancy.

References

Abbott, K.L., Ali, A., Reinfeld, B.I., Deik, A., Subudhi, S., Landis, M.D., Hongo, R.A., Young, K.L., Kunchok, T., Nabel, C.S., Crowder, K.D., Kent, J.R., Madariaga, M.L.L., Jain, R.K., Beckermann, K.E., Lewis, C.A., Clish, C.B., Muir, A., Rathmell, K., Rathmell, J.C., Vander Heiden, M.G. (2023). Metabolite profiling of human renal cell carcinoma reveals tissue-origin dominance in nutrient availability. bioRxiv *https://doi.org/10.1101/2023.12.24.573250*.

Amiott, E.A., Jaehning, J.A. (2006). Mitochondrial Transcription Is Regulated via an ATP ‘‘Sensing’’ Mechanism that Couples RNA Abundance to Respiration. Molecular Cell *22*, 329-338. https://doi.org/10.1016/j.molcel.2006.03.031.

Apiz Saab, J.J., Dzierozynski, L.N., Jonker, P.B., AminiTabrizi, R., Shah, H., Elena Menjivar, R., Scott, A.J., Nwosu, Z.C., Zhu, Z., Chen, R.N., Oh, M., Sheehan, C., Wahl, D.R., Rasca di Magliano, M., Lyssiotis, C.A., Macleod, K.F., Weber, C.R., Muir, A. (2023). Pancreatic tumors exhibit myeloid-driven amino acid stress and upregulate arginine biosynthesis. eLife *12*. https://doi.org/10.7554/eLife.81289.

Bajzikova, M., Kovarova, J., Coelho, A.R., Boukalova, S., Oh, S., Rohlenova, K., Svec, D., Hubackova, S., Endaya, B., Judasova, K., Bezawork-Geleta, A., Kluckova, K., Chatre, L., Zobalova, R., Novakova, A., Vanova, K, Ezrova, Z., Maghzal, G.J., Novais, S.M., Olsinova, M., Krobova, L., Jin An, Y., Davidova, E., Nahacka, Z., Sobol, M., Cunha-Oliveira, T., Sandoval-Acuña, C., Strnad, H., Zhang, T., Huynh, T., Serafim, T.L., Hozak, P., Sardao, V.A., Koopman, W.J.H., Ricchetti, M., Oliveira, P.J., Kolar, F., Kubista, M., Truksa, J., Dvorakova-Hortova, K., Pacak, K., Gurlich, R., Stocker, R., Zhou, Y., Berridge, M.V., Park, S., Dong, L., Rohlena, J., Neuzil, J. (2019). Reactivation of Dihydroorotate Dehydrogenase-Driven Pyrimidine Biosynthesis Restores Tumor Growth of Respiration-Deficient Cancer Cells. Cell Metabolism *29*, 399-416. 10.1016/j.cmet.2018.10.014.

Bao, X.R., Ong, S.-E., Goldberger, O., Peng, J., Sharma, R., Thompson, D. A., Vafai, S. B., Cox, A. G., Marutani, E., Ichinose, F., Goessling, W., Regev, A., Carr, S. A., Clish, C. B., & Mootha, V. K. (2016). Mitochondrial dysfunction remodels one-carbon metabolism in human cells. eLife *5*. https://doi.org/10.7554/elife.10575.

Bhardwaj, G., Penniman, C.M., Jena, J., Suarez Beltran, P.A., Foster, C., Poro, K., Junck, T.L., Hinton, A.O., Souvenir, R., Fuqua, J.D., Morales, P.E., Bravo-Sagua, R., Sivitz, W.I., Lira, V.A., Abel, E.D., O’Neill, B.T. (2021). Insulin and IGF-1 receptors regulate complex I–dependent mitochondrial bioenergetics and supercomplexes via FoxOs in muscle. Journal of Clinical Investigation *131*, e146415. 10.1172/JCI146415.

Bhutia, Y.D., Babu, E., Ramachandran, S., Yang, S., Thangaraju, M., Ganapathy, V. (2016). SLC transporters as a novel class of tumour suppressors: identity, function and molecular mechanisms. Biochemical Journal *473*, 1113-1124. 10.1042/BJ20150751.

Birsoy, K., Wang, T., Chen, W.W., Freinkman, E., Abu-Remaileh, M., Sabatini, D.M. (2015). An Essential Role of the Mitochondrial Electron Transport Chain in Cell Proliferation Is to Enable Aspartate Synthesis. Cell *162*, 540-551. https://doi.org/10.1016/j.cell.2015.07.016.

Borst, P. (2020). The malate–aspartate shuttle (Borst cycle): How it started and developed into a major metabolic pathway. IUBMB Life *72*, 2241-2259. 10.1002/iub.2367.

Broeks, M.H., Meijer, N.W.F., Westland, D., Bosma, M., Gerrits, J., German, H.M., Ciapaite, J., van Karnebeek, C.D.M., Wanders, R.J.A., Zwartkruis, F.J.T., Verhoeven-Duif, N., Jans, J.J.M. (2023). The malate-aspartate shuttle is important for de novo serine biosynthesis. Cell Reports *42*. https://doi.org/10.1016/j.celrep.2023.113043.
Caggiano, E.G., Taniguchi, C.M. (2024). UCP2 and pancreatic cancer: conscious uncoupling for therapeutic effect. Cancer and Metastasis Reviews. https://doi.org/10.1007/s10555-023-10157-4.

Calvo, E., Cogliati, S., Hernansanz-Augstin, P., Loureiro-Lopez, M., Guaras, A., Casuso, R.A., Garcia-Marques, F., Acin-Perez, R., Marti-Mateos, Y., Silla-Castro, J.C., Carro-Alvarellos, M., Huertas, J.R., Vazquez, J., Enriquez, J.A. (2020). Functional role of respiratory supercomplexes in mice: SCAF1 relevance and segmentation of the Qpool. Science Advances *6*. 10.1126/sciadv.aba7509.

Canto, C., Menzies, K., Auwerx, J. (2016). NAD+ metabolism and the control of energy homeostasis - a balancing act between mitochondria and the nucleus. Cell Metabolism *22*, 31-53. 10.1016/j.cmet.2015.05.023.

Chidley, C., Darnell, A.M., Gaudio, B.L., Lien, E.C., Barbeau, A.M., Vander Heiden, M.G., Sorger, P.K. (2023). A CRISPRi/a screening platform to study cellular nutrient transport in diverse microenvironments. bioRxiv. https://doi.org/10.1101/2023.01.26.525375.

Chike Nwosu, Z., Gu Song, M., Pasca di Magliano, M., Lyssiotis, C.A., Eun Kim, S. (2023). Nutrient transporters: connecting cancer metabolism to therapeutic opportunities. Oncogene *42*, 711-724. 10.1038/s41388-023-02593-x.

Couvillion, M.T., Soto, I.C., Shipkovenska, G., Churchman, L.S. (2016). Synchronized mitochondrial and cytosolic translation programs. Nature *533*, 499-503. https://doi.org/10.1038/nature18015.

Datta, R., Sivanand, S., Lau, A.N., Florek, L.V., Barbeau, A.M., Wyckoff, J., Skala, M.C., Vander Heiden, M.G. (2022). Interactions with stromal cells promote a more oxidized cancer cell redox state in pancreatic tumors. Science Advances *8*. 10.1126/sciadv.abg6383.

DeNicola, G.M., Chen P., Mullarky E., Sudderth, J.A., Hu, Z., Wu, D., Tang, H., Xie, Y., Asara J.M., Huffman, K.E., Wistuba, I.I., Minna, J.D., DeBerardinis, R.J., Cantley, L.C. (2015). NFR2 regulates serine biosynthesis in non-small cell lung cancer. Nature Genetics *47*, 1475-1481. 10.1038/ng.3421.

DeNicola, G.M., Karreth, F.A., Humpton, T.J., Gopinathan, A., Wei, C., Frese, K., Mangal, D., Yu, K.H., Yeo, C.J., Calhoun, E.S., Scrimieri, F., Winter, J.M., Hruban, R.H., Iacobuzio-Donahue, C., Kern, S.E., Blair, I.A., Tuveson, D.A. (2011). Oncogene-induced Nrf2 transcription promotes ROS detoxification and tumorigenesis. Nature *6*, 106-109. 10.1038/nature10189.

Derdak, Z., Mark, N.M., Beldi, G., Robson, S.C., Wands, J.R., Baffy, G. (2008). The mitochondrial uncoupling protein-2 promotes chemoresistance in cancer cells. Cancer Research *68*, 2813-2819. https://doi.org/10.1158/0008-5472.CAN-08-0053.
Dieckmann, C.L., Staples, R.R. (1994). Regulation of mitochondrial gene expression in Saccharomyces cerevisiae. International Review of Cytology *152*, 145-181. 10.1016/s0074-7696(08)62556-5.

Diehl, F.F., Lewis, C.A., Fiske, B.P., Vander Heiden, M.G. (2019). Cellular redox state constrains serine synthesis and nucleotide production to impact cell proliferation. Nature Metabolism *1*, 861-867. doi:10.1038/s42255-019-0108-x.

Dong, L., Kovarova, J., Bajzikova, M., Bezawork-Geleta, A., Svec, D., Endaya, B., Sachaphibulkij, K., Coelho, A.R., Sebkova, N., Ruzickova, A., Tan, A.S., Kluckova, K., Judasova, K., Zamecnikova, K., Rychtarcikova, Z., Gopalan, V., Andera, L., Sobol, M., Yan, B., Pattnaik, B., Bhatraju, N., Truksa, J., Stopka, P., Hozak, P., Lam, A.K., Sedlacek, R., Oliveira, P.J., Kubista, M., Agrawal, A., Dvorakova-Hortova, K., Rohlena, J., Berridge, M.V., Neuzil, J. (2017). Horizontal transfer of whole mitochondria restores tumorigenic potential in mitochondrial DNA-deficient cancer cells. eLife *6*. 10.7554/eLife.22187.

Ferraro, G.B., Ali, A., Luengo, A., Kodack, D.P., Deik, A., Abbott, K.L., Bezwada, D., Blanc, L., Prideaux, B., Jin, X., Possada, J.M., Chen, J., Chin, C.R., Amoozgar, Z., Ferreira, R., Chen, I., Naxerova, K., Ng, C., Westermark, A.M., Duquette, M., Roberge, S., Lindeman, N.I., Lyssiotis, C.A., Nielsen, J., Housman, D.E., Duda, D.G., Brachtel, E., Golub, T.R., Cantley, L.C., Asara, J.M., Davidson, S.M., Fukumua, D., Dartois, V.A., Clish, C.B., Jain, R.K., Vander Heiden, M.G. (2021). Fatty acid synthesis is required for breast cancer brain metastasis. Nature Cancer *in press*. 10.1038/s43018-021-00183-y.
Fiedorczuk, K., Sazanov, L.A. (2018). Mammalian Mitochondrial Complex I Structure and Disease-Causing Mutations. Trends in Cell Biology *28*, 835-867. 10.1016/j.tcb.2018.06.006.

Gravel, S., Hulea, L., Toban, N., Birman, E., Blouin, M., Zakikhani, M., Zhao, Y., Topisirovic, I., St-Pierre, J., Pollak, M. (2014). Serine Deprivation Enhances Antineoplastic Activity of Biguanides. Cancer Research *74*, 7521-7533. https://doi.org/10.1158/0008-5472.CAN-14-2643-T.

Greggio, C., Jha, P., Kulkarni, S.S., Lagarrigue, S., Broskey, N.T., Boutant, M., Wang, X., Conde Alonso, S., Ofori, E., Auwerx, A., Canto, C., Amati, F. (2017). Enhanced Respiratory Chain Supercomplex Formation in Response to Exercise in Human Skeletal Muscle. Cell Metabolism *7*, 301-311. 10.1016/j.cmet.2016.11.004.

Gu, J., Wu, M., Guo, R., Yan, K., Lei, J., Gao, N., Yang, M. (2016). The architecture of the mammalian respirasome. Nature *537*, 639-643. 10.1038/nature19359.

Hu, Q., Wu, D., Walker, M., Wang, P., Tian, R., Wang, W. (2021). Genetically encoded biosensors for evaluating NAD+/NADH ratio in cytosolic and mitochondrial compartments. Cell Reports Methods *1*. https://doi.org/10.1016/j.crmeth.2021.100116.

Jin, X., Demere, Z., Nair, K., Ali, A., Ferraro, G. B., Natoli, T., Deik, A., Petronio, L., Tang, A. A., Zhu, C., Wang, L., Rosenberg, D., Mangena, V., Roth, J., Chung, K., Jain, R. K., Clish, C. B., Vander Heiden, M. G., & Golub, T. R. (2020). A metastasis map of human cancer cell lines. Nature *588*, 331-336. https://doi.org/10.1038/s41586-020-2969-2.

King, M.P., Attardi, G. (1989). Human cells lacking mtDNA: repopulation with exogenous mitochondria by complementation Science *246*, 500-503. 10.1126/science.2814477.

Krall, A.S., Xu, S., Graeber, T.G., Braas, D., Christofk, H.R. (2016). Asparagine promotes cancer cell proliferation through use as an amino acid exchange factor. Nature Communications *11457*. https://doi.org/10.1038/ncomms11457.

Lanoue, K.F., Meijer, A.J., Brouwer, A. (1974). Evidence for electrogenic aspartate transport in rat liver mitochondria. Archives of Biochemistry and Biophysics *161*, 544-550. https://doi.org/10.1016/0003-9861(74)90337-3.

Lapuente-Brun, E., Moreno-Loshuertos, R., Acin-Perez, R., Latorre-Pellicer, A., Colas, C., Balsa, E., Perales-Clemente, E., Quiros, P.M., Calvo, E., Rodriguez-Hernandez, M.A., Navas, P., Cruz, R., Carracedo, A., Lopez-Otin, C., Perez-Martos, A., Fernandez-Silva, P., Fernandez-Vizarra, E., Enriquez, J.A. (2013). Supercomplex Assembly Determines Electron Flux in the Mitochondrial Electron Transport Chain. Science *340*, 1567-1570. 10.1126/science.1230381.

Le Gal, K., Ibrahim, M.X., Wiel, C., Sayin, V.I., Akula, M.K., Karlsson, C., Dalin, M.G., Akyürek, L.M., Lindahl, P., Nilsson, J., Bergo, M.O. (2015). Antioxidants can increase melanoma metastasis in mice. Science Translational Medicine *7*, 308re308. 10.1126/scitranslmed.aad3740.

Leif, H., Weidner, U., Berger, A., Spehr, V., Braun, M., van Heek, P., Friedrich, T., Ohnishi, T., Weiss, H. (1993). Escherichia coli NADH dehydrogenase I, a minimal form

of the mitochondrial complex I. Biochemical Society Transactions *21*, 998-1001. 10.1042/bst0210998.

Letts, J.A., Fiedordzuk, K., Sazanov, L.A. (2016). The architecture of respiratory supercomplexes. Nature *537*, 644-648. 10.1038/nature19774.

Li, Z., Ji, B.W., Dixit, P.D., Lien, E.C., Tchourine, K., Hosios, A.M., Abbott, K.L., Westermark, A.M., Gorodetsky, E.F., Sullivan, L.B., Vander Heiden, M.G., Vitkup, D. (2022). Cancer cells depend on environmental lipids for proliferation when electron acceptors are limited. Nature Metabolism *4*, 711-723. https://doi.org/10.1038/s42255-022-00588-8.

Lomelino, C.L., Andring, J.T., McKenna, R., Kilberg, M.S. (2017). Asparagine synthetase: Function, structure, and role in disease. Journal of Biological Chemistry *292*, 19952-19958. 10.1074/jbc.R117.819060.

Luengo, A., Li, Z., Gui, D. Y., Sullivan, L. B., Zagorulya, M., Do, B. T., Ferreira, R., Naamati, A., Ali, A., Lewis, C. A., Thomas, C. J., Spranger, S., Matheson, N. J., & Vander Heiden, M. G. (2021). Increased demand for NAD+ relative to ATP drives aerobic glycolysis. Molecular Cell *81*, 691–707. https://doi.org/10.1016/j.molcel.2020.12.012.

Lyssiotis, C.A., Kimmelman, A.C. (2017). Metabolic Interactions in the Tumor Microenvironment. Trends in Cell Biology *27*, 863-875. https://doi.org/10.1016/j.tcb.2017.06.003.

Maddocks, O.D.K., Berkers, C. R., Mason, S. M., Zheng, L., Blyth, K., Gottlieb, E., & Vousden, K. H. (2013). Serine starvation induces stress and p53-dependent metabolic remodelling in cancer cells. Nature *493* (*7433*), 542–546. https://doi.org/10.1038/nature11743.

Murtas, G., Marcone, G.L., Peracchi, A., Zangelmi, E., Pollegioni, L. (2021). Biochemical and Biophysical Characterization of Recombinant Human 3-Phosphoglycerate Dehydrogenase. International Journal of Molecular Sciences *22*. 10.3390/ijms22084231.

Ngo, B., Kim, E., Osorio-Vasquez, V., Doll, S., Bustraan, S., Liang, R. J., Luengo, A., Davidson, S. M., Ali, A., Ferraro, G. B., Fischer, G. M., Eskandari, R., Kang, D. S., Ni, J., Plasger, A., Rajasekhar, V. K., Kastenhuber, E. R., Bacha, S., Sriram, R. K., … Pacold, M. E. (2020). Limited Environmental Serine and Glycine Confer Brain Metastasis Sensitivity to PHGDH Inhibition. Cancer Discovery *10*, 1352–1373. https://doi.org/10.1158/2159-8290.cd-19-1228.

Nielsen, J. (2003). It Is All about Metabolic Fluxes. Journal of Bacteriology *185*, 7031-7035. 10.1128/JB.185.24.7031-7035.2003.

Papalazarou, V., Newman, A.C., Huerta-Uribe, A., Legrave, N.M., Falcone, M., Zhang, T., McGarry, L., Athineos, D., Shanks, E., Blyth, K., Vousden, K.H., Maddocks, O.D.K (2023). Phenotypic profiling of solute carriers characterizes serine transport in cancer. Nature Metabolism *5*. https://doi.org/10.1038/s42255-023-00936-2.

Park, J.O., Rubin, S.A., Xu, Y., Amador-Noguez, D., Fan, J., Shlomi, T., Rabinowitz, J.D. (2016). Metabolite concentrations, fluxes and free energies imply efficient enzyme usage. Nature Chemical Biology *12*, 482-489. https://doi.org/10.1038/nchembio.2077.

Pettit, F.H., Pelley, J.W., Reed, L.J. (1975). Regulation of pyruvate dehydrogenase kinase and phosphatase by acetyl-CoA/CoA and NADH/NAD ratios. Biochemical and Biophysical Research Communications *65*, 578-582. https://doi.org/10.1016/S0006-291X(75)80185-9.

Piskounova, E., Agathocleous, M., Murphy, M.M., Hu, Z., Huddleston, S.E., Zhao, Z., Marilyn Leitch, A., Johnson, T.M., DeBerardinis, R.J., Morrison, S.J. (2016). Oxidative stress inhibits distant metastasis by human melanoma cells. Nature *527*, 186-191. 10.1038/nature15726.

Santidrian, A.F., Matsuno-Yagi, A., Ritland, M., Seo, B.B., LeBoeuf, S.E., Gay, L.J., Yagi, T., Felding-Habermann, B. (2013). Mitochondrial complex I activity and NAD+/NADH balance regulate breast cancer progression. Journal of Clinical Investigation *123*, 1068-1081. https://doi.org/10.1172/JCI64264.

Sharma, L.K., Fang, H., Liu, J., Vartak, R., Deng, J., Bai, Y. (2011). Mitochondrial respiratory complex I dysfunction promotes tumorigenesis through ROS alteration and AKT activation Human Molecular Genetics *20*, 4605-4616. https://doi.org/10.1093/hmg/ddr395.

Sharma, L.K., Lu, J., Bai, Y. (2016). Mitochondrial Respiratory Complex I: Structure, Function and Implication in Human Diseases. Current Medicinal Chemistry *16*, 1266-1277. 10.2174/092986709787846578.

Shimizu, M. (2018). NAD+/NADH homeostasis affects metabolic adaptation to hypoxia and secondary metabolite production in filamentous fungi. Bioscience, Biotechnology, and Biochemistry *82*, 216-224. https://doi.org/10.1080/09168451.2017.1422972.

Siess, E.A., Nimmannit, S., Wieland, O.H. (1976). Kinetic and regulatory properties of pyruvate dehydrogenase from Ehrlich ascites tumor cells. Cancer Research *36*, 55-59.

Sporn, M.B., Liby, K.T. (2012). NRF2 and cancer: the good, the bad and the importance of context. Nature Reviews Cancer *12*, 564-571. https://doi.org/10.1038/nrc3278.

Sullivan, L.B., Gui, D.Y., Hosios, A.M., Bush, L.N., Freinkman, E., Vander Heiden M.G. (2015). Supporting Aspartate Biosynthesis Is an Essential Function of Respiration in Proliferation Cells. Cell *162*, 552-563. doi:10.1016/j.cell.2015.07.017.

Sullivan, M.R., Danai, L. V., Lewis, C. A., Chan, S. H., Gui, D. Y., Kunchok, T., Dennstedt, E. A., Vander Heiden, M. G., Muir, A. (2019a). Quantification of microenvironmental metabolites in murine cancers reveals determinants of tumor nutrient availability. eLife *8*. https://doi.org/10.7554/elife.44235.

Sullivan, M.R., Darnell, A.M., Reilly, M.R., Kunchok, T., Joesch-Cohen, L., Rosenberg, D., Ali, A., Rees, M.G., Roth, J.A., Lewis, C.A., Vander Heiden, M.G. (2021). Methionine synthase is essential for cancer cell proliferation in physiological folate environments. Nature Metabolism *3*, 1500-1511. https://doi.org/10.1038/s42255-021-00486-5.

Sullivan, M.R., Mattaini, K.R., Dennstedt, E.A., Nguyen, A.A., Reilly, M.F., Meeth, K., Muir, A., Darnell, A.M., Bosenberg, M.W., Lewis, C.A., Vander Heiden, M.G. (2019b). Increased serine synthesis provides an advantage for tumors arising in tissues where serine levels are limiting. Cell Metabolism *29*, 1410-1421,e1414. doi: 10.1016/j.cmet.2019.02.015.

Tan, A.S., Baty, J.W., Dong, L, Bezawork-Geleta, A., Endaya, B. Goodwin, J., Bajzikova, M., Kovarova, J., Peterka, M., Yan, B., Pesdar, E.A., Sobol, M., Filimonenko, A., Stuart, S., Vondrusova, M., Kluckova, K., Sachaphibulkij, K., Rohlena, J., Hozak, P., Truksa, J., Eccles, D., Haupt, L.M., Griffiths, L.R., Neuzil, J., Berridge, M.V. (2015). Mitochondrial genome acquisition restores respiratory function and tumorienic potential of cancer cells without mitochondrial DNA. Cell Metabolism *21*, 81-94.

Tasdogan, A., Ubellacker, J.M., Morrison, S.J. (2021). Redox Regulation in Cancer Cells during Metastasis. Cancer Discovery *11*, 2682-2692. 10.1158/2159-8290.CD-21-0558.

Tuschen, G., Sackmann, U., Nehls, U., Haiker, H., Buse, G., Weiss, H. (1990). Assembly of NADH: ubiquinone reductase (complex I) in Neurospora mitochondria. Independent pathways of nuclear-encoded and mitochondrially encoded subunits. Journal of Molecular Biology *213*, 845-857. https://doi.org/10.1016/S0022-2836(05)80268-2.

van Karnebeek, C.D.M., Ramos, R.J., Wen, X., Tarailo-Graovac, M., Gleeson, J.G., Skrypnyk, C., Brand-Arzamendi, K., Karbassi, F., Issa, M.Y., van der Lee, R., Brogemoller, B.I., Koster, J., Rousseau, J., Campeau, P.M., Wang, Y., Cao, F., Li, M., Ruiter, J., Ciapaite, J., Kluijtmans, L.A.J., Willemsen, M.A., Jans, J.J., Ross, C.J., Wintjes, L.T., Rodenburg, R.J., Huigen, M.C., Jia, Z., Waterham, H.R., Wasserman, W.W., Wanders, R.J.A., Verhoeven-Duif, N.M., Zaki, M.S., Wevers, R.A. (2019). Bi-allelic GOT2 Mutations Cause a Treatable Malate-Aspartate Shuttle-Related Encephalopathy. American Journal of Human Genetics *105*, 534-548. 10.1016/j.ajhg.2019.07.015.

Vaupel, P., Kallinowski, F., Okunieff, P. (1989). Blood flow, oxygen and nutrient supply, and metabolic microenvironment of human tumors: a review. Cancer Research *1*, 6449-6465.

Vemuri, G.N., Eiteman, M.A., McEwen, J.E., Olsson, L., Nielsen, J. (2007). Increasing NADH oxidation reduces overflow metabolism in Saccharomyces cerevisiae. PNAS *104*, 2402-2407. 10.1073/pnas.0607469104.

Wang, K., Luo, L., Fu, S., Wang, M., Wang, Z., Dong, L., Wu, X., Dai, L., Peng, Y., Shen, G., Chen, H., Nice, E.C., Wei, X., Huang, C. (2023). PHGDH arginine methylation by PRMT1 promotes serine synthesis and represents a therapeutic vulnerability in hepatocellular carcinoma. Nature Communications *14*. https://doi.org/10.1038/s41467-023-36708-5.

Wang, Y., Stancliffe, E., Fowle-Grider, R., Wang, R., Wang, C., Schwaiger-Haber, M., Shriver, L.P., Patti, G.J. (2022). Saturation of the mitochondrial NADH shuttles drives aerobic glycolysis in proliferating cells. Molecular Cell *82*, 3270-3283. https://doi.org/10.1016/j.molcel.2022.07.007.

Wiig, H., Swartz, M.A. (2012). Interstitial Fluid and Lymph Formation and Transport: Physiological Regulation and Roles in Inflammation and Cancer. Physiological Reviews *92*, 1005-1060. https://doi.org/10.1152/physrev.00037.2011.

Williamson, D.H., Lund, P., Krebs, H.A. (1967). The Redox State of Free Nicotinamide-Adenine Dinucleotide in the Cytoplasm and Mitochondria of Rat Liver. Biochemical Journal *103*, 514-527.

Zhao, R., Jiang, S., Zhang, L., Yu, Z. (2019). Mitochondrial electron transport chain, ROS generation, and uncoupling International Journal of Molecular Medicine *44*, 3-15. 10.3892/ijmm.2019.4188.

Appendix A: Pyruvate increases cancer cell sensitivity to boronic-acid containing proteasome inhibitors

This chapter is under preparation for submission for publication.

Authors: Sarah M. Chang[1], Sky Kim[1], Zhaoqi Li[1], Sam D. Block[1], Brian T. Do[1], Michele Ceribelli[2], Frances Tosto[2], Chen Lu[2], Craig J. Thomas[2], Matthew G. Vander Heiden[1,3]

Affiliations:
[1]Koch Institute for Integrative Cancer Research and Department of Biology, Massachusetts Institute of Technology, Cambridge, MA, USA.
[2]NIH Chemical Genomics Center, National Center for Advancing Translational Sciences, NIH, Bethesda, MD, USA
[3]Dana-Farber Cancer Institute, Boston, MA, USA.

Author Contributions

Conceptualization: **SMC,** ZL, MGVH; Small Molecule Screening: MC, FT, CL, CJT; Small Molecule Screening Analysis: BTD; Screen Validation: **SMC**, ZL, SK, SDB; Proliferation Assays: **SMC**, SK, ZL, SDB; Cell Line Production: **SMC**; Flow Cytometry: **SMC**; Immunoblotting: **SMC**; Proteasome Activity Assays: **SMC**; GC-MS analysis: **SMC**; Writing: **SMC**; Editing: **SMC**; Funding Acquisition: MGVH

Abstract

Metabolites in the tumor nutrient environment can alter the sensitivity of cancer cells to therapeutic agents. To broadly characterize how the metabolic environment influences therapeutic sensitivity, we conducted a small molecule screen using a diverse library of 2480 therapeutic agents in cells cultured with or without pyruvate, an important central carbon metabolite that also alters cellular redox state. Interestingly, we find that pyruvate and other α-ketoacids increase cancer cell sensitivity to boronic acid proteasome inhibitors, including Bortezomib, a current standard treatment for patients with multiple myeloma. Pyruvate enhances proteasome inhibition by Bortezomib but not non-boronic acid proteasome inhibitors, and its impact on proteasome inhibition is abolished in cell lysates. Upon cysteine or glutathione supplementation, cells are no longer sensitive to Bortezomib with or without pyruvate, yet proteasome activity is still inhibited. Together, our data suggest that pyruvate synergizes with boronic acid proteasome inhibitors by altering intracellular availability, leading to greater proteasome inhibition that causes cytotoxicity through altered glutathione metabolism. Our findings provide insight into combatting resistance to proteasome inhibitors observed in patients, expand the potential use of proteasome inhibitors beyond multiple myeloma, as well as inform novel drug design.

Introduction

The rise in cancer precision medicine leverages our discoveries that connect specific genetic lesions to oncogenesis. Certain therapies using this approach have been massively successful, such as treating chronic myelogenous leukemia (CML) with

imatinib or Gleevec, an inhibitor of the oncogenic fusion protein Bcr-Abl (Daley, 1990; Druker, 2001). However, despite the recent initiatives to target cancer based on genomic lesions, precision medicine trials have been disappointing (Letai, 2017). One important cell-extrinsic facet of cancer biology is the impact of the tumor nutrient environment in determining the biological processes on which tumors depend for growth (Muir, 2018). Consequently, differences in the nutrient environment can greatly alter the efficacy of certain therapeutics agents. For example, many cancer cells depend on extracellular glutamine for proliferation (Eagle, 1955; Hosios, 2016; Pavlova, 2017), which has generated interest in targeting glutamine metabolism to suppress cancer growth. The first step in glutamine utilization is its conversion to glutamate by glutaminase, leading to the development of glutaminase inhibitors which have yielded mixed results in clinical trials (Gross, 2014). It was discovered that the presence of a single metabolite, cystine, could dramatically alter the sensitivity of cancer cells to glutaminase inhibitors by modulating intracellular glutamate availability (Muir, 2017). Similarly, we showed that changes to cellular NAD+ availability by pyruvate can significantly influence sensitivity to biguanides that suppress electron transport chain complex I, such as the anti-hyperglycemic agent metformin (Gui, 2016). Accumulating evidence has supported the integral role the nutrient environment plays in influencing the success of cancer therapeutic agents and has driven the growing interest in quantifying different nutrient environments (Abbott, 2023b; Sullivan, 2019a), investigating how nutrient environment alters cancer cell metabolic dependencies (Cantor, 2017; Ferraro, 2021; Hennequart, 2021; Jin, 2020; Labuschagne, 2014; Li, 2022; Maddocks, 2017; Ngo, 2020; Rossiter, 2021; Sullivan, 2019b; 2021), and interrogating

therapeutic efficacy in different nutrient environments (Abbott, 2023a; Cantor, 2017; Tardito, 2015).

Pyruvate levels can be depleted in certain tissue environments, such as the interstitial fluid of pancreatic ductal adenocarcinoma (PDAC) (Sullivan, 2019a). Given our finding that pyruvate, through altering cellular redox state, or the NAD+/NADH ratio, can influence therapeutic efficacy, we performed a high throughput small molecule single agent screen on 2480 compounds at 11 concentrations in lung adenocarcinoma A549 cells with and without exogenous pyruvate. We found that surprisingly, cells were far more sensitive to certain proteasome inhibitors upon pyruvate supplementation (Supplementary Figure 1A,B). Intriguingly, pyruvate appeared to increase cellular sensitivity specifically to boronic acid proteasome inhibitors.

The 26S proteasome is a 2.4 MDa molecular machine that degrades ubiquitinated proteins and is integral not only for protein homeostasis and quality control, but also the regulation of the cell cycle, gene expression, and antigen presentation (Ciechanover, 1994). It consists of the 19S regulatory particle that binds to ubiquitinated protein and the 20S core particle that houses six proteolytically active β subunits: two β1, β2, and β5 subunits. Each β subunit cuts at different amino acid residues.The caspase-like β subunit (β1) cleaves after acidic residues, the trypsin-like β subunit (β2) cleaves after basic residues, and the chymotrypsin-like β subunit (β5) cleaves after large hydrophobic residues and also determines the rate of protein breakdown (Kisselev, 1999). Proteasome inhibitors are widely used to treat various diseases such as amyloidosis, mantle-cell lymphoma, and multiple myeloma (Manasanch, 2017). The first-in-class proteasome inhibitor Bortezomib, or Velcade, substantially improved the outcomes of patients with

multiple myeloma when it was first approved in 2003 (Moreau, 2012). Since then, both second and third generations of proteasome inhibitors have been approved for resistant and relapsed or refractory multiple myeloma (Besse, 2019). Because of multiple myeloma's tremendous protein production, proteasome inhibition leads to higher proteotoxic stress and greater cytotoxicity (Obeng, 2006). However, how proteasome inhibition leads to cell death is not well understood, as the doses required for proteasome inhibitors to alter levels of essential proteins is much higher than the doses that lead to cytotoxicity in patients (Fricker, 2020). One study finds that proteasome inhibition leads to cell death due to amino acid depletion (Suraweera, 2012). Other studies find that the peptides generated by proteasome cleavage play important functions within the cell and are suppressed by proteasome inhibition (Fricker, 2020). Nevertheless, proteasome inhibitors have had a tremendous impact on the treatment of certain hematological malignancies.

Proteasome inhibitors can be classified into three categories based on chemical structure: boronates, epoxyketones, and salinosporamides. Boronates, including Bortezomib, are slowly reversible proteasome inhibitors that target the chymotrypsin and caspase-like active sites. One major side effect of Bortezomib is painful peripheral neuropathy that affects more than 30% patients. This has been linked to an off-target effect of Bortezomib on serine proteases, including cathepsin G and the mitochondrial HtrA2/Omi (Arastu-Kapur, 2011; Moreau, 2012). New boronates have been developed, including ixazomib and delanzomib. Ixazomib is an oral boronate approved for the treatment of relapsed and refractory multiple myeloma (Besse, 2019). Epoxyketones include the second generation proteasome inhibitor Carfilzomib, which is used to treat

Bortezomib-resistant multiple myeloma. Carfilzomib irreversibly inhibits the chymotrypsin-like active site with low affinity to the caspase and trypsin-like subunits. Unlike Bortezomib, Carfilzomib has fewer off target effects, but shares similar potency to Bortezomib against the chymotrypsin-like active site. Salinosporamides, including the proteasome inhibitor Marizomib, are natural products from the marine bacterium *Salinospora tropica.* Marizomib is an irreversible proteasome inhibitor that targets both the chymotrypsin and trypsin-like active sites, distinct from both Bortezomib and Carfilzomib. Marizomib is used to treat both hematological malignancies as well as solid tumors (Potts, 2011).

In this study, we aim to uncover why pyruvate supplementation increases cellular sensitivity to boronic acid proteasome inhibitors. We find that pyruvate supplementation raises cytotoxicity to Bortezomib and not Carfilzomib by enhancing the inhibition of the chymotrypsin-like proteolytic site. The more severe proteasome inhibition caused by pyruvate supplementation depends on an intact cell membrane. Thus, our findings demonstrate that pyruvate, as well as other α-ketoacids, may modulate uptake of boronic acid containing proteasome inhibitors to alter effective dose.

Results

Pyruvate increases cellular sensitivity to boronic acid proteasome inhibitors

We confirmed the findings of the small molecule screen (**Supplementary Figure 1A,B**) by treating lung adenocarcinoma A549 cells with the boronic acid proteasome inhibitors Bortezomib and Ixazomib and non-boronic acid proteasome inhibitors Carfilzomib and MG132 with and without 1 mM pyruvate. Indeed, pyruvate altered cellular sensitivity to Bortezomib and Ixazomib but not Carfilzomib or MG132 (**Figure 1A-E**). We begin to see the effect of pyruvate between 0.1 and 0.5 mM pyruvate (**Supplementary**

Figure 2A). To directly examine whether the boronic acid directly modulated changes in drug sensitivity, we treated cells with MG262, a boronic acid-containing version of MG132, and compared the effect of pyruvate on cells treated with MG132. Pyruvate increased cellular sensitivity to MG262 only, demonstrating that the phenotype is specific for boronic acid proteasome inhibitors (**Figure 1D-F**). Because proteasome inhibitors are used to treat patients with multiple myeloma, we examined whether pyruvate increased sensitivity of multiple myeloma cells AMO-1 and L363 to boronic acid proteasome inhibitors. Indeed, multiple myeloma cells were more sensitive to Bortezomib and MG262 and not Carfilzomib or MG132 in the presence of pyruvate (**Figure 1G,H; Supplementary Figure 2B,C**). To test whether the changes in cell proliferation upon proteasome inhibitor and pyruvate treatment was due to cell death, we measured viability in AMO-1 cells with increasing concentrations of Bortezomib and Carfilzomib with and without pyruvate. We confirm that cell viability is decreased with Bortezomib and pyruvate treatment compared to Bortezomib alone, but is unaltered by pyruvate upon Carfilzomib treatment (**Supplementary Figure 2D,E**).

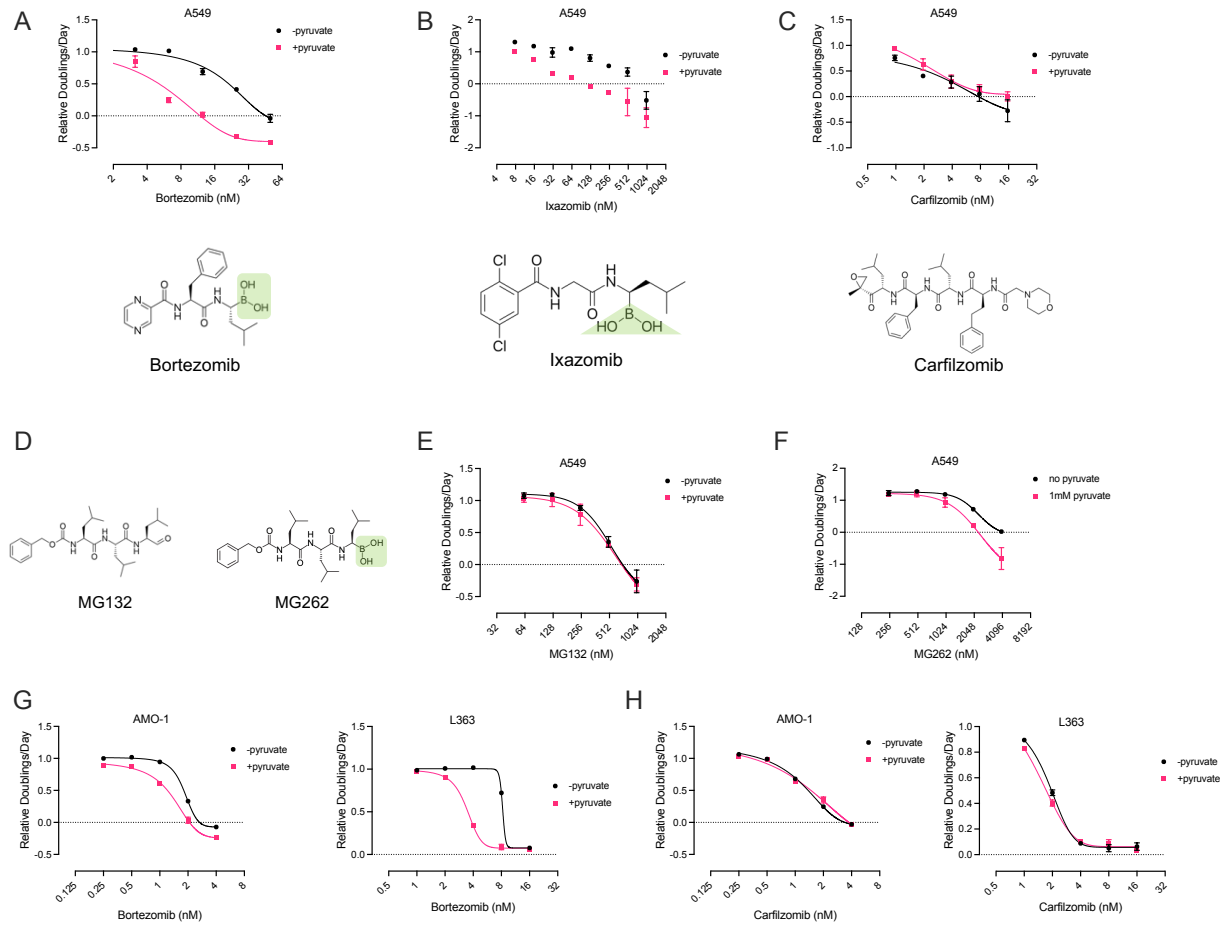

Figure 1. Pyruvate increases cellular sensitivity to boronic acid proteasome inhibitors. (A-C) Relative proliferation rates (doublings per day) of A549 cells treated with indicated concentrations of Bortezomib (A), Ixazomib (B), and Carfilzomib (C) with and without 1 mM pyruvate for three days with chemical structures of each proteasome inhibitors are shown. Boronic acids are highlighted in light green, n=2. **(D)** Chemical structure of MG132 (left) and its boronic acid version, MG262 (right) with the boronic acid highlighted in light green. **(E-F)** Relative proliferation rate (doublings per day) of A549 cells treated with MG132 (E) or MG262 (F) with and without 1 mM pyruvate for three days. **(G)** Relative proliferation rate (doublings per day) of AMO-1 cells (left) and L363 cells (right) treated with indicated concentrations of Bortezomib with and without 1 mM pyruvate for three days, n=3. **(H)** AMO-1 (left) and L363 (right) cells treated with indicated concentrations of Carfilzomib with and without 1 mM pyruvate for three days, n=3. All proliferation rate values are normalized to the untreated – pyruvate condition and represent means ± SD.

Pyruvate supplementation enhances Bortezomib mediated proteasome inhibition

We next asked whether pyruvate increased cellular sensitivity to boronic acid proteasome inhibitors due to greater proteasome inhibition or through an alternative process. To test this, we expressed ubiquitin fused to GFP in AMO-1 cells as a reporter

for activity of the ubiquitin-proteasome system (Dantuma, 2000). We treated cells with either 4 or 8 nM of Bortezomib or Carfilzomib with and without 1 mM pyruvate and measured GFP accumulation over time via flow cytometry. We saw GFP accumulation after thirty hours in cells treated with Bortezomib and pyruvate only, which we did not see in parental AMO-1 cells, suggesting that pyruvate increases cellular sensitivity to Bortezomib by further inhibiting proteasome activity (**Figure 2A,B, Supplementary Figure 3A**). As an orthogonal approach, we measured the accumulation of ubiquitinated proteins over time by Western blot. We found significant amounts of ubiquitinated protein in both Bortezomib and Carfilzomib treated cells, but pyruvate supplementation led to greater levels of ubiquitinated protein only in cells treated with Bortezomib (**Figure 2C,D**). To obtain greater resolution on the effect of pyruvate on proteasome inhibition, we used a cell-based proteasome activity assay that can assess the inhibition of the chymotrypsin-like, trypsin-like, and caspase-like proteasome activities over time. Consistent with our ubiquitin-GFP reporter and western blot results, pyruvate led to greater inhibition of chymotrypsin-like activity when cells were treated with Bortezomib and not Carfilzomib (**Figure 2E,F**). The effect of pyruvate occurs acutely, within one hour of treatment and is not further enhanced with long term pyruvate treatment (up to 24 hours), suggesting the effect of pyruvate does not require longer term metabolic changes incurred by pyruvate supplementation (**Figure 2E, Supplementary Figure 2B**). Boronic acid proteasome inhibitors suppress both chymotrypsin-like and caspase-like activity, whereas low dose Carfilzomib suppresses chymotrypsin-like activity only (Besse, 2019). We confirmed this in our cell-based activity assays monitoring trypsin-like and caspase-like activity (**Supplementary Figure 3C,D**). We also observe compensatory increases of trypsin-like

activity upon Bortezomib and Carfilzomib treatment (**Supplementary Figure 3C,D**). Pyruvate appears to suppress this compensatory increase of trypsin-like activity in cells treated with Bortezomib only, while mildly increasing caspase-like activity in Bortezomib-treated cells (**Supplementary Figure 3C**). We found no difference in protein expression of various proteasomal subunits upon Bortezomib and Carfilzomib treatment, with and without pyruvate supplementation (**Supplementary Figure 3E**). Together, our data demonstrate that pyruvate leads to greater cellular sensitivity to Bortezomib by enhancing the inhibition of chymotrypsin-like proteasomal activity.

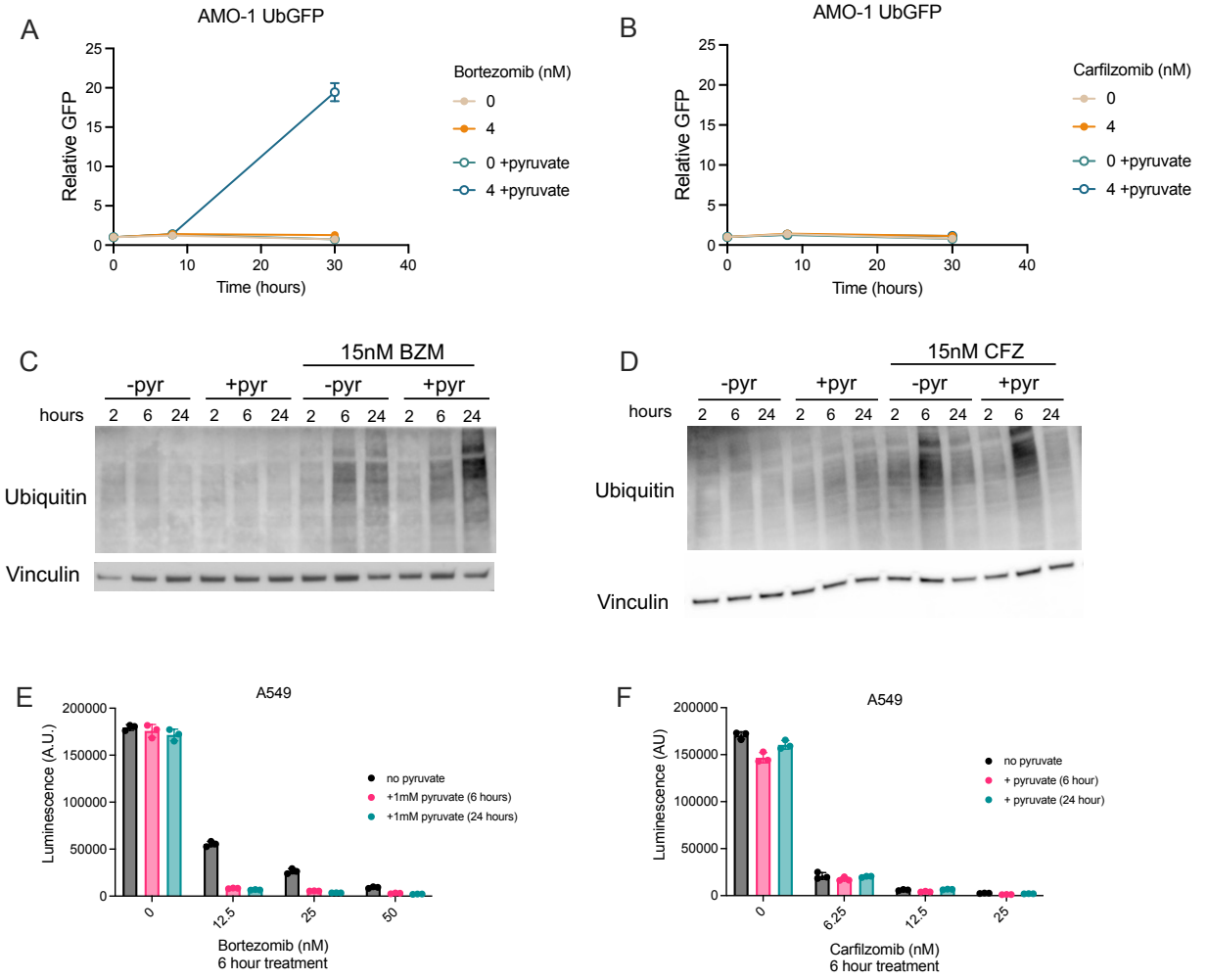

Figure 2. Pyruvate enhances proteasome inhibition by Bortezomib. (A,B) Relative GFP signal in AMO-1 expressing ubiquitin fused to GFP (UbGFP) treated with indicated concentratiosn of Bortezomib (A) or Carfilzomib (B) with and without 1 mM pyruvate over time. GFP signal is

normalized to untreated – pyruvate conditions, n=3. **(C,D)** Immunoblots displaying total ubiquitinated protein with 15 nM of Bortezomib (C) or 15 nM Carfilzomib (D) with and without 1 mM pyruvate for 2, 6, and 24 hours. Vinculin was used as a loading control. **(E,F)** Chymotrypsin-like proteasome activity was measured in A549 cells treated with indicated concentrations of Bortezomib (E) or Carfilzomib (F) with and without 1 mM pyruvate that was either simultaneously added with proteasome inhibitors or added 24 hours prior, n=3. All values are means ± SD.

Changes in the cellular NAD+/NADH ratio do not mediate increased sensitivity to Bortezomib by pyruvate

Pyruvate is a key central carbon metabolite that provides carbons to support the tricarboxylic acid (TCA) cycle, which is essential for amino acid, nucleotide, and fatty acid synthesis. Pyruvate is also an electron acceptor that facilitates the regeneration of NAD+ to support biomass synthesis (Gui, 2016; Sullivan, 2015). Altered cellular redox state has been linked to changes in proteasome assembly and activity in addition to modulating sensitivity to proteasome inhibitors (Meul, 2020; Sharma, 2022; Tsvetkov, 2014). We wondered if pyruvate caused greater proteasome inhibition by Bortezomib by increasing the cellular NAD+/NADH ratio. We treated cells with Bortezomib and pyruvate and measured changes in proliferation upon the addition of the complex I inhibitor rotenone, which suppresses mitochondrial respiration and decreases the NAD+/NADH ratio. As expected, pyruvate decreases proliferation of cells treated with Bortezomib and restores proliferation of cells treated with rotenone. Rotenone mildly improved the proliferation of Bortezomib treated cells, as previously described (Sharma, 2022), but does not modify the effect of pyruvate despite decreasing the NAD+/NADH ratio (**Figure 3A,B**). Consistently, lactate, through its conversion to pyruvate via lactate dehydrogenase, reduces the cellular NAD+/NADH ratio yet has no impact on cellular sensitivity to Bortezomib (**Figure 3C**). Lastly, we wondered if promoting pyruvate contribution to the TCA cycle by increasing pyruvate dehydrogenase activity, which reduces the

NAD+/NADH ratio, would alter cellular sensitivity to Bortezomib. We elevated pyruvate dehydrogenase activity by treated cells with the small molecule AZD7545, a pyruvate dehydrogenase kinase inhibitor (Luengo, 2021). We found no difference in proliferation when cells were treated with Bortezomib and pyruvate with or without AZD7545 (**Figure 3D**). These data argue that pyruvate does not lead to greater Bortezomib sensitivity by elevating the NAD+/NADH ratio.

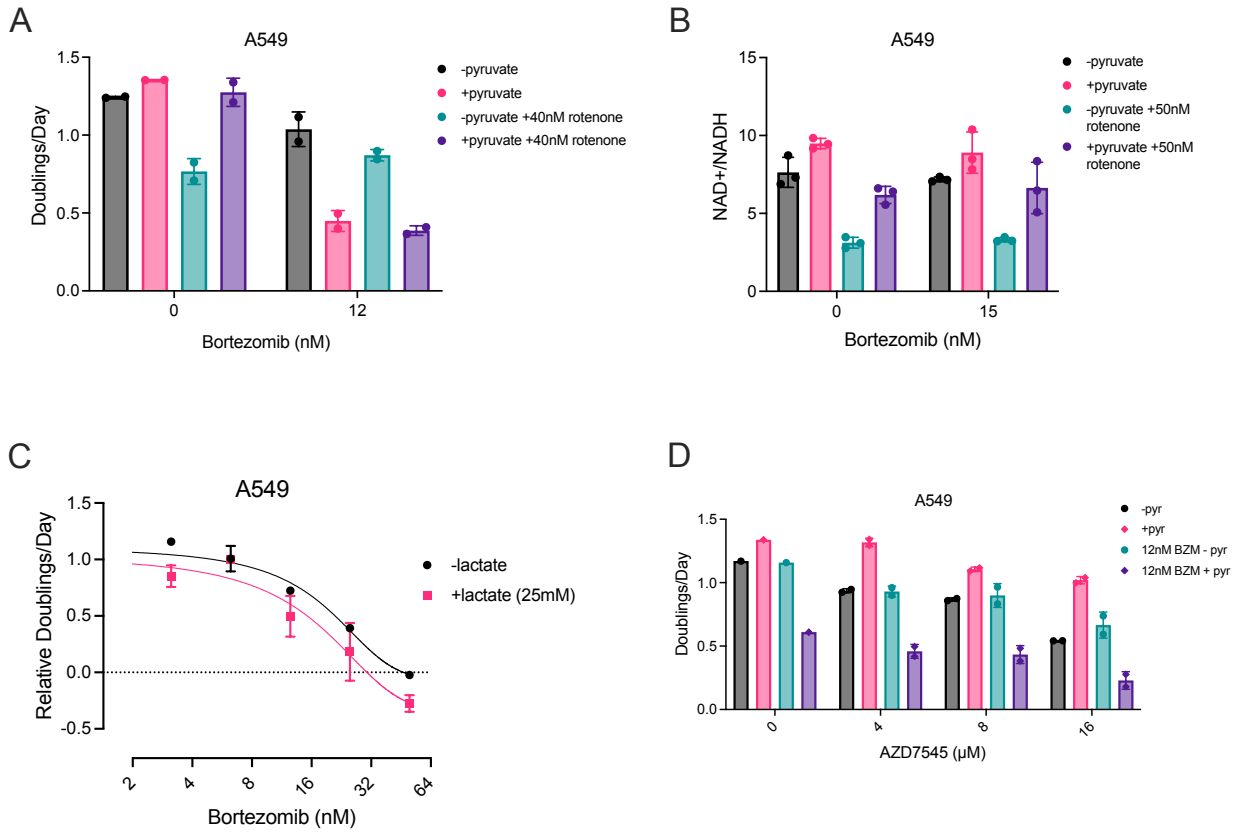

Figure 3. Higher NAD+/NADH ratio does not mediate greater sensitivity to Bortezomib. (A) Proliferation rate (doublings per day) of cells treated with and without 12 nM Bortezomib, 1 mM pyruvate, and 40 nM rotenone for three days, n=2. **(B)** NAD+/NADH ratio of cells treated with and without 15 nM Bortezomib, 1 mM pyruvate, and 50 nM rotenone for 24 hours, n=3. **(C)** Relative proliferation rate (doublings per day) of cells treated with indicated concentrations of Bortezomib with and without 25 mM lactate for three days. Values are normalized to the untreated – pyruvate condition, n=3. **(D)** Proliferation rate (doublings per day) of cells treated with indicated concentrations of AZD7545 with or without 12 nM Bortezomib and 1 mM pyruvate for three days, n=1-2. All values are means ± SD.

Cysteine supplementation rescues proliferation of cells treated with Bortezomib and pyruvate

Given the importance of the proteasome in maintaining amino acid homeostasis, we wondered if the enhanced proteasome inhibition imparted by pyruvate supplementation was related to changes in amino acid homeostasis. This is supported by findings that show that proteasome inhibitors cause cell death through amino acid depletion (Suraweera, 2012). To broadly examine this, we measured intracellular amino acid levels of cells treated with Bortezomib or Carfilzomib with and without pyruvate (**Figure 4A**). We observe that amino acid levels are mildly decreased in both Bortezomib and Carfilzomib treated cells in the absence of pyruvate. Certain amino acids are restored with pyruvate supplementation, but only in Bortezomib treated cells (valine, tyrosine, phenylalanine, methionine, lysine, leucine, isoleucine, histidine, asparagine, arginine, and alanine). On the other hand, pyruvate had no impact on amino acid levels in Carfilzomib treated cells. We were interested in cases where pyruvate further depleted amino acids in Bortezomib but not Carfilzomib treated cells: proline and cysteine. We wondered if supplementing cells with either proline or cysteine would rescue proliferation of Bortezomib treated cells and ablate the greater cellular sensitivity to Bortezomib by pyruvate. While proline supplementation did not alter proliferation (**Supplementary Figure 4A**), cysteine supplementation did restore proliferation of Bortezomib treated cells supplemented with pyruvate (**Figure 4B**). To test if cysteine supplementation led to improved proliferation via uptake of cystine, the oxidized derivative of cysteine, we added the reducing agent β-mercaptoethanol, which maintains cystine in its oxidized form, to cell culture media. Indeed, the addition of β-mercaptoethanol rescued proliferation of cells treated with Bortezomib and pyruvate (**Supplementary Figure 4B**). Cystine uptake is

mediated by the transporter SLC7A11, or xCT, which promotes cystine uptake in exchange for glutamate. As an orthogonal approach to test whether cystine uptake restored proliferation of Bortezomib treated cells, we suppressed xCT activity by supplementing cells with 5 mM glutamate or treating cells with the xCT inhibitor erastin (Dixon, 2014) and measured proliferation with and without pyruvate. As expected, inhibiting cystine uptake via xCT increased sensitivity to Bortezomib and pyruvate treatment while having no effect on Carfilzomib treated cells (**Supplementary Figure 4C,D**). Interestingly, pyruvate alone appeared to increase cellular sensitivity to erastin and led to lower xCT protein level (**Supplementary Figure 4D,E**). We also observed that pyruvate alone decreased intracellular cysteine levels (**Figure 4A**). To further test the effect of pyruvate on xCT expression and activity, we measured the impact of pyruvate on cellular sensitivity to the glutaminase inhibitor CB-839. Glutaminase converts glutamine to glutamate. Thus, greater cystine availability promotes glutamate secretion via xCT and increases cellular sensitivity to CB-839 (Muir, 2017). If pyruvate suppresses xCT activity, we predicted that pyruvate supplementation would lead to CB-839 resistance. Strikingly, pyruvate greatly rescues the proliferation of cells treated with CB-839, consistent with pyruvate suppressing xCT function (**Supplementary Figure 4F**).

Glutathione is an essential antioxidant and requires cystine for its production. It was previously shown that cystine and glutathione can rescue Bortezomib cytotoxicity while xCT inhibition increased Bortezomib cytotoxicity (Nerini-Molteni, 2008; Starheim, 2016). We wondered if elevated cystine availability rescued proliferation of Bortezomib and pyruvate treated cells due to greater glutathione production. Thus, we supplemented cells treated with Bortezomib or Carfilzomib with glutathione and found a dramatic

proliferation rescue of Bortezomib treated cells with and without pyruvate (**Figure 4C**). However, despite rescuing proliferation, both cysteine and glutathione supplementation did not restore proteasome activity in Bortezomib and pyruvate treated cells (**Figure 4D**). Additionally, cysteine supplementation not only rescued proliferation of Bortezomib treated cells, but also restored proliferation of MG132 (non boronic acid proteasome inhibitor) and MG262 (**Supplementary Figure 4G**). However, glutathione supplementation improved proliferation to a greater extent in MG262 treated cells compared to MG132 treated cells (**Supplementary Figure 4H**). Together, these data confirm that a major process that modifies Bortezomib cytotoxicity is cystine and glutathione availability, but does not appear to be specific to boronic acid containing proteasome inhibitors. Moreover, while pyruvate appears to modify xCT function, the greater proteasome inhibition observed upon pyruvate supplementation in Bortezomib treated cells is not explained by differences in cystine or glutathione levels, as cysteine and glutathione supplementation do not restore proteasome activity.

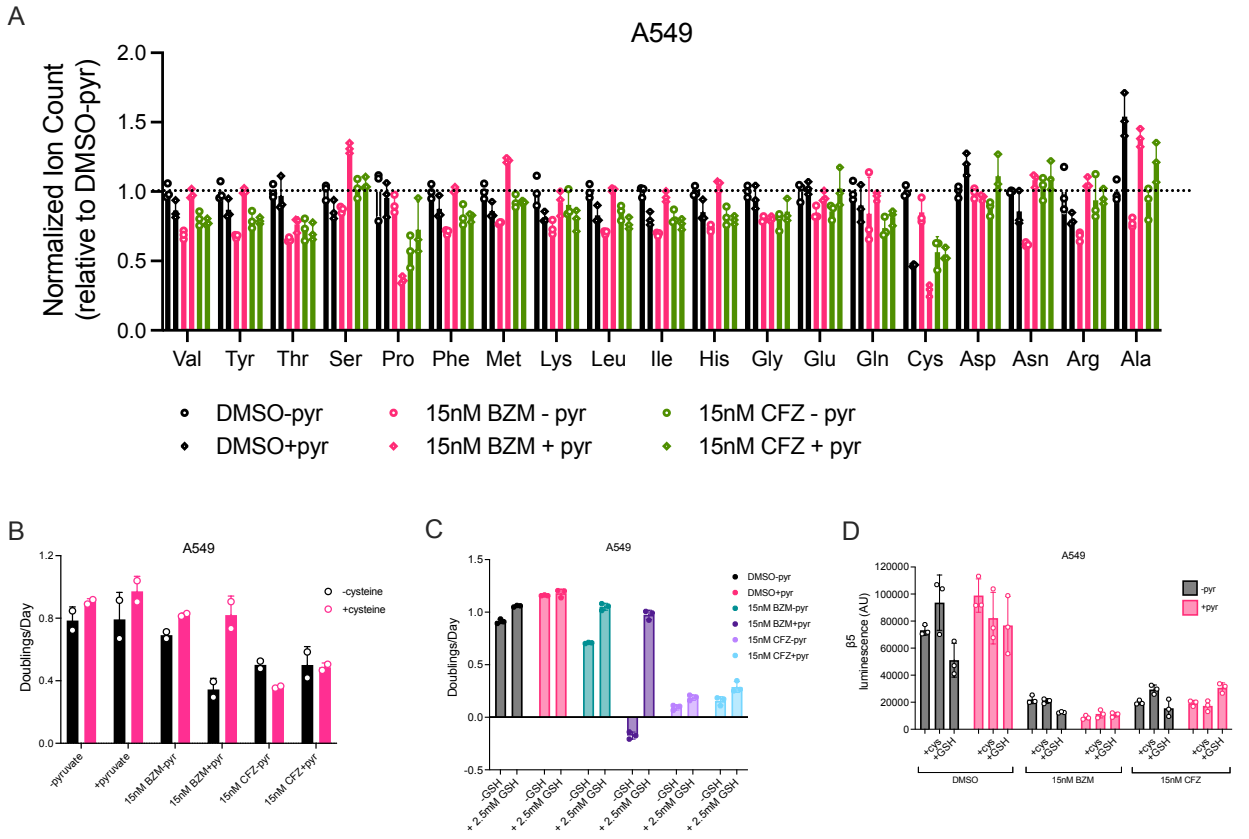

Figure 4. Cysteine and glutathione supplementation restore proliferation but not proteasome activity in Bortezomib treated cells. (A) Relative intracellular amino acid levels after 24 hour treatment of 15 nM Bortezomib (BZM) or Carfilzomib (CFZ) with and without 1 mM pyruvate. Total ion counts were normalized to internal standard norvaline and cell number. Values are relative to DMSO – pyruvate condition per each amino acid, n=3. **(B)** Proliferation rate (doublings per day) of cells treated with 15 nM Bortezomib or Carfilzomib with and without 1 mM cysteine after three days, n=2. **(C)** Proliferation rate (doublings per day) of cells treated with and without 15 nM Bortezomib, 15 nM Carfilzomib, 1 mM pyruvate, or 2.5 mM glutathione reduced ethyl ester (GSH) after three days, n=3. **(D)** Chymotrypsin-like (β5) proteasome activity after 24 hour treatment of 15 nM Bortezomib or Carfilzomib with and without 1 mM pyruvate, 1 mM cysteine (cys), and 2.5 mM GSH, n=3. All values are means ± SD.

Pyruvate enhances proteasome inhibition by altering Bortezomib availability

Our finding that cysteine and glutathione supplementation do not alter Bortezomib mediated proteasome inhibition is consistent with previous findings (Starheim, 2016). These observations argue that the cytotoxicity due to Bortezomib treatment is not necessarily due to inhibited proteasome activity but from altered glutathione metabolism

downstream of proteasome inhibition. Pyruvate supplementation enhances inhibition of the proteasome by Bortezomib, suggesting that pyruvate leads to greater cellular sensitivity by directly altering proteasome activity as opposed to processes downstream of proteasome inhibition. This is supported by cysteine and glutathione supplementation fully restoring proliferation in Bortezomib and pyruvate treated cells. Given the specificity of pyruvate's effect on boronic acid proteasome inhibitors, we predicted that the uptake of boronic acid proteasome inhibitors is modified by pyruvate as opposed to a biological consequence of pyruvate in conjunction with proteasome inhibition. Specifically, we hypothesized that pyruvate supplementation increased effective Bortezomib concentration intracellular, leading to greater proteasome inhibition. Thus, we collected cell lysates and treated samples with either Bortezomib or Carfilzomib with and without 1 mM pyruvate. Interestingly, we find that in lysates, pyruvate does not lead to greater proteasome inhibition in Bortezomib or Carfilzomib treated samples (**Figure 5A,B**). We then wondered whether other metabolites with similar chemical structures as pyruvate could increase cellular sensitivity to Bortezomib. Because pyruvate is an α-ketoacid, we treated cells with the α-ketoacids α-ketobutyrate (AKB), α-ketoglutarate (AKG), and α-phenylpyruvate (phpyr). Indeed, the presence of these α-ketoacids increased cellular sensitivity to Bortezomib (**Figure 5C-F**). This argues that α-ketoacids like pyruvate lead to greater cellular sensitivity to Bortezomib and likely other boronic acid containing proteasome inhibitors by increasing their intracellular levels and leading to greater proteasome inhibition.

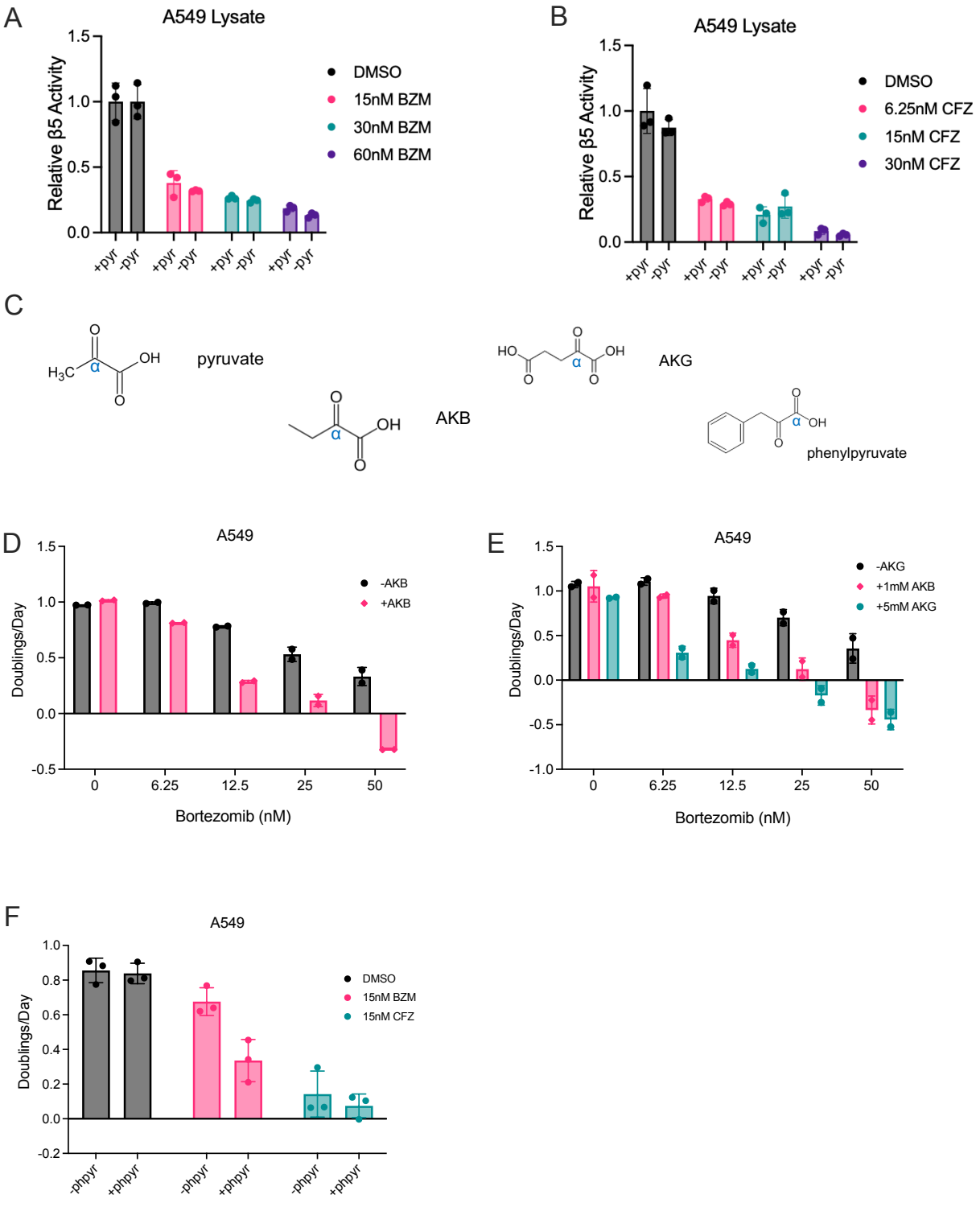

Figure 5. Increased cellular sensitivity to Bortezomib by α-ketoacids depends on uptake. **(A,B)** Chymotrypsin-like (β5) activity in A549 cell lysates treated with indicated concentrations of Bortezomib (BZM) (A) or Carfilzomib (CFZ) (B) with and without 1 mM pyruvate, n=3. Values are relative to DMSO – pyruvate conditions. **(C)** Chemical structures of α-ketoacids pyruvate, α-

ketobutyrate (AKB), α-ketoglutarate (AKG), and phenylpyruvate. **(D)** Proliferation rate (doublings per day) of cells treated with indicated concentrations of Bortezomib with and without 1 mM AKB for three days, n=2. **(E)** Proliferation rate (doublings per day) of cells treated with indicated concentrations of Bortezomib with and without 1 or 5 mM AKG for three days, n=2. **(F)** Proliferation rate (doublings per day) of cells treated with 15 nM BZM or CFZ with and without 1 mM phenylpyruvate (phpyr) for three days, n=3.

Discussion

Nutrient availability alters cellular sensitivity to therapeutic agents. Here, we show that pyruvate increases cellular sensitivity to boronic acid proteasome inhibitors while having no impact on sensitivity to non boronic acid proteasome inhibitors. Curiously, pyruvate is not the only metabolite that increases cellular sensitivity to boronic acid proteasome inhibitors. We uncover that other α-ketoacids share the same effect as pyruvate, demonstrating the chemical specificity of this phenotype. Consistent with the phenotype being mediated by chemical factors, we do not find known biological consequences of pyruvate supplementation, such as altered cellular redox state, to be involved in increasing cellular sensitivity to boronic acid proteasome inhibitors. Instead, our data highlight the role of α-ketoacids in modulating drug availability inside the cell as the enhanced proteasome inhibition observed with pyruvate supplementation was abolished in cell lysates.

Bortezomib can be taken up by cells via the organic anion-transporting polypeptide (OAT) 1B1 transporter and effluxed from cells via P-glycoprotein (multidrug resistance associated protein/ATP-binding cassette B1). However, OAT1B1 does not appear to significantly affect intracellular accumulation of Bortezomib (Clemens, 2015). On the other hand, altering P-glycoprotein expression does modulate intracellular concentrations of Bortezomib (Verbrugge, 2012), but also impacts carfilzomib availability (Besse, 2018).

Thus, it seems unlikely that pyruvate modulates boronic acid proteasome inhibitor uptake or efflux by influencing drug transporters to alter cellular sensitivity. One major difference between Bortezomib and Carfilzomib is their reversibility, where Bortezomib is reversible and Carfilzomib is irreversible. This difference could impact the effective concentration of each drug and the gradient of each drug across the cell membrane to influence drug uptake, as irreversible binding would reduce free intracellular levels (Schäfer, 2017). However, MG132, a non boronic acid proteasome inhibitor is reversible and is not impacted by pyruvate supplementation. Yet, depending on the affinities of each drug to their target and the amount of proteasomal subunits, different reversibility ranges could lead pyruvate to potentiate proteasome inhibition differently. We also found that glutathione supplementation rescued proliferation of cells treated with Bortezomib and MG262, the boronic acid version of MG132. This is interesting in light of the observation that glutathione can react with boronic acids to generate glutathione conjugates, which could inactive boronic acid proteasome inhibitors (Li, 2013). However, the inability for glutathione supplementation to rescue proteasome activity despite restoring cellular proliferation makes is less likely that glutathione metabolism, which could be altered by pyruvate through suppressed xCT activity, and the formation of glutathione-drug conjugates are involved in mediating lower proteasome activity upon simultaneous pyruvate and boronic acid proteasome inhibitor treatment.

Pyruvate levels in the blood have been documented to be around 50-100 μM (Landon, 1962). Additionally, pyruvate levels may be depleted in solid tumor microenvironments (Sullivan, 2019a). Notably, we see changes in cellular sensitivity to boronic acid proteasome inhibitors between 100-150 μM pyruvate, which is greater than

human plasma levels of pyruvate. It is intriguing to envision therapeutic alterations to pyruvate levels in different tumor nutrient environments to potentiate boronic acid proteasome inhibition efficacy. This could present a novel opportunity to use proteasome inhibitors in other clinical settings, including solid malignancies. Additionally, our finding that pyruvate can influence xCT function may reveal that pyruvate supplementation alters cellular sensitivity to ferroptosis inducers such as erastin, which requires further study.

In sum, there remain a plethora of processes that could mediate the increased cellular sensitivity to boronic acid proteasome inhibitors by α-ketoacids. Given the chemical specificity of the phenotype, we cannot rule out the potential that α-ketoacids and boronic acids react to modify proteasome inhibitor structures and impact drug uptake, efflux, or other factors that modulate effective intracellular availability. With further chemical resolution, our findings could lay the ground work for novel drug design and a better understanding for proteasome inhibitor drug kinetics.

Material and Methods

MIPE compound library

The library utilized in these studies is an NCATS internal collection of 1912 small molecules known to modulate oncology targets, pathways and phenotypes, referred to as the MIPE-oncology library (MIPE). The library includes approved drugs, compounds in clinical development for cancer treatment and compounds in pre-clinical development. In addition, where feasible, the library included several compounds for each target class or cellular mechanism and process. In many cases, a compound may have known polypharmacology, for example, kinase inhibitors, and the intended target for which the compound was developed, was used for target enrichment analysis.

Quantitative HTS

For the screen, the compounds in the MIPE library were transferred to columns 5–48, and controls were added in columns 1–4 of the 1536-well assay plate. Column 1 contained media only; column 2 contained cells with added DMSO, whereas columns 3 and 4 contained the proteasome inhibitor bortezomib or the antibiotic salinomycin in DMSO (final concentration 10 μM). Compounds were tested as dose responses starting at a stock concentration of 10 mM (final compound concentration of 46 μM) in DMSO, and diluted threefold, also with DMSO. The library was tested at 11 compound concentrations for qHTS analysis. RLU for each well were normalized to the median RLUs from the DMSO control wells as 100% viability, and median RLUs from control wells with media only as 0% viability.

Cell Culture Experiments

Cell lines were maintained in Dulbecco's Modified Eagle's Medium (DMEM) without sodium pyruvate (Corning 50-013-PC) supplemented with sodium bicarbonate (Sigma S6014) and 10% heat-inactivated Fetal Bovine Serum (FBS) or in RPMI 1640 (Corning 15-040-CV) supplemented with sodium bicarbonate, glutamine (Fisher Scientific 25-030-164), and 10% heat-inactivated FBS. All cells were cultured at 37°C with 5% CO_2, tested for mycoplasma contamination regularly, and confirmed negative before experimentation.

Proliferation Assays

Cells were plated in six-well plates in 2ml of DMEM with 10% heat-inactivated FBS at an initial seeding density of 40,000 cells. Cells were permitted to settle overnight, and cells on a six-well dish were counted to calculate the starting cell number at the start of the

experiment. For all remaining plates, cells were washed once with 1ml of 1X PBS and 2ml of treatment media was added to each well. All treatment media was made with 10% dialyzed serum. Three days after the initial treatment, cells were quantified using a Cellometer (Nexcelom Bioscience) or cells were quantified using a sulforhdamine B (SRB) (Sigma Aldrich 230162) colorimetric assay. All SRB measurements are normalized to a blank. Proliferation rates were calculated with the following formula:

Doublings per day = log_2(final cell count / initial cell count) / (total # of treatment days)

Ubiquitin-GFP Reporter Cell Line Generation

Ub-G76V-GFP (Addgene plasmid #11941) was acquired and introduced to AMO-1 cells via lentiviral infection. Lentiviral production was accomplished by transfecting Ub-G76V-GFP and third generation lentiviral plasmids into lentiX293T cells with lipofectamine 3000 (Thermo Fisher L3000001) following manufacturer's protocol.

Proteasome Activity Assays

Proteasome activity was measured using the Cell-Based Chymotrypsin-like Proteasome-Glo Assay (Promega G8660) per manufacturer's protocol. Briefly, cells were trypsinized and washed three times with 1X PBS before plated. 4000 cells were plated in a white-walled 96 well plate and allowed to settle in 250ul of media containing 10% dialyzed FBS. The next day, cells were washed twice in 200ul of treatment media before 100ul of treatment was added for the indicated amount of time. One hour before initiating the assay, the cell plate was taken out of the incubator and equilibrated at room temperature. 100ul of luciferin detection reagent with chymotrypsin-like, trypsin-like, or caspase-like substrates was added to each well with the exception of substrate-free controls, incubated

in the dark for ten minutes, and then placed in a plate reader (Tecan Infinite M200Pro) to measure luminescence over time. For proteasome activity assays on cell lysates, the manufacturer's protocol was followed. Briefly, cells were lysed in ice cold 1X RIPA buffer containing Halt Proteasome and Phosphatase Inhibitor Cocktail (Thermo Scientific 78442), clarified by rocking samples for thirty minutes at 4°C and then spun at maximum speed for ten minutes for collection of supernatant. Protein concentration was calculating using the BCA Protein Assay (Pierce, 23225) with BSA as a standard. 10 µg of protein in 25 µl of lysis buffer was analyzed for proteasome activity in a 96 well black-walled plate (Corning 3603). Proteasome inhibitors with and without pyruvate were incubated with lysates for one hour at 37°C. After incubating, 25 µl of luciferin detection reagent with chymotrypsin-like substrate was added per 10 µg of protein and incubated again for another hour before measuring luminescence in a plate reader (Tecan Infinite M200Pro).

Immunoblotting

Cells were washed with ice cold 1X PBS and lysed in cold RIPA buffer containing Halt Protease and Phosphatase Inhibitor Cocktail (Thermo Scientific 78442). Lysates were clarified by rocking samples for thirty minutes at 4°C and then spun at maximum speed for ten minutes for collection of supernatant. Protein concentration was calculating using the BCA Protein Assay (Pierce, 23225) with BSA as a standard. Lysates were resolved by SDS-PAGE using NuPAGE 4-12% Bis-Tris Protein Gels and run at 100V. Proteins were transferred onto nitrocellulose membranes via wet transfer at 100V. Membranes were blocked in 5% BSA in TBST before incubating membranes with primary antibodies at 4°C overnight (Vinculin [1:1000] Cell Signaling Technology 13901S; Ubiquitin [1:1000] Cell Signaling Technology 3933S; PSMD4 [1:1000] Cell Signaling Technology 3846S;

PSMA5 [1:1000] Cell Signaling Technology 2457S; PSMC3 [1:1000] Cell Signaling Technology 13923S; PSMB2 [1:1000] Abcam ab236752; xCT/SLC7A11 [1:1000] Cell Signaling Technology 98051). The next day, membranes were washed three times with TBST at room temperature and then incubated in secondary antibodies for one hour at room temperature. The secondary antibody used was anti-rabbit IgG horseradish peroxidase-linked antibody (1:4000 dilution; Cell Signaling Technologies, 7074S) or anti-mouse IgG horseradish peroxidase-linked antibody (1:4000, 7076S).

Gas Chromatography-Mass Spectrometry (GC-MS) Amino Acid Quantification

150,000 cells were plated in a six well plate and permitted to settle overnight. A parallel plate was plated for cell number quantification. The next day, cells were treated with the indicated treatment conditions for 24 hours. Following incubation, cells were washed twice with ice cold blood bank saline as quickly as possible and lysed with 500 µl of ice cold 80% HPLC-grade methanol (Sigma Aldrich, 646377) in HPLC-grade water (Sigma Aldrich, 270733) with heavy labeled metabolomics amino acid mix (Cambridge Isotope Laboratories MSK-A2-1.2) supplemented with ^{15}N-labeled asparagine (Cambridge Isotope Laboratories NLM-3286-PK) and ^{15}N-labeled glutamine (Cambridge Isotope Laboratories CLM-1822-H for amino acid quantification. Lysates were then vortexed at 4°C at maximum speed for ten minutes and then spun down at 4°C at maximum speed for thirty minutes. The supernatant was collected and then dried under nitrogen gas to prepare for metabolic analysis. Dried samples were derivatized by adding 16 µl of methoxamine reagent (Thermo Fisher, TS-45950) and incubated for an hour at 37°C followed by addition of 20 µl of *N*-*tert*-butyldimethylsilyl-*N*-methyltrifluoroacetamide with 1% *tert*-butyldimethylchlorosilane (Sigma 375934) and incubation of two hours at 60°C.

Samples were then centrifuged at maximum speed for ten minutes, and 20 µl of supernatant was used for analysis. Following derivatization, samples were analyzed using a DB-35MS column (30 m × 0.25 mm i.d. × 0.25 µm, Agilent J&W Scientific) in an Agilent 7890 gas chromatograph coupled to an Agilent 5975C mass spectrometer (GC–MS).

NAD+/NADH Measurements

NAD+/NADH measurements were performed using the NAD/NADH-Glo Assay (Promega G9072) with a modified version of manufacturer instructions as previously reported (Sullivan, 2015). Cells were plated at an initial seeding density of 20,000 cells and permitted to settle overnight. The next day, cells were washed once with 1X PBS and then incubated with 2ml of treatment media for the indicated times prior to preparation of cell extracts. For extraction, cells were washed once in ice cold 1X PBS and extracted in 100 µl ice-cold 1% dodecyltrimethylammonium bromide (DTAB) in 0.2N NaOH diluted 1:1 with 1X PBS. Each sample was flash-frozen in liquid nitrogen and immediately stored at -80°C. To measure NADH, 10 µl of sample was moved to PCR tubes, diluted with 10 µl of DTAB, and incubated at 75 °C for 30 min, where basic conditions selectively degrade NAD+. To measure NAD+, 10 µl of the samples was moved to PCR tubes containing 30 µl DTAB and 20 µl 0.4 N HCl and incubated at 60°C for 15 min, where acidic conditions selectively degrade NADH. Samples were then allowed to equilibrate to room temperature and quenched by neutralizing with 20 µl 0.25 M Tris in 0.2 N HCl (for NADH) or 20 µl 0.5 M Tris base (for NAD+). Manufacturer instructions were followed thereafter to measure NAD+/NADH using a luminometer (Tecan Infinite M200Pro). A standard curve

with representative samples was done with each assay to confirm that NAD+ and NADH measurements were in the linear range of detection.

References

Abbott, K.L., Ali, A., Casalena, D., Do, B.T., Ferreira, R., Cheah, J.H., Soule, C.K., Deik, A., Kunchok, T., Schmidt, D.R., Renner, S., Honeder, S.E., Wu, W., Chan, S.H., Tseyang, T., Stoltzfus, A.T., Michel, S.L.J., Greaves, D., Hsu, P.P., Ng, C.W., Zhang, C.J., Farsidjani, A., Kent, J.R., Madariaga, M.L.L., Gramatikov, I.M.T., Matheson, N.J., Lewis, C.A., Clish, C.B., Rees, M.G., Roth, J.A., Griner, L.M., Muir, A., Auld, D.S., Vander Heiden, M.G. (2023a). Screening in serum-derived medium reveals differential response to compounds targeting metabolism. Cell Chemical Biology *30*, 1156-1168. https://doi.org/10.1016/j.chembiol.2023.08.007.

Abbott, K.L., Ali, A., Reinfeld, B.I., Deik, A., Subudhi, S., Landis, M.D., Hongo, R.A., Young, K.L., Kunchok, T., Nabel, C.S., Crowder, K.D., Kent, J.R., Madariaga, M.L.L., Jain, R.K., Beckermann, K.E., Lewis, C.A., Clish, C.B., Muir, A., Rathmell, K., Rathmell, J.C., Vander Heiden, M.G. (2023b). Metabolite profiling of human renal cell carcinoma reveals tissue-origin dominance in nutrient availability. bioRxiv *https://doi.org/10.1101/2023.12.24.573250*.

Arastu-Kapur, S., Anderl, J.L., Kraus, M., Parlati, F., Shenk, K.D., Lee, S.J., Muchamuel, T., Bennett, M.K., Driessen, C., Ball, A.J., Kirk, C.J. (2011). Nonproteasomal targets of the proteasome inhibitors bortezomib and carfilzomib: a link to clinical adverse events. Clinical Cancer Research *17*. 10.1158/1078-0432.CCR-10-1950.

Besse, A., Besse, L., Kraus, M., Mendez-Lopez, M., Bader, J., Xin, B., de Bruin, G., Maurits, E., Overkleeft, H.S., Driessen, C. (2019). Proteasome Inhibition in Multiple Myeloma: Head-to-Head Comparison of Currently Available Proteasome Inhibitors. Cell Chemical Biology *26*, 340-351. https://doi.org/10.1016/j.chembiol.2018.11.007.

Besse, A., Stolze, S.C., Rasche, L., Weinhold, N., Morgan, G.J., Kraus, M., Bader, J., Overkleeft, H.S., Besse, L., Driessen, C. (2018). Carfilzomib resistance due to ABCB1/MDR1 overexpression is overcome by nelfinavir and lopinavir in multiple myeloma. Leukemia *32*, 391-401. 10.1038/leu.2017.212.

Cantor, J.R., Abu-Remaileh, M., Kanarek, N., Freinkman, E., Gao, X., Louissaint, A., Lewis, C.A., Sabatini, D.M. (2017). Physiologic medium rewires cellular metabolism and reveals uric acid as an endogenous inhibitor of UMP synthase. Cell *169*, 258-272.e217. doi: 10.1016/j.cell.2017.03.023.

Ciechanover, A. (1994). The Ubiquitin-Proteasome Proteolytic Pathway. Cell *79*, 13-21. https://doi.org/10.1016/0092-8674(94)90396-4.

Clemens, J., Seckinger, A., Hose, D., Theile, D., Longo, M., Emil Haefeli, W., Burhenne, J., Weiss, J. (2015). Cellular uptake kinetics of bortezomib in relation to efficacy in myeloma cells and the influence of drug transporters. Cancer Chemotherapy and Pharmacology *75*, 281-291.

Daley, G.Q., Van Etten, R.A., Baltimore, D. (1990). Induction of chronic myelogenous leukemia in mice by the P210bcr/abl gene of the Philadelphia chromosome. Science *247*, 824-830. 10.1126/science.2406902.

Dantuma, N.P., Lindsten, K., Glas, R., Jellne, M., Masucci, M.G. (2000). Short-lived green fluorescent proteins for quantifying ubiquitin/proteasome-dependent proteolysis in living cells. Nature Biotechnology *18*, 538-543. https://doi.org/10.1038/75406.

Dixon, S.J., Patel, D.N., Welsch, M., Skouta, R., Lee, E.D., Hayano, M., Thomas, A.G., Gleason, C.E., Tatonetti, N.P., Slusher, B.S., Stockwell, B.R. (2014). Pharmacological inhibition of cystine-glutamate exchange induces endoplasmic reticulum stress and ferroptosis. eLife *30*. https://doi.org/10.7554/eLife.02523.

Druker, B.J., Talpaz, M., Resta, D.J., Peng, B., Buchdunger, E., Ford, J.M., Lydon, N.B., Hantarjian, H., Capdeville, R., Ohno-Jones, S., Sawyers, C.L. (2001). Efficacy and safety of a specific inhibitor of the BCR-ABL tyrosine kinase in chronic myeloid leukemia. New England Journal of Medicine *344*, 1031-1037. 10.1056/NEJM200104053441401.

Eagle, H. (1955). Nutrient Needs of Mammalian Cells in Tissue Culture. Science *122*, 501-504. 10.1126/science.122.3168.50.

Ferraro, G.B., Ali, A., Luengo, A., Kodack, D.P., Deik, A., Abbott, K.L., Bezwada, D., Blanc, L., Prideaux, B., Jin, X., Possada, J.M., Chen, J., Chin, C.R., Amoozgar, Z., Ferreira, R., Chen, I., Naxerova, K., Ng, C., Westermark, A.M., Duquette, M., Roberge, S., Lindeman, N.I., Lyssiotis, C.A., Nielsen, J., Housman, D.E., Duda, D.G., Brachtel, E., Golub, T.R., Cantley, L.C., Asara, J.M., Davidson, S.M., Fukumua, D., Dartois, V.A., Clish, C.B., Jain, R.K., Vander Heiden, M.G. (2021). Fatty acid synthesis is required for breast cancer brain metastasis. Nature Cancer *in press*. 10.1038/s43018-021-00183-y.

Fricker, L. (2020). Proteasome Inhibitor Drugs. Annual Review of Pharmacology and Toxicology *60*, 457-476. https://doi.org/10.1146/annurev-pharmtox-010919-023603.

Gross, M.I., Demo, S.D., Dennison, J.B., Chen, L., Chernov-Rogan, T., Goyal B., Janes, J.R., Laidig, G.J., Lewis, E.R., Li, J., Mackinnon, A.L., Parlati, F., Rodriguez, M.L., Shwonek, P.J., Sjogren, E.B., Stanton, T.F., Wang, T., Yang, J., Zhao, F., Bennett, M.K. (2014). Antitumor activity of the glutaminase inhibitor CB-839 in triple-negative breast cancer. Molecular Cancer Therapeutics *13*, 890-901. https://doi.org/10.1158/1535-7163.MCT-13-0870

Gui, D.Y., Sullivan, L.B., Luengo, A., Hosios, A.M., Bush, L.N., Gitego, N., Davidson, S.M., Freinkman, E., Thomas, C.J., Vander Heiden, M.G. (2016). Environment dictates dependence on mitochondrial complex I for NAD+ and aspartate production and determines cancer cell sensitivity to metformin. Cell Metabolism *24*, 716-727. 10.1016/j.cmet.2016.09.006.

Hennequart, M., Labuschagne, C.F., Tajan, M., Pilley, S.E., Cheung, E.C., Legrave, N.M., Driscoll, P.C., Vousden, K.H. (2021). The impact of physiological metabolite levels on serine uptake, synthesis and utilization in cancer cells. Nature Communications *12*. https://doi.org/10.1038/s41467-021-26395-5.

Hosios, A.M., Hecht, V.C., Danai, L.V., Johnson, M.O., Rathmell, J.C., Steinhauser, M.L., Manalis, S.R., Vander Heiden, M.G. (2016). Amino acids rather than glucose account for the majority of cell mass in proliferating mammalian cells. Developmental Cell *36*, 540-549. doi: 10.1016/j.devcel.2016.02.012.

Jin, X., Demere, Z., Nair, K., Ali, A., Ferraro, G. B., Natoli, T., Deik, A., Petronio, L., Tang, A. A., Zhu, C., Wang, L., Rosenberg, D., Mangena, V., Roth, J., Chung, K., Jain, R. K., Clish, C. B., Vander Heiden, M. G., & Golub, T. R. (2020). A metastasis map of human cancer cell lines. Nature *588*, 331-336. https://doi.org/10.1038/s41586-020-2969-2.

Kisselev, A.F., Akopian, T.N., Castillo, V., Goldberg, A.L. (1999). Proteasome Active Sites Allosterically Regulate Each Other, Suggesting a Cyclical Bite-Chew Mechanism for Protein Breakdown. Molecular Cell *4*, 394-402. https://doi.org/10.1016/S1097-2765(00)80341-X.

Labuschagne, C.F., van den Broek, N.J.F., Mackay, G.M., Vousden, K.H., Maddocks, O.D.K. (2014). Serine, but not glycine, supports one-carbon metabolism and proliferation of cancer cells. Cell Reports *7*. doi: 10.1016/j.celrep.2014.04.045.

Landon, J., Fawcett, J.K., Wynn, V. (1962). Blood pyruvate concentration measured by a specific method in control subjects. Journal of Clinical Pathology *15*, 579-584. 10.1136/jcp.15.6.579.

Letai, A. (2017). Functional precision cancer medicine—moving beyond pure genomics. Nature Medicine *23*, 1028-1035. 10.1038/nm.4389.

Li, A.C., Yu, E., Ring, S.C., Chovan, J.P. (2013). Boronic Acid-Containing Proteasome Inhibitors: Alert to Potential Pharmaceutical Bioactivation. Chemical Research in Toxicology *26*, 608-615. https://doi.org/10.1021/tx400032n.

Li, Z., Ji, B.W., Dixit, P.D., Lien, E.C., Tchourine, K., Hosios, A.M., Abbott, K.L., Westermark, A.M., Gorodetsky, E.F., Sullivan, L.B., Vander Heiden, M.G., Vitkup, D. (2022). Cancer cells depend on environmental lipids for proliferation when electron

acceptors are limited. Nature Metabolism *4*, 711-723. https://doi.org/10.1038/s42255-022-00588-8.

Luengo, A., Li, Z., Gui, D. Y., Sullivan, L. B., Zagorulya, M., Do, B. T., Ferreira, R., Naamati, A., Ali, A., Lewis, C. A., Thomas, C. J., Spranger, S., Matheson, N. J., & Vander Heiden, M. G. (2021). Increased demand for NAD+ relative to ATP drives aerobic glycolysis. Molecular Cell *81*, 691–707. https://doi.org/10.1016/j.molcel.2020.12.012.

Maddocks, O.D.K., Athineos, D., Cheung, E. C., Lee, P., Zhang, T., Van Den Broek, N. J. F., Mackay, G. M., Labuschagne, C. F., Gay, D., Kruiswijk, F., Blagih, J., Vincent, D. F., Campbell, K. J., Ceteci, F., Sansom, O. J., Blyth, K., & Vousden, K. H. (2017). Modulating the therapeutic response of tumours to dietary serine and glycine starvation. Nature *544*, 372–376. https://doi.org/10.1038/nature22056.

Manasanch, E.E., Orlowski, R.Z. (2017). Proteasome inhibitors in cancer therapy. Nature Reviews Clinical Oncology *14*, 417-433. https://doi.org/10.1038/nrclinonc.2016.206.

Meul, T., Berschneider, K., Schmitt, S., Mayr, C.H., Mattner, L.F., Schiller, H.B., Yazgili, A.S., Wang, X., Lukas, C., Schlesser, C., Prehn, C., Adamski, J., Graf, E., Schwarzmayr, T., Perocchi, F., Kukat, A., Trifunovic, A., Kremer, L., Prokisch, H., Popper, B., von Toerne, C., Hauck, S.M., Zischka, H., Meiners, S. (2020). Mitochondrial Regulation of the 26S Proteasome. Cell Reports *32*. https://doi.org/10.1016/j.celrep.2020.108059.

Moreau, P., Richardson, P.G., Cavo, M., Orlowski, R.Z., San Miguel, J.F., Palumbo, A., Harousseau, J. (2012). Proteasome inhibitors in multiple myeloma: 10 years later. Blood *120*, 947-959. https://doi.org/10.1182/blood-2012-04-403733.

Muir, A., Danai, L.V., Gui, D.Y., Waingarten, C.Y., Lewis, C.A., Vander Heiden, M.G. (2017). Environmental cystine drives glutamine anaplerosis and sensitizes cancer cells to glutaminase inhibition. eLife *6*. https://doi.org/10.7554/eLife.27713.001.
Muir, A., Vander Heiden, M.G. (2018). The nutrient environment affects therapy. Science *360*, 962-963. 10.1126/science.aar5986.

Nerini-Molteni, S., Ferrarini, M., Cozza, S., Caligaris-Cappio, F., Sitia, R. (2008). Redox homeostasis modulates the sensitivity of myeloma cells to bortezomib. British Journal of Haematology *141*, 494-503. 10.1111/j.1365-2141.2008.07066.x.

Ngo, B., Kim, E., Osorio-Vasquez, V., Doll, S., Bustraan, S., Liang, R. J., Luengo, A., Davidson, S. M., Ali, A., Ferraro, G. B., Fischer, G. M., Eskandari, R., Kang, D. S., Ni, J., Plasger, A., Rajasekhar, V. K., Kastenhuber, E. R., Bacha, S., Sriram, R. K., … Pacold, M. E. (2020). Limited Environmental Serine and Glycine Confer Brain Metastasis Sensitivity to PHGDH Inhibition. Cancer Discovery *10*, 1352–1373. https://doi.org/10.1158/2159-8290.cd-19-1228.

Obeng, E.A., Carlson, L.M., Gutman, D.M., Harrington, W.J., Lee, K.P., Boise, L.H. (2006). Proteasome inhibitors induce a terminal unfolded protein response in multiple myeloma cells. Blood *15*, 4907-4916. 10.1182/blood-2005-08-3531.

Pavlova, N.N., Thompson, C.B. (2017). The Emerging Hallmarks of Cancer Metabolism. Cell Metabolism *23*, 27-47. 10.1016/j.cmet.2015.12.006.

Potts, B.C., Albitar, M.X., Anderson, K.C., Baritaki, S., Berkers, C., Bonavida, B., Chandra, J., Chauhan, D., Cusack, J.C., Fenical, W., Ghobrial, I.M., Groll, M., Jensen, P.R., Lam, K.S., Lloyd, G.K., McBride, W., McConkey, D.J., Miller, C.P., Neuteboom, S.T.C., Oki, Y., Ovaa, H., Pajonk, F., Richardson, P.G., Roccaro, A.M., Sloss, C.M., Spear, M.A., Valashi, E., Younes, A., Palladino, M.A. (2011). Marizomib, a Proteasome Inhibitor for All Seasons: Preclinical Profile and a Framework for Clinical Trials. Current Cancer Drug Targets *11*, 254-284. 10.2174/156800911794519716.

Rossiter, N.J., Huggler, K.S., Adelmann, C.H., Keys, H.R., Soens, R.W., Sabatini, D.M., Cantor, J.R. (2021). CRISPR screens in physiologic medium reveal conditionally essential genes in human cells. Cell Metabolism *33*, 1248-1263. https://doi.org/10.1016/j.cmet.2021.02.005.

Schäfer, J., Welti, L., Seckinger, A., Burhenne, J., Theile, D., Weiss, J. (2017). Cellular effect and efficacy of carfilzomib depends on cellular net concentration gradient. Cancer Chemotherapy and Pharmacology *80*, 71-79. 10.1007/s00280-017-3335-4.

Sharma, A., Nair, R., Achreja, A., Mittal, A., Gupta, P., Balakrishnan, K., Edgar, C.L., Animasahun, O., Dwivedi, B., Barwick, G.B., Gupta, V.A., Matulis, S.M., Bhasin, M., Lonial, S., Nooka, A.K., Wiita, A.P., Boise, L.H., Nagrath, D., Shanmugam, M. (2022). Therapeutic implications of mitochondrial stress-induced proteasome inhibitor resistance in multiple myeloma. Science Advances *8*. 10.1126/sciadv.abq5575.

Starheim, K.K., Holien, T., Misund, K., Johansson, I., Baranowska, K.A., Sponaas, A.M., Hella, H., Buene, G., Waage, A., Sundan, A., Bjørkøy, G. (2016). Intracellular glutathione determines bortezomib cytotoxicity in multiple myeloma cells. Blood Cancer Journal *6*. https://doi.org/10.1038/bcj.2016.56.

Sullivan, L.B., Gui, D.Y., Hosios, A.M., Bush, L.N., Freinkman, E., Vander Heiden M.G. (2015). Supporting Aspartate Biosynthesis Is an Essential Function of Respiration in Proliferation Cells. Cell *162*, 552-563. doi:10.1016/j.cell.2015.07.017.

Sullivan, M.R., Danai, L. V., Lewis, C. A., Chan, S. H., Gui, D. Y., Kunchok, T., Dennstedt, E. A., Vander Heiden, M. G., Muir, A. (2019a). Quantification of microenvironmental metabolites in murine cancers reveals determinants of tumor nutrient availability. eLife *8*. https://doi.org/10.7554/elife.44235.

Sullivan, M.R., Darnell, A.M., Reilly, M.R., Kunchok, T., Joesch-Cohen, L., Rosenberg, D., Ali, A., Rees, M.G., Roth, J.A., Lewis, C.A., Vander Heiden, M.G. (2021). Methionine synthase is essential for cancer cell proliferation in physiological folate environments. Nature Metabolism *3*, 1500-1511. https://doi.org/10.1038/s42255-021-00486-5.

Sullivan, M.R., Mattaini, K.R., Dennstedt, E.A., Nguyen, A.A., Reilly, M.F., Meeth, K., Muir, A., Darnell, A.M., Bosenberg, M.W., Lewis, C.A., Vander Heiden, M.G. (2019b). Increased serine synthesis provides an advantage for tumors arising in tissues where serine levels are limiting. Cell Metabolism *29*, 1410-1421,e1414. doi: 10.1016/j.cmet.2019.02.015.

Suraweera, A., Münch, C., Hanssum, A. Bertolotti, A. (2012). Failure of Amino Acid Homeostasis Causes Cell Death following Proteasome Inhibition. Molecular Cell *48*, 242-253. https://doi.org/10.1016/j.molcel.2012.08.003.

Tardito, S., Oudin, A., Ahmed, S.U., Fack, F., Keunen, O., Zheng, L., Miletic, H., Sakariassen, P.Ø., Weinstock, A., Wagner, A., Lindsay, S.L., Hock, A.K., Barnett, S.C., Ruppin, E., Mørkve, S.H., Lund-Johansen, M., Chalmers, A.J., Bjerkvig, R., Niclou, S.P., Gottlieb, E. (2015). Glutamine synthetase activity fuels nucleotide biosynthesis and supports growth of glutamine-restricted glioblastoma. Nature Cell Biology *17*, 1556-1568. https://doi.org/10.1038/ncb3272.

Tsvetkov, P., Myers, N., Eliav, R., Adamovich, Y., Hagai, T., Adler, J., Navon, A., Shaul, Y. (2014). NADH Binds and Stabilizes the 26S Proteasomes Independent of ATP. Journal of Biological Chemistry *289*, 11272-11281. 10.1074/jbc.M113.537175.

Verbrugge, S.E., Assaraf, Y.G., Dijkmans, B.A.C., Scheffer, G.L., Al, M., den Uyl, D., Oerlemans, R., Chan, E.T., Kirk, C.J., Peters, G.J., van der Heijden, J.W., de Gruijl, T.D., Scheper, R.J., Jansen, G. (2012). Inactivating PSMB5 mutations and P-glycoprotein (multidrug resistance-associated protein/ATP-binding cassette B1) mediate resistance to proteasome inhibitors: ex vivo efficacy of (immuno)proteasome inhibitors in mononuclear blood cells from patients with rheumatoid arthritis. Journal of Pharmacology and Experimental Therapeutics *341*, 174-182. 10.1124/jpet.111.187542.

Supplementary Figures

Supplementary Figure 1

A

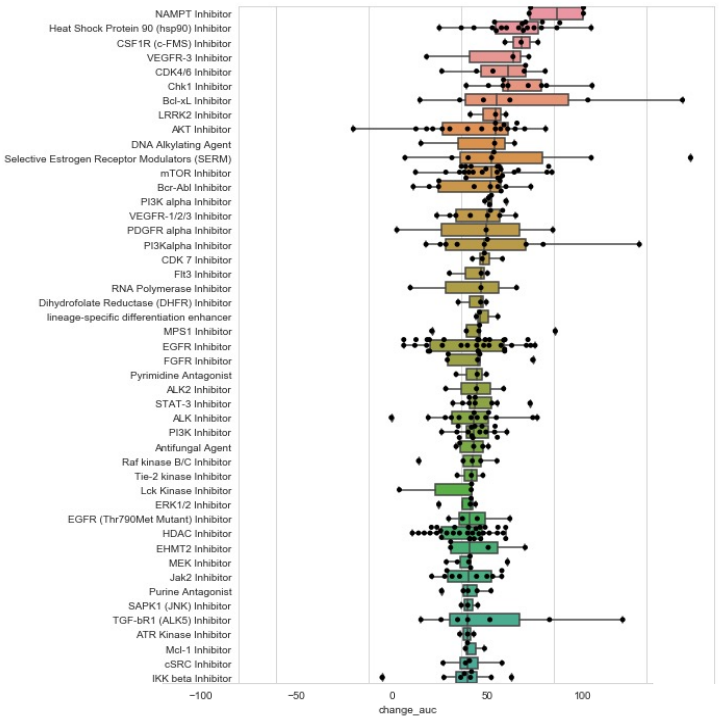

B

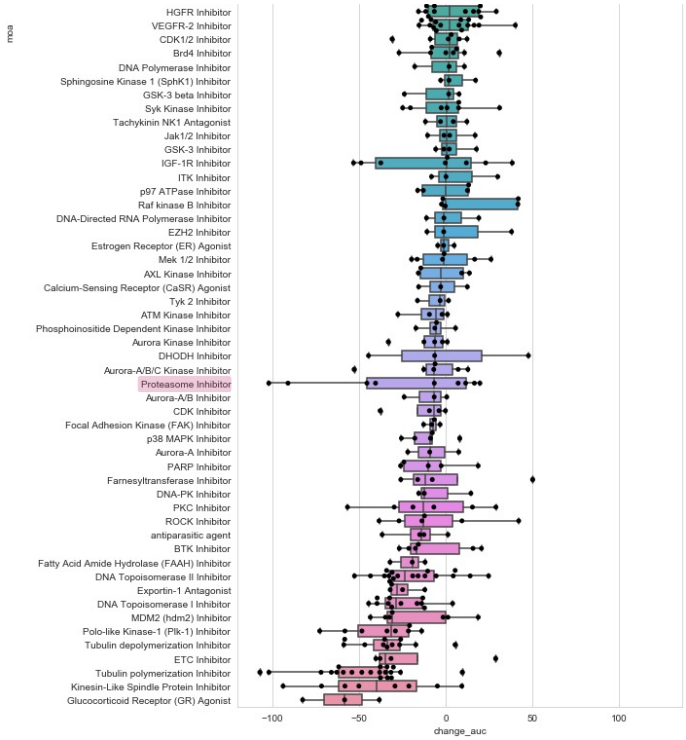

Supplementary Figure 1. Results of small molecule screen. Screen was conducted in A549 cells cultured in DMEM. The small molecule library consisted of 2480 small molecules starting at

40 mM and diluted 1:3 for a total of 11 concentrations tested. Cells were cultured with the small molecule library for 72 hours with and without 1 mM pyruvate and viability was measured using Cell Titer Glo. Changes in area under the curve (auc) were quantitated and classified as either drugs whose cellular sensitivity were decreased by pyruvate **(A)** or increased by pyruvate **(B).** Proteasome inhibitors are highlights in light red in **(B).**

Supplementary Figure 2

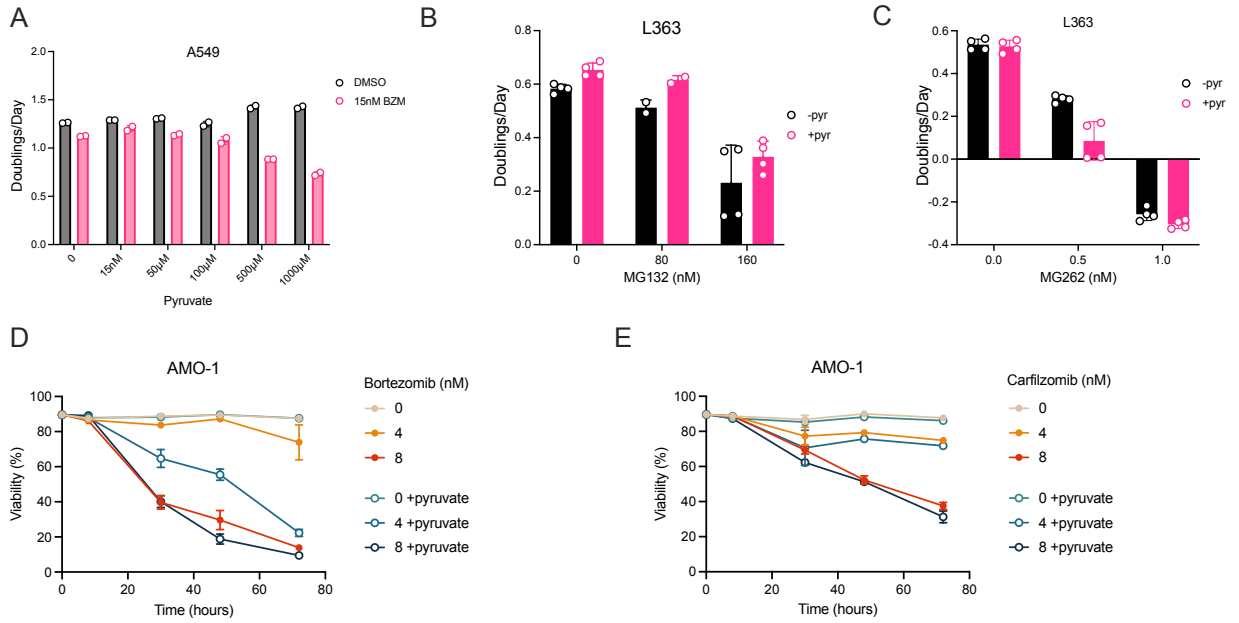

Supplementary Figure 2. Pyruvate leads to worse proliferation and viability in cells treated with boronic acid proteasome inhibitors. (A) Proliferation rate (doublings per day) of A549 cells treated with 15 nM of Bortezomib with indicated concentrations of pyruvate, n=2. **(B,C)** Proliferation rate (doublings per day) of L363 cells treated with indicated concentrations of MG132 (B) or MG262 (C) with and without 1 mM pyruvate, n=4. **(D,E)** Percent cellular viability of AMO-1 cells treated with indicated concentrations of Bortezomib (D) or Carfilzomib (E) with and without 1 mM pyruvate over time, n=3. All values are means ± SD.

Supplementary Figure 3

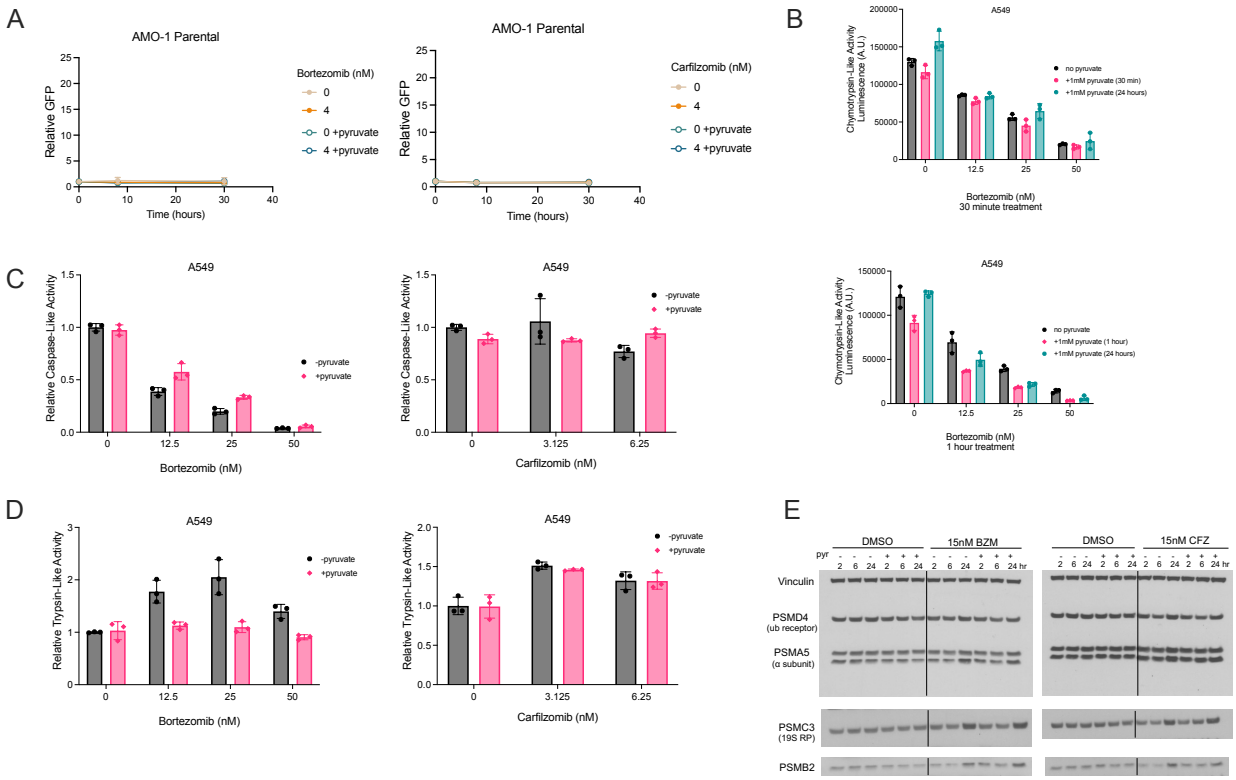

Supplementary Figure 3. Pyruvate acutely suppresses chymotrypsin-like activity in Bortezomib treated cells. (A) Relative GFP signal in parental AMO-1 cells not expressing ubiquitin-GFP reporter treated with indicated concentrations of Bortezomib (left) or Carfilzomib (right) with and without 1 mM pyruvate over time. Values are relative to untreated – pyruvate, n=3. **(B)** Chymotrypsin-like proteasome activity of cells treated with indicated concentrations of Bortezomib with and without 1 mM pyruvate for 30 minutes (top) or 1 hour (bottom). Pyruvate was either added simultaneously with Bortezomib or 24 hours prior. **(C)** Relative caspase-like proteasome activity in cells treated with indicated concentrations of Bortezomib (left) or Carfilzomib (right) with and without 1 mM pyruvate for six hours. Values are normalized to untreated – pyruvate conditions, n=3. **(D)** Relative trypsin-like activity in cells treated with indicated concentrations of Bortezomib (left) and Carfilzomib (right) with and without 1 mM pyruvate for six hours, n=3. **(E)** Immunoblots measuring protein expression of indicated proteasome subunits in cells treated with either 15 nM Bortezomib (BZM) or Carfilzomib (CFZ) with and without 1 mM pyruvate over time. Vinculin was used as a loading control. All values are means ± SD.

Supplementary Figure 4

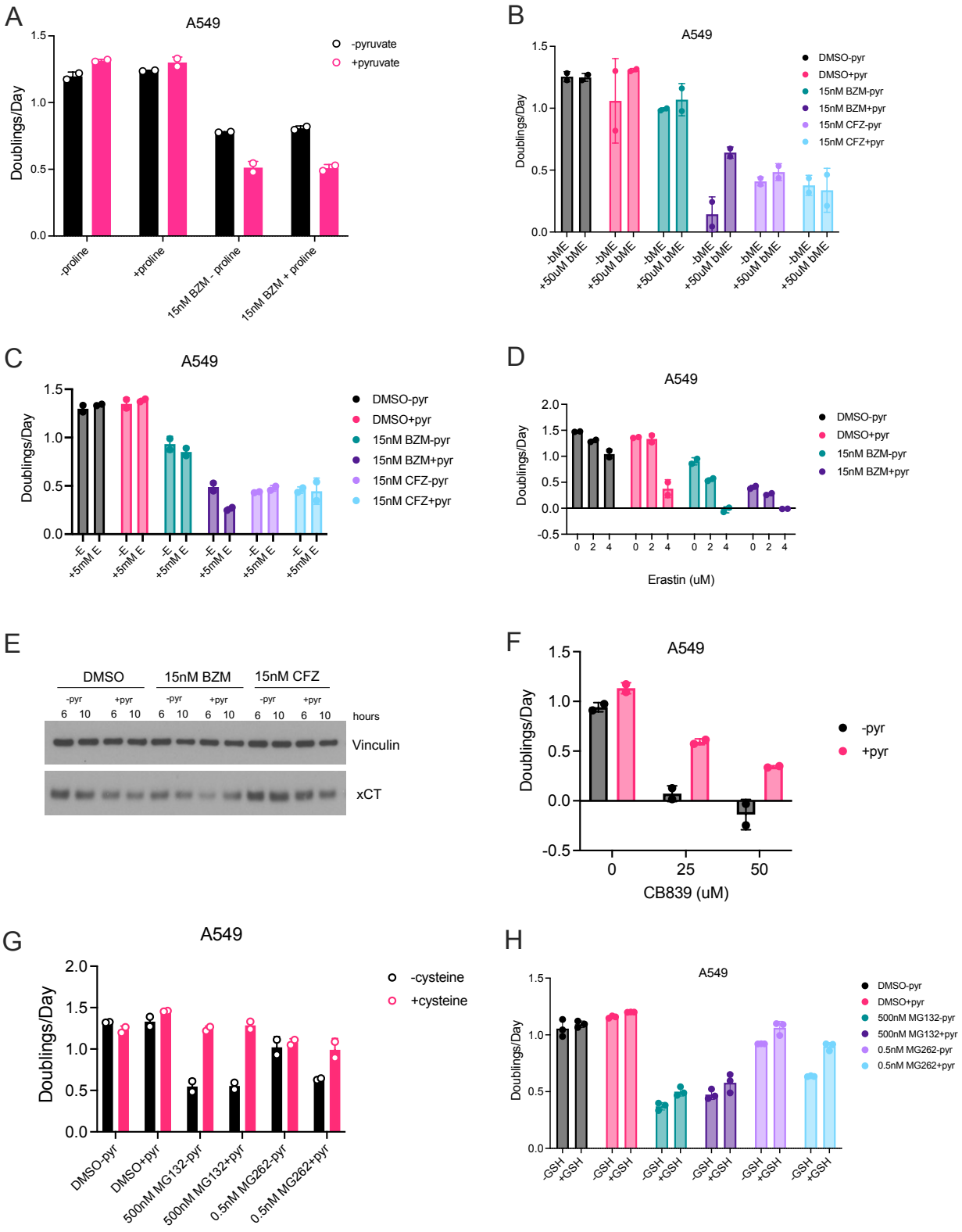

Supplementary Figure 4. xCT function, cysteine, and glutathione are involved in modulating sensitivity to proteasome inhibitors and impacted by pyruvate supplementation. (A) Proliferation rate (doublings per day) of cells treated with 15 nM Bortezomib (BZM) with and without 1 mM pyruvate and 2 mM proline for three days, n=2. **(B)** Proliferation rate (doublings per day) of cells treated with 15 nM Bortezomib (BZM) or Carfilzomib (CFZ) with and without 1 mM pyruvate and 500 μM β-mercaptoethanol (bME) for three days, n=2. **(C)** Proliferation rate (doublings per day) of cells treated with 15 nM Bortezomib (BZM) or Carfilzomib (CFZ) with and without 1 mM pyruvate and 5 mM glutamate (E) for three days, n=2. **(D)** Proliferation rate (doublings per day) of cells treated with 15 nM BZM with and without 1 mM pyruvate and indicated concentrations of erastin for three days, n=2. **(E)** Immunoblot measuring protein levels of xCT with 15 nM BZM or CFZ with and without 1 mM pyruvate after 6 and 10 hours. Vinculin was used as a loading control. **(F)** Proliferation rate (doublings per day) of cells treated with indicated concentrations of CB-839 with and without 1 mM pyruvate for three days, n=2. **(G)** Proliferation rate (doublings per day) of cells treated with 500 nM MG132 or 0.5 nM MG262 with and without 1 mM pyruvate for three days, n=2. **(H)** Proliferation rate (doublings per day) of cells treated with 500 nM MG132 or 0.5 nM MG262 with and without 1 mM pyruvate and 2.5 mM glutathione reduced ethyl ester (GSH), n=3. All values are means ± SD.